

Department of Materials Engineering and Materials Design

University of Nottingham

THE ELECTRODEPOSITION OF ZINC-MANGANESE

By

Karen Elizabeth Ferguson BEng (Hons) MPhil

Thesis submitted to the University of Nottingham
for the degree of Doctor of Philosophy

August 1999

**CONTAINS A
PULLOUT**

ABSTRACT

Electroplated zinc alloys can provide increased corrosion protection for automotive body panels compared with zinc coatings of similar thickness. As a result, their use is becoming widespread. In particular, outstanding results have been reported in the literature for the corrosion resistance of zinc-manganese, and the alloys are said to offer good paintability, weldability and formability. However, the production of zinc-manganese coatings is restricted by the instability of the sulphate-citrate bath from which the alloy is usually deposited. The solution deteriorates rapidly and precipitates appear in the bath. The aim of this research was to investigate both the process of alloy deposition from the sulphate-citrate bath and the solution instability.

The electrodeposition of zinc-manganese was assessed in terms of the polarisation behaviour of the system, in order to determine the role of the bath components and the operating parameters in the deposition process. The coatings were analysed using scanning electron microscopy, and the efficiency of metal deposition was established. The sodium citrate complexant was not found to significantly move the deposition potentials of zinc and manganese together. Instead, its action as a buffer can be used to explain metal deposition and the polarisation behaviour of the system. The sodium citrate suppresses the hydrogen evolution reaction, such that manganese can be deposited from the electrolyte.

The bath deterioration with time and the resulting precipitate were examined using a variety of chemical techniques including spectroscopic methods, namely ultraviolet and visible, atomic absorption and infrared. Bath discolouration and precipitation were found to be two separate phenomena. The precipitate was determined to be a citrate of known composition with a ratio of Mn^{2+} ions to Zn^{2+} ions of 2:1. The formation took several days, and it was precipitated once the solubility limit in the bath was exceeded. Solution discolouration resulted from reactions occurring after the oxidation of Mn^{2+} ions and could be delayed by the use of antioxidants.

A method for the manufacture and long-term storage of the solution has been developed, and recommendations are made for improvement of the bath composition and operating conditions.

GLOSSARY

Subscript Suffixes

Symbols for general terms may include subscript suffixes as follows:

A	Anodic
C	Cathodic
H ₂	Hydrogen
Mn	Manganese
O ₂	Oxygen
Zn	Zinc

General Terms

β	Symmetry factor
δ_N	Diffusion layer thickness
ϵ	Molar absorption coefficient
γ	Activity coefficient
η	Overpotential
η_{act}	Activation overpotential
η_{conc}	Concentration overpotential
η_{res}	Resistance overpotential
η_{total}	Total overpotential
λ	Wavelength
ν	Frequency
ρ	Density
υ	Wavenumber
a,b	Constants in the Tafel equation (Appendix 7)
a'	Activity
A	Atomic weight
A ₀	Intensity of incident light
A _T	Intensity of transmitted light
c	Concentration
c ₀	Bulk concentration
c _e	Surface concentration
D	Diffusion coefficient

E	Potential
E^0	Standard electrode potential
E_{eq}	Equilibrium potential
E_{total}	Total potential
ΔE	Energy gain
F	Faraday's constant (= 96480Cmol ⁻¹)
G	Free energy
G^*	Gibbs free energy for a reversible system
$(G^*)'$	Gibbs free energy for an irreversible system
ΔG	Change in free energy
ΔG^*	Change in standard free energy
h	Planck's constant (6.5×10^{-27} erg sec)
i	Current density (= I / area)
i_c	Cathodic partial current density
i_a	Anodic partial current density
i_0	Equilibrium exchange current density
i_L	Limiting current density ($c_e=0$)
i_{net}	Net current density
I	Current
J	Diffusion rate
k	Rate constant
K_{eq}	Equilibrium constant
l	Path length of absorbing solution
p	Partial pressure
Q	Charge passed
R	Universal gas constant ($8.31 \text{ J mol}^{-1} \text{ K}^{-1}$)
R_s	Solution resistance
t	Time
t	Transport number
T	Absolute temperature
δ	Thickness
v	Volume
w	Equivalent weight
wt%	Alloy percentage (by weight)
x	Distance from electrode
z	Ionic charge of the metal ions M^{z+}

Symbols and Abbreviations

[]	Denotes activity of species
CCE	Cathode current efficiency for metal deposition
CE	Counter electrode
GCL	Gouy-Chapman Layer
HC	Hull Cell
HDL	Helmholtz Double Layer
OHP	Outer Helmholtz Plane
RE	Reference electrode
SCE	Standard Calomel Electrode (+0.242mV with respect to the standard hydrogen electrode at 25°C)
SEM	Scanning electron microscope
WE	Working electrode

CONTENTS

	<u>PAGE</u>
CHAPTER 1 - INTRODUCTION	
1.1 The Use Of Steel In Automobiles	1
1.2 Corrosion Protection Systems	1
1.3 Electroplated Zinc Alloys	3
1.4 Electroplated Zinc-Manganese	4
1.5 Research Objectives	5
CHAPTER 2 - LITERATURE REVIEW	
PART ONE - RELEVANT ELECTROCHEMICAL THEORY	
2.1 The Electrodeposition Process	6
2.1.1 The Double Layer	6
2.1.2 Cathodic Deposition at the Metal Surface	7
2.1.3 Migration of Ions (Mass Transport)	7
2.1.4 Electron Transfer (Electrocrystallisation)	7
2.2 Equilibrium Electrode Processes	8
2.2.1 Single Electrode Potentials	8
2.2.2 Exchange Current Density	10
2.3 Non-Equilibrium Electrode Processes	10
2.3.1 Polarisation	10
2.3.1.1 Activation Polarisation	11
2.3.1.2 Concentration Polarisation	13
2.3.1.3 Resistance Polarisation	15
2.4 Polarisation Diagrams	15
2.4.1 Single Electrode Polarisation Diagrams	16
2.4.2 Polarisation of Two Electrodes	16
2.4.3 Factors Affecting Polarisation Curves	18
2.4.3.1 Multiple Cathodic Processes	18
2.4.3.2 Oxygen Reduction	19
2.4.3.3 Hydrogen Evolution	19
2.5 Potential-pH Diagrams (Pourbaix Diagrams)	21
2.5.1 Construction of a Pourbaix Diagram for Zinc in Aqueous Solution	21
2.6 Electrodeposition of Alloys	25
2.6.1 The Nernst Equation in Alloy Plating	26

PART TWO - ELECTRODEPOSITION OF ZINC MANGANESE

2.7	Introduction	27
2.8	Electroplating Baths And Conditions	28
2.9	Polarisation Behaviour For Zinc-Manganese Electrodeposition From A Sulphate-Citrate Bath	30
2.9.1	Total Polarisation Behaviour	30
2.9.2	Partial Polarisation Curves	31
2.9.3	Effect Of Operating Variables On The Partial Polarisation Curves	32
2.10	Effect Of Bath Composition And Operating Conditions On The Manganese Content Of The Deposit	35
2.10.1	Variation In Electroplating Bath Composition	35
2.10.2	Variation In Operating Conditions	35
2.11	Effect Of Bath Composition And Operating Conditions On The Cathode Current Efficiency During Electroplating	38
2.11.1	Variation In Electroplating Bath Composition	38
2.11.2	Variation In Operating Conditions	38
2.12	Structure and Appearance of Zinc-Manganese Electroplate	39
2.13	Corrosion Resistance Of Zinc-Manganese Electroplate	41
2.13.1	Corrosion Resistance Without Paint	43
2.13.2	Corrosion Resistance After Phosphating and/or Painting	44
2.13.2.1	Perforation Corrosion Resistance	45
2.13.2.2	Resistance to Paint Chipping	46
2.13.2.3	Paint Undercutting	46
2.14	Phosphating and Painting of Zinc-Manganese Electroplate	47
2.14.1	Phosphatability	47
2.14.2	Wet Adhesion of Paint	48
2.14.3	Cratering During Electrocoating	49
2.15	Coating Adhesion	49
2.16	Weldability	49
PART THREE - CHEMISTRY OF THE ELECTROPLATING BATH		
2.17	Electroplating Bath Chemistry	50
2.17.1	Electroplating Bath Stability	50
2.17.2	Electroplating Bath Additives	52
2.17.3	Alternative Baths	54
2.18	Analysis of Electroplating Bath Chemistry	54
2.18.1	Plating Bath Reactions During Electrodeposition	54
2.18.2	Analysis Techniques	54

2.18.2.1	Ultraviolet and Visible Spectroscopy	56
2.18.2.2	Infrared Spectroscopy	57

CHAPTER 3 - EXPERIMENTAL PROCEDURE

3.1	Introduction	61
-----	--------------	----

PART ONE - ELECTRODEPOSITION OF ZINC-MANGANESE

3.2	The Electroplating Bath	61
-----	-------------------------	----

3.2.1	Choice of Bath	61
3.2.2	Preparation of the Bath	62
3.2.3	Operating Conditions	63

3.3	Experimental Apparatus	64
-----	------------------------	----

3.3.1	The Circuit	64
3.3.2	The Cathode	65
3.3.3	Specimen Design	65
3.3.4	Electrode Preparation	67
3.3.5	Counter Electrode	67
3.3.6	Reference Electrode	68
3.3.7	Power Supply	68
3.3.8	The Hull Cell	69

3.4	Electrodeposition Of Zinc-Manganese	70
-----	-------------------------------------	----

3.4.1	Polarisation Behaviour	70
3.4.2	Cathode Current Efficiency	71
3.4.3	Electrodeposition of Coatings	72
3.4.3.1	Hull Cell Tests	72
3.4.3.2	Electroplated Specimens	73

3.5	Examination Of Zinc-Manganese Coatings	74
-----	--	----

3.5.1	Visual Examination	74
3.5.2	Scanning Electron Microscopy	74

PART TWO – CHEMISTRY OF THE ELECTROPLATING BATH

3.6	Chemical Techniques	75
-----	---------------------	----

3.6.1	Ultraviolet and Visible Spectroscopy	76
3.6.2	Infrared Spectroscopy	76
3.6.3	Atomic Absorption Spectroscopy	77

3.7	Chemistry of the Electroplating Solution	77
-----	--	----

3.7.1	Visual Examination and Bath Deterioration	78
3.7.2	Effect of Deoxygenation of the Solution	78
3.7.3	Ultraviolet and Visible Spectroscopy	79

3.8	Examination Of The Precipitate	80
-----	--------------------------------	----

3.8.1	Elemental Analysis of the Precipitate	80
3.8.1.1	Scanning Electron Microscopy	80

3.8.1.2	Atomic Absorption Spectroscopy	81
3.8.1.3	Microanalysis	81
3.8.1.4	Titration	81
3.8.2	Structure of the Precipitate	82
3.8.2.1	Infrared Spectroscopy	82
3.8.2.2	Ultraviolet and Visible Spectroscopy	82
CHAPTER 4 - EXPERIMENTAL RESULTS		
4.1	Introduction	83
PART ONE – ELECTRODEPOSITION OF ZINC-MANGANESE		
4.2	Polarisation Behaviour and Hull Cell Panels	83
4.2.1	Standard Bath	83
4.2.1.1	Related to Coating Appearance and Microstructure	84
4.2.1.2	Related to Cathode Current Efficiency	86
4.2.2	Effect of Variation in Operating Conditions	87
4.2.2.1	Effect of Sodium Citrate on Zinc Electrodeposition	88
4.2.2.2	Effect of Sodium Citrate on Manganese Electrodeposition	89
4.2.2.3	Effect of Sodium Citrate on Zinc-Manganese Electrodeposition	89
4.2.2.4	Constituent Solutions of a Standard Bath	90
4.2.2.5	Effect of pH	91
4.2.2.6	Effect of Sodium Citrate Content	92
4.2.2.7	Effect of Zinc Sulphate Content	92
4.2.2.8	Effect of Manganese Sulphate Content	93
4.2.2.9	Effect of Metal Salt Content	94
4.2.2.10	Effect of Additions	95
4.2.2.11	Effect of Aging a Standard Bath (With and Without Additions)	96
4.2.2.12	Effect of Repeated Use of the Standard Bath	97
4.2.2.13	Effect of Separating the Anode and Cathode	98
4.2.2.14	Effect of Oxygen Content	98
PART TWO – CHEMISTRY OF THE ELECTROPLATING BATH		
4.3	The Electroplating Bath	99
4.3.1	Preparation of the Bath	99
4.3.2	General Observations on Operating Conditions	99
4.4	Deterioration of the Bath	100
4.4.1	Standard Bath	100
4.4.2	Effect of Variation in Bath Composition	101
4.4.3	Effect of Deoxygenation of the Solution	101
4.5	Chemistry of the Electroplating Solution	102
4.5.1	Ultraviolet and Visible Spectroscopy	102
4.6	Examination of the Precipitate	105
4.6.1	Elemental Analysis of the Precipitate	105

4.6.2	Structure of the Precipitate	105
4.6.2.1	Infrared Spectroscopy	105
4.6.2.2	Ultraviolet and Visible Spectroscopy	106

CHAPTER 5 - DISCUSSION

PART ONE – ELECTRODEPOSITION OF ZINC-MANGANESE

5.1	Introduction	107
5.2	The Role of Citrate in Solution	108
5.2.1	Citrate as a Complexant	108
5.2.2	Citrate as a Buffer	109
5.3	Interpretation of Polarisation Behaviour	111
5.3.1	No Electrodeposition (Region A)	112
5.3.1.1	Hydrogen Evolution Reaction	113
5.3.1.2	Formation of a Cathode Surface Film	114
5.3.2	Zinc-Rich Coatings (Region B)	117
5.3.3	Limiting Current for Zinc-Rich Coatings (Region C)	119
5.3.4	Zinc-Manganese Alloys (Region D)	121
5.3.4.1	The Role of Zinc in Alloy Deposition	123
5.3.5	Limiting Current for Zinc-Manganese Alloys (Region E)	124

PART TWO – CHEMISTRY OF THE ELECTROPLATING BATH

5.4	Introduction	124
5.5	Chemistry of the Electroplating Solution	125
5.6	Examination of the Precipitate	128

PART THREE – PRACTICAL GUIDELINES FOR THE SULPHATE-CITRATE BATH

5.7	Introduction	130
5.8	Bath Composition	131
5.9	Operating Conditions	133

CHAPTER 6 - SUMMARY

6.1	Conclusions	134
-----	-------------	-----

PART ONE – ELECTRODEPOSITION OF ZINC-MANGANESE

PART TWO – CHEMISTRY OF THE ELECTROPLATING BATH

TABLES

FIGURES

ACKNOWLEDGEMENTS

REFERENCES

APPENDICES

CHAPTER 1

INTRODUCTION

1.1 The Use of Steel in Automobiles

For use in automobiles, steel has numerous advantages compared with alternative materials. These include favourable cost, availability, recyclability, a proven track record and a large engineering database. In addition, it is formable, weldable and paintable. The main drawback is its susceptibility to corrosion. Corrosion damage to an automobile is largely of two types. These are cosmetic corrosion of the exterior surface and perforation of the body by corrosion initiating from the underside.

The steel components of a car may be classified into two categories. The first is discrete parts, such as fasteners, brackets and engine components, which are formed into the desired shape before having a corrosion protection system applied either individually or in bulk. Such parts must fulfil their primary engineering function whilst providing corrosion protection to the sub-assembly. The second category includes simpler geometric configurations which can be processed continuously, namely strip, wire and tube. In particular, high corrosion resistance is now demanded from body panels which are formed from coated strip steel.

1.2 Corrosion Protection Systems

Early corrosion protection schemes were usually based on phosphate pre-treatment, often coupled with a multi-layer paint system. This provided adequate barrier protection, but was not successful in preventing corrosion of the steel if the paint system became damaged. As the car industry began to offer “anti-corrosion” guarantees, base steel under the paint no longer provided the expected protection. So, zinc coatings were introduced. Not only does the zinc provide a barrier between the environment and the substrate, but it also corrodes itself to form an insoluble “white

rust” film to protect the system. If the coating becomes damaged, the zinc further protects by its sacrificial action resulting from galvanic coupling with the steel.

Zinc may be applied to the steel by one of a number of methods, about which there are many published works ⁽¹⁾⁽²⁾⁽³⁾. The first widely used technique in the 1960’s was hot-dip galvanising. Other methods include spraying of the molten metal and electroplating. There are a wide range of zinc-rich paints and products in which zinc dust or flake are incorporated in organic or inorganic media. The combination of metallic zinc with paint, powder or plastic overcoats is of great importance and is the basis of an expanding industry, since the duplex coating has a greater corrosion life than a simple summation of those of the individual components.

With hot-dip coatings, the steel parts were initially covered in their entirety with a 6µm to 20µm thick layer of zinc ⁽⁴⁾. Whilst this method is still used today for unexposed parts, it was found not to be ideal for external parts such as body panels. Problems are encountered with the welding of two-sided galvanised coatings and with the surface appearance. There are also paint match difficulties when attempting to join a galvanised part to one made from cold-rolled steel. As a consequence, a one-sided product was manufactured. For sheet steel, zinc coatings of thickness 4µm to 14µm ⁽⁴⁾ with excellent properties were usually applied by electroplating. The coated side was applied to the interior of a body panel to protect against perforation corrosion, while the uncoated exterior gives a suitable surface for further processing and painting.

In recent years, however, the car manufacturers have been faced with even more strict anti-corrosion requirements. Guarantees of five years against cosmetic corrosion and ten years against perforation corrosion are common. The external paint coating does not provide the required protection against cosmetic corrosion if it becomes damaged and exposed to environments such as salt from road grit, so a two-sided zinc coated product was introduced. Since high standards must be reached for exterior use, the zinc is usually electroplated.

Due to the sacrificial corrosion mechanism of zinc, improved protection can be obtained by increasing the coating thickness. However, above about $7.5\mu\text{m}$ ⁽⁵⁾, formability deteriorates and weldability is impaired. The requirements of saving fuel costs emphasises the need to keep the coating thin, as does the fact that scrap disposal may become an issue in the future. Therefore, the trend has become to develop thinner, corrosion resistance coatings which can replace zinc for both the thick interior layers used on body panels for perforation protection and the high quality sacrificial coatings on the exterior. The search for a suitable coating that offers the required corrosion resistance together with good paintability, formability and weldability is complicated by the fact that these properties are not always mutually compatible. The constraints imposed lead directly to the rationale for using electroplated zinc alloys in place of pure zinc.

1.3 Electroplated Zinc Alloys

The general approach is to alloy the zinc with more noble metals such as nickel, iron or cobalt. The literature indicates that, in comparison with pure zinc, the corrosion resistance can be increased by a factor of two or more by using alloys of the same or even lower thickness. A vast majority of the research which has been carried out covers alloy systems which can be electroplated readily from commercially viable processes. Not only are such systems gaining worldwide approval as a replacement for zinc, but they are also used instead of cadmium where the demand for the electroplated finish has been declining due to its toxicity and that of its process solutions⁽⁶⁾.

Both zinc-nickel and zinc-iron are widely used by the automobile industry in Japan, whilst the Europeans appear to favour zinc-nickel and zinc-cobalt. These systems typically contain small amounts of the alloying element (0.3% to 12%). Each system has its advantages and disadvantages, and several excellent overviews of their properties⁽⁷⁾ and comparison with various zinc coatings⁽³⁾⁽⁴⁾⁽⁵⁾⁽⁸⁾⁽⁹⁾ are available. Other developmental systems which show excellent corrosion resistance but are not yet of

commercial significance include zinc alloyed with tin, aluminium, chromium and magnesium.

Suitable coatings appear only to be produced by electroplating. Since this process has high energy consumption and cost relative to a process such as hot-dip galvanising ⁽⁵⁾, zinc alloys are unlikely to totally replace the use of zinc. Electroplating cannot be competitive where high thickness is required on discrete parts, so the potential market for zinc alloys is predominantly restricted to continuous processes.

The corrosion resistance of zinc alloys is excellent. Brooman ⁽⁶⁾ shows a comparison of salt spray test results for the time to red rust of unchromated alloy coatings of thickness 7.62µm. Zinc-iron failed after 300 hours, zinc-cobalt after 450 hours and zinc-nickel after 700 hours. One system showed outstanding results, with no red rust exhibited after the test was concluded at 1000 hours. That alloy was zinc-manganese.

1.4 Electroplated Zinc-Manganese

Zinc-manganese electroplated coatings have been produced with a manganese content of about 50%. The alloys are said to offer good paintability, weldability and formability. The corrosion resistance of the alloy is impressive, and has been shown to be forty times better than that of conventional electrogalvanised steels in salt spray tests. Paint undercutting and perforation corrosion results found zinc-manganese to be equal to a zinc coating of twice the thickness. Zinc-manganese is said to be appropriate for both exposed and unexposed auto-body parts ⁽³⁾, and it has been applied using a conventional, industrial electrogalvanising line.

The alloy is usually deposited from a sulphate-citrate bath, in which the latter is said to act as a complexing agent. Despite its presence, the difference in deposition potentials between the two metals is still large, so co-deposition only occurs at high

current densities. The manganese content is dependent on the operating conditions, and its increase is accompanied by a decrease in cathode current efficiency. The main hindrance to its industrial adoption is the stability of its process solution. The solution appears to deteriorate quickly and precipitates appear in the bath. Hence, while other zinc alloys have been the subject of a vast amount of research in the last decade, relatively little work has been published on zinc-manganese.

1.5 Research Objectives

The aim of this work was to extend the knowledge available on the electrodeposition of zinc-manganese and its process solution. The behaviour of the sulphate-citrate bath has been examined with a view to understanding the problems encountered in electroplating the alloy such that the process may be improved. In order to achieve this objective, both the process of metal deposition and the solution instability needed investigation.

Having established the results achieved from a chosen sulphate-citrate bath in terms of appearance, structure and cathode current efficiency, the first area of this research investigates the effects of various process parameters on the polarisation behaviour of the alloy bath and the corresponding single metal baths.

In the second part of this work, the electroplating bath has been studied using a variety of chemical methods to assess the deterioration of the solution and to determine the reasons for its instability.

CHAPTER 2

LITERATURE REVIEW

PART ONE - RELEVANT ELECTROCHEMICAL THEORY

2.1 THE ELECTRODEPOSITION PROCESS

Basic electrochemical theory can be found in a number of texts ⁽¹⁰⁻¹⁵⁾. The majority of these cover the kinetics and thermodynamics from a corrosion viewpoint, concentrating on the anodic processes involved. The theory given below predominantly relates to the cathodic processes, as relevant to electrodeposition.

2.1.1 The Double Layer

A piece of metal comprises a regular lattice of metal ions in a sea of electrons. When initially immersed in a polar solvent, ligands such as water molecules or complexing ions are attracted to the metal surface. Metal atoms dissolve into solution to form solvated ions with overall positive charge. These are electrostatically attracted to the metal surface, the latter attaining an overall negative charge to preserve electroneutrality. These opposite charges become aligned in parallel layers to form the Helmholtz electrical double layer (Figure 2.1) ⁽¹²⁾.

The closest distance between opposing charges is called the Outer Helmholtz Plane. The Inner Helmholtz Plane is a region where unsolvated charges may be specifically adsorbed and cannot be distinguished electrically from the metal surface. Since the solvated ions are much larger than the central metal ion, insufficient of them can be aligned in the Helmholtz double layer to neutralise the charge on the metal surface. The excess charge required is located in the Gouy-Chapman layer, in which the

concentration of counter ions decreases with distance from the electrode until a homogeneous distribution occurs in the bulk electrolyte.

2.1.2 Cathodic Deposition at the Metal Surface

Equations for reactions at electrodes usually describe the overall process but neglect any intermediate steps. For the electrodeposition reaction, the metal ion in solution must first migrate to the metal surface before electron transfer occurs and it can be built into the lattice.

2.1.3 Migration of Ions (Mass Transport)

Migration from the bulk solution towards the cathode occurs by one of three methods ⁽¹⁶⁾.

1. By convection due to movement of the liquid which results from changes in density and temperature gradients in the solution. This can be influenced by agitation or temperature change.
2. By diffusion, which moves ions from areas of high concentration to less concentrated regions of the electrolyte, especially into and across the diffusion layer.
3. An electric field influences the migration of ions across the double layer.

2.1.4 Electron Transfer (Electrocrystallisation)

At the cathode surface, the solvated ion enters the diffusion layer and is distorted under the influence of the weak electric field. The dipoles are aligned with the

positively charged end towards the cathode. Under the influence of the higher field strength of the Outer Helmholtz Plane, the cation is divested of some of the solvation molecules and becomes attached to the electrode surface where it is known as an adion. This occurs randomly at any point on the cathode surface, then the adion migrates along the electrode surface to a suitable discontinuity where it completely loses the solvation molecules. Charge transfer occurs at the most energetically favourable site. This may be an imperfection in the substrate (kink site), a stable nucleus or cluster of adions may form a nucleus of critical radius. Hence, the ion becomes incorporated in the metal lattice. This process is illustrated in Figure 2.2.

Further adions become attached to nuclei and lateral monotomic growth layers are produced. These may be interrupted if, for example, adsorbed impurities are encountered and growth stacks result. Lateral growth occurs until the enlarged radii contact each other and growth projects from this nucleation centre. In this manner, grains are formed and further growth now proceeds outwards from the substrate.

2.2 EQUILIBRIUM ELECTRODE PROCESSES

2.2.1 Single Electrode Potentials

If a metal, M, is immersed in a solution of its own ions, M^{z+} , an equilibrium results between the oxidation reaction for anodic dissolution and the reduction reaction for cathodic deposition. That is



An equilibrium or reversible potential difference is set up across the electrical double layer which is characteristic of the specific metal. While this equilibrium potential cannot be measured directly, a relative potential difference can be obtained by connecting it to a reference electrode of known potential such as the standard

hydrogen electrode (SHE). By convention, the equilibrium potential of the latter is assumed to be zero at all temperatures. Such a value is known as the single potential of the electrode, E_{eq} , on the standard hydrogen scale. In experimental work, alternative reference electrodes may be chosen, such as the saturated calomel electrode (SCE). This has a value of +0.242V against the standard hydrogen electrode at 25°C⁽¹¹⁾.

An electrochemical series of electrode potentials for different metals can be produced. This is usually constructed in terms of standard electrode potentials, E^0 . The latter is defined as the potential of an electrode versus the standard hydrogen electrode at 25°C in equilibrium with a solution of its own ions of unit molar activity. The activity of an electrolyte reflects the interaction between ions of opposite charge which alters the behaviour of the solution from that which would be expected from the measured concentration. The activity, a' , is related to the concentration, c , according to

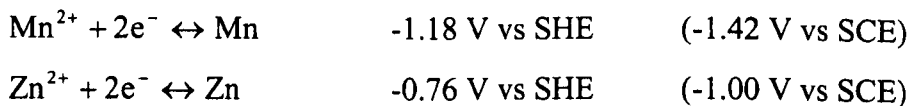
$$a' = \gamma c \quad \text{(Equation 2.2)}$$

where γ is the correction factor known as the activity coefficient of value less than 1. In a solid where interaction between the atoms is small or in a dilute solution where the distance between opposite charges reduces interaction, the activity coefficient is usually considered to be unity.

The electrode potential must be defined in terms of the activity of the ions since the equilibrium at the electrode and, therefore, the potential alters with the quantity of M^{z+} . This is shown quantitatively by the Nernst equation which is derived in Appendix 6. It is applicable only for reversible systems. For the deposition of metal ions at 25°C, this is commonly expressed as

$$E_{eq} = E^0 + \frac{0.059}{z} \log[M_{aq}^{z+}] \quad \text{(Equation 2.3)}$$

For manganese and zinc, the standard electrode potentials are given by Lowenheim ⁽¹⁶⁾ as



Such values should only be taken as guidelines in practical electroplating where the metal electrode is rarely in a solution of its own ions at unit activity.

2.2.2 Exchange Current Density

The equilibrium potential drives partial currents for anodic dissolution and cathodic deposition. These are equal and opposite, since no overall reaction results. The magnitude of these defines the exchange current density, i_0 , so

$$i_+ = |i_-| = i_0 \quad (\text{Equation 2.4})$$

2.3 NON-EQUILIBRIUM ELECTRODE PROCESSES

2.3.1 Polarisation

If equilibrium at the electrode is altered, the resulting change in potential across the double layer is called polarisation. The departure of the electrode potential from the equilibrium potential is known as the total overpotential, η_{total} , which is, therefore, given by

$$E_{\text{total}} = E_{\text{eq}} + \eta_{\text{total}} \quad (\text{Equation 2.5})$$

The total polarisation is the sum of partial polarisations, the most significant of which are the concentration polarisation (η_{conc}), the activation polarisation (η_{act}) and the resistance polarisation (η_{res}). That is

$$\eta_{\text{total}} = \eta_{\text{act}} + \eta_{\text{conc}} + \eta_{\text{res}} \quad (\text{Equation 2.6})$$

An electrode can either be polarised anodically or cathodically, and polarisation curves plotted accordingly. In the discussion below, cathodic polarisation as relevant to electroplating will primarily be considered.

2.3.1.1 Activation Polarisation

For ions to pass through the double layer and be deposited as metal, they must lose their solvation sheath and gain electrons. This requires a minimum activation energy. To promote the deposition reaction, it is necessary to move the energy level of ions closer to this activation energy. Simultaneously, the activation energy required by the lattice ions needs to be increased, so the rate at which they ions enter solution is reduced. Since this energy is related to the electrode potential as described in Appendix 6 by

$$\Delta G = -zFE \quad (\text{Equation A6.1})$$

these changes may be effected by applying a cathodic potential. The activation polarisation, η_{act} , is the portion of the total overpotential which causes these effects.

The magnitude of the activation polarisation is strongly affected by the physical and chemical nature of the electrode material. It is dependent on the number of ions in solution, the degree of complexing, the presence of other ions such as additives and the presence of surface films.

Activation polarisation can be described quantitatively by the Tafel Equation which is derived in Appendix 7 and can be generalised as

$$\eta_{\text{act}} = a + b \log i_{\text{net}} \quad (\text{Equation 2.7})$$

From this it can be seen that for a system under activation control, a linear relationship should be obtained between η_{act} and $\log i_{\text{net}}$, the net current density. The slope of the line, b , and the intercept at zero overpotential, a , are constants for a particular electrode reaction under specific experimental conditions.

It is useful to visualise polarisation graphically as follows. Consider the single electrode at equilibrium as described in Equation 2.1. Under activation control, cathodic polarisation will cause the equilibrium potential and the cathodic partial current density to alter according to the following Tafel relationship

$$\eta_{\text{act,C}} = -b_{\text{C}} \log \frac{|i_{-}|}{i_0} \quad (\text{Equation A7.4})$$

Similarly, for anodic polarisation the change will be described by

$$\eta_{\text{act,A}} = b_{\text{A}} \log \frac{i_{+}}{i_0} \quad (\text{Equation A7.5})$$

Graphically these changes in activation overpotential with partial current density are represented by the dashed lines in Figure 2.3. Alternatively, it is common to plot the magnitude of the current density on a semi-log scale (Figure 2.4), which shows more appropriately the linear nature of the Tafel equations. Also, the anodic and cathodic lines intersect at the exchange current density.

Experimentally, these partial oxidation or reduction rates are not evaluated individually. The difference between them is measured as a net current density, i_{net} , where, for cathodic polarisation

$$|i_{\text{net,C}}| = |i_-| - i_+$$

So, Equation A7.4 becomes

$$\eta_{\text{act,C}} = -b_C \log\left(\frac{|i_{\text{net,C}}| + i_+}{i_0}\right) \quad (\text{Equation 2.8})$$

This relationship between the activation polarisation and the net current density, $i_{\text{net,C}}$, is shown graphically in Figure 2.3 and 2.5. At values close to the equilibrium potential, the rate of oxidation is of the same order of magnitude as the reduction rate. Only when the reverse reaction becomes insignificant compared to the forward reaction can the anodic partial current density in Equation A7.5 be ignored and a linear Tafel relationship is observed (Figure 2.5). According to Shrier⁽¹⁰⁾, this occurs at overpotentials above about 0.052V.

2.3.1.2 Concentration Polarisation

As a metal is deposited, the concentration of metal ions at the surface of the cathode becomes less than that in bulk solution because replenishment by mass transport is not sufficient to maintain the original concentrations. This difference gives rise to a concentration gradient and the distance to which it extends into solution is called the diffusion layer. It is not limited to the double layer, but extends into the solution to a distance of about 0.5mm under steady state conditions of natural convection or 0.01mm under conditions of high forced convection⁽¹⁰⁾. A schematic diagram of the concentration profile across the diffusion layer is shown in Figure 2.6.

Under activation control as described above, ions are supplied to the cathode at a rate such that electrocrystallisation is rate determining. If the deposition rate is increased, the rate of supply does not rise sufficiently for this to continue and the movement of ions through the diffusion layer becomes influential. The flow of ions becomes dependent upon the concentration gradient in the diffusion layer. As the concentration at the electrode surface decreases, the diffusion process becomes more difficult, and an ever increasing degree of polarisation is required to maintain the discharge of metal ions. This partial polarisation is known as the concentration overpotential, η_{conc} .

If the electrode is polarised cathodically to an extent where the deposition rate results in the ion concentration at the electrode surface being zero (Figure 2.6), then a limiting current density, i_L , is reached. The process is totally controlled by mass transport of ions which are discharged as they reach the cathode. Metal deposition is occurring at the maximum rate. This should not be confused with the maximum current density at which an acceptable electrodeposit can be produced, which is usually considerably lower than i_L .

The limiting current density can be calculated by equating the rate at which ions are discharged to the rate at which they can diffuse to the electrode (Appendix 8) such that

$$i_L = \frac{zF D c_0}{\delta_N} \quad \text{(Equation A8.3)}$$

The concentration polarisation can be decreased, and the limiting current thereby raised, by increasing the bath concentration or by reducing the diffusion layer thickness by agitation. Increase in temperature also has the same effect since it lowers the viscosity and raises the rate of diffusion. It is unaffected by the nature of the cathode surface.

The concentration polarisation may be represented quantitatively as shown in equation A8.4 of Appendix 8 by

$$\eta_{\text{conc}} = \frac{2.303RT}{zF} \log \left(1 - \frac{|i_{\text{net,C}}|}{i_L} \right) \quad (\text{Equation A8.4})$$

Experimentally, concentration polarisation becomes significant when the net cathodic current density approaches $0.1 i_L$ ⁽¹⁹⁾. This relationship between the concentration polarisation and the net cathodic current density is shown graphically in Figure 2.7.

2.3.1.3 Resistance Polarisation

The electrolyte itself introduces a resistance to deposition since it is not of infinite conductivity. The resistance overpotential is given by the product of the net cathodic current density and the solution resistance, R_s , between the electrodes, that is

$$\eta_{\text{res}} = i_{\text{net,C}} R_s \quad (\text{Equation 2.9})$$

The effect can be reduced by keeping the distance between the anode and cathode small and by operating with a highly conductive solution. Extra resistance could also be introduced by poorly conducting surface films.

In measurements between working and reference electrodes, the effect due to the solution can be reduced and virtually eliminated by using a Luggin capillary which encloses the reference electrode from the solution and can be placed very close to the cathode surface.

2.4 POLARISATION DIAGRAMS

2.4.1 Single Electrode Polarisation Diagrams

A study of the cathode potential versus current density curve for metal deposition can give indications of the nature of the deposition process. The potential scale on polarisation curves may be plotted either as the overpotential itself, η_{total} , or as the total potential, E_{total} , according to Equation 2.5. Due to the nature of the Tafel equation, such curves are typically plotted using a semi-log scale for the net cathodic current density, $i_{\text{net,C}}$.

Since the total overpotential is equal to the sum of the partial polarisations (Equation 2.6), a plot showing total cathodic polarisation represents the combination of Equations 2.8, A8.4 and 2.9 and the amalgamation of Figures 2.5 and 2.7. Stern and Geary⁽¹⁹⁾ plotted a theoretical cathodic polarisation curve and found the form to agree with experimental data.

The generalised form of a cathodic polarisation curve for single metal deposition is shown in Figure 2.8. Deposition is under activation control in the linear region (AB) and follows the Tafel relationship. Deviation close to the equilibrium potential occurs where the forward and reverse reactions are of similar magnitude.

When the current reaches a significantly high value, departure from the linear plot occurs. Between B and C the reaction is under mixed activation and concentration control, since the rate of diffusion of ions to the metal surface through the double layer affects the deposition rate.

The migration of ions becomes totally rate determining when the limiting current is reached at C. If resistance polarisation is high, this will be evident at high current densities⁽¹⁹⁾ and the limiting current density may not be observed as a single value.

2.4.2 Polarisation of Two Electrodes

To discover experimentally the effect of polarisation on a single piece of metal, it is connected to a second electrode in an electrochemical cell. The application of an external electromotive force causes one to become more negative (the cathode) and the other (the anode) to become more positive, and the cell is described as being polarised. The more noble cathode consumes the electrons generated by the more base anode.

If the oxidation-reduction system M represents the cathode, and that for Z represents the anode, each of these systems has its own equilibrium potential, exchange current density and Tafel slope. In open circuit, a common mixed potential or rest potential, E_{rest} , will be adopted. This is a compromise between their individual equilibrium potentials and takes a value where the total rates of oxidation and reduction are equal. That is, where

$$|i_{-,z}| + |i_{-,m}| = i_{+,z} + i_{+,m}$$

Polarisation diagrams for such a mixed electrode system are a combination of two single exchange process diagrams. The relationship between the activation overpotential and the partial current densities is shown in Figures 2.9 and 2.10.

If the system is polarised cathodically, the net cathodic current density is equal to the difference between the sum of all the reduction reactions and the sum of the rates of all the oxidation reactions. Therefore

$$|i_{net,C}| = (|i_{-,z}| + |i_{-,m}|) - (i_{+,z} + i_{+,m})$$

or

$$|i_{-,m}| = |i_{net,C}| + i_{+,m} + (i_{+,z} - i_{-,z})$$

This equation can be substituted into Equations A7.4, A8.4 and 2.9 to calculate the partial polarisations for the two electrode system. These values can be summed and a

cathodic total polarisation curve plotted as before (Figure 2.11). If the difference between the equilibrium potentials is large enough, only the cathodic curve for the cathodic reaction and the anodic curve for the anodic reaction need to be considered. Hence, this total curve shows the same features as that for a single electrode (Figure 2.8).

2.4.3 Factors Affecting Polarisation Curves

2.4.3.1 Multiple Cathodic Processes

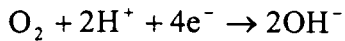
In practice, multiple reduction reactions may occur at the cathode. These may be irreversible, and a polarisation curve of the type shown in Figure 2.11 will represent the overall summation of all processes occurring. Single metal polarisation curves for the constituents of an alloy can give a guide as to whether co-deposition is possible. The range of current densities over which both metals are likely to be deposited together can be determined. However, the deposition potential of an alloy is affected by the substrate, alloy formation and solution interactions. A dual metal polarisation curve must be obtained to provide accurate representation of the deposition process for the alloy.

Multiple reactions may include the production of an alloy by the deposition of more than one type of metal ion. Alternatively, hydrogen evolution or oxygen reduction may occur. Both of these reactions result in a local increase in the pH at the cathode which can cause the precipitation of sparingly soluble metal hydroxides.

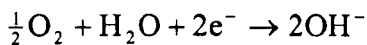
In general, the reaction requiring the least negative potential will take place until the potential is made significantly negative to produce a second reaction, which may occur simultaneously. At a given potential, the total current is the sum of the corresponding currents of the individual reactions. The portion of the total current involved in the metal deposition reaction is known as the cathode current efficiency.

2.4.3.2 Oxygen Reduction

Cathodic reduction of atmospheric oxygen dissolved in the solution may be represented in acid conditions by



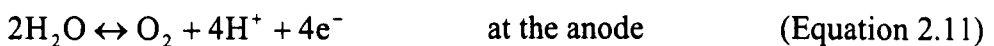
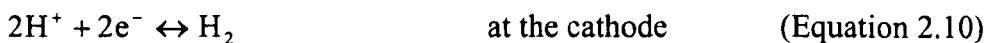
In alkaline and solutions close to neutral:



The solubility of oxygen in water is low (about 0.5M at 25°C⁽¹²⁾ or 4mg oxygen per 100g of water⁽¹³⁾), so the rate of oxygen reduction can become controlled by the mass transport of the molecules to the surface of the metal. The solubility of oxygen in water decreases with increasing temperature and is reduced to about 2mg oxygen per 100g of water⁽¹³⁾ at 50°C.

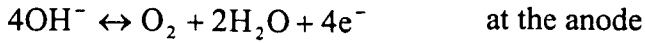
2.4.3.3 Hydrogen Evolution

The decomposition of water results in hydrogen evolution at the cathode. In acid, this occurs according to



and in neutral or alkaline solutions where there is low hydrogen ion concentration





Applying the Nernst equation (Equation A6.3) to the hydrogen evolution reaction in Equation 2.10

$$E_{\text{eq}} = E^0 + \frac{RT}{zF} \ln \frac{[\text{H}^+]^2}{p_{\text{H}_2}}$$

where p_{H_2} is the partial pressure of hydrogen. By definition

$$\text{pH} = -\log[\text{H}^+] \quad (\text{Equation 2.12})$$

So, at a partial pressure of 1 atmosphere and at 25°C on the standard hydrogen scale

$$E_{\text{eq}} = 0.00 - 0.059\text{pH} \quad (\text{Equation 2.13})$$

Similarly, applying the Nernst equation (Equation A6.3) to Equation 2.11 for oxygen evolution at the anode

$$E_{\text{eq}} = E^0 + \frac{RT}{zF} \ln \frac{p_{\text{O}_2} [\text{H}^+]^4}{[\text{H}_2\text{O}]^2}$$

and, under the same conditions,

$$E_{\text{eq}} = 1.23 - 0.059\text{pH} \quad (\text{Equation 2.14})$$

Hence, the evolution of hydrogen and oxygen due to dissociation of water is dependent upon both the electrode potential and the pH of the solution. A decrease in the partial pressure of oxygen will cause the equilibrium potential to become more

negative, whereas a decrease in that for hydrogen will displace the potential in the positive direction.

2.5 POTENTIAL-PH DIAGRAMS (POURBAIX DIAGRAMS)

A Pourbaix diagram presents the equilibria existing between a metal, metal ions and solid oxides in water as a plot of equilibrium potential versus pH at fixed temperature and pressure. The potential is usually given on the standard hydrogen scale (SHE), and the activity of ions is arbitrarily chosen as 10^{-6} M.

Pourbaix diagrams provide an excellent guide to the stability of species and the conditions where change becomes thermodynamically favourable. However, there are limitations to their use which should be considered. Firstly, such diagrams are based on thermodynamic data, but no details are included about the kinetics of reactions. Secondly, the diagrams are derived from reactions between pure metals and pure water at 25°C, which is rarely the case in practice.

Pourbaix collected thermodynamic data on the reactions between many metals and water⁽²⁰⁾. The diagrams produced for zinc and manganese are shown in Figures 2.12 and 2.13 respectively. The construction of the zinc diagram is discussed below.

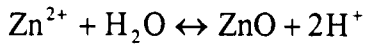
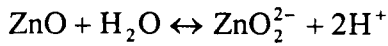
2.5.1 Construction of a Pourbaix Diagram for Zinc in Aqueous Solution

The reactions involved in constructing a diagram such as that shown in Figure 2.12 for the zinc system at 25°C can be considered to be of one of three types. (Values used in the equations below are taken from Pourbaix⁽²⁰⁾.)

1. Reactions dependent on pH but independent of equilibrium potential.

Such an equilibrium is a chemical reaction with no electrons involved and, hence, no single electrode potential. The Nernst equation does not apply and the ionic activities obey the equilibrium constant for the reaction.

Reactions of this type shown on the zinc diagram are



For the latter case, as an example, the equilibrium constant, K_{eq} , is given by

$$K_{\text{eq}} = \frac{[\text{H}^+]^2 [\text{ZnO}]}{[\text{Zn}^{2+}] [\text{H}_2\text{O}]} \cong \frac{[\text{H}^+]^2}{[\text{Zn}^{2+}]}$$

where the activities of the solid and water are assumed to be unity. According to Gellings⁽¹³⁾, K_{eq} takes the value of 1.11×10^{-11} at 25°C. Taking logarithms and substituting for pH from Equation 2.12 gives

$$\log K_{\text{eq}} = 2 \log [\text{H}^+] - \log [\text{Zn}^{2+}]$$

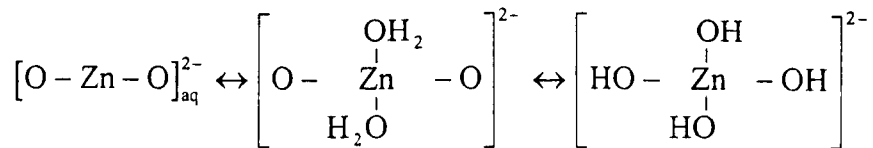
or

$$\log [\text{Zn}^{2+}] = 10.95 - 2 \text{pH}$$

This reaction is independent of potential and depends solely on pH. Hence, it is represented by a vertical line which will move to the right or left respectively by 0.5 pH for every tenfold increase or decrease in $[\text{Zn}^{2+}]$.

While the reactions above show the products of the zinc in aqueous solution to be oxides, it is to be expected that additional water molecules in the primary solvation

sheath will lead to an ion of higher symmetry ⁽¹²⁾. Zinc usually exists in the tetrahedral state so, for example



Hence, this hydrolysed oxide may be written more correctly as the hydroxide $\text{Zn}(\text{OH})_4^{2-}$. This phenomenon results from the tendency for water molecules to orientate with the negatively charged oxygen pointing inwards towards the positive metal ion nucleus.

2. Reactions dependent on equilibrium potential but independent of pH.

This type is exemplified by



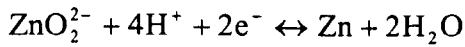
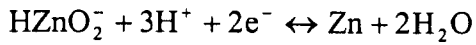
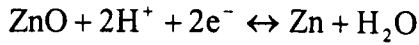
It is purely an electron transfer reaction which exhibits a single electrode potential. The Nernst equation (Equation A6.4) is obeyed at 25°C according to

$$E_{\text{eq}} = -0.763 + \frac{0.059}{2} \log[\text{Zn}^{2+}]$$

The equilibrium potential and the activity of the ions are, therefore, interdependent variables. There are no hydrogen ions involved so there is no pH dependence, and the equilibrium is represented as a horizontal line.

3. Reactions dependent on both equilibrium potential and pH.

These reactions involve both hydrogen ions and electrons and are shown as sloping lines. Examples on the zinc diagram are



Applying the Nernst equation to the latter, for example

$$E_{\text{eq}} = 0.441 - 0.118\text{pH} + \frac{0.059}{2} \log[\text{ZnO}_2^{2-}]$$

If the activity of the ions is constant, this equation will be a straight line with gradient -0.118.

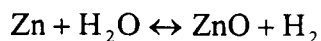
For completion of the phase diagram for zinc in aqueous solution, the lines for the dissociation of water need to be superimposed. These are given by Equations 2.13 and 2.14. Above the oxygen line, water is decomposed to oxygen, while below the hydrogen line water is decomposed to hydrogen. Therefore, the region between these two lines defines the domain of thermodynamic stability of water.

Examination of these lines in conjunction with a diagram indicates the conditions under which a metal will release the gases as a cathodic product. In acid solutions, the line corresponding to Equation 2.16 is below the hydrogen line, so the reaction cannot be in equilibrium in water because the total reaction



will proceed to the right. If zinc is polarised to a potential below the line representing this reaction into the immune region, then the dissolution will stop. The hydrogen evolution will still continue.

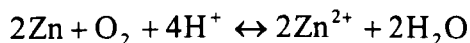
If the pH of the solution is raised, the reaction in Equation 2.15 occurs. This is below the hydrogen line, so the total reaction



will proceed to the right forming the passive product. At still higher pH, the zinc corrodes again according to



All zinc dissolution reactions lie below the oxygen line, so only in a solution containing dissolved oxygen will oxygen reduction as a cathodic reaction be possible according to simultaneous reactions such as



From the electrochemical series, it appears that metals with electrode potentials more negative than that for hydrogen could not be deposited from aqueous solution since the gas would be evolved in preference. In practice, hydrogen may be evolved at a more negative potential than would be expected because the activation polarisation, or hydrogen overvoltage, for the hydrogen reaction is extremely high.

2.6 ELECTRODEPOSITION OF ALLOYS

In order to co-deposit two different metals, two criteria must be met. Firstly, it must be possible to individually deposit at least one of the metals. Secondly, the deposition potentials of the metals must be close together. Usually, one metal will be deposited at a more noble potential than the other and there will be a separation in their equilibrium potentials. It may be possible to deposit two metals by electroplating at the potential of the more negative metal. However, the more noble metal may then be

co-deposited above its limiting current density, the result of which is a powdery or “burnt” deposit.

The electrochemical series gives a guideline as to the possibility of co-deposition of metals from simple salt solutions. Metals with similar standard electrode potentials are easier to co-deposit. It should, however, be remembered that the series has been evaluated under equilibrium conditions, and that electrodeposition at a polarised electrode usually occurs at potentials more negative than the standard electrode potentials.

In addition, it would be predicted that metals with electrode potentials more negative than hydrogen would not be deposited from aqueous solution. However, such metals may be deposited since the activation potential for hydrogen is extremely high, and hydrogen may be evolved at a more negative potential than would be predicted. This is known as hydrogen overvoltage, and it depends on the nature of the cathode surface. It may be greater than 1V on metals such as zinc, and is at its lowest on platinum.

2.6.1 The Nernst Equation in Alloy Electroplating

An electrode can only have one potential at any given time. Therefore, for the simultaneous electrodeposition of two different metals A and B, the deposition potentials E_{eq}^A and E_{eq}^B must be equal. That is to say, from the Nernst equation (Equation A6.3)

$$E_{eq}^A = E_A^0 + \frac{RT}{zF} \ln[A^{z+}] + \eta_A$$

must be equal to

$$E_{eq}^B = E_B^0 + \frac{RT}{zF} \ln[B^{z+}] + \eta_B$$

The potentials for deposition of the two metals can be moved closer together by either lowering the concentration of the more noble metal and raising the concentration of the less noble metal, or changing the activity of the ions.

Varying the concentration of the ions is impractical since, in the case of divalent ions, a thousandfold change in the concentration would result in only a 0.087V change in potential according to the Nernst equation (Equation A6.3). This method is, therefore, only useful where the difference between the electrode potentials of the two metals is small.

The activity of the ions may be changed by using a complexant. Aqueous metal ions are attached by co-ordinate bonds to water molecules in a solvation sheath. It is possible to replace these water molecules by alternative ligands which substitute into the structure. By donating their lone electrons to the positively charged cation, they form a more stable configuration. A complexant may, thereby, act to impede the electrodeposition of a metal from the solution, and subsequently increase the overvoltage required such that the metal can be co-deposited. The size of the shift in potential is related to the strength of the metal ion complex which is dependent on the stability of the metal/complex bond.

PART TWO - ELECTRODEPOSITION OF ZINC-MANGANESE

2.7 INTRODUCTION

The mechanical, physical and chemical properties of an electroplated coating can be varied considerably by changing the conditions associated with electrodeposition. Therefore, it is necessary to understand the operating variables involved in order to be able to provide a deposit which meets any given specifications.

Research has been reported on the effects of various plating variables on the properties of zinc-manganese. These include bath composition, complexing agents,

addition agents, current density, temperature and pH. Their effect on the manganese content and cathode current efficiency are described, since these are of importance in determining the properties of the coating and the feasibility of the process respectively. Results have been produced describing the type of deposition and the mechanism by which two metals with deposition potentials $-0.417\text{V}^{(21)}$ apart can be co-deposited. The various characteristics of the polarisation behaviour during deposition are reported. These include a comparison between the curves for alloy deposition and those for the deposition of zinc and manganese individually, the relationship of the potentials to the composition of the deposit, and the effect of plating variables on these curves.

Close control of the electrodeposition process is required since the coating properties may depend critically on the alloy composition. Variables affecting the properties have been investigated and are reported. These should be known since the optimum coating for one property may not be that for another, and a compromise may have to be reached. In addition, if the steel sheet is to be coated on the outer surface as well as the inside, then strict requirements will be imposed on the coating properties. As well as being corrosion resistant, a successful coating needs to have good finishability in terms of cratering and surface appearance, phosphatability and paint adherence. The coating must be compatible with all subsequent processing. It must be able to withstand the stress of forming operations without cracking or peeling off, and be easily weldable. The performance of zinc-manganese in terms of these properties will be discussed. These are divided into corrosion properties, processing requirements (workability, weldability and paintability) and functional requirements (appearance and paint adherence).

Zinc-manganese is included in a review of electrodeposited zinc alloy coatings by Wilcox and Gabe⁽²²⁾. An overview of literature dealing specifically with zinc-manganese electrodeposition has been produced by Wilcox and Petersen⁽²³⁾.

2.8 ELECTROPLATING BATHS AND CONDITIONS

Published works to date predominantly describe zinc-manganese coatings produced from a sulphate-citrate bath. This trend is almost certainly due to the information given by Brenner ⁽²⁴⁾ who cites the work of Faust and co-workers ⁽²⁵⁾. The latter made a comprehensive investigation of the protective value of electrodeposited coatings and alloys for aircraft parts, some of which covered manganese coatings and alloys. The research was active for about eight years, but the work was only published in reports to sponsors ⁽²⁵⁾ and not in scientific literature.

Faust et al ⁽²⁵⁾ deemed the following baths to be unsatisfactory for various reasons, such as yielding a deposit with too low a manganese content or at too low a current efficiency, or a powdery or poor quality deposit: sulphate-acetate, sulphate-borocitrate, fluoborate, sulphate-sulphamate, sulphate-pyrophosphate, sulphate-borate, sulphate-fluoride, sulphate-gluconate, sulphate-thiocyanate, fluosilicate, alkane sulphonate, ethylenediamine tetra-acetate and a concentrated caustic bath. A simple sulphate bath was also disregarded since the pH of the bath changed rapidly and the maximum manganese content which could be obtained was only 5%.

The most promising results were obtained with the sulphate-citrate bath. However, the resulting zinc-manganese coatings contained “microholes” through which the steel substrate corroded in accelerated corrosion tests. The cause of these was never discovered, but they were possibly a reason why Faust et al ⁽²⁵⁾ did not find the corrosion performance of these electroplated alloys satisfactory, even though they contained up to 85% manganese. In outdoor exposure tests, these coatings were abandoned in favour of a coating containing 50% manganese produced by the thermal diffusion of zinc and manganese coatings. These were inferior to both zinc and cadmium in protective value.

The composition and working parameters of typical baths are given in Table 2.1. The literature available covers both flowing and static conditions, with inert anodes and cathodes of either copper, mild steel or stainless steel. Baths are operated at a temperature between 25°C and 60°C, with a pH between pH5.4 and pH5.6. The bath

composition does not vary greatly between authors and comprises zinc sulphate, manganese sulphate and sodium citrate. Limited work has been done with addition agents and alternative baths (see Part Three of this Literature Review). The optimum manganese content in a zinc-manganese coating with respect to its properties is reported to be between 40% and 50% (by weight) (see Figure 2.14)⁽²⁶⁾⁽²⁷⁾⁽²⁸⁾. This is generally produced at a low cathode current efficiency of about 40%.

2.9 POLARISATION BEHAVIOUR FOR ZINC-MANGANESE ELECTRODEPOSITION FROM A SULPHATE-CITRATE BATH

The total polarisation behaviour for the system has been presented⁽²⁶⁻³¹⁾. In order to clarify the electrodeposition characteristics of the various reactions involved in the process, partial polarisation curves have also been shown.

2.9.1 Total Polarisation Behaviour

The total polarisation curves for baths containing zinc sulphate, zinc sulphate with sodium citrate, manganese sulphate with sodium citrate, and the whole bath as determined by these authors are shown in Figure 2.15. The reader should note when making comparisons that Gabe et al⁽²⁹⁾⁽³⁰⁾ employ a mercury/mercury sulphate reference electrode and Selvam and Guruviah⁽³¹⁾ a saturated calomel electrode (+0.242V against the standard hydrogen electrode at 25°C)⁽³⁵⁾. Both show the current density on a linear scale. Akiyama et al⁽³²⁾ use a saturated calomel electrode, but show current density on a logarithmic scale. Sagiya et al⁽²⁶⁾⁽²⁷⁾⁽²⁸⁾⁽³⁴⁾ give the potential against a silver/silver chloride reference electrode (+0.29V against the standard hydrogen electrode at 25°C⁽³⁵⁾) with current density on a logarithmic scale.

For the electrodeposition of zinc from the sulphate alone, Gabe et al⁽²⁹⁾⁽³⁰⁾ describe a rapid rise in current with no indications of mass transport limitations (Curve 1, Figure 2.15 b)). When the sodium citrate was added (Curve 2), a limiting current is

discernible followed by an increase in current due to combined metal deposition and increasing hydrogen evolution. The actual onset of zinc deposition appears to occur at more negative potentials, illustrating the complexing nature of the citrate.

According to Sagiya et al ⁽²⁶⁾⁽²⁷⁾⁽²⁸⁾, the displacement of the zinc sulphate curve by addition of the citrate complexant causes the deposition potential of zinc to become more negative than that of manganese, which permits the co-deposition of the two metals.

Akiyama et al ⁽³²⁾ found that the addition of sodium citrate caused the deposition potential of both zinc and manganese in single metal baths to become more negative by approximately 0.15V. In an alloy bath, the zinc was deposited at similar potentials to a single metal bath. However, at potentials where manganese was deposited with the zinc in the alloy curve, this occurred at more positive values than for manganese alone. They conclude that the shift must be caused by the co-deposition of manganese with zinc.

The total polarisation curves for the whole sulphate-citrate bath are given in Figure 2.15. Gabe et al ⁽²⁹⁾⁽³⁰⁾ describe the curve as follows. The onset of metal deposition as is at -1550mV. A limiting current is observed before the initiation of hydrogen evolution. The reduction of both metals is not evident on the curve, the initial peak at -1650mV is probably due to zinc reduction. The manganese electrodeposition is not clearly definable, occurring at more negative potentials than zinc and probably being “masked” by the hydrogen evolution process.

2.9.2 Partial Polarisation Curves

Sagiya et al ⁽³³⁾⁽³⁴⁾ have split the total polarisation behaviour into its components, namely zinc reduction, manganese reduction and hydrogen evolution (Figure 2.16), as have Selvam and Guruviah ⁽³¹⁾. The results of Gabe et al ⁽²⁹⁾⁽³⁰⁾ are given in tabular form in Table 2.2.

Sagiyama et al ⁽³³⁾⁽³⁴⁾ have described the curves in Figure 2.16 as follows. Although citrate was added as a complexing agent, there is still a large difference in deposition potential between zinc and manganese. Hence, zinc was deposited alone in the potential range between -1100mV and -1500mV. At potentials more negative than this, manganese and zinc co-deposited. In this region, the deposition rate of manganese increased with decrease in potential. Therefore, the manganese content of the deposit increased with current density. Manganese deposition in this range is not diffusion-controlled.

The partial polarisation curve for zinc deposition reached limiting current density in the potential range between -1400mV to -1600mV. Therefore, in the range of co-deposition, zinc reduction is diffusion controlled. There are decreases in the partial current density at potentials in the limiting current region between -1500mV and -1700mV, and between -1700mV to -1900mV. The first is attributed to agitation effects caused by an increase in hydrogen evolution in this range. The second is said to be the result of an increase in the pH in the vicinity of the cathode due to increased hydrogen evolution. This is said to stabilise the formation of zinc citrate complex ions and suppress zinc deposition.

The hydrogen evolution partial polarisation curve was affected by diffusion at potentials more noble than -1700mV. Below this it was not affected and hydrogen evolution was promoted as indicated by the steeper slope of the graph.

2.9.3 Effect of Operating Variables on the Partial Polarisation Curves

The effect of flow rate, temperature and pH on these partial polarisation curves was also examined (Figures 2.17 and 2.18) ⁽³³⁾⁽³⁴⁾. Gabe et al ⁽²⁹⁾⁽³⁰⁾ produced data from which partial current information can be calculated for variation in pH and flow rate but at fixed current densities (Tables 2.3 and 2.4 respectively). Gabe et al ⁽²⁹⁾⁽³⁰⁾ discuss the mechanisms inferred from the observations in terms of manganese content and cathode current efficiency. These are described in the relevant sections below.

However, the trends observed will be compared here to the partial polarisation curves produced by Sagiya et al ⁽³³⁾⁽³⁴⁾.

Sagiya et al ⁽³³⁾⁽³⁴⁾ found that the effect of increasing the flow rate from 1m/sec to 2m/sec or raising the temperature of the bath was to increase the partial current density of zinc. Gabe et al ⁽²⁹⁾⁽³⁰⁾ examined the effect of flow rate between 0 rpm and 500 rpm but at a single current density of 7Adm^{-2} (This approximates to a potential of -1650mV according to the total polarisation curve of Figure 2.15 a.) The increase in zinc partial current was again observed, particularly at speeds faster than 100 rpm (Table 2.4).

This trend is observed within the wide range of potential over which the partial current of zinc is controlled by diffusion. The increased partial current of zinc is attributed ⁽³³⁾⁽³⁴⁾ to the higher flow rate or temperature promoting the diffusion of zinc ions and zinc citrate ions, which results in an increase in the diffusion constant. Raising the temperature is said to increase the concentration of simple zinc ions due to a decrease in the formation constant of zinc citrate complex ions.

According to Sagiya et al ⁽³³⁾⁽³⁴⁾, the partial polarisation curve of manganese is relatively unaffected by flow rate except in the region where a “burnt” coating was deposited (Figure 2.17 b)). Here, limiting current density increased with flow rate. Temperature had almost no effect. These results are said to demonstrate that the deposition rate of manganese is not diffusion controlled in the potential range where sound deposits are produced. However, the partial current results of Gabe et al ⁽²⁹⁾⁽³⁰⁾ (Table 2.4) suggest that, at constant current density within the co-deposition range, the partial current decreases with increase in flow rate. This is particularly noticed at speeds greater than 100 rpm.

Due to the effects on both the zinc and manganese partial currents together, the percentage of manganese in the deposit increases with decreased flow rate or temperature (Figures 2.19 and 2.20 respectively) ⁽³³⁾⁽³⁴⁾⁽³⁷⁾.

In describing Figure 2.21, Sagiya et al ⁽³³⁾⁽³⁴⁾ say that the ratio of the partial current density of hydrogen to manganese is constant, and is unaffected by flow rate or temperature. Again, Gabe et al ⁽²⁹⁾⁽³⁰⁾ agree with this trend at flow rates below 100 rpm (Table 2.4). Above this value, the ratio was found to increase markedly.

The effect of pH on the partial polarisation curves is shown in Figure 2.18 ⁽³³⁾⁽³⁴⁾. By changing the pH from pH5.6 to pH5.0:

- The deposition potential of zinc shifted to more positive values, and the partial current density for zinc increased. Sagiya et al ⁽³³⁾⁽³⁴⁾ explain that the decrease in pH reduces the formation of zinc citrate complex ions and increases the concentration of simple zinc ions. The limiting current is, thereby, raised.
- The deposition potential of manganese shifted to less noble values. Therefore, decrease in pH is said to promote the formation of manganese citrate complex ions.

The change in the formation of the two kinds of complex ions results in the promotion of zinc deposition and the suppression of manganese deposition. Thus, the manganese content of the deposit is decreased with pH ⁽³³⁾⁽³⁴⁾⁽³⁷⁾ (Figure 2.22).

Gabe et al ⁽²⁹⁾⁽³⁰⁾ studied the effect of pH on the partial current data at constant current density of 20Adm^{-2} (which is at approximately -2050mV according to Figure 2.15a)). By changing the pH in the range from pH6.5 to pH3.5, the same trends as above were observed. That is to say, decrease in pH resulted in an increase in the partial current density for zinc deposition but a decrease in that for manganese. A decrease in the partial current for hydrogen was also observed, which agrees with the curves of Sagiya et al ⁽³³⁾⁽³⁴⁾ in Figure 2.17 b).

Although no graph is shown ⁽³³⁾⁽³⁴⁾, lowering the concentration of sodium citrate may cause an increase in the partial current density of zinc due to a decrease in the

formation of zinc citrate complex ions. The increased zinc deposition rate may lower the manganese content of the deposit, thus explaining the trend in Figure 2.23.

2.10 EFFECT OF BATH COMPOSITION AND OPERATING CONDITIONS ON THE MANGANESE CONTENT OF THE DEPOSIT

The effect of varying the bath composition and operating conditions of the sulphate-citrate electrolyte on the manganese content of the coating has been evaluated by several groups of workers. The deposit composition is important since the properties of the coating have been shown to be related to it (Figure 2.14).

2.10.1 Variation in Electroplating Bath Composition

If all other variables are fixed, the manganese content of the deposit can be increased by:

- Increasing the manganese content of the bath ⁽³¹⁾⁽³²⁾⁽³³⁾⁽³⁴⁾⁽³⁷⁾ (Figure 2.24).
- Decreasing the zinc content of the bath ⁽³¹⁾⁽³⁸⁾.
- By increasing the Mn^{2+}/Zn^{2+} ratio in the bath ⁽²⁶⁾.
- By increasing the sodium citrate content of the bath ⁽²⁴⁾⁽³¹⁾⁽³³⁾⁽³⁴⁾ (Figure 2.23). Danilov et al ⁽³⁸⁾ observed an increase in manganese content of the alloy with sodium citrate content of the bath up to 0.8M, and a decrease thereafter.

2.10.2 Variation in Operating Conditions

Keeping all other variables constant, the manganese content of the deposit can be increased by:

- Increasing the pH of the bath ⁽²⁴⁾⁽²⁹⁾⁽³⁰⁾⁽³¹⁾⁽³³⁾⁽³⁴⁾⁽³⁷⁾⁽³⁹⁾⁽⁴⁰⁾ (Figure 2.22). An explanation for this trend is offered by Gabe et al ⁽²⁹⁾⁽³⁰⁾. The pH at the cathode surface is higher than that of the bulk solution. Due to this difference, the onset of zinc hydroxide precipitation at the cathode will occur at a lower bulk pH than would be predicted. As the pH of the bulk solution is increased, that at the cathode is also raised. As a result, zinc in the diffusion layer will be less likely to be reduced to the metallic state and more likely to form zinc hydroxide as described by the potential pH diagram for the zinc-water system at 25°C ⁽²⁰⁾ (Figure 2.12). Therefore, as the pH increases, the amount of metallic zinc deposited decreases. Eyraud et al ⁽³⁷⁾ observed that the effect of a pH increase from only pH5.7 to pH6.3 had a marked effect on the manganese content.
- Decreasing the bath temperature ⁽³³⁾⁽³⁴⁾, although Selvam and Guruviah ⁽³¹⁾ and Govindarajan et al ⁽⁴⁰⁾ found that the effect was minimal (Figure 2.20). Faust et al ⁽¹²⁾ discovered that lowering the temperature from 25°C to 10°C did not “improve” results. However, Eyraud et al ⁽³⁷⁾ observed an increase in manganese content of approximately 10% over the current density range between 1.5 Adm⁻² and 5.0 Adm⁻² when the temperature was decreased from 50°C to 20°C.
- Decreasing the flow rate ⁽²⁹⁾⁽³⁰⁾⁽³³⁾⁽³⁴⁾⁽³⁷⁾ (Figure 2.19). Above approximately 100 rpm, the manganese content falls markedly with increasing rotation speeds ⁽²⁹⁾⁽³⁰⁾ indicating that manganese deposition under these conditions is not mass transport limited. Conversely, zinc content increased with rotation speed, indicating a process under diffusion control. Rotation speed has relatively less effect on the hydrogen reaction, a slight decrease in gas production resulting from increased rotation speed.

- Increasing the current density⁽²⁴⁾⁽²⁹⁻³⁴⁾⁽³⁷⁻⁴¹⁾. As a percentage of metal deposition, increase in current density leads to increase in manganese content and decrease in zinc content. However, if the process is considered in terms of three components (namely, zinc deposition, manganese deposition and hydrogen evolution), then the same results reveal a slightly different trend (Table 2.2)⁽²⁹⁾⁽³⁰⁾. Increase in current density still reveals decrease in zinc deposition, especially at high values where the process is under mass transfer control. The weight percentage of manganese, however, increases with current density to a peak (at 20Adm⁻²) then decreases thereafter. Gabe et al⁽²⁹⁾⁽³⁰⁾ explain that as the current density at the electrode increases, it gradually becomes more favourable to deposit manganese and reduce hydrogen ions than it does to electrodeposit zinc. A further increase in current density (at about 20Adm⁻²) results in hydrogen evolution becoming more favourable than manganese electrodeposition.

The effect on the manganese content of the deposit of altering the current density together with other operating variables has been documented. Results are shown for change in manganese (Figure 2.24), zinc and sodium citrate (Figure 2.23) contents of the bath, and change in pH (Figure 2.22 and Table 2.3), temperature (Figure 2.20) and flow rate (Figures 2.19, and Table 2.4) respectively. The general trend of increased manganese content of the deposit with increased current density is still observed, but is lessened and becomes virtually undetectable by lowering the citrate content towards 0.2mol/l (Figure 2.23)⁽²⁹⁾⁽³⁰⁾, by altering the metal percentage of manganese in the bath towards 20% or 80%⁽²⁹⁾⁽³⁰⁾, or by decreasing the pH of the bath towards pH3 (Figure 2.22 and Table 2.3)⁽²⁹⁾⁽³⁰⁾.

Figures 2.20 and 2.19 show the variation in manganese content of the deposit with current density, but at variable temperature and flow rate respectively. At low current densities only zinc is deposited. This range can be extended by increasing either temperature or flow rate. Thereafter, the manganese content increases with current density until a peak value is reached above which the coating is “burnt”. The highest peak value for manganese content was achieved by either lowering both the current

density and the temperature (Figure 2.20), or by raising the current density and the flow rate (Figure 2.19).

Pulse plating has been found by Foo et al ⁽⁴²⁾ to reduce the manganese content of the deposit in comparison with direct current plating. In experiments where pulse on times and off times were varied between 1ms and 50ms, the manganese content of the alloy was increased by short off times, particularly when associated with long on times.

2.11 EFFECT OF BATH COMPOSITION AND OPERATING CONDITIONS ON THE CATHODE CURRENT EFFICIENCY DURING ELECTROPLATING

From an industrial viewpoint, a disadvantage of electroplating zinc-manganese from a sulphate-citrate bath is the low cathode current efficiency, typically about 40%.

2.11.1 Variation in Electroplating Bath Composition

Keeping all other variables constant, an increase in cathode current efficiency can be affected by:

- Increasing the zinc content of the bath ⁽³¹⁾.
- Decreasing the sodium citrate content of the bath ⁽³¹⁾.
- Decreasing the manganese content of the bath ⁽³²⁾⁽³⁷⁾ (Figure 2.25).

2.11.2 Variation in Operating Conditions

Under otherwise constant conditions, the cathode current efficiency can be raised by:

- Increasing the bath temperature ⁽³¹⁾⁽³⁷⁾ (Figure 2.26). Eyraud et al ⁽³⁷⁾ observed an increase in cathode current efficiency of approximately 15% over the current density range between 1.5 adm⁻² and 5.0 Adm⁻² when the temperature was increased from 20°C to 50°C.
- Increasing the flow rate ⁽²⁹⁾⁽³⁰⁾⁽³⁷⁾ (Table 2.4 and Figure 2.27). As the rotation speed is increased, it becomes more favourable to reduce hydrogen ions on the manganese than to reduce manganese species to the metallic state.
- Decreasing the current density ⁽²⁴⁾⁽²⁹⁻³¹⁾⁽³⁷⁾⁽⁴¹⁾ (Table 2.2).
- Decreasing the pH, according to Gabe et al ⁽²⁹⁾⁽³⁰⁾ (Table 2.3). Eyraud et al ⁽³⁷⁾ observed that the effect of a pH decrease from only pH6.3 to pH 5.7 had a marked effect on the cathode current efficiency.

Unfortunately, for the above operating conditions, those which promote an increased current efficiency are also those which result in a decrease in the manganese content of the deposit. Sagiyaama et al ⁽³³⁾⁽³⁴⁾ show this to be a clear relationship which is unchanged by variation in current density, flow rate or temperature (Figure 2.28), but can be shifted by pH (Figure 2.29).

A cathode current efficiency of 42% was observed with direct current plating by Foo et al ⁽⁴²⁾. The value could be increased with pulse plating up to 86%.

2.12 STRUCTURE AND APPEARANCE OF ZINC-MANGANESE ELECTROPLATE

The crystal structure of zinc-manganese alloys has been identified using x-ray diffraction methods ⁽²⁶⁻²⁸⁾⁽³⁷⁾⁽⁴¹⁾⁽⁴³⁾. In the range between 20% and 30% manganese content, ε-phase was found. This has a hexagonal close packed structure. Above

60% manganese, γ -manganese of tetragonal structure is the major phase. In between 30% and 60% manganese, a mixture of these two phases was seen. By calculating the x-ray peak intensity ratio, the division of these phases has been shown in graphical form (Figure 2.30) ⁽²⁶⁻²⁸⁾⁽⁴⁶⁾. The manganese-zinc phase diagram reveals that these phases exist in non-equilibrium state at room temperature (Figure 2.31) ⁽⁴⁷⁾. There is no data currently available for zinc-manganese alloys in the JCPDS Powder Diffraction Files ⁽⁴⁸⁾. Eyraud et al ⁽³⁷⁾ compared the spectra obtained with the patterns provided for the isostructural zinc-iron system.

Comparing these phases with the deposit morphology examined using a scanning electron microscope ⁽²⁶⁻²⁸⁾⁽³¹⁾⁽³⁹⁾⁽⁴⁴⁾⁽⁴⁵⁾, the ϵ -phase is a fine structure whereas the γ -manganese comprises larger, round nodules.

Brenner ⁽²⁴⁾ says that Faust et al ⁽²⁵⁾ found the appearance of the “best” deposits to be grey and matt. Hull Cell panels are presented by Selvam and Guruviah ⁽³¹⁾ for baths with varying sodium citrate content and including addition agents. Addition of gelatin or agar-agar can produce semi-bright deposits, whereas selenic acid alters the appearance over the entire panel. These authors have not related the appearance to the manganese content along the panel, except to say that the current density range between 1Adm^{-2} and 8Adm^{-2} corresponds to manganese contents from 2% to 33%.

The uniformity and composition through the thickness of a zinc-manganese coating was found to vary very little by Sagiya et al ⁽³³⁾⁽³⁴⁾ using glow-discharge spectrometry. The electroplate was deposited onto steel strip on an industrial scale, horizontal-type electrogalvanising line equipped with slit-type electrolyte injecting nozzles. Wielage et al ⁽⁴³⁾ show cross-sections through zinc-manganese coatings containing between 19% and 24% manganese. The coating appears to be very porous, with increasing columnar structure with manganese content.

The uniformity of the coating across a flat panel was commented on by Faust et al ⁽²⁵⁾. The appearance was not even and this correlated with a large variation in the composition of the alloy from the edges towards the centre. The edges the deposit

contained 70% manganese (ϵ -phase), whereas the centre of the panel comprised 45% manganese (γ -manganese). This “edge effect” was improved but not removed by a more uniform current distribution over the panel. Composition variations between the centre and the edge of coatings can be reduced by pulse plating ⁽⁴²⁾.

2.13 CORROSION RESISTANCE OF ZINC-MANGANESE ELECTROPLATE

From a corrosion viewpoint, automobile manufacturers are primarily interested in zinc alloys to protect against two types of damage, namely perforation and cosmetic corrosion. Perforation corrosion initiates at an interior surface of a body panel, penetrates the sheet steel and eventually results in red rust on the exterior surface. It often occurs at locations which are difficult to clean, phosphate and coat during manufacture because of limited accessibility, or at crevices which collect dirt, salt and moisture. Cosmetic corrosion describes attack which initiates at the exterior surface, usually at regions where a paint film is damaged. Although this form may eventually lead to perforation, the main concerns are with appearance. These concerns are threefold. Firstly, red rust stains and bleeding may occur at scratches in the paint. This represents the failure of the coating to protect the underlying steel. Secondly, undercutting of the paint film may occur at the scratches. Thirdly, the chipping of paint and corrosion of steel due to the combined effects of corrosion and impact damage by stones and debris.

Zinc and zinc alloy coatings can protect steel from corrosion by one or a combination of cathodic protection and barrier action. Steel exposed at coating voids is galvanically protected by preferential anodic dissolution of the sacrificial coating and simultaneous cathodic polarisation of the steel. If this were the only mechanism, the protective life would be severely limited. As the coating dissolves, it also forms a rust (white in the case of zinc) of insoluble salts such as the carbonate or oxide. These salts plug the pores of the coating and form a layer on the metal surface, thus providing a barrier isolating the steel from the atmosphere. The coating lies dormant on the surface until mechanical damage to the film occurs. The damaged area is

protected through sacrificial action until a barrier is again built. Zinc alloys are generally not as active as pure zinc, so tend to corrode at lower rates and provide less galvanic action.

While the major reason for the improvement in corrosion resistance of cars in recent years has almost certainly been due to the use of coated steels, other factors such as improved design, better pre-treatments and more effective paint systems have undoubtedly contributed. Good corrosion resistance can be achieved by adequate painting of conversion-coated steel, with excellent coverage of the substrate being achieved by a primer layer applied by anaphoresis or cataphoresis. However, although these layers provide an excellent barrier, without the metallic coating no sacrificial corrosion resistance is achieved. Problems will occur at areas not easily reached by paint and at spots where the substrate is accidentally uncovered.

Therefore, to investigate the corrosion properties and behaviour of zinc-manganese, authors have produced results both for coatings without paint and those which have been phosphated and/or painted. The sacrificial and barrier actions of the coating itself are discussed, and the resistances to both perforation and cosmetic corrosion have been investigated. In the latter category, red rust formation, paint chipping and undercutting are included. Sagiya et al ⁽²⁶⁻²⁸⁾⁽³³⁾⁽³⁴⁾ give the quantity of coatings on the specimens in terms of a mass per unit area. For easy comparison with other work, these units can be converted to coating thickness according to Appendix 1.

The salt spray test is commonly used to assess the corrosion performance of a coating and the protection afforded to the underlying substrate, usually to the specifications of ASTM B117-97 ⁽⁴⁹⁾. It is possible to draw conclusions as to how the coating itself corrodes, and also the time taken until the coating breaks down completely and the steel substrate corrodes giving red rust. However, Porter et al ⁽⁸⁾ doubt the usefulness of accelerated tests such as this for predicting the service behaviour of zinc coatings in the atmosphere since they magnify any differences. Such tests are useful for guidelines, and there is no doubt that zinc alloys give substantial improvement of corrosion resistance in use.

2.13.1 Corrosion Resistance Without Paint

Sagiyama et al ⁽²⁶⁻²⁸⁾⁽³⁹⁾⁽⁴⁴⁻⁴⁶⁾ report the performance of unpainted zinc-manganese coatings on steel in a salt spray test. The corrosion resistance increased with the proportion of γ -manganese in the microstructure. At manganese contents above 40%, the time to red rust (and total breakdown of the coating) exceeded 1000 hours and the coating could provide forty times the corrosion resistance to steel than a zinc layer of similar thickness. The time to red rust increased with coating thickness ⁽³⁶⁾.

Zinc-manganese itself corrodes to give a black product, as opposed to the white product produced from zinc and other zinc alloys. Gabe et al ⁽²⁹⁾⁽³⁰⁾ suggest this is probably manganese (III) oxide or manganese dioxide. Sagiyama et al ⁽²⁶⁻²⁸⁾⁽⁴⁶⁾ identified γ - Mn_2O_3 and $ZnCl_2 \cdot 3Zn(OH)_2$ in the corrosion products from a salt spray test using x-ray diffraction. Increase in manganese content, and thereby the corrosion resistance, of the coatings showed an increase in the ratio of manganese corrosion product to that of zinc.

To examine the mechanism by which zinc-manganese protects the steel, anodic and cathodic polarisation curves were obtained in 5% sodium chloride solution by Sagiyama et al ⁽²⁶⁻²⁸⁾⁽⁴⁴⁾⁽⁴⁵⁾ for a variety of salt spray tested zinc and zinc-manganese coatings. From these, the corrosion potential and the corrosion current were obtained to show further relationships.

Comparison has been made between zinc-53% manganese and zinc after salt spray testing for 24 hours ⁽²⁶⁻²⁸⁾⁽⁴⁵⁾. The corrosion current density, or the corrosion rate, was lower for the alloy on steel than for zinc on steel. The zinc-manganese coating will, therefore, dissolve at a slower rate and protect the steel for longer. Furthermore, Urakawa et al ⁽⁴⁴⁾ show that over the majority of a 1000 hour salt spray test, increase in manganese content of the alloy gives a slower corrosion rate. The γ - Mn_2O_3 is

thought to act as a protective barrier ⁽⁴⁴⁾ which suppresses oxygen reduction at the cathode and, thereby, increases corrosion resistance.

The corrosion potential for the steel substrate can be obtained from electrochemical measurements and is that at which the coating totally breaks down and red rust appears (approximately -600mV). The corrosion potential of both zinc and zinc-manganese are more cathodic than that of steel, and that of the alloy becomes increasingly so with increase in manganese content. These values can be obtained from the electropotentials. Therefore, at the start of a salt spray test the manganese content clearly affected the corrosion potential ⁽²⁶⁻²⁸⁾⁽⁴⁴⁾⁽⁴⁵⁾⁽⁵⁰⁾.

However, once the coating has started to corrode, the manganese content has little effect on the corrosion potential ⁽²⁶⁻²⁸⁾⁽⁴⁴⁾⁽⁴⁵⁾. Coatings with manganese contents of 39%, 53% and 76% all behaved similarly. The potential rapidly dropped to between -920mV and -960mV where it remained until just before red rust appeared.

Sagiyama et al ⁽²⁶⁻²⁸⁾ concluded that this trend indicates the sacrificial behaviour of zinc-manganese on steel.

Therefore, corrosion protection for this system is provided by the combination of the protective barrier and the galvanic sacrificial action, in a manner similar to zinc and other zinc alloys ⁽⁵¹⁾.

2.13.2 Corrosion Resistance after Phosphating and/or Painting

For the results of Sagiyama et al ⁽²⁶⁻²⁸⁾ which concern painted zinc-manganese coated steel, there is no mention of a phosphate layer also being applied, even though full details are given of paint layers. The paint layer may have been applied directly to the alloy coating, especially since phosphatability is described in the paper after these results are presented.

The galvanic sacrificial nature of a coating can be retained in many corrosion conditions ⁽²⁹⁾⁽³⁰⁾. It can be affected if the coating becomes more noble to steel by the effect of ions in solution, the formation of a passive film or by increased temperature. Alloys of zinc with nickel, cobalt or tin become increasingly noble as the alloy content increases and at a critical content will cease to sacrificially protect the steel. A critical alloy content exists (for example, 12% nickel in zinc) for maximum protective ability.

Zinc-manganese, however, becomes increasingly base as the manganese content increases. This is attributed to the formation of the passive film ⁽²⁹⁾⁽³⁰⁾ which allows galvanic polarity to be maintained whilst acting itself as a kinetic barrier. Such behaviour is analogous to the “weathering steels” where iron, in the presence of certain alloying elements, can produce a film of γ -Fe.OH. This offers stable passive film protection.

The properties of perforation and undercutting resistance described below show the maximum protection to be offered by an alloy of 50% manganese. Gabe et al ⁽²⁹⁾⁽³⁰⁾ suggest that this 50% manganese content in zinc alloys may represent the ability to form an oxide film of this type.

2.13.2.1 Perforation Corrosion Resistance

Sagiyama et al ⁽²⁶⁻²⁸⁾ evaluated the relationship between corrosion depth and manganese content of the coatings by weight loss in 0.01N sodium hydroxide at pH12. Minimum corrosion was found in the range of alloys containing 30% to 50% manganese. It is interesting to note, however, that alloys with 70% to 80% manganese behaved similarly to electrodeposited zinc. (Although a 20 μ m cathodically deposited electrocoat was used on these specimens, there is no mention as to whether they are phosphated as well).

Perforation corrosion is said to be predominantly determined by the extent of the sacrificial protection action of the coatings⁽²⁶⁻²⁸⁾. Since both zinc and manganese are electrochemically less noble than iron, electrodeposited zinc-manganese alloys are found to exhibit sacrificial action as described previously.

2.13.2.2 Resistance to Paint Chipping

Steel, galvanealed zinc and zinc-53% manganese were coated with a triple paint layer of total thickness 90 μm ⁽²⁶⁾⁽²⁸⁾. (Again, no mention of phosphating is made). The specimens were chipped using a gravelometer then subjected to a salt spray test. Red rust was observed on the steel in less than 240 hours and on the zinc after 720 hours when the test was concluded. No corrosion was found on the zinc-manganese specimens, and the excellent performance was credited to the good corrosion resistance of the alloy and the adhesion of the paint to it.

2.13.2.3 Paint Undercutting

Gabe et al⁽²⁹⁾⁽³⁰⁾ compared the performance of panels of zinc, zinc-nickel and zinc-manganese of varying thickness in a salt spray test (Table 2.5). All panels were phosphated and cathodically electroplated (25 μm), then scribed to allow exposure of the substrate. After 1000 hours, the zinc system showed red rust. The 6.0 μm zinc-nickel and 2.5 μm zinc-manganese panels performed in an equivalent manner, both showing the coloured rust characteristic of the alloy system - black for zinc-manganese and white for zinc-nickel. The zinc-manganese coatings with thickness of 5.0 μm and greater withstood the entire time of the test with no undercutting.

The effect of the manganese content of the alloy on the “blistering” resistance was assessed by Sagiyama et al⁽²⁶⁻²⁸⁾. The samples were electrocoated (20 μm) and scribed in a comparable manner to those of Gabe et al⁽²⁹⁾⁽³⁰⁾ above, but the presence

of a phosphate layer is unmentioned. After 840 hours, 20g/m² (approximately 2.8µm thickness) of zinc-30% manganese performed in an equivalent manner to zinc coatings of twice the thickness. Thereafter, the “blistering resistance” increased with manganese content.

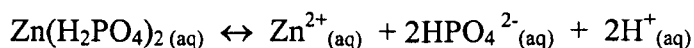
According to Sagiya et al ⁽²⁶⁾, undercutting is known to be the result of alkaline attack dissolving the coating. Dissolution of the coatings is considered to correlate with increased undercutting. The dissolution of zinc-manganese alloys in an alkaline solution at pH12 was studied. The amount of the dissolved deposit, which is exclusively zinc, decreased with increased manganese content. Thus, dissolution of the deposit in alkaline solution and the degree of undercutting may be suppressed by the resistance of manganese to such solutions.

2.14 PHOSPHATING AND PAINTING OF ZINC-MANGANESE

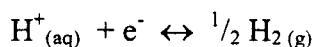
A phosphate or chromate conversion coating is applied to zinc or its alloys to provide a further layer for protection against corrosion and also a suitable surface to which paint can successfully adhere. The ability of zinc-manganese to be phosphated and the parameters affecting the adhesion of paint to this layer have been reported ⁽²⁶⁾. Also, cathodically electrodepositing paint onto zinc-manganese was found to be successful.

2.14.1 Phosphatability

During phosphating, the metal is subjected to an oxidising chemical treatment which produces a relatively thick (approximately 2µm) layer of corrosion product, of a form suitable for resisting further attack ⁽³⁵⁾. As a result of chemical reaction with free phosphoric acid, iron phosphate and a phosphate of either zinc or manganese are precipitated as an insoluble film. Thus, zinc phosphate dissociates:



followed by proton reduction:



with simultaneous oxidation of the substrate to aqueous ions. The film forms as the double layer becomes depleted of protons and the pH rises. Oxidising agents, such as NO_3^- and/or Cu^{2+} , may be added in 0.1 mol/kg quantities to accelerate the process and may give rise to some substrate ions in the film. Usually this does not damage its properties.

Sagiyama et al ⁽²⁶⁻²⁸⁾ applied zinc phosphate to zinc-manganese alloys using an immersion phosphating process. Both fine and dense crystals were formed. No crystals were formed on pure manganese. The phosphate film was attributed to hopeite ($\text{Zn}_3(\text{PO}_4)_2 \cdot 4\text{H}_2\text{O}$) by x-ray diffraction. Using energy dispersive x-ray spectroscopy, manganese was detected in this film and its percentage increased with manganese content of the deposit. It was concluded that manganese atoms substituted for some of the zinc atoms in the hopeite to give a structure of $\text{Zn}_{3-x}\text{Mn}_x(\text{PO}_4)_2 \cdot 4\text{H}_2\text{O}$.

2.14.2 Wet Adhesion of Paint

The adhesion of a 3-layered paint system of total thickness 90 μm to phosphated zinc-manganese alloys was assessed by Sagiyama et al ⁽²⁶⁻²⁸⁾. The samples were immersed in water for 240 hours, then a cross hatch cut was made and the paint was pulled off using tape. The paint remained adhered in the range between 10% to 80% manganese ⁽²⁶⁻²⁸⁾⁽⁴⁴⁾.

The phosphate film is said to dissolve during cathodic electropainting due to an increase in pH ⁽²⁶⁾. As manganese content of the deposit increases, the zinc dissolves decreased but the phosphorous dissolution increased. Manganese from the phosphate

film was not detected in the solution. According to Sagiya et al ⁽²⁶⁾, these results indicate that manganese precipitates on the surface as manganese oxide, and this may contribute to good wet adhesion of the paint.

2.14.3 Cratering During Electrocoating

Results were produced showing the production of craters during electrocoating of zinc-manganese ⁽²⁶⁻²⁸⁾. Craters were generated on galvanised steel, but few were found when applying paint either directly to the steel substrate or on the zinc-manganese.

2.15 COATING ADHESION

Drawability and coating adhesion were evaluated using a draw bead test ⁽²⁶⁻²⁸⁾. Good coating adhesion was found in the range of 20 % to 50 % manganese content.

2.16 WELDABILITY

Zinc-manganese can be welded under the same conditions as zinc ⁽²⁶⁻²⁸⁾. It provides good multiple spot weldability or electrode life.

The welding of coated steel is discussed by Roach ⁽⁵²⁾. Zinc has a much lower melting point than steel (420°C compared to 930°C) ⁽⁵³⁾. Before a weld can be formed in the steel, the molten zinc diffuses into the copper electrodes forming a brass alloy and contaminating the electrode. Brass has a higher resistivity than zinc, so in subsequent welds the heat is generated in the contaminated electrode rather than in the zinc coating, thus reducing the size of the weld nugget. Also, higher currents and pressures are used in welding coated steel, so electrode wear is higher. This wear increases the electrode area which reduces the current density and, subsequently, the

weld nugget diameter. These effects of wear and contamination reduce the electrode life to one tenth of that for welding steels alone.

The electrode contamination is highly inconsistent between different electrodes. Batches of steel with electrocoatings have more consistent surfaces, which give larger electrode life compared to hot-dipped materials.

PART THREE - CHEMISTRY OF THE ELECTROPLATING BATH

2.17 ELECTROPLATING BATH CHEMISTRY

Work has been reported on the reactions occurring in the bath during electrodeposition, the lack of stability in the electrolyte and the effect of addition agents on the bath, deposit and cathode current efficiency.

2.17.1 Electroplating Bath Stability

The sulphate-citrate bath for electrodepositing zinc-manganese has the problem of being unstable and, therefore, of relatively little use for industrial purposes. This is reported in some papers but not mentioned in others, even though there is little difference in bath composition or operating conditions throughout the literature.

Eyraud et al⁽³⁷⁾ observed precipitation from a bath after 12 hours. A pink precipitate was observed from a bath at pH3, but at pH9 a brown precipitate, thought to be manganese dioxide, was formed. Sulcius et al⁽⁵⁴⁾ have recorded precipitation from a bath at pH3.2 after 24 hours, at pH5.3 after 22 to 24 hours, and at pH6.3 after 96 hours.

Faust et al⁽²⁵⁾ observed the precipitation of a manganese compound from a bath which had been operated for several hours, but found this did not occur in an unworked bath.

The cause of the precipitation was not ascertained, but it could be prevented by separating the anode and cathode compartments with a diaphragm. Selvam and Guruviah⁽³¹⁾ have used this method, but they have not commented on the reasons for doing so or the effect this had on the process. The latter paper does not mention bath instability. Sulcius et al⁽⁵⁴⁾ found that precipitation could not be avoided by separating the anode and the cathode with a diaphragm.

Selvam and Guruviah⁽³¹⁾⁽⁵⁴⁾ developed a three-stage method for manufacture of the bath. This involved preparing separate solutions of each of the zinc sulphate, manganese sulphate and sodium citrate components. The zinc and sodium citrate solutions were then mixed, followed by addition of the manganese sulphate solution 8 hours later. This is said to improve the stability of the bath. Eyraud et al⁽³⁷⁾ could not produce a coating containing manganese from this bath, regardless of the current density employed, with or without agitation. Hence, the latter researchers prepared the electroplating bath by preparation of the manganese sulphate solution, followed by addition of zinc sulphate and finally the addition of the sodium citrate component.

The bath pH has been reported to be a determining factor in the precipitate formation. Sagiyaama et al⁽³³⁾⁽³⁴⁾ observed no precipitate in a bath stored for 20 days at 50°C if the value was higher than pH5.4 (Figure 2.32). Furthermore, they showed that less precipitation occurred in a bath with the composition:

Zinc	0.5 mol/l
Manganese	0.2 mol/l
Sodium Citrate	0.85 mol/l

compared with:

Zinc	0.4 mol/l
Manganese	0.3 mol/l
Sodium Citrate	0.85 mol/l

Gabe et al ⁽²⁹⁾⁽³⁰⁾ summarises the results given by Sagiyama et al ⁽³³⁾⁽³⁴⁾ on bath instability. It was concluded that the precipitate is likely to be a trivalent citrate complex, and that the problem might be alleviated by the addition of metallic manganese or zinc.

Sagiyama et al ⁽³³⁾⁽³⁴⁾ reduced manganese (III) to manganese (II) using metallic zinc and manganese. The manganese (III) ions result from oxidation of the manganese (II) ions in the bath by dissolved oxygen in the electrolyte or by oxidation at an insoluble anode. After electroplating, an absorbance peak at 430nm (Figure 2.33) was identified to be that of manganese (III) citrate complex ions. Treatment with the metallic pieces restored the spectrum to that of the unused bath.

Bozzini et al ⁽⁴¹⁾ added 0.1M to 1.0M potassium bromide to the electroplating bath to improve its stability. The addition is reported to stabilise manganese (II) and thereby eliminate the precipitation of manganese (III) species.

The precipitate produced from the sulphate-citrate bath has been analysed using x-ray diffraction and thermal analysis by Sulcius et al ⁽⁵³⁾. It was found to contain approximately 48.5% manganese, 22% carbon and 3.5% hydrogen, with no zinc. This stoichiometry differed from that of a known sample of manganese citrate. The precipitate was identified as $Mn_3O_4(MnO.Mn_2O_3)$ which is thought to result from the oxidation of manganese (II) in the bath to manganese (III).

2.17.2 Electroplating Bath Additives

Gabe et al ⁽²⁹⁾⁽³⁰⁾ found that small amounts of ascorbic acid (typically 2.0g/l) were successful in inhibiting the appearance of the precipitate during bath storage at 50°C.

Sagiyama et al ⁽³³⁾⁽³⁴⁾ discovered that additions of small amounts of sulphur compounds such as telluric acid or selenic acid could markedly increase the cathode current efficiency. A cathode current efficiency of greater than 60% could be

achieved when producing a deposit containing 50% manganese by adding 0.15g/l sodium thiosulphate as a reducing agent (Figure 2.34).

Akiyama et al ⁽³²⁾ found that the observed relationship of decrease in current efficiency with increase in manganese content of the deposit did not apply if selenious acid or sodium thiosulphate was added to the bath. The current efficiency was almost constant at 70% during the production of deposits with a manganese content of between 20% to 80% in baths containing an addition of 2mmol/l selenious acid. Over a similar range, an addition of 1mmol/l sodium thiosulphate or thiourea produced deposits at about 50% efficiency.

Similarly, Sulcius et al ⁽⁵⁵⁾ report that the addition of 0.5g/l ammonium selenate produces a deposit containing about 70% manganese at a current efficiency of 70% throughout the current density range of 5 Adm⁻² to 20 Adm⁻². Again, the inverse relationship between manganese content and current efficiency is not observed in the bath containing the additive. This has also been found in the electrodeposition of manganese-iron alloys with the addition of 0.1g/l to 0.5g/l selenium dioxide ⁽⁵⁶⁾.

According to Brenner ⁽²⁴⁾, Faust et al ⁽²⁵⁾ observed a decrease in manganese content of the deposit with increase in ammonium content of the bath. However, ammonium ions are not mentioned as a bath component elsewhere in the article.

Gelatin, agar-agar and selenic acid were found to alter the appearance of the alloys over Hull Cell panels by Selvam and Guruviah ⁽³¹⁾.

In the electrodeposition of nickel-manganese-zinc alloys from a sulphate bath, the manganese content of the deposit increased with increasing addition of dextrin or l-serine, but decreased with increasing additions of glucose, β -alanine or glycine ⁽⁵⁷⁾. The cathode current efficiency was unaffected by these additives. While the zinc content of these deposits is approximately 90%, it should be noted that the manganese content is only of the order of 0.5%. The additive concentration was between 1g/l and

2g/l. The bath contained not only the metal sulphates, but also 30g/l ammonium sulphate, 18g/l thiourea and 0.8g/l ascorbic acid.

2.17.3 Alternative Baths

As cited by Gabe ⁽²⁹⁾⁽³⁰⁾, Sugimoto et al ⁽⁵⁸⁾ have examined a fluoborate bath containing both zinc and manganese fluoborate, boric acid and polyethylene glycol. Cathode efficiencies of up to 80% are reported.

Zinc-manganese has been deposited from a bath containing EDTA as a complexing agent by Agladze et al ⁽⁵⁹⁾. The bath also contained 30g/l manganese sulphate, 4g/l zinc sulphate, 150g/l ammonium sulphate and 0.33g/l ammonium selenate. The EDTA content was varied from 0.8g/l to 10g/l. The manganese content of the alloy increased with EDTA content, and was found to vary between 75% and 99.2% over this range. Decrease in flow rate, temperature or manganese content of the bath was found to promote increase in manganese content of the alloy.

2.18 ANALYSIS OF ELECTROPLATING BATH CHEMISTRY

2.18.1 Plating Bath Reactions During Electrodeposition

In order to determine the chemical reactions occurring in the sulphate-citrate bath during the deposition of zinc-manganese, Yoshikawa et al ⁽⁶⁰⁾ analysed the solution from a flow cell in an atomic absorption spectrophotometer. The results are summarised in Figure 2.35. They concluded that the zinc and manganese ions complexed with the citrate ions and showed a “typical” peak at 225nm on the spectrum.

2.18.2 Analysis Techniques

Electromagnetic radiation including light (visible, ultraviolet and infrared), x-rays, radio and radar waves are part of a broad spectrum which ranges from gamma rays (with wavelength in fractions of an angstrom) to radio waves (with wavelength measured in meters or even kilometres). All these waves have the same velocity, namely 3×10^{10} cm/sec. Since their frequency is equal to their wavelength divided by this velocity, it follows that the shorter the wavelength, the higher the frequency.

When a beam of electromagnetic radiation is passed through a substance, the radiation can be either absorbed or transmitted, depending upon its frequency and the structure of the molecules it encounters. Electromagnetic radiation is energy, so when a molecule absorbs radiation, it gains energy. The energy gain depends on the frequency of the radiation. The higher the frequency (the shorter the wavelength), the greater is the energy gain in accordance with

$$\Delta E = h\nu$$

where ΔE is the energy gain in ergs, h is Planck's constant and ν is the frequency in Hertz.

The energy gained by a molecule in this way may bring about increased vibration or rotation of the atom, or may raise electrons to higher energy levels. The particular frequency of radiation that a given molecule can absorb depends upon the changes in vibrations or rotations or electronic states that are permitted by that structure. A spectrum can be obtained which shows how much electromagnetic radiation is absorbed (or transmitted) at each frequency. This can be highly characteristic of a particular structure.

Light of wavelength between about 400nm and 750nm is visible. The ultraviolet region occurs at wavelengths below 400nm, and the infrared region above 750nm. Absorption of ultraviolet or visible light results in electronic transitions within an atom or molecule. Absorption of infrared radiation results in molecular vibrations.

2.18.2.1 Ultraviolet and Visible Spectroscopy

Absorption of ultraviolet or visible light results in electronic transitions within an atom or molecule, that is, promotion of valence electrons from low-energy, ground-state orbitals to higher energy excited-state orbitals. The transitions are generally between a bonding or lone-pair orbital and an unfilled non-bonding or anti-bonding orbital.

The energies involved in vibration and rotation of a molecule are smaller than those involved in electronic transitions. When the electronic transition occurs it will, therefore, be accompanied by vibrational and rotational energies. The magnitude of the energy change will approximate to the larger electronic transition, but will vary by the amounts of energy involved in the other transitions. All possible combinations will occur. The result is that the absorption peak is not a sharp line, but a broad peak whose position for that molecule is specific to that electronic transition. Furthermore, since the spectrum may represent a number of such possible electronic transitions occurring within the molecule, a series of peaks will be observed.

Hence, the wavelength of the absorption is a measure of the separation of the energy levels of the orbitals concerned, and the spectral band intensity, or absorbance, is directly proportional to the number of absorbing atoms.

The wavelength range of the ultraviolet, visible and near-infrared regions of the electromagnetic spectrum is 100 to 900nm. The highest energy separation is found when electrons in σ -bonds are excited, giving rise to absorption in the 120 to 200nm range, called the vacuum ultraviolet. This range is relatively uninformative and is usually outside the range of a spectrometer. However, above 200nm, excitation of electrons from p- and d-orbitals, and π -orbitals, gives rise to easily measured and informative spectra. From 200 to 400nm is the ultraviolet region, with the visible region occurring above 400nm.

Each atom or molecule has a unique characteristic series of energy levels. The spectrum for $[\text{Mn}(\text{H}_2\text{O})_6]^{2+}$ is given by Greenwood and Earnshaw⁽⁶¹⁾ (Figure 2.36).

2.18.2.2 Infrared Spectroscopy

The energies of most molecular vibrations correspond to that of the infrared region of the electromagnetic spectrum. It is possible to identify an unknown sample by obtaining an infrared spectrum and assigning the characteristic vibrations of specific functional groups. The usual range of an infrared spectrum is between 4000cm^{-1} at the high frequency end and 625cm^{-1} at the low frequency end.

For a complexed molecule, the overall infrared spectrum comprises the frequencies resulting from the ligand, together with those from the metal-ligand bond.

Some of the molecular vibrations detected in infrared spectroscopy are associated with individual bonds or functional groups. Since these have characteristic vibration frequencies within well-defined regions, a sample molecule can often be identified using them. These localised vibrations may be stretching, bending, rocking, twisting or wagging. They are exhibited in the infrared spectrum in a region above 1500cm^{-1} , where the absorption bands are can be assigned to these specific functional groups.

Other vibrations involve the whole molecule. These are shown in the region below 1500cm^{-1} , called the fingerprint region, where the series of bands are characteristic of the specific molecule. However, within this region, some bands do occur which can be assigned to localised vibrations of functional groups. The usual method of confirming the identity of a compound using infrared spectrometry is to compare this fingerprint region with a known spectrum of an authentic sample.

Bands are frequently observed which do not correspond to any of the fundamental vibrations of the molecule and are due to overtone bands and combination bands. The latter results from the interaction between two or more vibrations.

In interpreting the infrared spectrum, the order of stretching frequencies of bonds generally follows a logical order. The stretching vibrations of single bonds to hydrogen give rise to the absorption at the high frequency end as a result of the low mass of the hydrogen atom. Thereafter, triple bonds are observed at higher frequency than double bonds, followed by single bonds. Multiple bond stretching usually occurs in the region 1500 to 2500cm^{-1} ⁽⁶²⁾. The greater the strength of the bond between two similar atoms, the higher the frequency of the vibration. Bending vibrations are of much lower frequency and usually appear in the fingerprint region below 1500cm^{-1} .

Carboxylic acids usually exist as dimers with very strong hydrogen bridges between the carbonyl and hydroxyl groups of the two molecules. This association can exist in dilute solutions which considerably modifies the infrared spectrum. For this reason, the spectra are best measured in the solid, as in this research, or liquid state ⁽⁶³⁾. A solid sample is usually either prepared as a potassium bromide disc or as a mull with the liquid paraffin, Nujol ⁽⁶⁴⁾. Nujol possesses only C-H and C-C bonds. A spectrum captured using this method will show strong peaks due to these features at 2940 , 2860 , 1465 and 1380cm^{-1} , together with a weaker band at 720cm^{-1} . Potassium bromide eliminates these bands but a weak band almost always appears at 3450cm^{-1} from the O-H group of traces of water.

Although the whole of the spectrum should be assessed, there are certain outstanding characteristic absorptions shown by carboxylic acids, particularly in the regions from 2500cm^{-1} to 3600cm^{-1} , and 1200cm^{-1} to 1700cm^{-1} . The infrared spectrum for zinc citrate ⁽⁶⁵⁾ is shown in Figure 2.37. Spectral data for two manganese citrate complexes is given in Figure 2.38 ⁽⁶⁶⁾. Key regions are labelled and described below:

- A. The α -hydroxyl group in an α -hydroxycarboxylic acid shows a very sharp O-H stretch band (medium height) at 3570cm^{-1} .

- B. The O-H stretch of the carboxyl group is observed as a broad band between 2500 to 3335cm^{-1} ⁽⁶⁷⁾. The position, shape and intensity is consistent throughout the carboxylic acid series and is due to the strong hydrogen bonding of the acid dimer.
- C. A C-H stretch band occurs around 2940cm^{-1} , which increases in intensity relative to the O-H stretch absorption as the chain length increases in the acid series⁽⁶⁷⁾. C-H bonds do not take part in hydrogen bonding, therefore their position is little affected by the state of measurement or their chemical environment⁽⁶⁴⁾.

There is a characteristic series of bands produced by most carboxylic acids within this region between 2500 and 3000cm^{-1} . These bands are usually seen as a jagged series on the low frequency side of any C-H absorption which may be present. The main peak is usually near 3000cm^{-1} , with a main satellite band near 2650cm^{-1} . The highest frequency band is due to the O-H stretching vibration and the others are combination bands of lower frequency vibrations of the COOH group⁽⁶⁴⁾. However, these peaks are usually overlaid to some extent by the C-H absorption⁽⁶³⁾.

There is a characteristic series of bands produced by most carboxylic acids within this region between 2500 and 3000cm^{-1} . These bands are usually seen as a jagged series on the low frequency side of any C-H absorption which may be present. The main peak is usually near 3000cm^{-1} , with a main satellite band near 2650cm^{-1} . The highest frequency band is due to the O-H stretching vibration and the others are combination bands of lower frequency vibrations of the COOH group⁽⁶⁴⁾. However, these peaks are usually overlaid to some extent by the C-H absorption⁽⁶³⁾.

- D. Carboxylic acids usually exist as dimers and exhibit their carbonyl stretch bands between 1695 to 1725cm^{-1} . In α -hydroxycarboxylic acids, this is shifted to a lower wavelength⁽⁶⁷⁾.

In a carboxylic acid salt, ionisation results in equilibration of the two oxygen atoms attached to the carbon with the disappearance of the carbonyl absorption and the appearance of two new bands. Antisymmetrical stretching of the COO^- structure is shown as a peak between 1550 to 1610cm^{-1} (D'), and symmetrical stretching at 1300 to 1420cm^{-1} (64) (D'').

- E. An O-H deformation near 1430cm^{-1} appears within CH_2 bending bands (67).
- F. A C-O stretch vibration appears around 1250cm^{-1} , of intensity similar to the 2500 to 3335cm^{-1} band (63)(67). The longer chain compounds, examined as solid samples, have this band broken into a number of sharp peaks which increase in number with the length of the chain.
- G. There is an O-H deformation band between 910 to 950cm^{-1} (63)(67).

There are other vibrations which are appropriate to the structure of the carboxylic acids and their salts:

- H. C-C vibrations, which absorb in the fingerprint region, are generally weak and are not practically useful.
- I. Strong bands associated with O-H stretching vibrations of water and hydroxyl groups occur between 3200 and 3700cm^{-1} (62). The hydroxyl group is characterised by a strong sharp absorption band in the region 3650 to 3700cm^{-1} . Water of hydration usually exhibits one strong sharp band near 3600cm^{-1} , and one or more strong sharp bands near 3400cm^{-1} . Water of hydration can be distinguished from hydroxyl groups by the presence of the H-O-H bending motion which produces a medium band (often multicomponent) in the region 1600 to 1650cm^{-1} (62).

CHAPTER 3

EXPERIMENTAL PROCEDURE

3.1 INTRODUCTION

The literature indicates that the benefits which can be obtained from the zinc-manganese system in terms of corrosion resistance are excellent. However, there still appears to be much scope for fundamental investigation. The research in this project concentrates on two areas, namely the process of electrodeposition of zinc-manganese and the chemistry of the electroplating bath.

In particular, the electrodeposition of zinc-manganese was assessed in terms of the polarisation behaviour of the system, in order to establish the role of the bath components and the operating parameters in the deposition process. The coatings produced were examined using microscopy, and the efficiency of deposition was established.

The chemistry of the electroplating bath was investigated to provide understanding about the stability problems encountered in the bath. Both the electrolyte and the precipitate were examined using a variety of chemical techniques.

This chapter describes the procedures for the experiments performed, together with details of the electrolyte and apparatus used.

PART ONE – THE ELECTRODEPOSITION OF ZINC-MANGANESE

3.2 THE ELECTROPLATING BATH

3.2.1 Choice of Bath

Zinc-manganese is usually electroplated from a sulphate-citrate bath. There have been very few results published using alternative solutions. This appears to originate from the work of Faust et al ⁽²⁵⁾ who report this to be the only electrolyte from which the alloy could be deposited in a satisfactory manner.

A sulphate-citrate bath was used for this research. The composition chosen was similar to that used by Gabe et al ⁽²⁹⁾⁽³⁰⁾ and Sagiya et al ⁽³³⁾⁽³⁴⁾ so that results would be comparable.

As a standard bath, the following reagents of standard laboratory grade were added to double distilled water per litre of bath:

Manganese sulphate, $\text{MnSO}_4 \cdot \text{H}_2\text{O}$	40g	(0.24M)
Zinc sulphate, $\text{ZnSO}_4 \cdot 7\text{H}_2\text{O}$	70g	(0.24M)
Sodium citrate, $\text{Na}_3\text{C}_6\text{H}_5\text{O}_7 \cdot 2\text{H}_2\text{O}$	180g	(0.60M)

3.2.2 Preparation of the Bath

For pure research purposes it is preferable to use Analar grade chemicals of high purity to minimise impurities and to ensure high accuracy of results. However, standard laboratory reagents were used in this research for two reasons. Firstly, this solution was designed to be commensurate with an industrial bath which would contain a higher percentage of impurities. Secondly, the bath decayed, so fresh solution was used for every experiment to ensure consistent conditions. Continuous use of Analar grade reagents would be expensive.

Usually in making up electroplating solutions these salts would simply be dissolved in the distilled water. However, problems were encountered in making up the bath in this way. The successful method adopted to avoid bath deterioration before electroplating involved mixing two solutions of double concentration as follows. The

0.24M zinc sulphate and 0.24M manganese sulphate were dissolved in almost half a litre of distilled water with heating and agitation. When this had cooled completely, the volume was made up to precisely half a litre. Similarly, a half litre solution containing the 0.6M sodium citrate was made up. When required, the two solutions could be mixed together.

Gabe et al ⁽²⁹⁾⁽³⁰⁾ found 2g/l ascorbic acid to be suitable for inhibiting the appearance of the precipitate during bath storage. Therefore, in some tests for this research 2g/l ascorbic acid or 2g/l sodium sulphite were added. The chemical was introduced to the electroplating bath in the double concentrate sodium citrate solution. To maximise its action, it was dissolved in the double distilled water and left for 24 hours before adding the sodium citrate.

Two further operations are usually considered for the preparation of electroplating baths ⁽⁶⁸⁾. Firstly, it is usual to purify an electroplating bath by chemical treatment and/or plating out operations to remove trace quantities of impurities. Secondly, an electroplating bath usually provides more consistent results if it is “aged”, that is, used repeatedly. Due to the instability of the solution and to preserve the chemical composition of the solution, these operations were not considered as suitable for this electrolyte.

3.2.3 Operating Conditions

A majority of the work was performed at 25°C. This was chosen to simulate room temperature. It was controlled by positioning the electrolytic cell in a water bath and was monitored using a thermometer.

The electrolyte has a natural pH of 5.6. This was used as the standard operating value since it is within the range over which Sagiya et al ⁽³³⁾⁽³⁴⁾ observed bath stability. Downwards pH adjustment was carried out using 10% (by volume) sulphuric acid which did not result in foreign ions being added to the bath. An attempt was made to

raise the pH of the bath using additions of zinc powder or granules, and by the addition of sodium hydroxide solution and ammonia solution. The pH meter was calibrated daily against freshly made buffers of pH4.0 and pH7.0. Readings of pH were left to stabilise for three minutes before they were noted.

The bath was oxygenated since it was exposed to the atmosphere. With the exception of Hull Cell tests, all experiments were performed using one litre of bath. No forced agitation of the electrolyte was used.

According to the literature ⁽²⁶⁻²⁸⁾, the properties of the coating are improved with increase in manganese content of the alloy. Hence, when altering bath composition and operating conditions in this experimental work, parameters were varied to promote manganese deposition. Increases in forced agitation and temperature are reported to result in decrease in manganese content according to Figures 2.19 and 2.20 and were, therefore, not investigated.

3.3 EXPERIMENTAL APPARATUS

3.3.1 The Circuit

The simplest practical arrangement for an electrolytic cell comprises an anode and a cathode positioned in the electroplating solution. This is known as a two-electrode system. A continuous supply of direct current is driven through the circuit connecting these two electrodes by a power supply. The current applied is usually measured by placing a known resistance in parallel with the cathode and reading the voltage across it, then applying Ohm's Law. Thurlby 1503 digital multimeters were used during this work for this purpose.

The potential difference between these two electrodes cannot be taken as the potential of the working electrode. Current flow results in the polarisation of the system and the potential changes from its known equilibrium value. Hence, a third electrode,

known as a reference electrode, may be included. The potential of the working electrode is then measured with respect to this electrode which provides a fixed reference value. The three-electrode circuit is shown in Figure 3.1.

3.3.2 The Cathode

In electroplating, the cathode is the working electrode and the metal is deposited onto its surface.

The simplest and most even current distribution is obtained by using a planar cathode facing a similarly shaped anode, with all points between them being equidistant. This arrangement is often used in the industrial scale electroplating of continuously processed steel strip⁽⁶⁹⁾. To allow a similar arrangement to be used in this research, all cathode specimens were produced from flat sheet metal.

Except where stated, the cathode was formed from mild steel. This is the most common substrate onto which zinc-manganese would be electroplated to act as a corrosion resistant coating. The specimens to be electroplated were made from mild steel Pyrene panels (from Pyrene Chemical Services, Buckingham) with a ground finish to ensure a standard and reproducible surface. The specimen design and pre-electroplating preparation is described below.

3.3.3 Specimen Design

Several factors needed to be considered when designing the cathode:

- It is desirable for the cathode to have an area which is significantly less (approximately ten times⁽⁷⁰⁾) than that of the anode. This allows even distribution of current and potential, and ensures that the performance of the electrochemical cell is dominated by the processes at the cathode.

- The specimens had to be of a size which could be electroplated at the high current densities involved, but within the output capabilities of the power supplies available.
- In relation to the cathode area, the volume of electrolyte had to be large such that the bulk solution would not become depleted of metal ions during electroplating, particularly during the lengthy polarisation tests. However, it needed to be as small as possible to allow the use of a new solution for each test to be within economic constraints.
- The specimens needed to be large enough to eliminate any edge effects.

Therefore, it was decided to predominantly use disc specimens of 0.5cm^2 in area. For ease of connection and handling during electroplating, a larger specimen was machined from the steel. The discs were partly punched out from this, such that they were raised slightly from the surface. Apart from on the front faces of the discs and leaving an area for electrical connection at the top, the front and back of the steel specimen was covered with two layers of air dried "Fortolac" lacquer (from W Canning and Co Ltd, Birmingham).

After electroplating, the disc could be pushed out from the back. This specimen design avoided damaging or cracking of the deposit by post-electroplating machining, since they were already of convenient size for further processing such as examination under a microscope.

The size of the steel specimen machined from the Pyrene panel varied according to the experiment. For polarisation work, a $1\text{cm} \times 10\text{cm}$ specimen was used with one disc face exposed. For electroplating samples, a $4\text{cm} \times 6\text{cm}$ specimen was used with four disc faces exposed.

For the cathode efficiency experiments where the specimen had to be weighed before and after electroplating, steel rings of height 0.33cm were used. These were mounted on a stainless steel rod in a PTFE collar. Only the disc face of area 1.97cm² and the PTFE collar were exposed to the electroplating solution.

3.3.4 Electrode Preparation

All mild steel cathodes were cleaned immediately prior to electroplating using the routine described in Appendix 2. This was developed using guidelines from several sources ⁽⁶⁸⁾⁽⁷¹⁾. It comprises degreasing in an organic solvent, followed by a hot alkaline soak, then anodic and cathodic electrocleaning. The process was finished with acid pickling and a final anodic electroclean.

After electroplating, the specimens were rinsed well in distilled water and air dried.

3.3.5 Counter Electrode

The counter, or auxiliary, electrode in electroplating is the anode. Its function is to supply electrons needed by the cathode.

For a majority of this work a soluble zinc sheet anode of high purity was used. This was chosen so that the anode material did not introduce any foreign ions into the bath. It was positioned parallel and opposite to the cathode.

For cathode current efficiency tests, the zinc sheet anode was cylindrical and the ring-shaped cathode was positioned in the centre.

However, for the polarisation studies an insoluble platinum foil electrode was used. This type of anode was felt to be more appropriate in these tests since they involved a lengthy time period at very high current densities. A zinc anode would have

replenished the electrolyte with zinc ions and thereby altered the solution composition under these conditions.

These anodes were scoured frequently and cleaned by immersion in 20% (by volume) nitric acid.

3.3.6 Reference Electrode

The reference electrode must have a potential which is stable throughout the experiment. Furthermore, for comparison with results from other authors, it must be possible to convert this potential value to other standard reference electrode scales, such as the Standard Hydrogen scale.

The reference electrode chosen was a mercury/mercurous chloride electrode (Standard Calomel Electrode (SCE)) with a potential of 0.244V versus the Standard Hydrogen Electrode at 25°C. This electrode has traditionally been one of the most widely used due to its versatility and its reliability at temperatures up to 70°C.

The reference system needs to be placed as close to the surface of the working electrode as possible without touching it to minimise the IR drop across the solution. A practical arrangement for achieving this is to use a Luggin capillary⁽⁷⁰⁾. The tip of this was placed as near as possible to the exposed cathode surface, but not directly in front of it. It was positioned at an angle to avoid bubble formation over the electrode tip.

3.3.7 Power Supply

A potentiostat applies and automatically controls an accurate external potential between the anode and the cathode. No current passes through the reference electrode circuit, the potential of which remains fixed. It is possible to set up a potentiostat as a

galvanostat by connecting an external resistance between the relevant instrument terminals. In this mode, the current can be set precisely instead of the potential.

For work requiring currents below 2A, the circuit included a “Ministat” (from H B Thompson and Associates, Newcastle Upon Tyne) which was wired as a galvanostat as shown in Figure 3.1.

At high current densities where the output of this machine was not sufficient, a stabilised power supply (Type AP30-80 Regulated Power Supply from Farnell) was used.

The polarisation work was carried out with an ACM Gill 8AC computerised potentiostat.

3.3.8 The Hull Cell

The Hull Cell is an extremely versatile electroplating tool capable of producing an electrodeposit for a wide range of current densities on one cathode panel in a single test.

The guidelines set out by Cannings⁽⁶⁸⁾ for Hull Cell tests were followed. The cathode was 100cm x 75cm, which is a half Pyrene panel. A high purity zinc sheet anode was used. The Hull Cell was used in a two-electrode circuit.

The volume of solution needed was 267cm³. This was designed to give a concentration relationship between the Hull Cell and a full-scale industrial tank, such that adding 1g of chemical to the cell is equivalent to adding 0.5oz per US gallon⁽⁷²⁾.

After electroplating, the panels were rinsed well in distilled water and air dried.

3.4 ELECTRODEPOSITION OF ZINC-MANGANESE

3.4.1 Polarisation Behaviour

For all polarisation curves, the system was allowed to stabilise for 15 minutes at the rest potential before data collection began using the ACM Gill 8AC. The entire curve could be captured by collecting data between -600mV and -3000mV (versus SCE).

Sweep rates of 10, 15, 20 and 100mV/min were tried. In choosing a sweep rate, a compromise had to be made. The slow sweep rates gave the cathode process optimum time to stabilise as the potential was being altered, but resulted in a thick coating on the cathode and increasing specimen area due to dendritic growth. A fast sweep rate resulted in thinner coatings but the system did not have enough time to stabilise. A sweep rate of 15 mV/min gave the best compromise, allowing the system time to adjust as readings were being taken, but being the fastest sweep rate at which a representative curve was obtained.

All polarisation curves were repeated at least three times to ensure reproducible and representative results.

Due to the difficulties experienced in raising the bath pH, if the natural value for one of the solutions in a series was less than pH5.6 then the curves for that series were obtained at pH5.0. This was assumed to produce comparative results since the standard curve and that obtained at pH5.0 are similar. Unless otherwise stated, standard bath composition and operating conditions were used.

Experimental details of the bath compositions and operating conditions used for the polarisation curves are given in Table 3.1. Aged baths were filtered before tests to remove any precipitate. Oxygen-free (white spot) nitrogen was bubbled through the bath in a sealed porthole beaker for an hour before the deoxygenated test commenced. The data was obtained to investigate the following:

- The form of the standard curve.
- The effect of deterioration due to aging of the bath. The solutions for these tests were kept open to the atmosphere for 30 days, and topped up daily to the original volume with double distilled water to account for evaporation.
- The effects of anode and cathode separation using a glass frit, the continuous use of the standard bath and the oxygen content of the electrolyte.
- The effect of variation in pH of the bath.
- The role of the individual components of a standard bath. The sulphate ions aid bath conductivity, so this molarity in the standard bath was maintained throughout by appropriate additions of sodium sulphate.
- The effect of sodium citrate on manganese, zinc and zinc-manganese electrodeposition.
- The effect of variation in the concentrations of each of sodium citrate, zinc sulphate, manganese sulphate and the total salt content in the bath.
- Effect of additions of 2g/l ascorbic acid or 2g/l sodium sulphite, to both fresh and aged baths.

3.4.2 Cathode Current Efficiency

Over a large range of current densities in zinc-manganese electroplating, the current is not totally consumed in metal deposition but is partly expended in the evolution of hydrogen at the cathode. The cathode current efficiency expresses, as a percentage,

the maximum amount of metal that can be deposited at a given current according to Faraday's Law.

The cathode current efficiencies for electroplating at various current densities were established using a copper coulometer placed in series with the cathode. The bath and operating conditions for this are detailed in Appendix 3. The principle behind this method is dependant on copper being deposited from the coulometer solution at 100% efficiency, and uses the fact that the quantity of current passed is the same through both the coulometer and the electroplating bath on test. The cathode current efficiency for zinc-manganese electrodeposition was calculated as shown in Appendix 4.

Experimental values were obtained at current densities of 1, 2, 4, 6, 8, 10, 12, 14, 16, 20, 30, 40, 50, 60, 70, 80 and 90Adm⁻². Three values were obtained at each current density. A placebo test was run with both the copper and steel in place but with no current passing in order to validate the method.

3.4.3 Electrodeposition of Coatings

The potential ranges over which the component metals of the system deposit, both separately and together, were determined by electroplating disc specimens at key points.

3.4.3.1 Hull Cell Tests

The Hull Cell was used to establish the effects of current density on the composition and morphology of electroplated zinc-manganese from a standard bath within the range 0.15Adm⁻² to 15Adm⁻². A current of 3A was applied for 5 minutes.

A central horizontal strip of depth 1cm was removed from the electroplated panel. Using the calibration chart from Cannings⁽⁶⁸⁾, the points “a” to “n” were marked as shown in Figure 3.2. These indicated the position of specific current densities in Adm^{-2} . The strip was then cut into samples for examination under the scanning electron microscope.

Hull Cell panels were also produced similarly for visual examination from baths corresponding to those used for the polarisation curves in Section 3.4.1. Details of these solutions are given in Table 3.1. Aged baths were filtered to remove any precipitate prior to the test.

3.4.3.2 Electroplated Specimens

The form of the standard polarisation curve indicated that the region of interest for zinc-manganese electrodeposition included higher current densities than can be accurately obtained on a Hull Cell panel. Therefore, to investigate the morphology and composition of the alloy above 15Adm^{-2} , disc specimens were electroplated at 20, 30, 40, 50, 60, 70, 80 and 90Adm^{-2} for 10 minutes.

These disc specimens and those from the Hull Cell provided deposits of varying thickness. After their composition and cathode current efficiency of electrodeposition had been obtained, samples could be produced at current densities of interest with a calculated thickness according to the calculations in Appendix 5.

Disc specimens were produced with a thickness of $7.5\mu\text{m}$. This was in line with a typical industry standard for sheet steel coatings. The current densities selected were 0.15, 1.5, 3.0, 6.0, 15, 20 and 30Adm^{-2} .

To confirm that 0.5cm^2 disc specimens were representative of larger areas of electroplate, full Pyrene panel samples were similarly electroplated at 15 and 20Adm^{-2} to a calculated thickness of $7.5\mu\text{m}$.

In addition, the form of the standard polarisation curve showed a region of interest at low current densities. To investigate this further, a specimen was electroplated at each of -850mV and -1050mV (versus SCE) to a calculated thickness of 7.5µm.

3.5 EXAMINATION OF ZINC-MANGANESE COATINGS

3.5.1 Visual Examination

The general appearance of all the electroplated coatings produced was observed and visually compared. Any distinguishing features were noted.

3.5.2 Scanning Electron Microscopy

The Hull Cell samples, disc specimens and discs from the Pyrene panels electroplated as described in Section 3.4.3.2 were all examined and analysed. In addition, a disc specimen of the cleaned mild steel substrate was inspected.

Specimens were mounted onto an aluminium disc with an adhesive, conductive carbon disc. They were blown with a clean air spray before being inserted into the Jeol 6400 microscope. The low current density specimens produced at -850mV and -1050mV (versus SCE) were gold-coated using an Emscope SC500 Coating Unit to prevent them from charging up in the microscope.

The centre of each specimen was examined and any characteristic features noted and photographed. The composition of this region was analysed using the attached Tracor Noran Series II EDX system. Unless stated, all analysis of composition was carried out at a magnification of x200. The composition of the coatings produced at -850mV and -1050mV (versus SCE) was analysed at x1000.

PART TWO – CHEMISTRY OF THE ELECTROPLATING BATH

3.6 CHEMICAL TECHNIQUES

Visible and ultraviolet spectra are usually presented as a graph of wavelength, λ , versus absorbance. Infrared spectra are commonly presented as wavenumber, ν , versus % transmission.

Absorbance is inversely proportional to transmission since, when a compound absorbs radiation, the intensity of that being transmitted decreases. Therefore, in an infrared spectrum, the base line (at zero absorbance) occurs at 100% transmission, which is recorded at the top of the spectrum and the graph shows a series of downwards absorbance peaks. In the case of visible and ultraviolet spectra, the base line occurs at the bottom of the spectrum, and absorption is shown as an increase in the signal.

The band position in spectroscopy may be expressed as a wavelength, λ , or as a wavenumber, ν , where

$$\nu = \lambda^{-1}$$

Since the wavelength is usually expressed in nm and the wavenumber is conventionally expressed in cm^{-1} , then

$$\nu = \frac{10^7}{\lambda}$$

It should be noted that the intensity of a transition should technically be measured by the area under the absorption peak rather than by the maximum of the peak. For

convenience and the difficulty in dealing with overlapping bands, the latter procedure is commonly adopted.

3.6.1 Ultraviolet and Visible Spectroscopy

The ultraviolet and visible spectra were obtained in this research using a Perkin-Elmer Lambda 5 ultraviolet-visible spectrophotometer, with quartz cells. This is a double-beam instrument which automatically changes the light source at the appropriate wavelength. A tungsten filament lamp is used for the visible and near-infrared region between approximately 350nm and 1000nm. A hydrogen lamp is used at wavelengths shorter than 350nm.

A portion of the solution under test was transferred to one of the quartz cells. It was placed in the spectrometer along with the second cell containing the solvent, that is, distilled water. These cells are arranged such that two equal beams of ultraviolet or visible light are passed, one through the sample and one through the solvent. The intensities of the transmitted beams are then compared over the whole wavelength range of the machine.

The error in this technique is usually between 0.5 and 5% ⁽⁷³⁾.

3.6.2 Infrared Spectroscopy

The Perkin-Elmer 577 spectrometer used for this research comprises a source of infrared light which is split into two beams of equal intensity. One is passed through the sample and if the vibration of the sample molecule falls within the range of the instrument, the molecule may absorb energy at a particular frequency. The resulting spectrum is a comparison of the intensity of the two beams after one has passed through the sample. This process is automated and results in a spectrum showing transmission plotted against wavenumber.

3.6.3 Atomic Absorption Spectroscopy

The electronic spectra of atoms, unlike molecules, take the form of discrete lines of small bandwidth in the gas phase. These absorption lines are very narrow (less than 0.1nm) and are characteristic of the analyte element. Thus, by converting an element into the gas phase atoms, measurement of absorption of light at one of these characteristic wavelengths may be used to determine its concentration within a sample.

Atomic absorption is a comparative technique whereby the concentration of an element in the sample is assessed against that of a standard solution. In the atomic absorption spectrometer, a source lamp produces a beam covering a specific, narrow range of wavelengths. The source lamp is chosen such that the beam is characteristic of electronic transitions in the outer orbitals of the atoms of the sample. In the sample chamber, an aqueous solution of the sample is aspirated into a flame and atomised. If the sample contains the element to be measured, a proportion of the light from the source is absorbed and measured by a detector. The extent of absorption gives a quantitative measure of the concentration of ground state atoms in the sample.

The error in this type of analysis is typically between 1 and 3% ⁽⁷³⁾.

3.7 CHEMISTRY OF THE ELECTROPLATING SOLUTION

The largest problem with electroplating zinc-manganese from the sulphate-citrate bath is the lack of stability of the electrolyte. There is virtually no information about this in either metallurgical or chemical literature. Therefore, it was decided to examine both the solution and the precipitate formed from the bath.

3.7.1 Visual Examination and Bath Deterioration

To compare the effect of time on the standard bath and its component solutions, 1 litre quantities of solutions were produced and observed for a month at natural pH and room temperature. Unless otherwise stated, the solutions were kept open to the atmosphere, and topped up daily to the original volume with double distilled water to account for evaporation.

A detailed list of the solution compositions prepared is given in Table 3.2. To record their appearance, photographs were taken of the freshly made solutions, then again on days 3, 9 and 30. The quantity of precipitate formed was recorded on a comparative scale. The solutions observed were chosen to illustrate the following:

- The deterioration of the standard bath.
- The stability of the constituent solutions of the standard bath, namely zinc sulphate and manganese sulphate, and sodium citrate.
- The effect of variation in the concentrations of each of sodium citrate, zinc sulphate and manganese sulphate in the bath.
- The effect of additions of 2g/l ascorbic acid or 2g/l sodium sulphite on the deterioration of the bath.
- The effect of exclusion of the atmosphere on both the standard bath and baths with such additives, at both room temperature and 50°C.
- The effect of variation of metal salt content in the standard bath.

3.7.2 Effect of Deoxygenation of the Solution

In order to establish the extent of the solution decay caused by aerial oxidation, experiments were performed at room temperature which excluded oxygen from the bath.

The two component solutions used to make up the standard bath were placed in individual porthole beakers connected together with a tube. The system was sealed and the two solutions were deaerated using sintered glass bubblers through which oxygen-free (white spot) nitrogen flowed for two hours. The solutions were then mixed, while still being deoxygenated, and observed.

3.7.3 Ultraviolet and Visible Spectroscopy

Ultraviolet and visible spectroscopy was used to examine the behaviour of the manganese in the solution.

When aged baths were used, the solutions had been left open to the atmosphere and were topped up with distilled water to the appropriate level to account for evaporation. Aged solutions were filtered immediately prior to testing to remove any precipitate.

The tests were performed at room temperature. The following solutions were examined:

- A trace was obtained for aqueous Mn^{2+} ions. The peaks in the trace for a solution of 0.24M manganese sulphate are very low, and at this level there was interference from the background spectrum. So, a fresh solution of 0.48M manganese sulphate was used, at its natural pH of 4.37. This produced the same trace but with larger, more visible peaks.

- Spectra were recorded to show the deterioration of a standard bath over a time period of 30 days.
- The effect of variation in the pH of a solution of manganese sulphate and sodium citrate was investigated. A solution of 0.24M manganese sulphate and 0.6M sodium citrate was compared at pH5.6 and pH6.8.
- The effect of aging on manganese sulphate and sodium citrate solution was examined. Solutions of 0.48M manganese sulphate containing 0.6M sodium citrate at pH5.6 were compared, both freshly prepared and aged for 30 days.

3.8 EXAMINATION OF THE PRECIPITATE

All precipitates examined were produced from an unused standard electroplating bath at natural pH (pH5.6) and room temperature. The baths were aged for one month by exposure to the atmosphere, with the water lost due to evaporation being continuously replenished with distilled water to retain the original volume.

The precipitate was washed in distilled water and air dried before being analysed.

3.8.1 Elemental Analysis of the Precipitate

The precipitate was analysed for metallic and non-metallic elements as described below.

3.8.1.1 Scanning Electron Microscopy

The precipitate was examined using a Jeol 6400 scanning electron microscope. It was mounted on an aluminium disc with an adhesive, conductive carbon disc. It was

gold-coated using an Emscope SC500 Coating Unit to prevent it from charging up when in the microscope. The composition was analysed using the attached Tracor Noran Series II EDX system at a magnification of x5000. Using this technique, it was only possible to analyse for metallic elements. The scanning electron microscope analyses the surface of the specimen to a depth of approximately 1µm to 2µm.

3.8.1.2 Atomic Absorption Spectroscopy

Atomic absorption spectroscopy was performed to ascertain the composition of the precipitate. The precipitate was analysed for zinc and manganese, as well as for sodium which may have been present due to the sodium citrate in the bath. An average of three results was obtained.

3.8.1.3 Microanalysis

Microanalysis was performed using a Perkin-Elmer Model 240B elemental analyser. The percentage of carbon, hydrogen and nitrogen was obtained. This was assessed by combustion of the precipitate in oxygen and the detection of the products carbon dioxide, water and nitrogen by means of a calibrated gas chromatograph. An average of three results was obtained.

3.8.1.4 Titration

The sulphur content was evaluated by burning 5.89mg of the precipitate in oxygen and titrating with 2M barium perchlorate. The gas evolved was absorbed into water and (100 volume) hydrogen peroxide. This method of analysis is relatively precise, with an error of about 0.1% to 2%⁽⁷³⁾.

3.8.2 Structure of the Precipitate

The structure of the precipitate was examined using infrared spectroscopy and ultraviolet and visible spectroscopy.

3.8.2.1 Infrared Spectroscopy

Infrared spectra were obtained for the precipitate from a standard bath and zinc citrate. Approximately 10mg to 15mg of the solid was ground in a small agate mortar with more than ten times its bulk of Analar grade potassium bromide. The mixture was pressed into a disc.

The spectra were scanned in the range 4000cm^{-1} to 400cm^{-1} .

3.8.2.2 Ultraviolet and Visible Spectroscopy

Ultraviolet and visible spectra were obtained for a precipitate from a standard bath which had been aged for 30 days. The precipitate was dissolved in a background matrix of 20% (by volume) nitric acid. 0.9984g of precipitate was added to 3.5cm^3 of the acid.

CHAPTER 4

EXPERIMENTAL RESULTS

4.1 INTRODUCTION

This chapter presents the results obtained using the experimental procedures outlined in Chapter 3. Part One details the outcome of the research on the process of electrodeposition of zinc-manganese and its properties. Part Two presents the investigation of the electroplating bath chemistry.

For ease of reference when viewing the results for any one particular solution, the figures showing the polarisation behaviour, Hull Cell panels and bath deterioration are presented together. All potentials given are values against the Standard Calomel Electrode (SCE) and composition percentages are by weight.

PART ONE – ELECTRODEPOSITION OF ZINC-MANGANESE

4.2 POLARISATION BEHAVIOUR AND HULL CELL PANELS

By altering the potential of the cathode at the low rate of 15mV/min, the polarisation behaviour obtained was accurate with high reproducibility. The use of the Luggin capillary reference electrode positioned very close to the cathode surface and the highly conducting nature of the solution minimised the IR drop between the two electrodes. All polarisation curves were plotted as electrode potential against log current density. In this way, limiting current densities can easily be distinguished.

4.2.1 Standard Bath

4.2.1.1 Related to Coating Appearance and Microstructure

Zinc-manganese coatings produced from a standard bath at current densities up to 70Adm^{-2} using operating conditions of 25°C and $\text{pH}5.6$ were examined visually and using scanning electron microscopy. These results can be related to the polarisation behaviour of the bath.

The microstructures of the coatings are shown in Figures 4.1 to 4.10. Intermediate structures are produced between the specific structures detailed below. The porosity of the coatings was low. For example, analysis showed only 1.60% of iron from the exposed substrate in a coating produced at a current density of 15Adm^{-2} and 1.47% at 20Adm^{-2} .

The total polarisation curve for zinc-manganese electrodeposition from a standard bath using standard operating conditions of 25°C and $\text{pH}5.6$ is shown in Figure 4.11. Five regions, labelled A to E, can be identified and related to the coatings produced as described below. The appearance of the range of coatings produced between 0.15Adm^{-2} and 15Adm^{-2} can be seen on the photograph of the Hull Cell panel produced from a fresh standard bath (Figure 4.12).

An attempt was made to identify the microstructures shown in Figures 4.1 to 4.10 using x-ray diffraction, but it was found to be difficult to identify the peaks. The data could not be matched in a database⁽⁴⁸⁾ as no zinc-manganese metal information was available, and it was impossible find a match with any particular oxides. The technique suggested by Eyraud et al⁽³⁷⁾ of comparing the x-ray diffraction pattern with those for the isostructural zinc-iron alloys was unsuccessful, as was creating a pattern using known crystal parameters⁽⁴⁷⁾⁽⁷⁴⁾⁽⁷⁵⁾ using CaRine Crystallographie Version 3.0 (Compiègne, France).

Region A - No Electrodeposition

Between -600mV and -1150mV, Figure 4.11 exhibits a “nose”. Specimens electroplated in this region at -850mV and -1050mV had the same visual appearance as the mild steel substrate. Examination of the cleaned substrate and these two specimens under the scanning electron microscope confirmed that no metal was electroplated at either of these potentials (Figures 4.1 and 4.2).

Region B - Zinc-Rich Coatings

Zinc electrodeposition occurs at potentials lower than -1150mV. From -1150mV to -1200mV (with corresponding current densities up to 0.6Adm^{-2}), matt, mid blue-grey deposits are produced. The manganese content of the coating increases with current density up to 2.20% at 0.6Adm^{-2} . Within this region, a specimen produced at a current density of 0.15Adm^{-2} (Figure 4.3a) reveals a key structure comprising hexagonal platelets. The composition of this is almost entirely zinc, with only 0.36% manganese.

Region C - Limiting Current for Zinc-Rich Coatings

A limiting current region for zinc deposition occurs at potentials between -1200mV to -1550mV, with corresponding current densities of 0.9Adm^{-2} to 1.5Adm^{-2} . These coatings have higher manganese contents of between 12.79% and 16.08%. The deposit is semi-matt silver and comprises irregular nodules typical of those shown in Figure 4.4c) at 1.5Adm^{-2} , which contains 16.08% manganese.

Region D - Zinc-Manganese Alloys

Between -1550mV and -1800mV (at current densities over 1.5Adm^{-2}), zinc-manganese alloys with higher manganese contents between 18.41% and 44.10% are produced. At 3Adm^{-2} , the matt silver deposit comprises angular, pyramidal nodules as shown in Figure 4.5b) which has a composition containing 24.62% manganese.

At current densities up to about 3.75Adm^{-2} , the nodules are of the order of approximately $1\mu\text{m}$ in size and examination of the coating at a lower magnification shows it to be relatively flat. At 3.75Adm^{-2} , the coating is cracked and some raised nodules are observed in the structure at low magnifications (Figure 4.5c)).

At 9Adm^{-2} , the coating is matt silver-grey and the structure is large, round nodules approximately $4\mu\text{m}$ in diameter. A peak manganese content of 44.1% is observed in the dull grey coating at 15Adm^{-2} (Figure 4.7b)), with the nodules being covered with small, spiky crystallites.

At potentials below -1680mV and the corresponding current densities higher than 15Adm^{-2} , the coating becomes of less interest to the practical electroplater. Above this value, the manganese content of the alloy decreases and the coating is matt dark grey or black (“burnt”) and powdery. The nodular structures grow around the gas bubbles evolved during electroplating, producing the microstructure shown for 30Adm^{-2} in Figure 4.8a). The nodules, as observed in Figure 4.8c) for 40Adm^{-2} , are relatively manganese-rich (37.12% manganese), with the dendritic coating in the holes being relatively zinc-rich with only 17.41% manganese. By 50Adm^{-2} less manganese-rich nodules are observed (Figure 4.9a)), and by 70Adm^{-2} (Figure 4.10) the cracked coating consists almost entirely of the dendritic structure seen in the holes at 40Adm^{-2} .

Region E - Limiting Current for Zinc-Manganese Alloys

The electrodeposition of the zinc-manganese alloys reaches its limiting current at potentials below -1800mV .

4.2.1.2 Related to Cathode Current Efficiency

The cathode current efficiency of the coatings and the manganese content for deposition from a standard bath under standard conditions are shown in Figures 4.13 and 4.14 respectively.

Increase in manganese content is accompanied by decrease in cathode current efficiency, which is observed as increased hydrogen production during electroplating. At the maximum useful current density of 15Adm^{-2} , the highest manganese content of 44.1% was recorded but the cathode current efficiency for metal deposition is only 35%. This value of cathode current efficiency is almost constant at current densities above 15Adm^{-2} .

At current densities of 15Adm^{-2} and above, there was violent agitation of the solution in the vicinity of the electrodes due to gas evolution from both the anode and the cathode.

Figure 4.14 also shows the composition of $7.5\mu\text{m}$ thick coatings produced on full Pyrene panels at 15Adm^{-2} and 20Adm^{-2} . The compositions are slightly lower for the Pyrene panels than for the 0.5cm^2 discs, but the discs were found to be relatively representative of larger scale coatings providing compositional analysis and microstructure examination were performed at the centre rather than the edges of the disc. Edge effects on disc specimens were found to be negligible at low current density in terms of appearance and composition. At high current densities they were exaggerated, but usually only extended into the specimen by about 1mm.

4.2.2 Effect of Variation in Operating Conditions

The effect of variation in bath composition and operating conditions from those used in a standard bath on the total polarisation behaviour of the zinc-manganese system and the appearance of the coatings is described below. The results can be compared with the total polarisation behaviour of the standard bath shown in Figure 4.12 and

the Hull Cell panel for a fresh bath in Figure 4.13. The deterioration of the bath during polarisation tests was noted.

In Hull Cell tests, ideally temperature should remain constant. Under the operating conditions employed in this research, it was found that the temperature increased by approximately 2°C during the experiment.

4.2.2.1 Effect of Sodium Citrate on Zinc Electrodeposition

Figure 4.15 shows the effect of sodium citrate on the polarisation curve for zinc electrodeposition from a sulphate bath. The sodium citrate alters the curve in three ways. Firstly, the shape of the “nose” in Region A where no electrodeposition occurs is altered, and is moved to higher current densities. Secondly, the potential at which zinc electrodeposition commences is lowered slightly from -1073mV to -1162mV when sodium citrate is present (Region B). Thirdly, in the presence of sodium citrate, a limiting current is apparent at 1Adm⁻² (Region C) and, at higher current densities, the polarisation curve is lowered to a constant potential value of -2150mV.

There was no discolouration of the clear solution during electroplating from the bath, either with or without sodium citrate.

The appearance of zinc electrodeposited from these two baths is shown in the Hull Cell panels on Figure 4.16. As observed in the polarisation behaviour, the major difference caused by the addition of sodium citrate is at the higher current densities where substantial hydrogen evolution occurs. Here, the sodium citrate addition results in a more even, less dendritic, less “burnt” coating without the white gelatinous precipitate observed in the Hull Cell panel for sodium sulphate and zinc sulphate alone.

4.2.2.2 Effect of Sodium Citrate on Manganese Electrodeposition

The polarisation behaviour and appearance of Hull Cell panels for solutions of manganese sulphate and sodium sulphate, with and without sodium citrate, are shown in Figures 4.17 and 4.18 respectively.

Without sodium citrate, large quantities of black-brown and white gelatinous precipitates were produced during electroplating. These precipitates were deposited on the Hull Cell panel as can be seen in Figure 4.18, but no manganese metal was deposited. The form of the polarisation curve is a straight line.

With the sodium citrate, a brown coating was produced at the high current density end of the Hull Cell. This darkened rapidly once it was removed from the electroplating bath. This deposit is produced at potentials below -1610mV , which coincides with a change in the shape of the polarisation curve. There was vigorous gas evolution from the panel even after the circuit was disconnected, possibly implying chemical dissolution of any coating deposited.

4.2.2.3 Effect of Sodium Citrate on Zinc-Manganese Electrodeposition

The effect of sodium citrate on the electrodeposition of zinc and manganese together can be seen in the polarisation curves of Figure 4.19 and the Hull Cell panel in Figure 4.20.

Electroplating from a solution of zinc sulphate and manganese sulphate in the absence of sodium citrate gives a combination of the individual effects described above for the zinc or manganese baths without sodium citrate. The gelatinous precipitates observed with attempted manganese deposition are produced in the bath. The polarisation behaviour and appearance on a Hull Cell panel is very similar to those for zinc sulphate with sodium sulphate. (A comparison of the two polarisation curves can be made in Figure 4.15, and between the Hull Cell panels in Figures 4.16 and 4.20.)

These observations indicate that, in agreement with results for the separate baths above, only zinc is being electrodeposited from the alloy bath without the citrate but not manganese.

Figure 4.19 shows the effect of adding sodium citrate to produce a standard bath. At the “nose” (Region A) and in the zinc deposition region of the graph (Regions B and C), the curves themselves and the changes observed are almost identical to those seen in Figure 4.15 which shows the effect of sodium citrate on zinc electrodeposition alone.

In the alloy region of the polarisation curves (Region D), the presence of the sodium citrate allows manganese to be electroplated together with zinc as an alloy at potentials below -1550mV . Addition of the sodium citrate completely changes the appearance of the Hull Cell panel, as can be seen by comparing that for the standard bath (Figure 4.12) with the panel for the zinc sulphate and manganese sulphate bath (Figure 4.20). The presence of the sodium citrate allows a sound deposit to be produced over a wide range of current densities.

4.2.2.4 Constituent Solutions of a Standard Bath

The role of each of the individual components of a standard bath as electroplated from baths containing sodium citrate can be seen in Figure 4.21. (In this diagram, the effect of sodium citrate on zinc electrodeposition is taken from Figure 4.15 above, and on manganese electrodeposition from Figure 4.17.)

Comparison between the red and black lines in Figure 4.21 shows that addition of manganese sulphate to the bath does not alter the polarisation behaviour for zinc electrodeposition from a bath containing sodium citrate (Regions A and B). The presence of manganese in the standard bath does, however, slightly increase the limiting current density observed in Region C.

From the standard bath, zinc-manganese metal is deposited in Region D at potentials below -1550mv. The curve in this region is observed to be at higher potentials than the graphs for the individual baths containing sodium citrate with either zinc or manganese sulphate. Whereas zinc-manganese alloy can be electroplated in this region, no metal is deposited from either of the individual baths.

Obviously the line for 0.48M sodium sulphate and 0.6M sodium citrate does not show metal deposition, but has been included to show the polarisation behaviour of secondary electrode reactions in the presence of sodium citrate. Hydrogen evolution accompanied alloy electrodeposition from the standard bath throughout Region D, at current densities above the limiting current density for zinc electrodeposition (Region C). This was particularly vigorous at current densities above 15Adm^{-2} .

4.2.2.5 Effect of pH

The effect of pH on zinc-manganese electrodeposition from a standard bath is shown in Figures 4.22 and 4.23. The polarisation behaviour could only be assessed for pH values below that of the standard bath due to the problems with raising the solution pH as described in Section 4.3.2. The assumption made in Section 3.4.1 that it was valid to compare polarisation results obtained at pH5.0 and pH5.6 is justified in Figure 4.22, since the curves at both values are similar. The colour of the solution became lighter with decreasing pH.

Figure 4.22 shows that pH has a large effect on all regions of the polarisation behaviour of zinc-manganese electrodeposition from the standard bath. The lower the pH, the higher the current density required to polarise the cathode. In the region where zinc is electrodeposited (Regions A and B), the form of the polarisation curve is relatively unaffected by pH, although its position varies. With progressive increase in pH, the “nose” (Region A) is moved to lower current densities, and the potential at which zinc deposition begins becomes more negative.

Lowering the pH also moves the potentials at which the alloy can be electroplated from the bath (Region D). The higher the pH, the lower the potential.

The Hull Cell panels in Figure 4.23 show a successive shift with pH in the position of the electroplated alloys from the standard bath, comparable with the observations of the polarisation behaviour. Vigorous evolution of gas was observed during electroplating in the bath of pH3.0 at the high current density end of the panel.

4.2.2.6 Effect of Sodium Citrate Content

The effect of varying the sodium citrate content of the bath on the polarisation behaviour is shown in Figures 4.24 and 4.25. A concentration of 0.48M sodium citrate supplies the same quantity of citrate ions to the solution as metal ions. An increase in sodium citrate concentration progressively moves both the position of the “nose” to higher current densities and lowers the potential at which zinc deposition commences (Region A). The limiting current density in Region C is progressively lowered, and the potentials over which alloy deposition occurs (Region D) decrease.

Figure 4.26 shows Hull Cell panels for baths with a sodium citrate content of 0.2M and 1.0M. These can be compared with that for the standard bath (0.6M sodium citrate) shown in Figure 4.12. At a sodium citrate concentration of 0.2M, the low current density region on the panel does resemble that of the standard bath. However, at higher current densities the coating looks similar to that observed in Figure 4.16 on the panel for a bath containing 0.24M sodium sulphate, 0.24M zinc sulphate and 0.6M sodium citrate. For 1.0M sodium citrate, the low current density region again resembles that for the standard bath. At high current densities where the zinc-manganese alloy would be expected, the coating appears very “burnt”.

4.2.2.7 Effect of Zinc Sulphate Content

The effect of variation in zinc sulphate content of the standard bath on the polarisation behaviour can be seen in Figures 4.27 and 4.28. An equal number of citrate and metal ions is provided in solution at a zinc sulphate concentration of 0.36M. Increase in zinc sulphate content lowers the current densities at which the “nose” is observed (Region A), and progressively moves the potential at which metal deposition starts to less negative values. Increase in zinc sulphate concentration also lowers the limiting current density for zinc deposition (Region C), and at a concentration of 0.024M this feature is not observed. It also moves the potentials at which alloy is deposited to less negative values (Region D).

The Hull Cell panels produced at 0.12M and 0.48M zinc sulphate are shown in Figure 4.29 and can be compared with that for the standard bath in Figure 4.12. The three panels are very different in appearance, in particular at the low current density end at which zinc electrodeposition predominates.

The manganese sulphate content was fixed in these tests. However, at constant pH5.0, the higher the zinc sulphate content, the paler orange the solution was at the start of the test and the more difficult it was to alter the pH. No precipitate is produced during tests with up to 0.12M zinc sulphate. At concentrations above this, the precipitate quantity increases with zinc sulphate content. The discolouration of the bath during electroplating increased with zinc sulphate content.

4.2.2.8 Effect of Manganese Sulphate Content

The effect of manganese sulphate content on the polarisation behaviour of the standard bath is shown in Figures 4.30 and 4.31. For an equal proportion of citrate ions as metal ions to be present, the bath needs to have a manganese sulphate concentration of 0.36M. These curves were difficult to reproduce.

In the same manner as for increase in zinc sulphate, increase in manganese sulphate content moves the position of the “nose” to lower current densities (Region A). However, the potentials at which zinc is deposited from the bath is relatively unaffected by manganese content (Region B). Providing some manganese sulphate is present, increase in manganese sulphate content up to 0.24M increases the limiting current density for zinc deposition (Region C), but has relatively little effect on the region of the curve where the alloy is deposited (Region D). This is a converse pattern to that observed with zinc sulphate content. At concentrations greater than 0.24M, no further change in the limiting current density is observed in Region C, but the potentials at which the alloy is deposited in Region D become progressively less negative.

The Hull Cell panels for variation in manganese sulphate content are shown in Figure 4.32 and can be compared with that for the standard bath in Figure 4.12. At the low current density end where zinc electrodeposition predominates, the panels are relatively similar. In the region where the alloy is electroplated, the width of the panel covered by dark coating increases with manganese content of the bath.

With no manganese sulphate present, no discolouration occurs in the clear solution during electroplating. The orange colour of the fresh solutions became darker with increased manganese sulphate content. The bath containing 0.12M manganese sulphate was very pale orange, but after electroplating became dark orange and a hard and dendritic precipitate was produced. At 0.48M manganese sulphate, the solution was dark but was more pink than orange, and chrysanthemum-like balls of metal were deposited. A precipitate was produced in all baths at manganese sulphate contents above 0.12M.

4.2.2.9 Effect of Metal Salt Content

The ratio of zinc to manganese salts in this series of tests was fixed at 1:1 as in the standard bath. An equal quantity of citrate ions and metal ions are present in solution at a ratio of 0.3M:0.3M.

The results of the polarisation behaviour for these baths can be seen in Figures 4.33 and 4.34. In Region A and B, increase in metal salt content in the bath follows the same trend as increase in zinc sulphate concentration. That is to say, increase in metal salt content moves the “nose” to lower current densities and the potential at which zinc electrodeposition starts to less negative potentials. The metal salt content does have a relatively large effect on the limiting current density for zinc electrodeposition (Region C), with a progressively higher current being observed with increase in metal salt concentration. A marked effect is also seen in the alloy deposition region (Region D), where increase in metal salts results in a shift in the deposition potentials to less negative potentials.

Hull Cell panels for metal salt ratios of 0.12M:0.12M and 0.48M:0.48M are presented in Figure 4.34. These can be compared with that for the standard bath of metal salt ratio 0.24M:0.24M in Figure 4.12. The appearance of the deposit on each of the panels is similar, allowing for the shift in the current densities observed in the polarisation behaviour in Figure 4.33. Vigorous gas production was observed across the whole Hull Cell panel during the testing of the 0.12M:0.12M bath. Relatively little gassing was observed during the Hull Cell test of the 0.48M:0.48M bath.

Precipitates were produced at all metal salt concentrations above 0.12M:0.12M. All solutions, including this bath, were dark orange at end.

4.2.2.10 Effect of Additions

Ascorbic acid and sodium sulphite were added to the bath for their antioxidant properties in an attempt to decrease the effects of any deterioration of the bath caused by oxygen.

The effect of these additions on the polarisation behaviour of the zinc-manganese standard bath are shown in Figure 4.35. Ascorbic acid does not appreciably alter the curve. Nor does it alter the appearance of a Hull Cell panel. This can be seen by comparing that for a fresh standard bath (Figure 4.12), with that for a similar bath with the ascorbic acid addition (Figure 4.36).

However, sodium sulphite does have some effect on the zinc electrodeposition region of the polarisation curve. This is seen as an alteration in the shape of the “nose” (Region A). The “nose” occurs at similar potentials but at lower current densities than in the standard bath. Zinc electrodeposition (Region B) occurs from a slightly lower potential of -1200mV , and this process limits at a higher current density of 2.5Adm^{-2} (Region C). Correspondingly, there is also a change in the appearance of the Hull Cell panel (Figure 4.37). In comparison with that for the standard bath (Figure 4.12), the deposits are much darker and less silver in colour when the additive is present.

In a standard bath with an addition of 2g/l ascorbic acid, there was no discolouration of the solution during electroplating. Conversely, a bath with 2g/l sodium sulphite discoloured in a similar manner to the standard bath, but not to such a degree. During electroplating, hydrogen sulphite was released from the bath due to breakdown of the addition. On standing for several days, the discolouration in this bath diminished, but it did not return to the original colour.

4.2.2.11 Effect of Aging a Standard Bath (With and Without Additions)

The effect of bath aging on the polarisation behaviour of zinc-manganese electrodeposition from a standard solution, both with and without additions of 2g/l ascorbic acid or 2g/l sodium sulphite, was evaluated.

In a standard bath without additions, aging for 30 days had virtually no effect on the polarisation behaviour (Figure 4.38). However, the Hull Cell panel did reveal darker and less silver-coloured electroplate in the aged bath (Figure 4.12). The aged standard bath was dark orange and darkened further during the polarisation experiment.

As described in Section 4.2.2.11, the fresh standard bath both with and without a 2g/l ascorbic acid addition showed comparable results. In a similar manner, as with the standard bath, aging for 30 days had no appreciable effect on the on the polarisation behaviour of the bath containing 2g/l ascorbic acid (Figure 4.39), but the appearance of the Hull Cell panel was darker and less silver-coloured (Figure 4.36). The bath containing ascorbic acid was dark straw coloured, and no discolouration was observed during the test.

The effect of aging a standard bath with a 2g/l sodium sulphite addition can be seen in Figure 4.40. As with the fresh bath, the polarisation curve is altered in the zinc electrodeposition regions. Aging moves the “nose” (Region A) to higher current densities than in the fresh bath, and reduces the limiting current density for zinc electrodeposition (Region C) to lower current densities. The Hull Cell panels for both the fresh and aged bath are identical (Figure 4.37), allowing for the shift in the limiting current density for zinc electrodeposition as observed in the polarisation curves.

With sodium sulphite added, the aged bath was pale pink and with virtually no change from the fresh bath. However, during the polarisation test it darkened in a similar manner to the standard solution.

4.2.2.12 Effect of Repeated Use of the Standard Bath

An electroplating bath is rarely replaced after every test, as was the case in this research. In order to give an indication of the effect on the polarisation behaviour

which would be caused by continuous use of the solution, a standard bath was subjected to repeated tests. The results are shown in Figure 4.41.

No change was observed in the regions of the curve where metal deposition occurs. However, the current density at which the “nose” occurred in Region A was increased successively with each repeat test.

4.2.2.13 Effect of Separating the Anode and Cathode

Separating the anode and the cathode in the electroplating cell had no effect on the polarisation behaviour of the standard bath in the regions of the curve where metal deposition occurs (Figure 4.42). However, a decrease in the current density at which the “nose” occurs was observed in the bath with the separated electrodes (Region A).

During the polarisation test, the anolyte became dark, bright orange with an end value of pH3.9, and the catholyte became straw yellow with an end value of pH5.4.

4.2.2.14 Effect of Oxygen Content

The polarisation behaviour of a bath deoxygenated with oxygen-free nitrogen is shown in Figure 4.43. The effect of deoxygenating the solution was to lower the current density at which the “nose” and the limiting current density for zinc electrodeposition occurred (Regions A and C respectively). No effect was seen in the regions of the curve concerned with metal deposition.

Discolouration still occurred in the bath due to oxygen production at the anode during alloy deposition.

PART TWO – CHEMISTRY OF THE ELECTROPLATING BATH

4.3 THE ELECTROPLATING BATH

4.3.1 Preparation of the Bath

Problems were encountered when preparing the electroplating bath by the usual method of dissolving all the salts in the distilled water. The large quantity of salts in the bath, in particular the sodium citrate, were difficult to dissolve. During the time taken to make up the bath, even with agitation, the bath would start to discolour. If the temperature was raised to speed up the dissolution, the solution discoloured to an even larger extent. The solution then needed to be cooled to room temperature before the volume could be altered to the precise value and experiments could commence. This resulted in further decay.

The bath could not be made up and stored in its entirety, as is common practice in electroplating. Over time the bath continued to discolour and a precipitate formed. Therefore, the method of mixing the bath from solutions of double concentration was developed. The sodium citrate solution and the solution of manganese sulphate and zinc sulphate could be stored separately successfully for long time periods. There was no discolouration or precipitation. They could be mixed cold immediately prior to experimentation with minimum decay.

The exception to this was the sodium citrate solution containing ascorbic acid. This was pale straw yellow when immediately made up but darkened over a period of time. This was, therefore, made up and used immediately unless an aged solution was required.

4.3.2 General Observations on Operating Conditions

It was found that it was very easy to raise the pH of baths which did not contain sodium citrate by using 10% (by volume) sulphuric acid. If the citrate was added, an increased volume of acid was required. Alteration of the pH became progressively more difficult with increasing sodium citrate content of the bath. Also, a large pH drop would be observed during electroplating in solutions which did not contain sodium citrate. During a polarisation test, the zinc sulphate and sodium sulphate bath exhibited a drop from pH5.6 to pH1.9, the bath containing manganese sulphate and sodium sulphate from pH5.6 to pH2.3, and the zinc sulphate and manganese sulphate solutions from pH5.0 to pH1.3. However, for a citrate containing bath, a typical pH drop was from pH5.6 to pH5.4.

While the bath pH could easily be made more acidic, problems were encountered when attempting to make it more alkaline. When adding 20% sodium hydroxide solution, a white precipitate formed in the bath. This could not be incorporated, even with vigorous agitation. Ammonia solution could be used but a large quantity was needed. This was not desirable since it altered the composition of the bath by adding significant quantities of ammonium ions.

The pH of the bath was found to be stable with time.

4.4 DETERIORATION OF THE BATH

4.4.1 Standard Bath

The solution of the zinc and manganese sulphates in distilled water was pale pink, and the sodium citrate solution was colourless (see Figure 4.20). As shown in Figure 4.12, immediately on mixing, the colour became very pale orange (Day 1). Over time this continued to deepen to dark orange.

At room temperature, a very pale pink, almost white precipitate started to fall from the bath after about three days as a fine powder. This fell to the bottom of the bath

and over time formed a hard, solid, crystalline layer. As seen in Figure 4.12, after 30 days a moderate amount (Level D) of precipitate was observed. This decay was found in both worked and unworked baths.

4.4.2 Effect of Variation in Bath Composition

The effect of varying the solution composition on the deterioration of the bath was studied. These results are grouped with those for the polarisation behaviour and the Hull Cell tests for the same baths (within Figures 4.12 to 4.45). The discolouration is recorded as photographs of the baths taken on days 1, 3, 9 and 30. The degree of precipitation is described using a scale of A (none) to F (very heavy). A summary of the results is given in Table 4.1.

4.4.3 Effect of Deoxygenation of the Solution

The effect of exclusion of the atmosphere is shown in Figures 4.44 and 4.45, with a summary given in Table 4.1. Raising the temperature of solutions in sealed bottles to 50°C for 30 days showed a decrease in discolouration in the standard bath, and less precipitation was observed.

Placing a lid on a dark orange aged bath caused it to slowly become lighter in colour.

When fresh solutions deoxygenated with nitrogen were mixed, no colour change occurred. Over time this continued to be the case. A pale pink, almost white precipitate was formed in a similar manner to the standard bath left open to the atmosphere. This occurred at a faster rate than in the standard solution. The continuous bubbling of nitrogen through the solution caused agitation which may be responsible for this observation.

4.5 CHEMISTRY OF THE ELECTROPLATING SOLUTION

4.5.1 Ultraviolet and Visible Spectroscopy

The graphs for ultraviolet and visible spectroscopy show the absorbance or optical density (no units) of the solution as a function of wavelength (in nm). The absorbance is given as $\log (A_o/A_T)$, where A_o and A_T are the intensities of the incident and transmitted light respectively.

Usually in ultraviolet and visible spectroscopy, the molar absorption (or extinction) coefficient of the solute, ϵ , is calculated from the absorbance values, and an ϵ (or $\log \epsilon$) versus wavelength or wavenumber graph is shown. The intensity, A_T , of a beam of light that is passed through a solution is related to the concentration, c , of the solute by the Beer-Lambert Law, such that

$$\log \left(\frac{A_o}{A_T} \right) = \epsilon \cdot c \cdot l \quad (\text{Equation 4.1})$$

where l is the thickness (path length) of the absorbing solution in cm. When c is in mol/l and l is in cm, ϵ is defined as the molar absorption coefficient (or extinction coefficient) of the solute. It has units of $1000\text{cm}^2\text{mol}^{-1}$ but the units are, by convention, never expressed.

To do this requires precise knowledge of the concentration of the compound in solution. In this research, due to bath instability and precipitation, the precise composition and nature of the solution is not always known so these calculations cannot be done. However, such conversions are unnecessary here since the aim of these experiments was to provide qualitative information about the changes occurring in solutions. This can be obtained from the wavelength of the absorption peaks and their relative absorbance values as shown on the graph, so calculations of the more precise molar absorptions are unnecessary.

In this research, the spectrum peaks are small showing low absorbance values because the solutions were relatively weak for use in this technique. However, the shape of the spectra are clear and comparable.

In the region below 250nm, large peaks are observed. These are due to charge transfer reactions between metal and ligand. This is less interesting than the spectra in the visible region at higher wavelengths, where the peaks give information about the metal ion. The spectra only give information about the manganese in the solution.

Please note that when comparing Figures 4.46 to 4.50, the y-axis scales are not identical. It was very difficult to judge the level of absorbance for different solutions so that results could consistently be captured on the same scale. This was particularly a problem with the aged solutions which were tested over a lengthy time period, where the level of absorbance changed to a large degree. The spectrum for each solution was captured at several scales in an attempt to provide comparable results, but this has not always been successful. The best comparisons have been shown.

The results from ultraviolet spectroscopy and visible are shown in Figures 4.46 to 4.53.

- The spectrum shown in Figure 4.46 obtained for 0.48M manganese sulphate solution shows absorbance peaks at the following positions:

	Band Position							
Wavelength / nm	248	314	336	358	396	402	434	532

- If 0.6M sodium citrate is added to 0.48M manganese sulphate solution, similar absorbance peaks are observed to those in the bath above (Figure 4.47) at:

	Band Position				
Wavelength / nm	356	402	406	428	524

If this solution is aged for 30 days, the resulting spectrum is seen in Figure 4.47 to exhibit a large absorbance peak at 430nm. There appears to be two peaks at approximately 464nm and 520nm which are very difficult to distinguish, together with a broad peak at 740nm. The absorbance values are much higher than for a fresh solution.

- The deterioration of a standard bath over a time period of 30 days is shown in Figures 4.48 and 4.49. On Day 1, absorbance peaks are observed at similar wavelengths as in the bath above containing 0.48M manganese sulphate solution:

	Band Position					
Wavelength / nm	336	356	403	406	430	532

Over time, the spectrum changes and two absorbance peaks at 440nm and 470nm become progressively more dominant. It is difficult to distinguish, but the spectrum may contain further peaks at:

	Band Position			
Wavelength / nm	406	440	452	470

- The effect of variation in the pH of a solution of 0.24M manganese sulphate and 0.6M sodium citrate is shown in Figure 4.50. At both pH5.6 and pH6.8 the absorbance peaks are at the same positions as in the similar solution containing 0.48M manganese sulphate as described above and shown in Figure 4.47. The peak heights are higher at increased pH.

4.6 EXAMINATION OF THE PRECIPITATE

4.6.1 Elemental Analysis of the Precipitate

The results of analysis of this precipitate for metallic and non-metallic elements are given in Table 4.2. The EDX system attached to the scanning electron microscope detected only zinc and manganese. The percentages shown for this technique are relative to each other, unlike the other results shown which are as a proportion of the whole compound.

4.6.2 Structure of the Precipitate

The infrared spectroscopy was carried out in order to determine the structure of the precipitate. The ultraviolet and visible spectroscopy was performed to assess the oxidation state of the manganese in it.

4.6.2.1 Infrared Spectroscopy

The infrared spectrum obtained for zinc citrate is shown in Figure 4.51. Bands of importance are labelled from A to F on the diagram. These are:

- A. A band at 3500cm^{-1} .
- B. A broad band between 2500cm^{-1} and 3335cm^{-1} .
- C. The band at 2940cm^{-1} , with a jagged series of bands on the low frequency side.
- D. The two bands between 1550cm^{-1} and 1610cm^{-1} , and 1300cm^{-1} to 1420cm^{-1} .

E. The bands near 1430cm^{-1} .

F. The band at 1250cm^{-1} .

The infrared spectrum for the precipitate from a standard bath aged for 1 month is shown in Figure 4.52. This is of similar form to the spectrum for zinc citrate, but differs in that the regions A, B and C are masked by a large peak. Regions D, E and F are visible.

4.6.2.2 Ultraviolet and Visible Spectroscopy

Figures 4.53 show the spectrum for the precipitate from a standard bath aged for 1 month at room temperature. It is similar in form to the spectrum shown in Figure 4.47 for 0.48M manganese sulphate and 0.6M sodium citrate solution. Absorbance peaks occur at the following positions:

	Band Position			
Wavelength / nm	396	401	428	530

To obtain these results, the precipitate was dissolved in 20% (by volume) nitric acid. Nitric acid is a strong oxidising agent and it could have increased the oxidation state of the manganese and, hence, masked the true oxidation state in the precipitate. However, since the results show a low oxidation state spectrum, the nitric acid was found not to affect the results and was deemed a suitable matrix for the test.

CHAPTER 5

DISCUSSION

The results presented in Chapter 4 are discussed in three parts. Part One relates to the process of zinc-manganese electrodeposition. In particular, the role of sodium citrate and zinc in promoting alloy deposition will be discussed. In Part Two, the deterioration of the bath by discolouration and precipitation is discussed in terms of the chemistry of the solution. The final section, Part Three, will summarise the effect of variation in bath composition and operating conditions on the electrodeposition of zinc-manganese, and guidelines will be given for an improved sulphate-citrate electrolyte.

PART ONE – ELECTRODEPOSITION OF ZINC-MANGANESE

5.1 INTRODUCTION

It is proposed that the primary role of sodium citrate in the electrodeposition of zinc-manganese alloy is not to act as a complexant in the usual manner by moving the deposition potentials of the individual metals together to allow alloy coatings to be produced. Instead, its action as a buffer resisting pH changes at the cathode surface and suppressing hydrogen reduction can be used to explain the observed polarisation behaviour of zinc-manganese electrodeposition from the sulphate-citrate bath.

Furthermore, it is thought that zinc must be present in the bath along with sodium citrate for manganese to be deposited in an appropriate form. An explanation will be given for this observation.

5.2 THE ROLE OF CITRATE IN SOLUTION

In a bath without sodium citrate, the zinc and manganese ions are hydrated. That is, they are attached to water molecules by co-ordinate bonds in a solvation sheath. As can be seen from the Hull Cell panels shown in Figures 4.16, 4.18 and 4.20, zinc metal can be electroplated from such a simple salt solution at potentials more negative than -1075mV (vs SCE) (Figure 4.15), whereas manganese metal cannot be deposited at all.

If sodium citrate is added to these individual baths, the potentials below which the metals can be deposited are -1150mV (vs SCE) for zinc (Figure 4.15) and -1550mV (vs SCE) for manganese (Figure 4.17). In order to electroplate two such metals from an alloy bath, it would be usual to move these two potentials together to allow them to be co-deposited. One method of achieving this is by changing the concentration of the salts in the bath. From the Nernst equation (Equation A6.4), the electrode potentials could be brought together by lowering the concentration of zinc in the bath, or increasing the concentration of manganese. This effect is observed in the Tafel regions for zinc deposition in Figures 4.27 and 4.28, and for manganese deposition in Figures 4.30 and 4.31. However, this does not provide the required shift and, indeed, the Nernst equation predicts that a change in divalent ion concentration to a hundred times the original would only move the potential of the electrode by 60mV .

5.2.1 Citrate as a Complexant

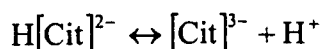
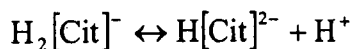
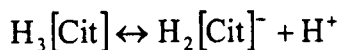
In alloy electroplating, another method which is often employed for moving the potentials closer together is the addition of a complexant to the bath. The complexant may associate with one or both types of metal ions present, and one or more of the water molecules surrounding the ions are replaced by the alternative ligand ions. Sodium citrate is reported in the literature as being added to the zinc-manganese bath as a complexant ⁽²²⁾⁽²³⁾⁽²⁶⁾⁽²⁷⁾⁽²⁹⁻³⁴⁾⁽³⁶⁾⁽³⁷⁾.

It is known that both zinc and manganese form a 1:1 complex with citrate in solution ⁽⁷⁶⁾. The colour change from pale pink to pale orange observed when mixing the constituent solutions of the standard bath is an indication that a complex is formed ⁽⁷⁷⁾. The total metal ion concentration in the standard bath is 0.48M. Therefore, in a standard bath containing 0.6M sodium citrate, there is sufficient citrate ions to complex all of the metal ions with 0.12M of free complexing agent. The relationships between the polarisation behaviour and concentrations of zinc sulphate, manganese sulphate and sodium citrate described below are followed for bath compositions up to a 1:1 ratio of metal ion to complexant. A limit to the trend will often be observed at the concentration at which this ratio occurs.

In a standard bath (Figure 4.15), the presence of sodium citrate does move the deposition potential for zinc closer to that of manganese but only by the relatively insignificant value of 75mV. Furthermore, increase in sodium citrate content shifts both the potentials for zinc and manganese deposition to more negative potentials (Figures 4.24 and 4.25), since both metals are complexed in solution by the citrate ions. Therefore, clearly in the case of zinc-manganese electrodeposition, the primary method by which sodium citrate promotes alloy deposition from the bath is not by moving the deposition potentials of the individual metals closer together.

5.2.2 Citrate as a Buffer

Citric acid, hydrated $C_6H_8O_7$, is a tricarboxylic acid (2-hydroxypropane-1,2,3-tricarboxylic acid). Three forms of its salts may be found in aqueous solution by disassociation of its acid groups:



In addition, further hydrogen ions can be supplied by disassociation of the hydroxyl group. When its sodium salt is added to the electroplating bath, it will dissociate completely. The citrate ion will then combine with H^+ ions to form weakly dissociated citric acid as above until all the citrate ion is exhausted.

The citric acid limits variation in the pH of the solution by equalising changes in the hydrogen ion concentration by this disassociation behaviour. Hence, the combined effect between the acid and the salt acts to buffer the solution ⁽⁷⁸⁾. The buffering ranges of the individual stages of dissociation link up such that a buffering range is obtained which extends from pH2 to above pH12, as can be seen in Figure 5.1. Baths containing sodium citrate were indeed found to be buffered, since it was difficult to alter the pH using sulphuric acid and the pH drop during electroplating in such electrolytes was small.

From Figure 5.1, the predominant species in the standard electroplating bath at pH 5.6 will be the dihydrogen citrate. Due to the buffering effect, the pH of the solution will not change substantially until either sufficient hydrogen or hydroxyl ions are added to alter the concentration of the various species present in the bath.

Figure 4.17 compares the polarisation of manganese sulphate both with and without sodium citrate. Without the citrate buffer, hydrogen is formed by the hydrolysis of water with a Tafel slope of 164mV/decade. However, in the presence of sodium citrate, water molecules are not hydrolysed and hydrogen ions are supplied for hydrogen evolution by the conversion of the dihydrogen citrate ions to monohydrogen citrate with only small changes in solution pH. Due to the high concentration of the dihydrogen ions in the solution, high current densities will be necessary to substantially convert it into the monosodium citrate. As a result of this conversion and the buffering effect, the manganese deposition potential can be reached in a bath containing sodium citrate without substantial hydrogen evolution from water hydrolysis.

From recent theory ⁽⁸³⁾, zinc electrodeposition is said to occur from a hydroxide layer at the cathode surface and not directly from the ions in the solution itself. This layer forms as a result of pH changes caused by the evolution of hydrogen from solution. The layer of zinc hydroxide is formed at the cathode surface followed by reduction of the hydroxide to zinc metal. When the film is depleted, the hydrogen evolution reaction is reintroduced and the pH at the surface increases again with the resulting formation of the hydroxide film. The film formation is, therefore, cyclic.

In solutions containing sodium citrate, the buffering action acts to delay such hydroxide film formation, but is not be able to prevent it completely. It is, therefore, proposed that zinc deposition occurs through such a hydroxide film under conditions where citrate is able to act as a buffer.

5.3 INTERPRETATION OF POLARISATION BEHAVIOUR

When interpreting polarisation behaviour, three equations are useful. These are:

- i) The Nernst equation, as derived in Appendix 6, which relates the potentials and activities of the system. At 25°C,

$$E_{eq} = E^0 + \frac{0.059}{z} \log[M_{aq}^{z+}] \quad (\text{Equation A6.4})$$

- ii) The Tafel equation for a cathodic process as given in Appendix 7:

$$\eta_{act} = a + b_c \lg i_{net} \quad (\text{Equation A7.6})$$

By plotting the polarisation behaviour in this research as the potential versus the log of the current density, the Tafel equation can be easily applied and a process under activation control should be a straight line with a slope of b_c , where

$$b_c = -\frac{2.303RT}{(1-\beta)zF}$$

- iii) The equation describing the behaviour of a system under diffusion control which relates the limiting current density to the bulk metal ion concentration as described in Appendix 8:

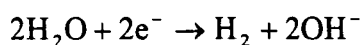
$$i_L = \frac{zFDc_0}{(1-t)\delta_N} \quad \text{(Equation A8.5)}$$

5.3.1 No Electrodeposition (Region A)

As labelled in Figure 4.11, Region A of the polarisation curve resembles a “nose”. It was found that no metal was deposited at the potentials associated with this region.

It is predicted that the rest potential is a mixed potential for two reactions, namely the corrosion of the steel in acid solution as predicted by the Pourbaix diagram for iron⁽²⁰⁾ and the hydrogen evolution reaction. The equilibrium potential at which the iron oxidation and reduction rates are equal can be calculated as follows. Since E^0 is -682mV (vs SCE) and assuming that $[Fe^{2+}]$ is $10^{-6} M$ ⁽²⁰⁾, then the equilibrium potential can be calculated from the Nernst equation (Equation A6.4) given above as -830mV (vs SCE).

During electroplating, hydrogen is often evolved at the cathode in accordance with the following reaction:



The potential below which this occurs in a solution of bulk pH5.6 can be calculated using the Nernst equation as given in Equation A6.5:

$$E_{\text{eq}} = E^0 - 0.059\text{pH} \quad (\text{Equation A6.5})$$

Since, by definition, E^0 is 0mV (vs SHE) or -242mV (vs SCE), then the hydrogen ion potential at equilibrium is -572mV (vs SCE).

The initial rest potential of the steel cathode in the electroplating bath is seen from Figure 4.11 to be -696mV. This does indeed lie between the corrosion potential of the steel in acid solution calculated above to be at -830mV (vs SCE), and the hydrogen ion potential at equilibrium at -572mV (vs SCE). The rest potential could, therefore, represent a mixed potential for these two reactions.

From the last calculation it can be seen that metal deposition from this bath will always be accompanied by hydrogen evolution. This is observed in the polarisation behaviour, since as the electrode is cathodically polarised and the potential is made more negative than the rest potential, the polarisation curve follows a Tafel slope of approximately 120mV/decade for hydrogen evolution.

5.3.1.1 Hydrogen Evolution Reaction

The Tafel slope for metal deposition is typically 60mV/decade to 70mV/decade. For hydrogen discharge, slopes of both 120mV/decade and 180mV/decade are possible, with the latter predominating in the potential range between -600mV and -2000mV. It is possible for the slope to be doubled to 240mV/decade to 360mV/decade when hydrogen evolution occurs on a non-conducting film ⁽¹⁹⁾⁽⁸⁰⁾.

In a bath without metal ions, the hydrogen evolution reaction in the “nose” region exhibits a Tafel slope of 164mV/decade, as shown by the polarisation behaviour of 0.6M sodium citrate and 0.48M sodium sulphate in Figure 4.21. This is identical to that for a bath containing 0.24M manganese sulphate and 0.24M sodium citrate from which no metal deposition occurs (Figure 4.17).

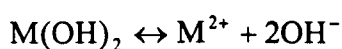
In a bath containing only zinc sulphate and sodium sulphate, the Tafel slope for the hydrogen evolution reaction in the “nose” region is very high at 535mV/decade (Figure 4.15), irrespective of the presence of manganese. With the addition of sodium citrate, and thereby the addition the buffering effect to the bath, the Tafel slope becomes 200mV/decade, as shown for a standard bath.

Variation in zinc or manganese ion concentration in a standard bath will not alter the hydrogen ion concentration at the cathode surface. Therefore, the Tafel slope would not be expected to alter from the value found in the standard bath. This is seen to be the case as the Tafel slope is virtually constant when the concentration of these salts is varied (Figures 4.27, 4.28, 4.30 and 4.31).

However, where hydrogen ions are supplied to the cathode surface, the Tafel slope would be expected to decrease towards that of 164mV/decade observed for the hydrogen reaction alone. Accordingly, reduction in pH is observed in Figure 4.22 to promote a progressive decrease in the Tafel slope, with that for the bath at pH3.0 reaching 182mV/decade. Similarly, the Tafel slope decreases with increasing sodium citrate content (Figures 4.24 and 4.25) due to the increased buffering effect, with that for the highest concentration of 1.0M being 172mV/decade.

5.3.1.2 Formation of a Cathode Surface Film

Evolution of hydrogen will cause the pH at the cathode surface to be raised from the bulk value of pH5.6. It is possible that the localised depletion of hydrogen ions could result in the metal ions precipitating at the cathode surface as metal hydroxide in accordance with:



where M is either zinc or manganese. In confirmation of this, the “nose” observed in Region A of the polarisation curves shown in Figure 4.15 is a typical feature of an anodic curve showing passive film formation.

From the Pourbaix diagrams for zinc and manganese (Figures 2.12 and 2.13 respectively), the pH at which this hydroxide film would be formed can be calculated for each of the metals as follows.

The solubility product for the reaction above is given by:

$$K_{M(OH)_2} = [M^{2+}][OH^-]^2 \quad (\text{Equation 5.1})$$

For the reaction:



the solubility product at 25°C is given by:

$$K_{H_2O} = [H^+][OH^-] = 10^{-14} \text{ mol/l}$$

Taking logarithms gives:

$$\log[H^+] + \log[OH^-] = -14$$

or

$$\log[OH^-] = \text{pH} - 14$$

Taking logs of Equation 5.1 and substituting gives:

$$\log[M^{2+}] + 2\text{pH} - 28 = \log K_{M(OH)_2} \quad (\text{Equation 5.2})$$

In this equation, $[M^{z+}]$ represents the activity, a' , of the ions M^{z+} where:

$$a' = \gamma c \quad (\text{Equation 2.2})$$

where γ the activity coefficient and c is the concentration. The activity coefficient is given by Parsons⁽⁸¹⁾ as 0.083 for a solution with a zinc sulphate concentration of 0.3M, and 0.085 for manganese sulphate concentration of 0.3M at 25°C. The solubility product $K_{M(OH)_2}$ has the value 3×10^{-17} mol/l for zinc and 8×10^{-14} mol/l for manganese⁽⁷⁸⁾. Therefore, in a standard solution where each of the metal sulphates is present in a concentration of 0.24M, the critical pH for hydroxide formation can be calculated from Equation 5.2. Accordingly, the critical pH for zinc hydroxide formation is pH7.08, and for manganese hydroxide is pH8.80. In the alloy bath, therefore, once the pH at the cathode surface has reached pH7.08, zinc hydroxide could be precipitated preferentially as a surface film.

In confirmation of this, the presence of zinc sulphate in the bath is observed to be the controlling factor in the appearance of the "nose". Addition of only 0.024M zinc sulphate causes this feature to appear (Figure 4.27), whereas the "nose" is present regardless of the manganese sulphate content of the bath (Figure 4.30).

Since zinc and manganese are both known to be complexed by citrate ions, it is therefore possible that any film at the surface could involve citrate and not just hydroxide. It is known that both zinc citrate and manganese (II) citrate are very slightly soluble in water⁽⁸²⁾, but no values are available in the literature for either their solubility products or activity coefficients to enable the pH at which they would be deposited to be evaluated as above. However, the above calculations make no allowance for the time of formation of the surface film. Hydroxides were found to be precipitated immediately from the standard bath when attempting to raise the pH with sodium hydroxide, whereas the time for citrate precipitation from the solution is of the order of days, as observed when the solution deteriorated (see Section 5.5). Hence, a cathode film would be assumed to be solely a hydroxide layer.

Addition of sodium citrate to the bath will alter the formation of the cathode surface film. Through its buffer action it will provide hydrogen ions to equalise the pH changes at the cathode. The increase in pH at the cathode will, thereby, become more difficult to achieve, and the film formation will occur at higher current densities as shown in Figure 4.15. Increase in sodium citrate concentration would be expected to further delay the onset of film formation since it increases the concentration of buffer in the bath. This is seen to be the case in Figures 4.24 and 4.25.

Film formation will be encouraged by alterations in bath composition or electrodeposition conditions which promote increase in pH from the bulk pH5.6 towards the critical pH of pH7.08. This will be observed as a shift in the “nose” to lower current densities in the polarisation curves. Such alterations include increasing the bulk pH of the solution (Figure 4.22), decrease in zinc ion concentration at the cathode surface (in accordance with Equation 5.2) (Figures 4.27 and 4.28) and increasing the manganese content (Figures 4.30 and 4.31) which relatively reduces the zinc ion concentration at the cathode surface.

5.3.2 Zinc-Rich Coatings (Region B)

If the cathodic polarisation of the electrode is increased, Region B of the polarisation curve is reached where metal deposition occurs under activation control with a Tafel slope of 10mV/decade, and zinc-rich coatings are produced.

In the zinc-manganese bath, the metal ions are complexed by the citrate. However, since the addition of sodium citrate to the bath does not cause a large shift in the deposition potential for zinc, it can be concluded that the complex releases the metal ions easily near the cathode surface and the metal is unlikely to be deposited directly from the complex. It is, therefore, proposed that the citrate releases the metal ions which are able to move to the cathode surface to form the layer of hydroxide as proposed by Yan et al ⁽⁸³⁾ (see Section 5.2.2). Once the film becomes a complete

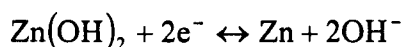
barrier, it prevents any further increase in pH at the surface by restricting the diffusion of hydrogen ions towards the cathode. It will also prevent the migration of manganese and further zinc ions towards the cathode.

The potential below which zinc would be electrodeposited from ions in the solution itself can be calculated using the Nernst equation given in Equation A6.4. The standard electrode potential, E^0 , is -1005mV (vs SCE) ⁽⁸¹⁾ for the following reaction:



Using the activity coefficient given by Parsons ⁽⁸¹⁾ as 0.083 for a 0.3M zinc sulphate solution, then for a bath in which the concentration of zinc sulphate is 0.24M, the equilibrium potential is -1055mV (vs SCE). In Figure 4.15, the potential below which zinc is deposited from a sulphate solution is -1075mV (vs SCE) in agreement with this calculation.

From this theoretical value for the equilibrium potential, the pH at the cathode surface at the onset of zinc deposition from a hydroxide film can be estimated. Assuming that formation occurs according to:



then, since E^0 is -681mV (vs SCE) ⁽²⁰⁾ and using Equation A6.5, the pH at the cathode surface in the bath without sodium citrate will be approximately pH6.34. At this value, the cathode surface has not reached the critical pH of pH7.08 for the formation of zinc hydroxide, so the cathode surface film will not cover the entire surface and zinc will be deposited from the ions in the solution. This occurrence of an incomplete film explains the irregular shape of the “nose” for the bath without citrate in Figure 4.15.

Addition of sodium citrate to the bath moves the potential at which zinc deposition commences to -1150mV (vs SCE) (Figure 4.15). The pH at the surface can be similarly estimated to be pH7.95. This is above the critical pH for film formation, so the cathode will be completely covered with zinc hydroxide as indicated by the shape of the “nose” region shown in Figure 4.15. Deposition will take place directly from the zinc hydroxide layer and not from the ions in solution, which causes the shift in deposition potential in a negative direction by 75mV .

From the model presented above, it would be predicted that addition of manganese to the zinc bath (Figures 4.15 and 4.21) and variation of its concentration (Figures 4.30 and 4.31) has no effect on the polarisation behaviour or the deposition potentials observed in the zinc deposition region. This can be seen to be the case. A decrease in the deposition potential for zinc would be expected with increase in zinc concentration (according to Equation A6.4) as seen in Figures 4.27 and 4.28, or with increase in pH (according to Equation A6.5) as seen in Figure 4.22. Increase in sodium citrate concentration does move the deposition potential for zinc closer to that for manganese deposition, but by a relatively insignificant value. Variation of sodium citrate content between 0.0M and 1.0M only results in a shift of 115mV (Figures 4.24 and 4.25). Therefore, the deposition of zinc from this bath can be predicted simply from electrochemical theory, and electrodeposition from this bath is not found to be of a complex nature.

5.3.3 Limiting Current for Zinc-Rich Coatings (Region C)

The zinc deposition potential of -1150mV in the bath with citrate relates to a current density of 0.03Adm^{-2} , with an estimated pH of pH7.95. Above pH7.0, Pearson⁽⁸⁰⁾ predicts an increase in surface pH during electroplating of one unit for every decade increase of current density. At 0.3Adm^{-2} , the polarisation behaviour shown in Figure 4.15 starts to deviate from Tafel behaviour, and electrodeposition begins to be under mixed activation and diffusion control. At this current density, the surface pH

would be predicted by Pearson to be pH8.95 which should still be within the range over which citrate acts as a buffer (Figure 5.1).

However, a limiting current for zinc deposition occurs at a current density of 1 A dm^{-2} (Figure 4.15). It is proposed that this occurs when citrate can no longer act to control this reaction, not due to its buffering capacity, but due to a limit in the rate at which the bulky complexed zinc ions can move towards the cathode and supply zinc ions relative to the rate of zinc ion reduction at the cathode surface. At this point, the electrodeposition rate will be such that zinc deposition is under diffusion control. Hydrogen evolution becomes the predominant reaction. For this to be the case, the limiting current for zinc deposition would also be found to be dependent on the zinc sulphate content of the bath.

For zinc deposition under diffusion control, the limiting current will be related to the concentration of zinc ions in the bath by Equation A8.3:

$$i_L = \frac{zFDc_0}{\delta_N} \quad (\text{Equation A8.3})$$

Assuming all other values are constant, the limiting current, i_L , would be expected to be directly proportional to the zinc ion concentration in the bulk solution. The citrate concentration affects the limiting current since the higher its concentration at the cathode surface, the lower the concentration of zinc ions which can reach the surface and, thus, the lower the limiting current. The limiting current density is, therefore, observed to be inversely proportional to the citrate content of the bath in Figure 5.2 and proportional to the zinc ion concentration in Figure 5.3. The limiting current for zinc deposition would not be expected to be pH dependent from Equation A8.3. This is confirmed in Figure 4.22.

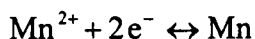
In this region, addition of sodium citrate to the bath results in a limiting current for hydrogen evolution. This effect is observed in Figure 4.15 for zinc deposition alone, in Figure 4.17 for manganese deposition alone, and in Figures 4.19 for zinc-

manganese electrodeposition. The buffering effect of the citrate is suppressing the breakdown of water to a potential below which manganese can be deposited. In confirmation of this effect, it is within this region that zinc-manganese alloys start to be produced. The higher the sodium citrate content of the bath, the greater this effect is observed to be in Figures 4.24 and 4.25.

5.3.4 Zinc-Manganese Alloys (Region D)

If the cathodic polarisation of the electrode is increased further, Region D of the polarisation curve is reached where zinc-manganese alloy is deposited with a Tafel slope for metal deposition of 30 mV/decade.

The potential below which manganese would be predicted to be electrodeposited from ions in the solution itself can, once again, be calculated using the Nernst equation given in Equation A6.4 applied to the following reaction:



Parsons ⁽⁸¹⁾ gives the standard electrode potential, E^0 , for this reaction as -1422mV (vs SCE). Using the activity coefficient of 0.085 ⁽⁸¹⁾ for a 0.3M manganese sulphate solution, then for a bath in which the concentration of manganese sulphate is 0.24M , the equilibrium potential would be calculated as -1472mV (vs SCE). This potential is within the range over which substantial quantities of manganese start to be co-deposited from the bath in the limiting current region for zinc deposition.

At the potentials for alloy deposition, the surface is under the conditions dictated by the limiting current of zinc with vigorous hydrogen evolution. It is not known whether manganese is deposited through a manganese or mixed metal hydroxide cathode film as in the case of zinc. Similarly, it is not known whether manganese is deposited either from simple ions or complexed citrate ions. However, the addition of sodium citrate to the bath does not make manganese electrodeposition more difficult.

Figure 4.21 shows that addition of sodium citrate does, in fact, slightly raise this potential.

At the current densities associated with alloy deposition, the role of the citrate as described above with respect to the hydrogen evolution reaction is seen clearly in Figure 4.15 which shows the deposition of zinc alone from a citrate bath. Without sodium citrate, no limiting current occurs for the zinc deposition reaction, and the breakdown of water occurs at potentials above -1472mV (vs SCE). Hence, the potential required for manganese deposition could not be reached and manganese metal cannot be produced from a bath without sodium citrate. The addition of sodium citrate suppresses the electrolysis of water to potentials below which manganese can be deposited and, thus, zinc-manganese alloys can be produced.

This effect is confirmed by examination of the Hull Cell panels. For the zinc sulphate bath without sodium citrate, the Hull Cell panel in Figure 4.16 reveals that white zinc hydroxide is produced at high current densities. The metal deposition region is extended if sodium citrate is added to the bath. Similarly, Figure 4.18 shows the deposit produced in a corresponding bath containing manganese sulphate without sodium citrate. The coating produced is manganese hydroxide, which rapidly converts to brown hydrated manganese (III) oxide, $\text{Mn}_2\text{O}_3 \cdot x\text{H}_2\text{O}$, in air⁽⁸⁴⁾. Manganese metal is not deposited since hydrogen evolution occurs more readily. Addition of sodium citrate to this bath produces manganese metal but not in an appropriate form (see Section 5.3.4.1), and the coating dissolves in the bath. Brenner⁽²⁴⁾ attributes this to the presence of impurities in the bath and in the deposit which set up local galvanic couples. This problem is overcome in the electrowinning of manganese by purifying the feed solution which is circulated through the cathode compartment.

This suppression of hydrogen evolution is observed even for the lowest sodium citrate concentration used in this work, that is, 0.2M (Figure 4.24). However, in accordance with the polarisation behaviour observed for variation in sodium citrate content of the bath in Figures 4.24 and 4.25, there was vigorous gassing during the electroplating of

a Hull Cell panel from a bath with a sodium citrate content as low as 0.2M. This was also the case for a sodium citrate content as high as 1.0M, since the limiting current for zinc-manganese deposition had been exceeded.

The suppression of hydrogen production in the presence of sodium citrate is the controlling factor in the polarisation behaviour of zinc-manganese electrodeposition. It is not dependent on the zinc or manganese content of the bath, as variation of either zinc sulphate (Figures 4.27 and 4.28) or manganese sulphate (Figures 4.30 or 4.31) content is observed to have no effect.

5.3.4.1 The Role of Zinc in Alloy Deposition

According to Brenner⁽²⁴⁾ and Safranek⁽⁸⁵⁾, ductile γ -manganese can be deposited from a purified manganese plating bath, but on standing at room temperature for days or weeks it changes to brittle α -manganese. This transition can be retarded or prevented by the presence of certain alloying elements such as copper, iron, nickel or cobalt.

It is possible that this phenomenon is observed for coatings produced from the zinc-manganese bath. When sodium citrate is added to the manganese sulphate bath, the brown coating observed on the Hull Cell panel in Figure 4.18 might be α -manganese. If zinc sulphate is added to the bath, a structure comprising round nodules was observed at current densities above 9Adm^{-2} (as described in Section 4.1.1.1 and Figures 4.6 to 4.10). This is thought to be a γ -manganese type structure in accordance with the literature⁽²⁶⁻²⁸⁾⁽³¹⁾⁽³⁹⁾⁽⁴⁴⁾⁽⁴⁵⁾. Therefore, the role of zinc in this bath may be similar to that for the other elements mentioned above in conjunction with manganese plating. That is, it allows the deposition and stabilisation of a more desirable phase.

Zinc-manganese alloy electrodeposition has been found to be of the regular type, with zinc being deposited above its limiting current density. The portion of the current used for discharging zinc will be constant throughout the alloy deposition range.

Also, alloy deposition will always be accompanied by hydrogen discharge, thus reducing the cathode current efficiency for metal deposition as shown in Figure 4.13.

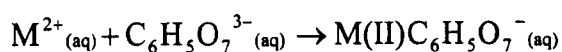
5.3.5 Limiting Current for Zinc-Manganese Alloys (Region E)

The practical limit for electroplating was found to be at a current density of 15Adm^{-2} . The true limiting current density for the alloy electrodeposition process where metal deposition is entirely diffusion controlled is seen to be at 200Adm^{-2} (Figure 4.21). At this value, there is excessive hydrogen evolution at the cathode and oxygen evolution at the anode due to the breakdown of water. Manganese nodules are no longer visible in the microstructure (Figure 4.10), and the limiting current is only dependent on the zinc sulphate concentration in the bath (Figure 4.27 and 4.28) in accordance with Equation A8.3.

PART TWO – CHEMISTRY OF THE ELECTROPLATING BATH

5.4 INTRODUCTION

In common with other transition metals such as nickel⁽⁸⁶⁾⁽⁸⁷⁾ and iron⁽⁷⁶⁾⁽⁸⁸⁾, both manganese⁽⁷⁶⁾⁽⁸⁹⁻⁹¹⁾ and zinc⁽⁷⁶⁾ form a discrete 1:1 complex with citrate in solution⁽⁹⁰⁾. The form of the citrate ligand in the complex is related to the pH as shown in the distribution diagram in Figure 5.4⁽⁷⁶⁾. At pH5.4, the predominating complex formation reaction will be⁽⁹²⁾:



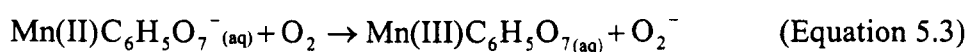
where M is either manganese or zinc.

The change in colour of the bath from pale pink to pale orange on mixing of the constituent solutions indicates the reactions of manganese in solution, since the zinc

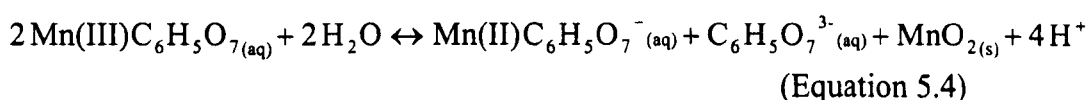
complex is colourless⁽⁷⁷⁾. Both worked and unworked aerated baths were observed to decay with time. This was seen as a gradual deepening in colour of the solution and precipitation from the bath. If the component solutions were deoxygenated with nitrogen and then mixed, no colour change occurred but precipitation was still observed. Thus, the deepening in colour and precipitation are confirmed to be due to two separate reactions, and the colour change is due to the effect of aerial oxidation on the solution.

5.5 CHEMISTRY OF THE ELECTROPLATING SOLUTION

Aerial oxidation of the bath results in a change in the complex of aqueous manganese (II) ions to aqueous manganese (III) in accordance with the following reaction⁽⁹²⁾:



While manganese (II) is the most stable oxidation state of the metal, all manganese (III) salts have a low stability. The aqueous manganese (III) complex will undergo internal electron transfer, and a range of organic oxidation products of citrate may be formed⁽⁹³⁾. Aqueous manganese (III) ions will not be obtained in high concentrations in the bath, as in weakly acid solution there is a strong tendency for them to hydrolyse and to disproportionate into manganese (IV) and manganese (II)⁽⁹⁴⁾. In the electroplating bath, therefore, the following reaction will also occur⁽⁹²⁾:



This is confirmed by the results of visible and ultraviolet spectroscopy on the baths as follows.

The visible and ultraviolet spectrum for aqueous manganese (II) ions is shown for a fresh solution of 0.48M manganese sulphate in Figure 4.46. This is of similar form to that given by Greenwood and Earnshaw⁽⁶¹⁾. The peaks represent the change in electronic state of the five unpaired 3d electrons present in the manganese (II) ion. Zinc cannot be observed using this technique since it has a completely filled 3d orbital and, therefore, no excitation of unpaired electrons can be detected.

Figure 4.47 shows the effect of adding sodium citrate to the solution for both a fresh and aged bath. (Note the difference in scales when comparing the spectra.) In a fresh bath, the manganese (II) spectrum is similar to that observed in Figure 4.46, although it is slightly modified due to the presence of the sodium citrate. Upon aging, this spectrum is replaced by a large peak at 430nm. A similar effect is observed during the aging of the standard bath (Figures 4.48 and 4.49), with an additional large peak at 470nm.

Increase in pH will promote the production of the aqueous manganese (III) complex according to the reaction shown in Equation 5.4. The effect of pH on the visible and ultraviolet spectrum for a solution of 0.24M manganese sulphate and 0.6M sodium citrate is shown in Figure 4.50. Increase in pH promotes the appearance of the peak at 430nm. This peak must, therefore, represent the presence of the aqueous manganese (III) complex. Both Gmelin⁽⁹⁵⁾ and Klewicki and Morgan⁽⁹²⁾ quote the appearance of a peak at 430nm due to the presence of manganese (III) in aqueous solution.

In addition, Gmelin⁽⁹⁵⁾ reports the presence of a red to cinnamon coloured colloidal complex with a broad absorption band at about 500nm in solutions containing a citrate to manganese (III) ratio of less than 2:1 or at less than pH8, together with the separation of a precipitate. This absorption band correlates with the second large peak observed in Figure 4.49.

Experimentally it was observed that increasing the pH caused the bath to darken in colour. The orange discolouration in the bath results from the reaction in Equation 5.4. However, it is uncertain as to whether the colour is due to one or more

of the reaction products, since octahedral aqueous manganese (III) complexes such as the hexaaquamanganese (III) ion, $[\text{Mn}(\text{H}_2\text{O})_6]^{3+}$, are red⁽⁹⁶⁾ and manganese dioxide hydrate is brown.

In confirmation of the effect of aerial oxidation, the degree of discolouration in a standard bath (Figure 4.12) was decreased by exclusion of the atmosphere (Figure 4.44). Exclusion of oxygen prevents the formation of the aqueous manganese (III) complex in accordance with Equation 5.3 and thereby prevents the reaction in Equation 5.4 occurring. Addition of an antioxidant to the bath was also found to reduce discolouration. A successful antioxidant for this bath needs not only to counteract the effect of aerial oxidation during aging, but also the production of oxygen at the anode during electrodeposition. Although no discolouration occurred during the aging of a solution containing sodium sulphite (Figure 4.37), this antioxidant could not counteract the effects of production of oxygen during electroplating. Ascorbic acid was more successful (Figure 4.36) and, although the solution did darken slightly during aging of the bath, there was no further discolouration during electroplating.

The effect of bath composition on the discolouration of the solution can be seen within Figures 4.12 to 4.45. These results are summarised in Table 4.1. If insufficient sodium citrate is present to form a 1:1 complex with both the zinc and manganese ions present, discolouration is reduced. The discolouration also varies with the relative concentrations of zinc sulphate and manganese sulphate in the bath. Thus, for a ratio of 1:1 manganese sulphate to zinc sulphate in the bath, the discolouration is similar, regardless of variation in each of the metal ion contents between 0.12M and 0.2M. If the relative concentration of manganese sulphate is decreased, a lower degree of discolouration is observed.

The time taken for complex formation in solution varies according to the reaction. For example, in attempting to raise the pH of the bath with sodium hydroxide solution, white zinc hydroxide was precipitated immediately. The reaction rate for Equation 5.4 is slower, which explains the gradual discolouration of the bath. It is

known that the proportion of aqueous manganese (II) oxidised to aqueous manganese (III) is approximately 10% of the initial concentration in 30 days in a solution open to the atmosphere ⁽⁹²⁾.

5.6 EXAMINATION OF THE PRECIPITATE

The results of infrared spectroscopy on the known sample of zinc citrate and the precipitate from the standard bath are shown in Figures 4.51 and 4.52 respectively. It is usual to identify such compounds by comparison with published results, in particular in the fingerprint region which is specific to an individual compound. However, neither the infrared spectrum for zinc citrate nor a full spectrum for manganese citrate could be located in the literature or in reference manuals such as those produced by Aldrich ⁽⁶⁷⁾ and Sigma ⁽⁹⁷⁾. The chemical manufacturers ICN Flow, Thame provided a spectrum for zinc citrate (Figure 2.37), and partial spectra for two forms of manganese (II) citrate are given by Fujita ⁽⁶⁶⁾ (Figure 2.38). The relevance of the bands labelled A to F on Figures 4.51 and 4.52 in identifying the samples as carboxylic acid derivatives are explained in Section 2.18.2.2.

The zinc citrate spectrum produced in this research (Figure 4.51) and that provided by ICN Flow (Figure 2.37) are virtually identical in form. However, the precise structure and degree of hydration of the two samples is unknown. The strong peak in region C of the manufacturers spectrum is due to the Nujol mulling agent used in the sample. The masking effect of this agent was avoided in this research by presenting the sample as a potassium bromide disc.

For the precipitate from the standard bath (Figure 4.52), the regions A, B and C cannot be seen separately and a large peak is observed. The region in which this occurs, at wavenumbers between 2500 and 3600 cm^{-1} , is where spectra often show strong bands associated with O-H stretching and water of hydration (see I in Section 2.18.2.2). An effect such as increased water of hydration could be causing this large peak, which is masking the individual regions A, B and C. It is impossible

to definitely attribute this effect to one of either the hydroxyl groups or the water of hydration, since the distinguishing H-O-H bending motion band which would be produced in the region of 1600 to 1650 cm^{-1} by water of hydration would be masked by the carbonyl absorption in the spectra presented here (Region D). This explanation of differing degrees of hydration of the compounds may also explain the differences in peak intensity found between otherwise similar zinc citrate spectra produced in this research and that provided by ICN Flow.

By comparison of Figure 4.52 with the partial spectra given by Fujita ⁽⁶⁶⁾ for two structures of manganese (II) citrate (Figure 2.38), the precipitate can be identified as that with structure $[\text{Mn}(\text{H}_2\text{O})_6][\text{Mn}(\text{C}_6\text{H}_5\text{O}_7)\text{H}_2\text{O}]_2 \cdot 2\text{H}_2\text{O}$. The results of ultraviolet spectroscopy on this precipitate (Figure 4.53) confirm the presence of the metal as manganese (II) ions, by comparison with the known spectrum for manganese (II) sulphate shown in Figure 4.46. This is further substantiated by the pale pink colour of the precipitate, as manganese (II) compounds are known to be light in colour, often pink when in an octahedral structure ⁽⁹⁴⁾. Gmelin ⁽⁹⁵⁾ reports that manganese (II) citrate of the structure suggested above is a light pink crystalline powder, of monoclinic structure. Each citrate ion forms a tridentate chelate to one manganese ion as can be seen in Figure 5.5 ⁽⁹⁵⁾⁽⁹⁸⁾⁽⁹⁹⁾. Complexes of manganese in higher oxidation states are darker in colour, and manganese (III) citrate is known to be light to dark green ⁽⁹⁵⁾.

The results of the elemental analysis in Table 4.2 show the precipitate to contain both zinc and manganese. Zinc citrate is known to exist in an isomorphous form ⁽⁸²⁾⁽¹⁰⁰⁾ to that identified for manganese (II) above. Summation of the weight percentages of the two metals and comparison with the structures predicted by Fujita ⁽⁶⁶⁾ (Table 5.1), confirm that the stoichiometry of the compound does indeed indicate the above structure. The precipitate is, therefore, a mixed zinc-manganese (II) citrate of the structure given above, with the ratio of manganese to zinc being 2:1.

Manganese (II) and zinc citrates are known to be only slightly soluble in cold water ⁽⁸²⁾. A precise value for solubility could not be found, but would be comparable

with that for iron (II) citrate at 9g/l⁽⁸⁸⁾. Due to the high concentration of salts in the electroplating bath, it can be assumed that the precipitate appears since its solubility limit is exceeded. Its appearance is not immediate due the time taken for complex formation, as discussed above.

Bath deterioration was reduced by storage at 50°C, both in terms of discolouration and the quantity of precipitation. Such an observation has also been made in the literature⁽³³⁾⁽³⁴⁾. At such a raised temperature, it is usual to store the solutions in a sealed container to reduce evaporation. This reduces the degree of aerial oxidation and thereby the formation of the manganese (III) citrate complex in accordance with Equation 5.3 with the resulting discolouration. In addition, the solubility of the precipitate may be increased at the raised temperature, hence the degree of precipitation is reduced.

PART THREE - PRACTICAL GUIDELINES FOR THE SULPHATE-CITRATE BATH

5.7 INTRODUCTION

A summary of the results discussed which are of interest to the practical electroplater is given below.

The electroplating bath was manufactured by preparing separate, double concentrate solutions of each of sodium citrate and zinc sulphate with manganese sulphate. In this form, the bath can be successfully stored for long time periods without deterioration. Bath decay was minimised by mixing equal volumes of the two solutions immediately prior to experimentation.

For electrodeposition from the sulphate-citrate bath at 25°C and pH5.6, it has been found that zinc-manganese alloys can be produced at current densities above

0.9Adm⁻². Although alloys with relatively high manganese content of approximately 40% (by weight) and containing γ -manganese can be produced between 10Adm⁻² and 50Adm⁻² (Figure 4.14), the practical range extends only to 15Adm⁻². Above this, “burnt” deposits are produced. The electrodeposition of zinc-manganese is always accompanied by hydrogen evolution. This reduces the cathode current efficiency for metal deposition to approximately 40% throughout this range (Figure 4.13).

From the experimental results obtained in this research, the range over which the bath composition and operating conditions can be varied to allow the most successful alloy deposition can be predicted. Hydrogen evolution must be suppressed to a potential which allows the deposition of manganese, but without the limiting current for zinc-manganese deposition being exceeded as this results in a black and “burnt” coating being produced.

Further experimentation in terms of the coating properties is necessary to confirm the following predictions.

5.8 BATH COMPOSITION

In terms of variation in sodium citrate, zinc sulphate (Figures 4.29) and manganese sulphate (Figures 4.30 to 4.32) concentrations, the optimum bath would appear to contain a ratio of sodium citrate to total metal ions of approximately 1:1. At this ratio, all zinc and manganese ions will be complexed in solution.

For the standard bath, a sodium citrate concentration of between 0.48M and 0.8M should be used (Figures 4.24 to 4.26). Below this range, the hydrogen evolution reaction is not sufficiently suppressed and above 0.8M, a black and “burnt” coating is observed.

The actual limiting current for alloy deposition is controlled by the zinc sulphate content of the bath. It increases with increasing salt content until a limit is reached at

a zinc sulphate to sodium citrate ratio of approximately 1:1. Above this, the potential at which the alloy is produced becomes more negative.

The manganese sulphate content of the bath appears to have very little effect on the deposition of the alloy in terms of the suppression of the hydrogen reaction. At manganese sulphate to sodium citrate ratios greater than 1:1, the potential at which the alloy is produced becomes slightly more negative.

In a standard bath, the production of precipitate cannot be avoided since its solubility limit has been exceeded. To eliminate precipitation, it has been found that the total metal ion concentration of the bath must be lower than 0.36M. Therefore, it is recommended that further work on this system should include research into a bath containing 0.18M zinc sulphate with 0.18M manganese sulphate and 0.36M sodium citrate. This would contain the salts in a similar ratio to that found in the standard bath, but at a content below that at which precipitation would be expected.

Preliminary experimentation on a bath with reduced salt content and including antioxidants has indeed shown a reduction in precipitation from the bath and a lower degree of discolouration (Figure 5.6).

The discolouration of the bath is due to the effect of oxygen on the manganese (II) citrate complexes formed in the solution. Decreased exposure to aerial oxidation reduced discolouration of the bath (Figures 4.45 and 4.46). Deoxygenation of the bath prior to electroplating prevented initial discolouration, but it did not alter the polarisation behaviour (Figure 4.42) since oxygen is produced at the anode during electroplating and subsequently causes discolouration of the solution. The anode and cathode can be separated without affecting the system (Figure 4.42). During electroplating, the catholyte discoloured relatively little, whereas the anolyte darkened significantly. To prevent this, the anolyte could be replaced with a carrier solution without a manganese component.

Alternatively, an antioxidant can be employed to reduce discolouration. Of the two antioxidants researched, namely sodium sulphite and ascorbic acid, the latter was the more successful in preventing discolouration of the bath. It did not alter either the polarisation behaviour (Figure 4.35) or the electroplate produced (Figure 4.36) from a fresh solution. No difference was observed on the polarisation behaviour of an aged solution (Figure 4.39).

5.9 OPERATING CONDITIONS

Figures 2.19 and 2.20 indicate that decreases in flow rate and temperature promote increased manganese content in the alloy deposit. This is said to be desirable for optimum coating properties ⁽²⁶⁻²⁸⁾. Hence, increase in temperature and flow rate were not considered in this research.

In terms of pH, the hydrogen reaction was not found to be sufficiently suppressed at values less than pH5.0 (Figures 4.22 and 4.23) to allow efficient metal electrodeposition. Since difficulty was found in raising the pH of the solution, the appropriate pH range for alloy production was found to be between pH5 and the natural pH of the solution, pH5.6.

Aging of the bath for 30 days and the subsequent increase in discolouration of the bath had no appreciable effect on either the polarisation behaviour of the system (Figure 4.38) or the appearance of the electroplate (Figure 4.12). The repeated use of the bath accompanied by increasing discolouration was also found to have no effect (Figure 4.41).

CHAPTER 6

SUMMARY

6.1 CONCLUSIONS

For the operating conditions used in this research, the following can be concluded about the electrodeposition of zinc-manganese:

PART ONE - ELECTRODEPOSITION OF ZINC-MANGANESE

- The standard sulphate-citrate bath used throughout this research contained 0.24M manganese sulphate, 0.24M zinc sulphate and 0.6M sodium citrate. Under the operating conditions of 25°C and pH5.4, zinc-manganese alloys are produced at current densities above 0.9Adm⁻². Alloys with high manganese content of 40% can be produced between 10Adm⁻² and 50Adm⁻², but the practical electroplating range only extends up to 15Adm⁻². Zinc-manganese deposition is always accompanied by hydrogen evolution. The cathode current efficiency for metal deposition is approximately 40% throughout this range.
- The primary role of sodium citrate in the bath is not to act as a complexant by moving the deposition potentials of zinc and manganese together to allow co-deposition. It has been found that it acts as a buffer resisting pH changes at the cathode surface and suppressing hydrogen reduction. This has been used to explain the polarisation behaviour of zinc-manganese electrodeposition.
- The polarisation behaviour of the zinc-manganese system exhibits five distinct regions, as confirmed by examination of the electroplate:

Region A - Between -600mV and -1150mV no electrodeposition occurs and a "nose" is observed. This represents the formation of a passive hydroxide film, the production of which is affected by the sodium citrate buffer since it supplies hydrogen ions to equalise the pH changes.

Region B - Zinc deposition occurs at potentials below -1150mV. It can be predicted that at this value the metal would be deposited from the zinc hydroxide layer. When this layer is depleted of zinc ions, the hydrogen reaction is reintroduced and the hydroxide film reforms.

Region C - Zinc deposition reaches a limiting current density at the point when sodium citrate can no longer act to control to this reaction. This is not due to its buffering capacity, but due to a limit in the rate at which the bulky complexed zinc ions can move towards the cathode surface relative to the rate of zinc deposition.

Region D - Zinc-manganese alloys are deposited at potentials between -1550mV and -1800mV. The zinc component is deposited above its limiting current. Thus alloy deposition is always accompanied by hydrogen evolution, which results in a reduced cathode current density for metal deposition. The action of the sodium citrate is to suppress the hydrogen reaction to potentials below which manganese can be deposited, so that it is possible to electrodeposit the two metals together.

Region E - The electrodeposition of zinc-manganese reaches its limiting current at potentials below -1800mV.

PART TWO - CHEMISTRY OF THE ELECTROPLATING BATH

- A successful method for the manufacture and storage of the bath has been developed. Double concentrate solutions of each of sodium citrate and zinc sulphate with manganese sulphate were prepared, which could be successfully

stored for long time periods. Mixing equal volumes of the solutions immediately prior to experimentation was found to reduce bath decay.

- Both worked and unworked aerated baths decayed with time. The gradual deepening in colour of the bath from pale pink to dark orange was due to oxidation of the aqueous manganese (II) citrate complex to an aqueous manganese (III) complex, with subsequent disproportionation resulting in the reformation of the manganese (II) complex and manganese dioxide hydrate. This was confirmed by visible and ultraviolet spectroscopy.
- Discolouration of the bath can be reduced by exclusion of the atmosphere, or by the use of an antioxidant. Ascorbic acid was the most successful antioxidant employed in this research, as it reduced discolouration due to both aerial oxidation and the production of oxygen at the anode during electroplating. It did not alter either the polarisation behaviour of the system or the resulting electroplate.
- The discolouration was not found to affect the polarisation behaviour of the system and the appearance of the electroplate, either during tests on aging of the bath or the repeated use of the bath.
- The pale pink deposit precipitated from the bath has been found by infrared spectroscopy and elemental analysis to be a mixed manganese (II) zinc citrate of known composition, containing the metal ions in the ratio of 2:1 respectively. The precipitate appears since its solubility limit is exceeded. Precipitation can be reduced by increasing the temperature or reducing the total metal salt content to below 0.36M.
- It is predicted that the optimum bath will contain a ratio of sodium citrate to total metal ions of approximately 1:1. At this ratio, all zinc and manganese ions will be complexed in solution. The sodium citrate content of the bath should be within the range 0.48M to 0.8M. The bath should be operated at pH value between pH5.0 and pH5.6. Temperature and flow rate have not been varied in this

research, but the literature indicates that lower flow rate and temperature promote optimum coating properties.

6.2 SUGGESTIONS FOR FURTHER WORK

With reference to the experimental techniques used in this research and the results obtained, the following suggestions are made for further related work:

- In accordance with the guidelines given in Part Three of Chapter 5, further experimental work could be performed to produce an improved electroplating bath. This electrolyte may include antioxidant additions (either those used in this research or alternatives) to reduce bath discolouration. The salt content of the bath should be lowered to reduce precipitation, and the composition which provides the optimum compromise between the properties of the electroplate and the deterioration of the bath needs to be ascertained. A study of possible addition agents which increase the cathode current efficiency for metal deposition without reducing the manganese content of the coating would be useful.
- The operating conditions chosen for this research were those which were indicated by the literature to increase the manganese content of the alloy and, thereby, produce a more corrosion resistant coating. For completion, the work performed in this research could be extended by investigating variation in temperature and flow rate which have not been considered due to these criteria.
- The appearance of the Hull Cell panel can only give guidelines about the range of coatings which can be produced from any particular bath. It is very useful for determining any bath which might be of interest, but the electroplate must be further analysed and tested to determine the precise compositions and properties.
- The structure of zinc-manganese alloys could be further investigated using transmission electron microscopy. This would lead to increased understanding of

the corrosion resistance of the alloys, and the mechanism of corrosion. It will also clarify the form in which the metal is deposited, which may be as an oxide or hydroxide rather than as the metal itself.

- The replacement of sodium citrate by ammonium citrate in the bath has produced interesting results which could be further investigated. Initial results showing the appearance of Hull Cell panels, bath deterioration and polarisation behaviour for a standard bath with such a substitution is shown in Figures 6.1 and 6.2. (These results were not discussed previously since the pH of the solution photographed to show bath deterioration is pH3.75, which is not commensurate with that used throughout the remainder of the research).

Manganese cannot be deposited from either a sulphate or chloride solution alone, but can be produced if ammonium sulphate or chloride is added ⁽¹⁰¹⁾. The rate of deposition increases with the ammonium content of the bath. Since this addition is also found to cause a marked increase in the rate of auto-dissolution of the manganese, the authors assume that the action of the ammonium salts is to activate the surface of the manganese which allows electrodeposition of the metal.

However, this observation may be explained by the effect of the ammonium salts on the formation of a cathode hydroxide film. According to Gonsalves ⁽¹⁰²⁾, the ammonium salt aids deposition by reduction to ammonia at the cathode. Insoluble hydroxides will then dissolve in the ammonia to give soluble complexes.

In this research, the addition of sodium citrate to a manganese sulphate bath (Figure 4.18) was also found to promote the deposition of metal, and the auto-dissolution of the deposit was observed. This similarity may occur since both the citrate and the ammonium ions will form a complex with the manganese ions in the bath. The citrate complex will be stronger than the ammonium complex, and it may be found that the latter will not suppress hydrogen evolution sufficiently to allow manganese deposition in an appropriate form. Along with the possible alteration of the hydroxide film, this may explain the differences observed in the

Hull Cell panels and polarisation behaviour of the bath containing ammonium citrate in Figures 6.1 and 6.2 from that of the standard bath (Figures 4.11 and 4.12). Precipitation still occurred in the bath containing ammonium citrate, but there was no discolouration. However, the discolouration would be expected to be less in the photographed case since the pH of the solution was lower.

- The role of sodium in the discolouration of the bath with time could be investigated. This is suggested after the following observations were made during this research, whilst also considering that no discolouration was observed over time in a bath where sodium citrate was substituted for ammonium citrate (Figure 6.1). Baths containing neither zinc nor citrate ions were stirred vigorously to observe the effect of the sodium on the manganese salts. A bath containing 0.24M manganese sulphate with 0.24M ammonium sulphate (pH5.17) did not discolour. A solution containing 0.24M manganese sulphate and 0.24M sodium sulphate (pH5.6) became progressively darker orange.
- Alternative baths to the commonly used sulphate-citrate bath could be researched. Guidelines may be sought from literature pertaining to the deposition of other manganese alloys. For example, manganese-tin alloys are deposited from an alkaline tartrate bath, and manganese-nickel alloys from a pyrophosphate bath⁽²⁴⁾. Ideally the bath requires the metal ions to be held in solution as a soluble complex which is stable over time. However, the degree of complexing of the ions must not be so great that electrodeposition of the alloy only occurs with difficulty at extremely negative potentials. Examination of available stability constants for zinc and manganese complexes may be helpful⁽¹⁰³⁾ in assessing their relative strengths. In terms of the hydroxyacids, the chemistry of some aliphatic and aromatic manganese complexes is given by Magers et al⁽¹⁰⁴⁾.

Regarding the solubility of such complexes, literature on wastewater treatment often evaluates the performance of both zinc and, in particular, manganese. The electroplater and the water treatment engineer look at the same chemistry from a

different viewpoint. The electroplater needs to keep the complexes in solution, whereas the water treatment engineer uses them to remove unwanted metal ions.

- In terms of electrodeposition, zinc and zinc alloys are often classified together because of the end usage of the product. As a result, the process of zinc-manganese electrodeposition is usually compared with that for zinc and other zinc alloys.

However, the problems of bath deterioration and precipitation are related more to the chemistry of manganese and citrate than that of zinc. Therefore, it might perhaps be more appropriate to approach zinc-manganese electrodeposition in terms of its similarity to manganese electroplating. A review of the literature pertaining to manganese deposition ⁽¹⁵⁾⁽⁷⁴⁾⁽⁸⁵⁾⁽¹⁰²⁾⁽¹⁰⁴⁻¹¹²⁾ would be useful to determine how researchers have overcome similar problems with the electrolyte as those found in the electrodeposition of zinc-manganese.

TABLES

Author	Manganese Sulphate (M/l)	Zinc Sulphate (M/l)	Sodium Citrate (M/l)	Operating Conditions	Typical Results	
					Mn Content of Deposit (%)	CCE (%)
FAUST ET AL ⁽²⁵⁾	0.65	0.18	0.72	pH5.3, 30°C, 11Adm ⁻²	39	26
SAGIYAMA ET AL ⁽²⁶⁻²⁸⁾	0.24	0.24	0.61	pH5-6	40-50	-
GABE ET AL ⁽²⁹⁾⁽³⁰⁾	0.25	0.25	0.6	pH5.4, 20-40°C, 20Adm ⁻² Anode: 316 stainless steel Cathode: Copper (RCE) or iron foil (static)	37.6	29.5
SELVAM AND GURUVIAH ⁽³¹⁾	0.36	0.18	0.68	pH5.6, ambient temp, 8Adm ⁻² Separated electrodes Anode: Bagged stainless steel or graphite Cathode: Stainless or mild steel Static conditions	55	10
SAGIYAMA ET AL ⁽³³⁾⁽³⁴⁾	0.18	0.24	0.61	pH5.6, 50-60°C, 35Adm ⁻² Anode: Platinum coated titanium Cathode: Mild steel Flow cell	65	30

TABLE 2.1: Operating Conditions and Typical Results from Published Literature on Zinc-Manganese Electrodeposition

Current Density (A/dm ²)	Zn (wt%)	Mn (wt%)	H ₂ (wt%)	Cathode Current Efficiency (%)
5.0	44.1	1.5	54.3	45.7
7.0	35.7	3.3	61.0	39.0
10.0	31.5	3.8	64.7	35.3
15.0	26.6	7.4	66.0	34.0
20.0	18.4	11.1	70.5	29.5
25.0	8.6	9.5	81.9	18.1
40.0	4.1	6.4	89.5	10.5

TABLE 2.2: Effect of Current Density on the Manganese Content of the Deposit and the Cathode Current Efficiency for Deposition from a Sulphate-Citrate Bath ⁽²⁹⁾⁽³⁰⁾

(Deposited at 500 rpm, 40°C, pH 5.4)

pH	Zn (wt%)	Mn (wt%)	H ₂ (wt%)	Cathode Current Efficiency (%)
3.5	76.1	1.6	22.3	77.7
4.5	50.7	3.8	45.5	54.5
5.0	27.6	8.1	64.3	35.7
5.3	22.7	10.4	66.9	33.1
5.4	18.4	11.1	70.5	29.5
5.8	13.8	9.7	76.5	23.5
6.5	7.4	15.1	77.5	22.5

TABLE 2.3: Effect of pH on the Manganese Content of the Deposit and the Cathode Current Efficiency for Deposition from a Sulphate-Citrate Bath ⁽²⁹⁾⁽³⁰⁾

(Deposited at 500 rpm, 40°C, 20Adm⁻²)

Rotation Speed (rpm)	Zn (wt%)	Mn (wt%)	H ₂ (wt%)	Cathode Current Efficiency (%)
0	12.5	13.5	74.0	26
50	13.4	13.6	73.0	27
100	15.2	13.3	71.5	29
300	22.9	8.1	69.0	31
500	35.7	3.3	61.0	39

TABLE 2.4: Effect of Flow Rate on the Manganese Content of the Deposit and the Cathode Current Efficiency for Deposition from a Sulphate-Citrate Bath ⁽²⁹⁾⁽³⁰⁾

(Deposited at 40°C, 7Adm⁻²)

Sample	Corrosion Performance ^a	Electrocoat Performance ^b	Comment
Bare steel	High/red	2	Unacceptable
7.5 µm Zn	Med/red+white	5	Unacceptable
6.0 µm Zn-Ni	Med/white	2	Unacceptable
2.5 µm Zn-Mn	Low/black	2	Unacceptable
5.0 µm Zn-Mn	None	0	Very good
7.5 µm Zn-Mn	None	0	Very good
10.0 µm Zn-Mn	None	0	Excellent

^a Low/Medium/High = degree of rust; White/Red/Black = type of rust.

^b 0 = no undercutting; 1 = up to 1 mm; 2 = up to 2 mm; 3 = up to 3 mm; 4 = up to 4 mm; 5 = >4 mm (delamination).

TABLE 2.5: Corrosion Performance of Zinc-50% Manganese Coatings ⁽²⁹⁾⁽³⁰⁾

(All panels phosphated and cathodically electrocoated (25µm), then scribed and subjected to ASTM 117B Salt Spray testing for 1000 hours)

Manganese Sulphate Concentration / M	Zinc Sulphate Concentration / M	Sodium Citrate Concentration / M	Other Salts	pH
Standard bath (fresh and aged) (HC)				
Effect of anode and cathode separation				
Effect of repeated use of the standard bath				
Effect of oxygen content				
0.24	0.24	0.6		5.6
Effect of pH on a standard bath				
0.24	0.24	0.6		3.0 (HC), 4.0 (HC), 5.0 (HC), 5.6 (HC)
Constituent solutions of a standard bath				
0.24	-	0.6	0.24M sodium sulphate	5.6 (HC)
-	0.24	0.6	0.24M sodium sulphate	5.6 (HC)
-	-	0.6	0.48M sodium sulphate	5.6 (HC)
0.24	0.24	0.6		5.6 (HC)
Effect of sodium citrate on manganese electrodepositon				
0.24	-	-	0.24M sodium sulphate	5.6 (HC)
0.24	-	0.6	0.24M sodium sulphate	5.6 (HC)
Effect of sodium citrate on zinc electrodepositon				
-	0.24	-	0.24M sodium sulphate	5.6 (HC)
-	0.24	0.6	0.24M sodium sulphate	5.6 (HC)
Effect of sodium citrate on zinc-manganese electrodepositon				
0.24	0.24	-		5.0 (HC)
0.24	0.24	0.6		5.0 (HC)
Effect of sodium citrate content				
0.24	0.24	0.0, 0.2 (HC), 0.4, 0.8, 0.6 (HC), 1.0 (HC)		5.0
Effect of metal salt content (in the same ratio as a standard bath)				
0.12	0.12	0.6		5.0 (HC)
0.24	0.24	0.6		5.0 (HC)
0.36	0.36	0.6		5.0
0.48	0.48	0.6		5.0 (HC)
Effect of zinc sulphate content				
0.24	0.00, 0.024, 0.12 (HC), 0.24 (HC), 0.36, 0.48 (HC)	0.6		5.0
Effect of manganese sulphate content				
0.00, 0.024, 0.12 (HC), 0.24 (HC), 0.36, 0.48 (HC)	0.24	0.6		5.0
Effect of additions (fresh and aged baths)				
0.24	0.24	0.6	2g/l ascorbic acid	5.4 (HC)
0.24	0.24	0.6	2g/l sodium sulphite	5.4 (HC)

(HC) Hull Cell Test performed on these solutions

TABLE 3.1: Baths Used for Polarisation Curves and Hull Cell Tests

Manganese Sulphate Concentration / M	Zinc Sulphate Concentration / M	Sodium Citrate Concentration / M	Other Salts
Standard bath			
0.24	0.24	0.6	
Constituent solutions of a standard bath			
0.24	-	-	
-	0.24	-	
0.24	0.24	-	
-	-	0.6	
Effect of sodium citrate content			
0.24	0.24	0.2	
0.24	0.24	0.4	
Effect of zinc sulphate content			
0.24	0.12	0.6	
Effect of manganese sulphate content			
0.12	0.24	0.6	
Effect of additions			
0.24	0.24	0.6	2g/l ascorbic acid
0.24	0.24	0.6	2g/l sodium sulphite
Effect of exclusion of atmosphere (solutions in sealed bottles)			
0.24	0.24	0.6	
0.24	0.24	0.6	2g/l ascorbic acid
0.24	0.24	0.6	2g/l sodium sulphite
Effect of metal salt content (in the same ratio as a standard bath)			
0.12	0.12	0.6	
0.2	0.2	0.6	

TABLE 3.2: Baths Used for Visual Examination

Bath Composition	Degree of Precipitation	Deterioration in Colour
Standard bath (Figure 4.12)		
0.24M manganese sulphate + 0.24M zinc sulphate + 0.6M sodium citrate	D	Pale orange fresh solution, gradually darkening to dark orange
Constituent solutions of a standard bath (Figure 4.20)		
0.24M manganese sulphate + 0.24M zinc sulphate	A	Pale pink - no discolouration with time
0.6M sodium citrate	A	Colourless - no discolouration with time
Effect of sodium citrate content (Figure 4.26)		
0.24M manganese sulphate + 0.24M zinc sulphate + 0.2M sodium citrate	E	Some discolouration – decreased relative to standard bath
0.24M manganese sulphate + 0.24M zinc sulphate + 0.4M sodium citrate	E	Moderate discolouration – decreased relative to standard bath
Effect of zinc sulphate content (Figure 4.29)		
0.24M manganese sulphate + 0.12M zinc sulphate + 0.6M sodium citrate	B	Very dark orange at end – increased relative to standard bath
Effect of manganese sulphate content (Figure 4.32)		
0.12M manganese sulphate + 0.24M zinc sulphate + 0.6M sodium citrate	A	Slight decrease in discolouration relative to standard bath
Effect of metal salt content (in the same ratio as a standard bath) (Figure 4.34)		
0.12M manganese sulphate + 0.12M zinc sulphate + 0.6M sodium citrate	A	As standard bath
0.2M manganese sulphate + 0.2M zinc sulphate + 0.6M sodium citrate	C	As standard bath
Effect of additions (Figures 4.36 and 4.37)		
0.24M manganese sulphate + 0.24M zinc sulphate + 0.6M sodium citrate + 2g/l ascorbic acid	D	Straw yellow – decrease relative to standard bath
0.24M manganese sulphate + 0.24M zinc sulphate + 0.6M sodium citrate + 2g/l sodium sulphite	D	Virtually no discolouration
Effect of exclusion of atmosphere (solutions in sealed bottles) (Figures 4.44 and 4.45)		
Standard Bath - 0.24M manganese sulphate + 0.24M zinc sulphate + 0.6M sodium citrate +	D	Slight discolouration – decreased relative to standard bath open to atmosphere
0.24M manganese sulphate + 0.24M zinc sulphate + 0.6M sodium citrate + 2g/l ascorbic acid	D	Slight discolouration but pale yellow – decreased relative to identical bath open to atmosphere
0.24M manganese sulphate + 0.24M zinc sulphate + 0.6M sodium citrate + 2g/l sodium sulphite	D	Virtually no discolouration – similar to identical bath open to atmosphere

Key for precipitation: A – None B – Very slight C – Slight D – Moderate E – Heavy F – Very heavy

TABLE 4.1: Summary of Effects of Bath Deterioration after 30 Days
(Figures 4.12 to 4.45)

	Mn	Zn	Na	C	H	N	S
SEM EDX System	63.14 %	36.86 %					
Atomic Absorption	14.36 %	7.64 %	0.02 %				
Microanalysis				19.59 %	4.30 %	0.00%	
Titration							0.00%

All percentage values are by weight.

TABLE 4.2: Elemental Analysis of the Precipitate Deposited from a Standard Bath

	Mn	Zn	C	H
Experimental				
Results (Table 4.2)	14.36 %	7.64 %	19.59 %	4.30 %
Theoretical				
$[\text{Mn}(\text{H}_2\text{O})_6][\text{Mn}(\text{C}_6\text{H}_5\text{O}_7)\text{H}_2\text{O}]_2 \cdot 2\text{H}_2\text{O}$	22.79%		19.93%	4.18%
$\text{Mn}(\text{C}_6\text{H}_6\text{O}_7) \cdot \text{H}_2\text{O}$	20.88%		27.40%	3.07%

All percentage values are by weight.

TABLE 5.1: Comparison of Elemental Analysis of the Precipitate Deposited from a Standard Bath with Known Manganese Citrate Complexes ⁽⁶⁶⁾⁽⁹⁵⁾⁽⁹⁸⁾⁽⁹⁹⁾

FIGURES

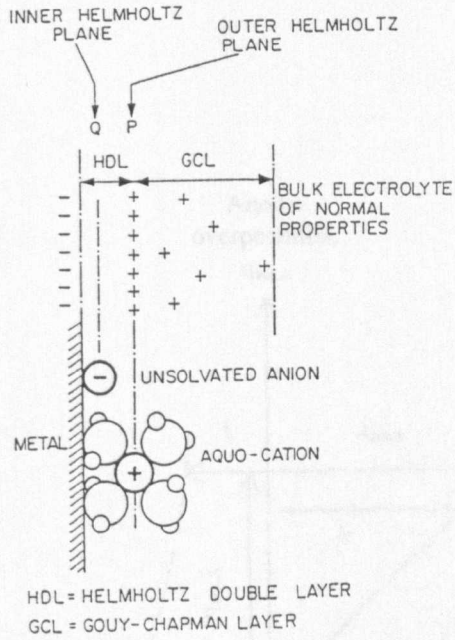
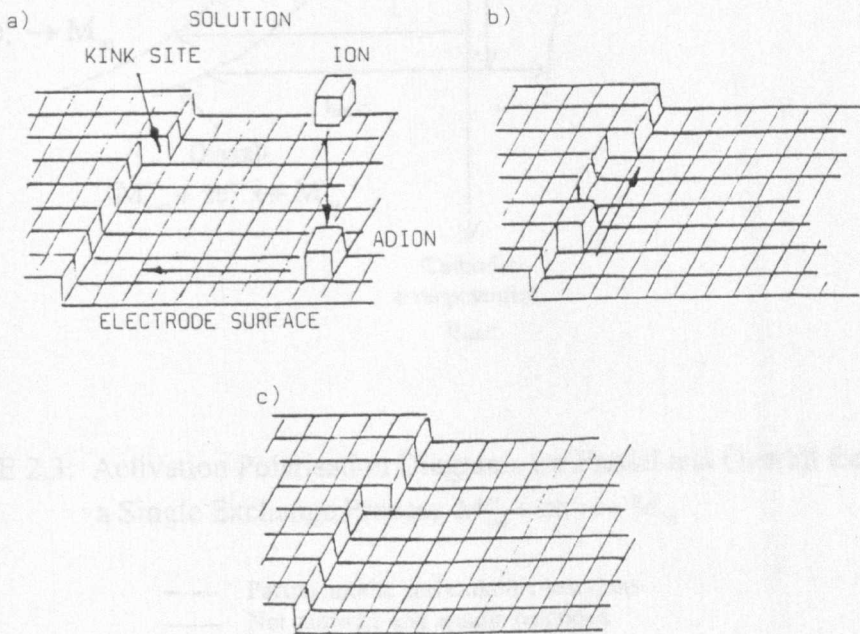


FIGURE 2.1: The Structure of the Electrical Double Layer⁽¹²⁾



- a) Transfer of the ion from the solution to a site on the metal surface and the diffusion of such an adion along the surface to a growth step;
- b) Diffusion of the ion along the growth step;
- c) Incorporation of the ion into a kink site.

FIGURE 2.2: Metal Ion Deposition at the Cathode Surface⁽¹⁷⁾

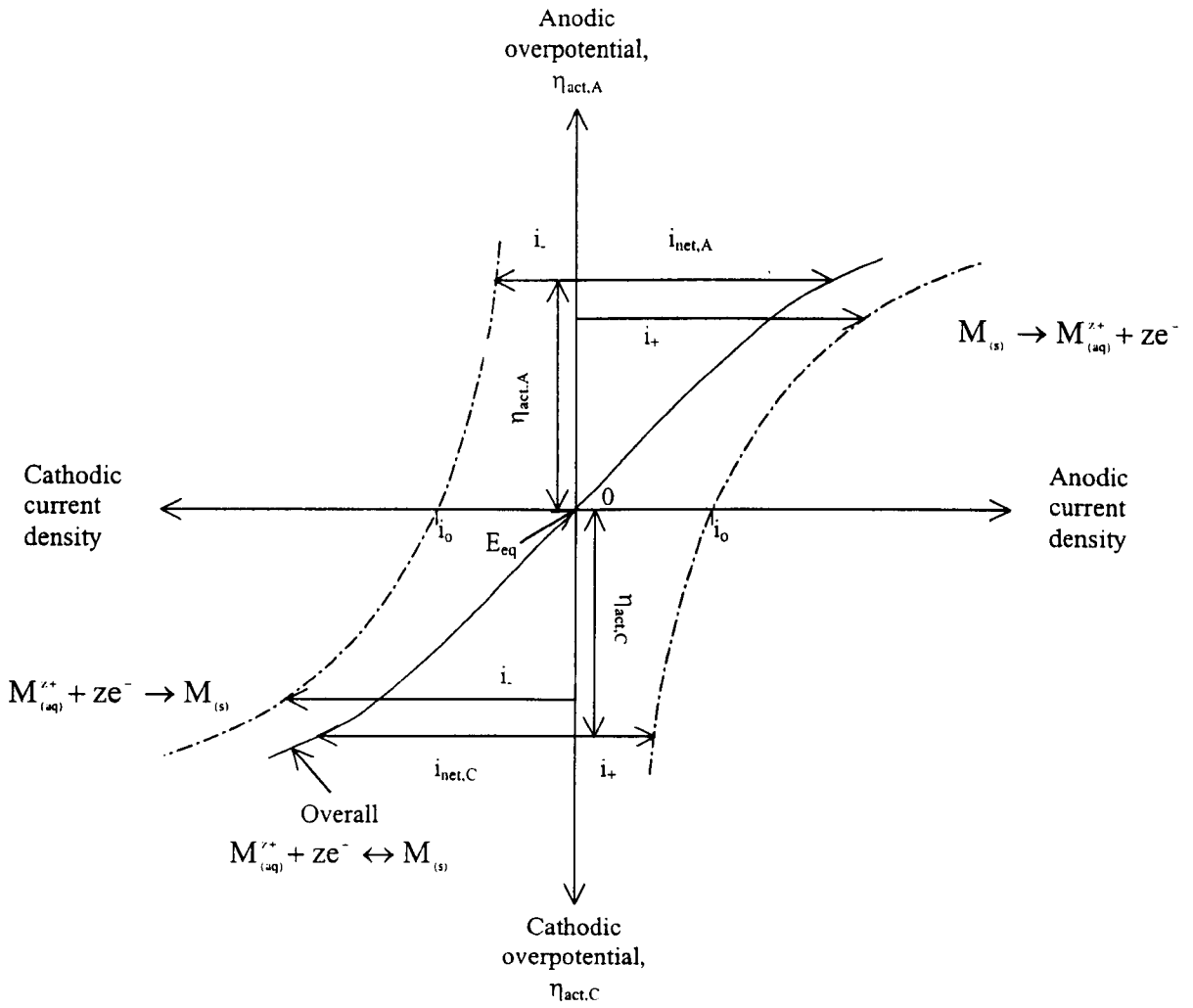


FIGURE 2.3: Activation Polarisation Diagrams for Partial and Overall Reactions for a Single Exchange Process $M_{(aq)}^{z+} + ze^- \leftrightarrow M_{(s)}$

- Partial anodic and cathodic reactions
- Net cathodic and anodic reactions

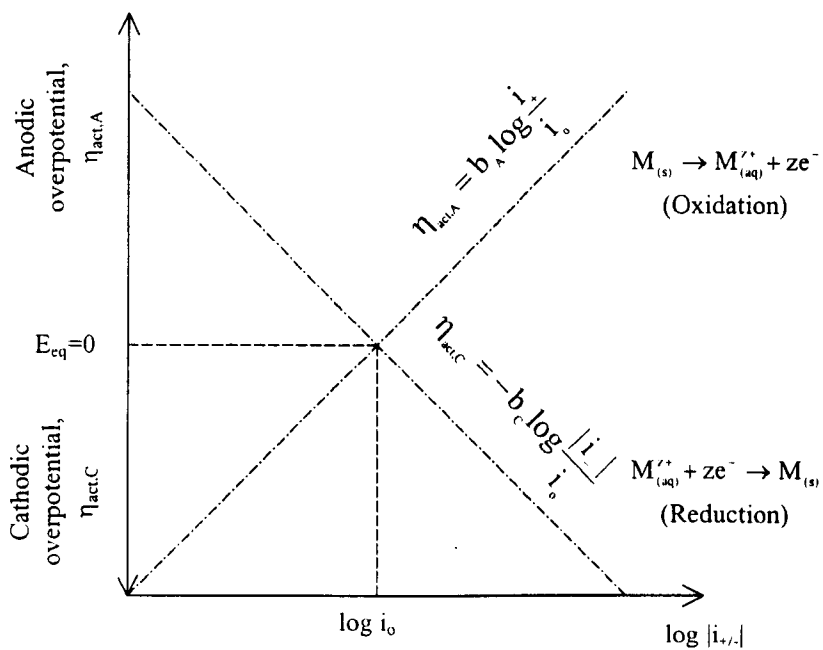


FIGURE 2.4: Activation Polarisation Diagrams for Partial Reactions for a Single Exchange Process $M_{(aq)}^{z+} + ze^{-} \leftrightarrow M_{(s)}$

(Both anodic and cathodic reactions plotted to the right on a semi-log scale)

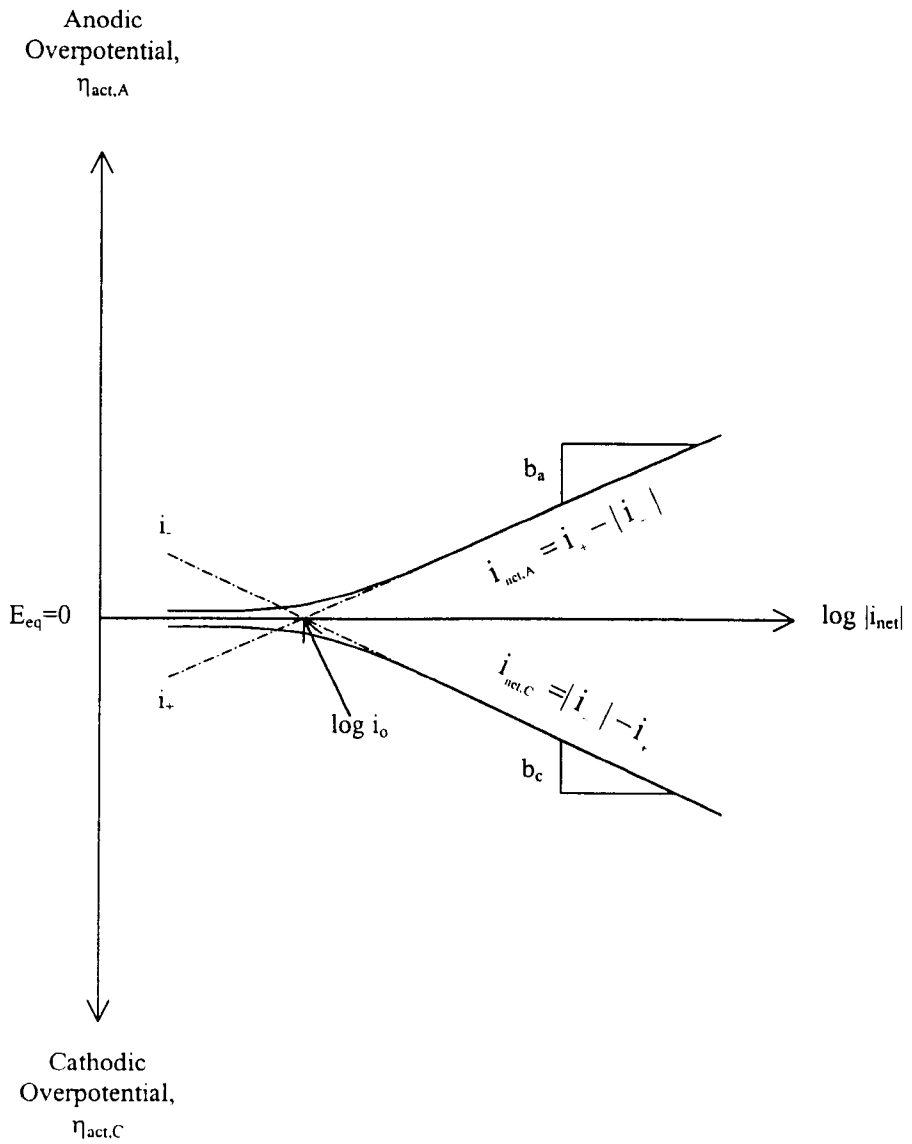
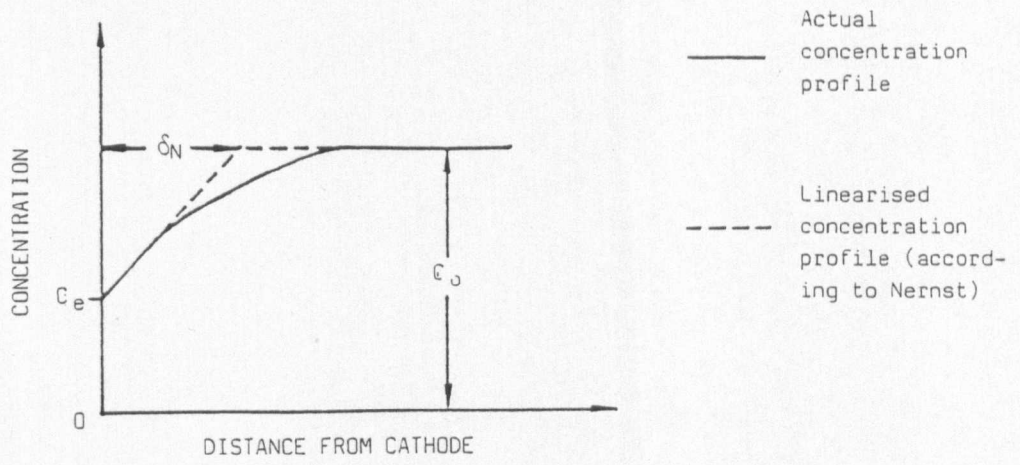


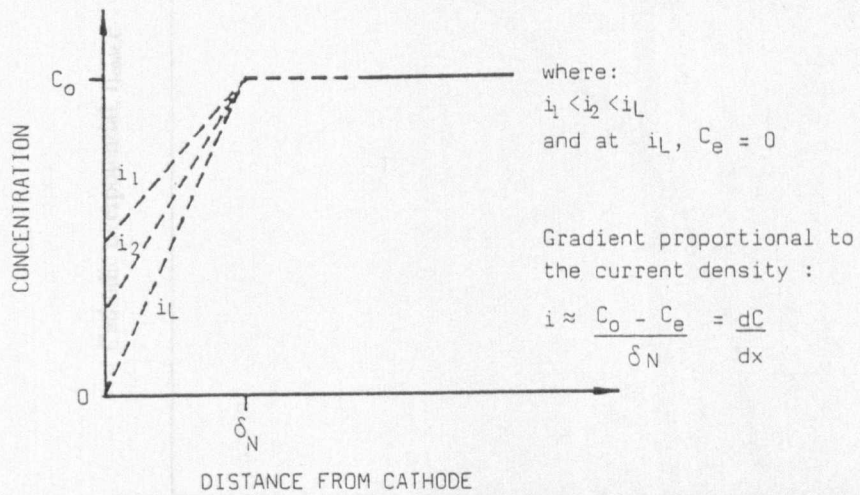
FIGURE 2.5: Activation Polarisation Diagram for Overall Reaction for a Single Exchange Process $M_{(aq)}^{z+} + ze^- \leftrightarrow M_{(s)}$

(As Figure 2.3, but both anodic and cathodic curves plotted to the right on a semi-log scale)

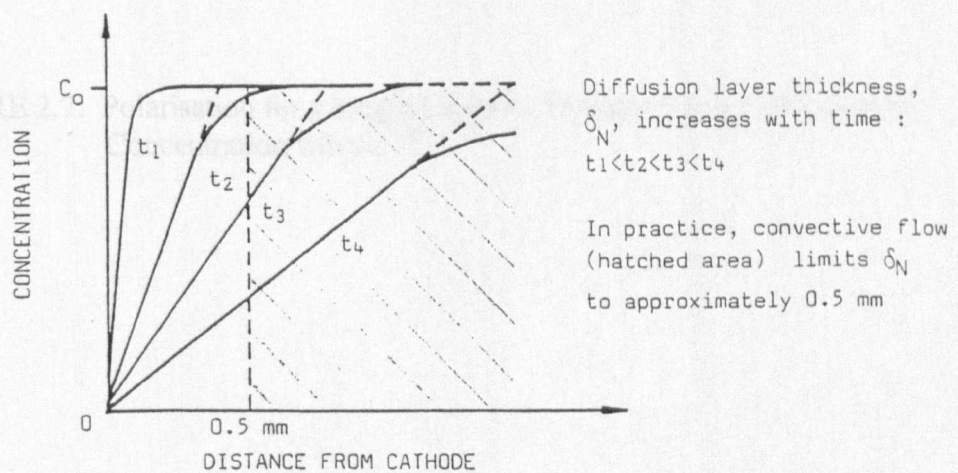
- Partial anodic and cathodic reactions (as Figure 2.4)
- Net cathodic and anodic reactions



- a) Schematic representation of metal ion concentration at the cathode during deposition



- b) Change in concentration profile with current density for values smaller than the limiting current density



- c) Concentration profiles across the diffusion layer at the limiting current density

FIGURE 2.6: Metal Ion Concentration at the Cathode During Electrodeposition ⁽¹⁵⁾⁽¹⁸⁾

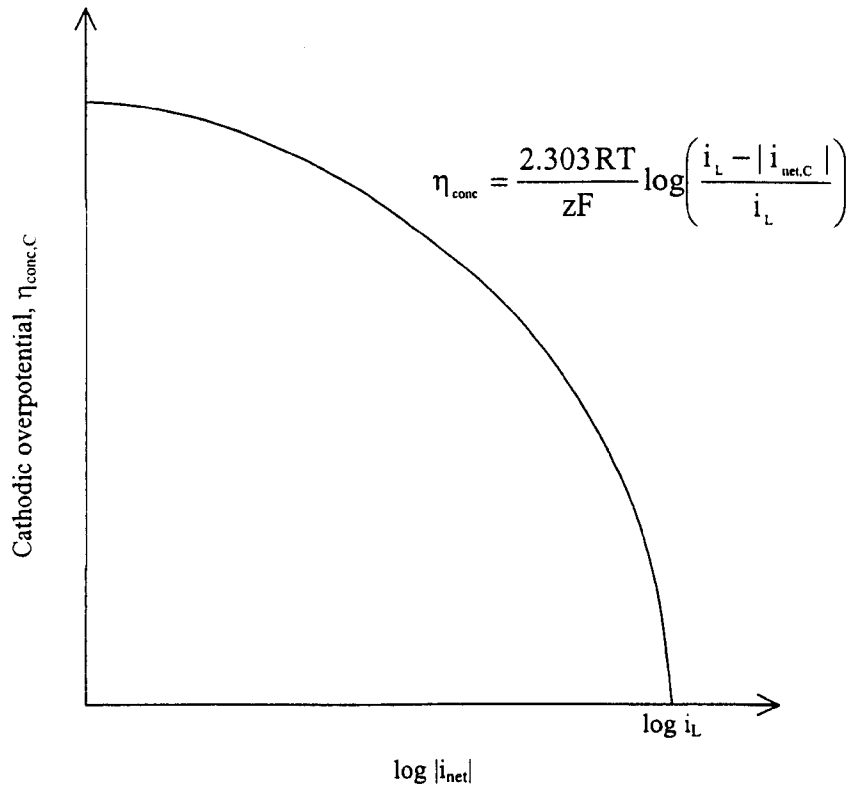


FIGURE 2.7: Polarisation for a Single Cathodic Process Solely Controlled by Concentration Effects ⁽¹⁰⁾

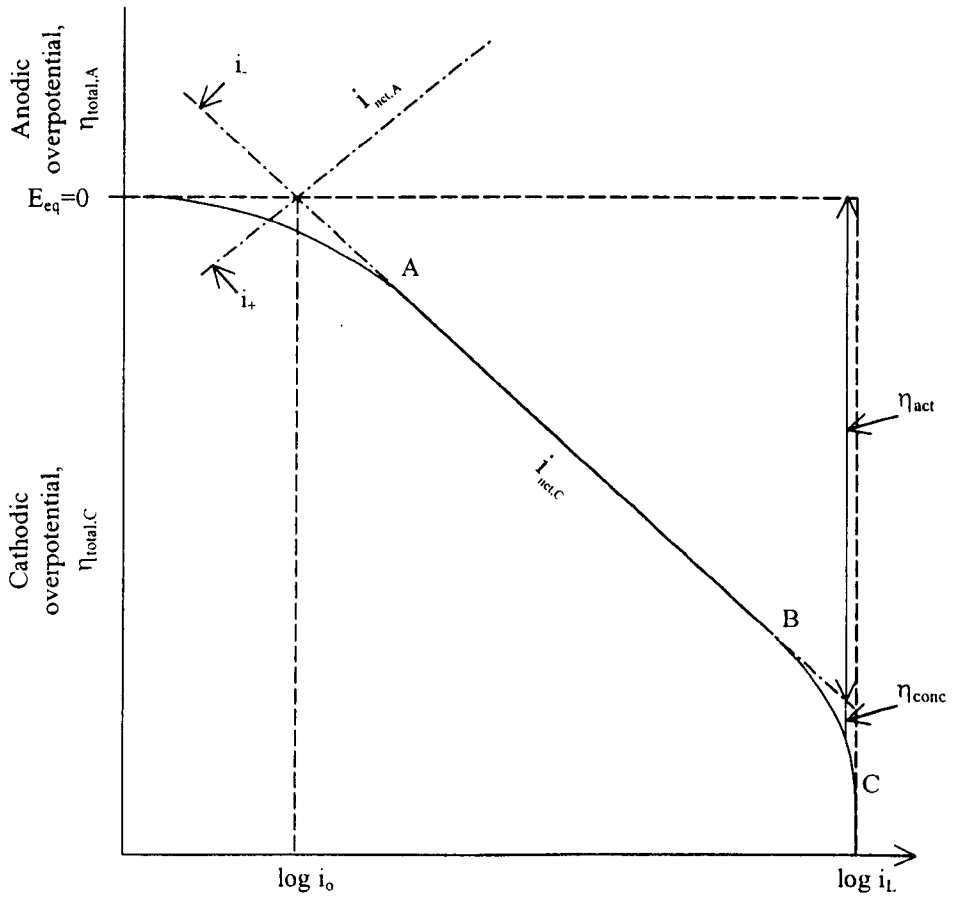


FIGURE 2.8: Generalised Cathodic Total Polarisation Curve for a Single Exchange Process

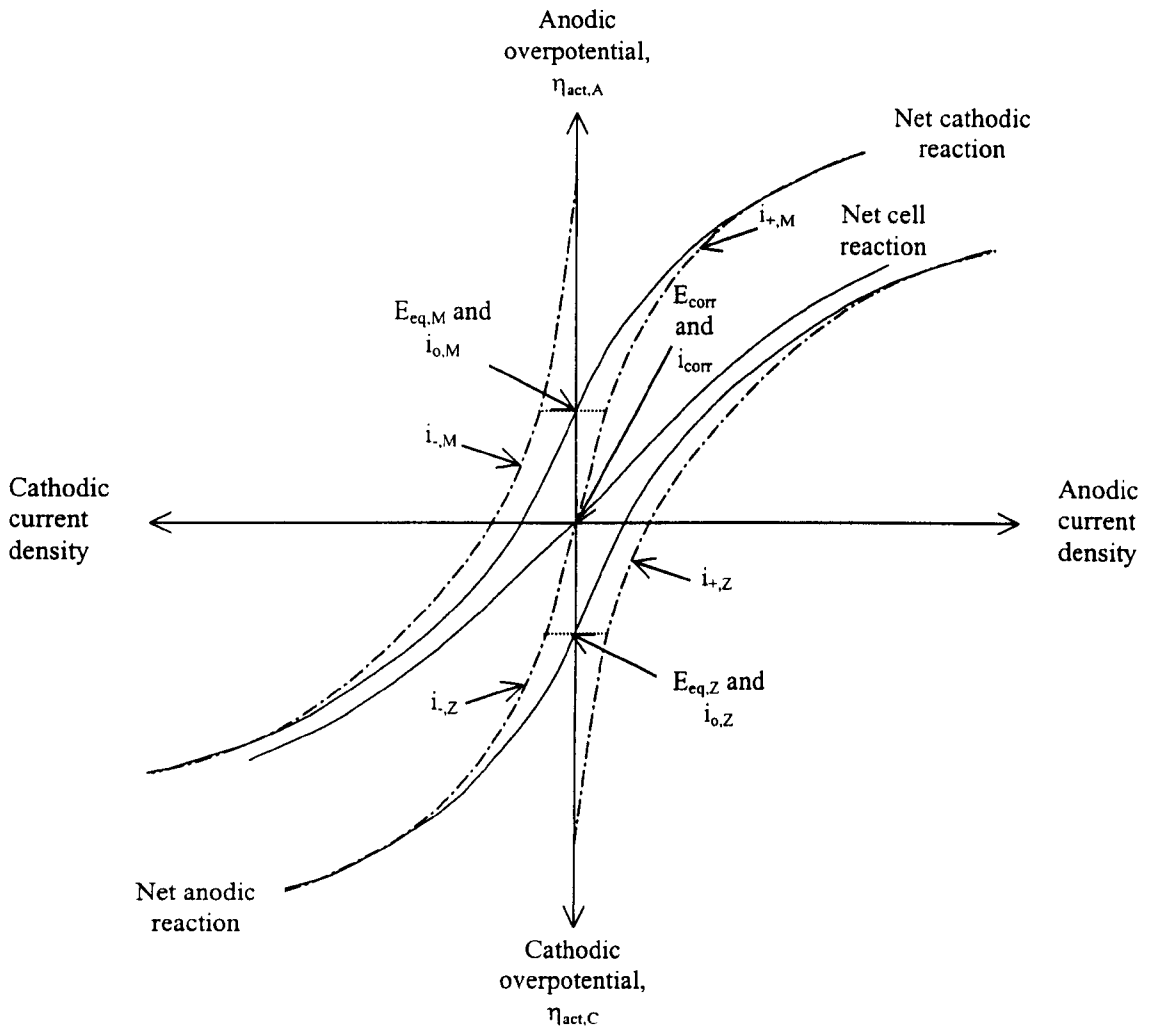


FIGURE 2.9: Activation Polarisation Diagrams for Partial and Overall Reactions for Two Exchange Processes

- Partial anodic and cathodic reactions
- Net cathodic, anodic and cell reactions

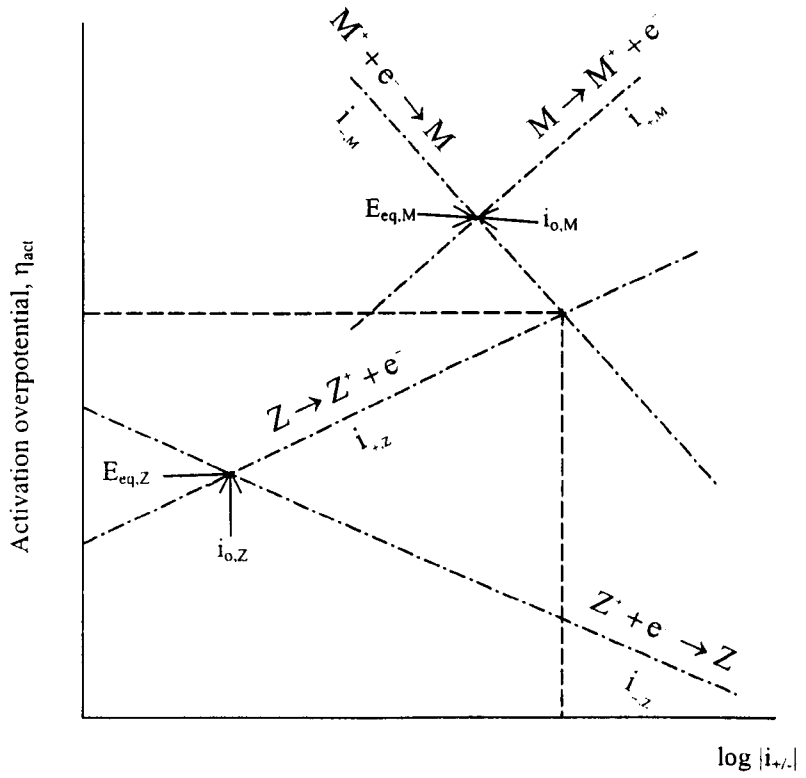


FIGURE 2.10: Activation Polarisation Diagrams for Partial Reactions for Two Exchange Processes

(Both anodic and cathodic reactions plotted to the right on a semi-log scale)

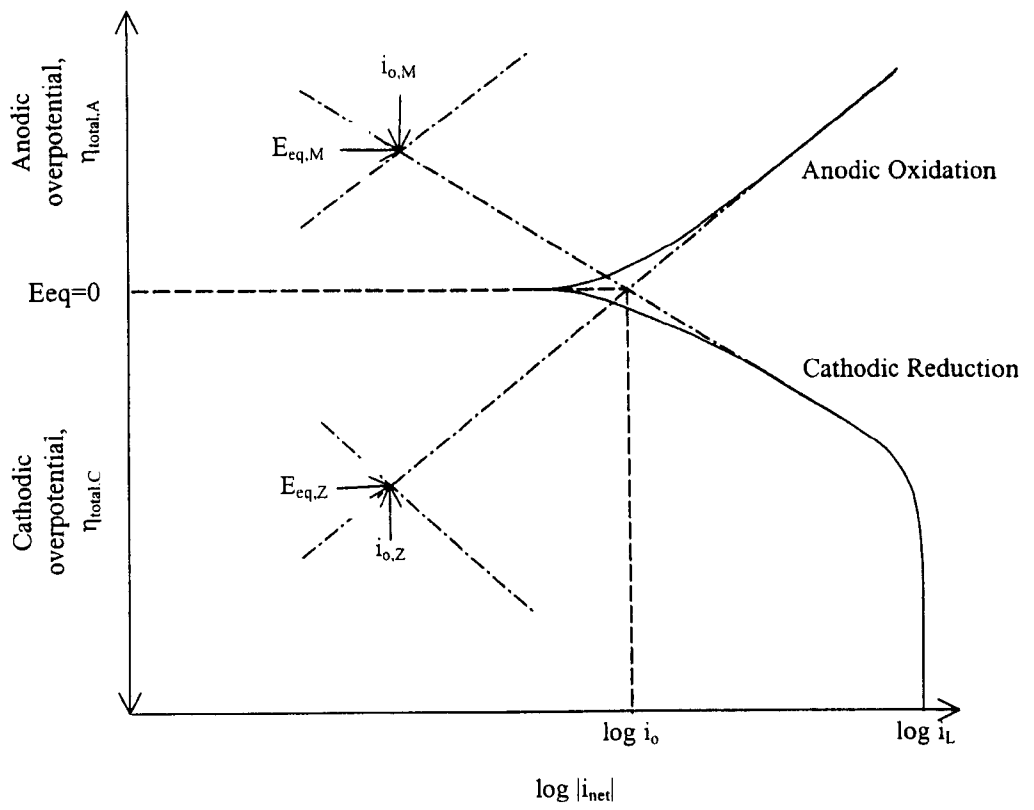


FIGURE 2.11: Generalised Total Polarisation Curve for a Two Exchange Process

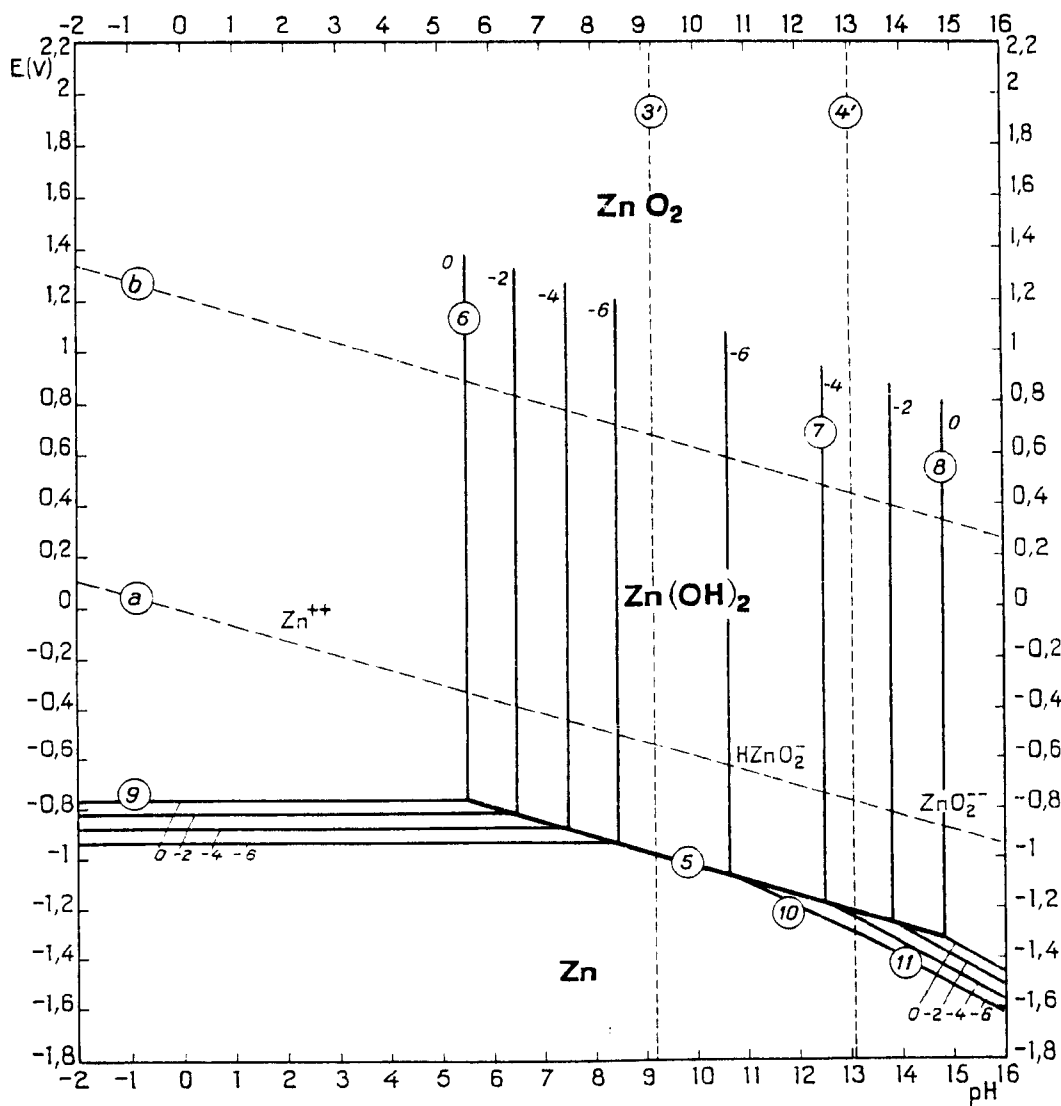


FIGURE 2.12: Equilibrium Potential-pH (Pourbaix) Diagram for the Zinc-Water System at 25°C ⁽²⁰⁾

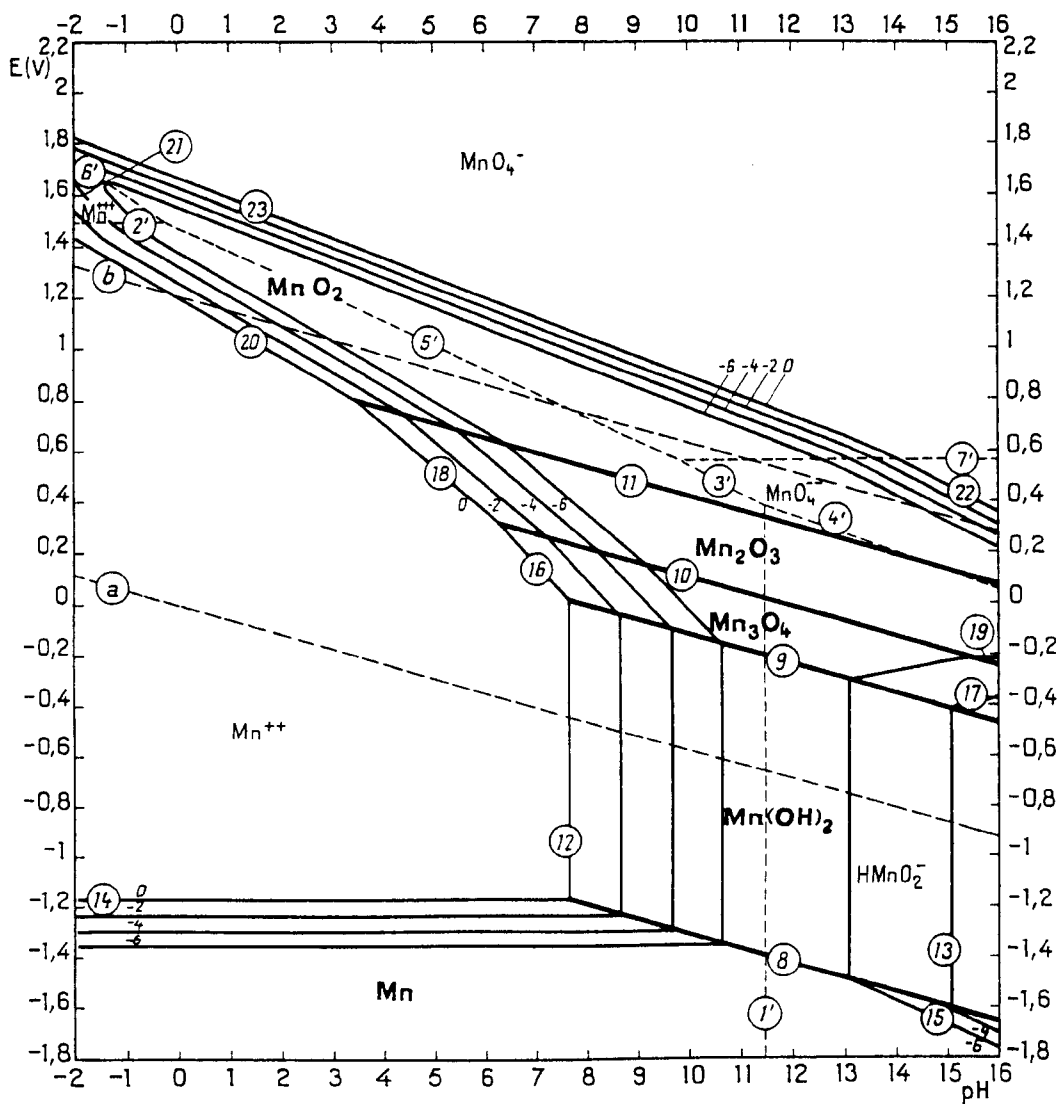
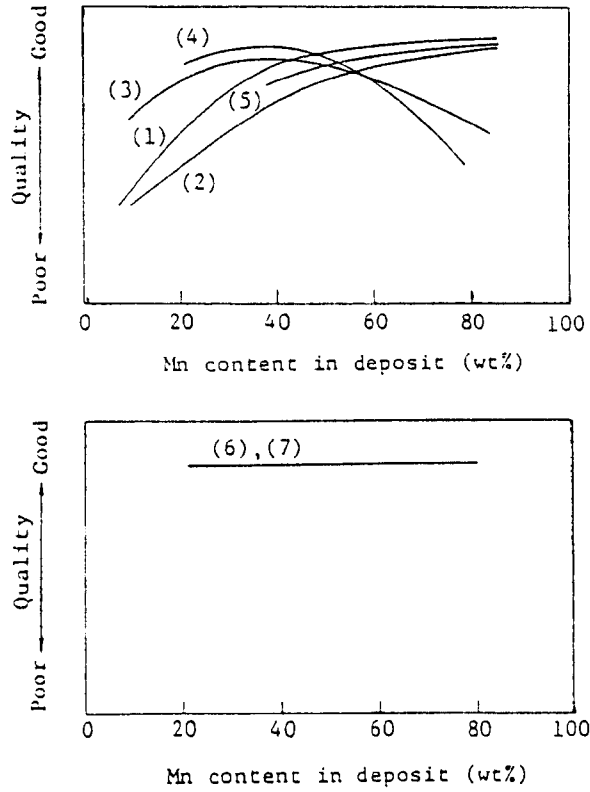
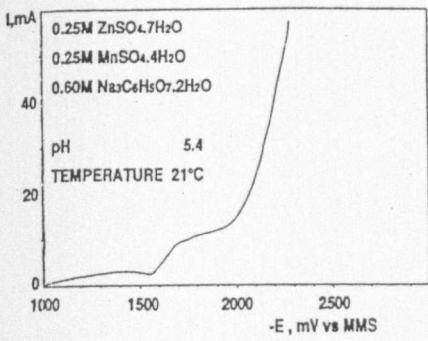


FIGURE 2.13: Equilibrium Potential-pH (Pourbaix) Diagram for the Manganese-Water System at 25°C ⁽²⁰⁾

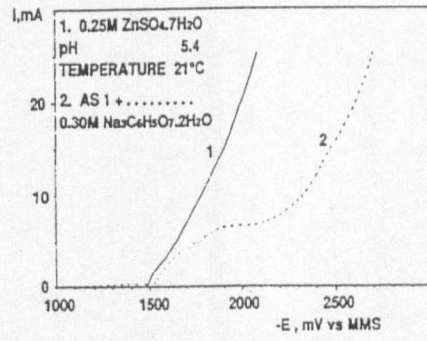


- (1): Corrosion resistance without painting
- (2): Blistering resistance
- (3): Perforation corrosion resistance
- (4): Workability
- (5): Weldability
- (6): Wet adhesion of paint
- (7): Anti-cratering property

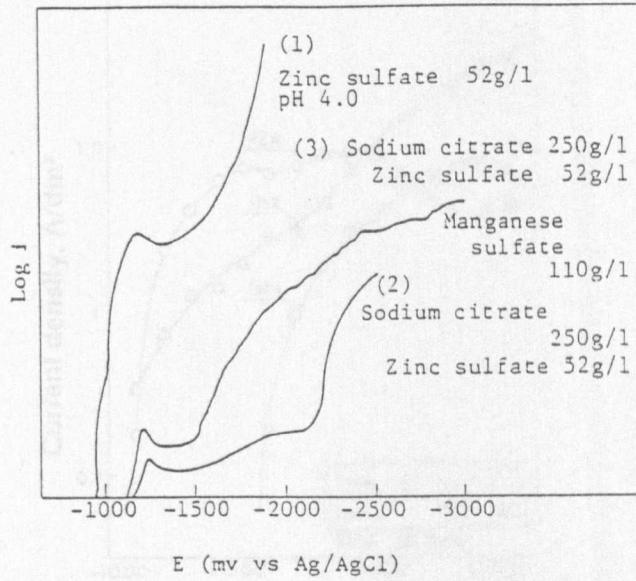
FIGURE 2.14: Summary of the properties of Zinc-Manganese Electroplate as a Function of Manganese Content of the Coating ⁽²⁶⁻²⁸⁾



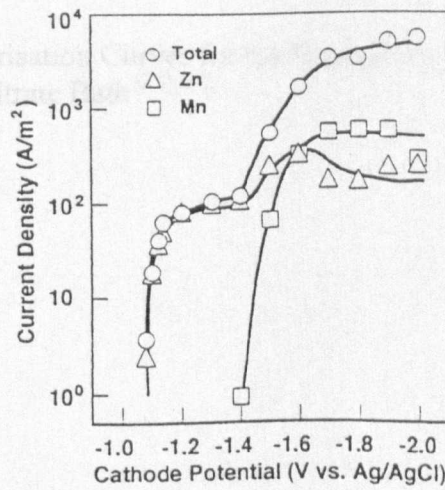
a) (29)(30)



b) (29)(30)



c) (26-28)(36)



d) (32)

FIGURE 2.15: Total Polarisation Behaviour of Zinc-Manganese Electrodeposition from a Sulphate-Citrate Bath

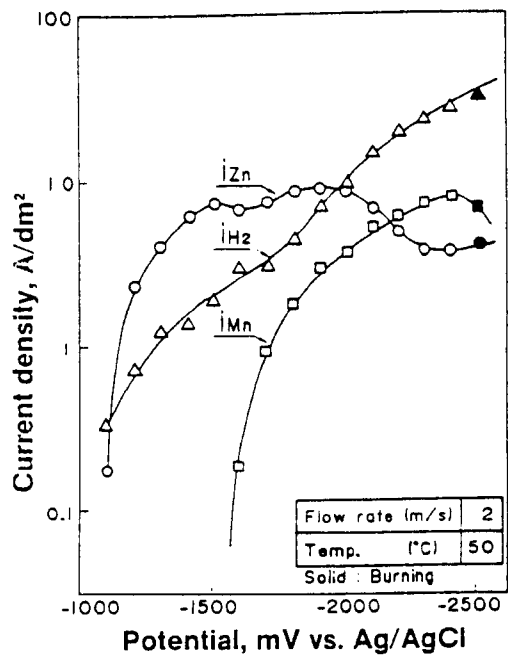


FIGURE 2.16: Partial Polarisation Curves for the Deposition of Zinc-Manganese from a Sulphate-Citrate Bath ⁽³³⁾⁽³⁴⁾

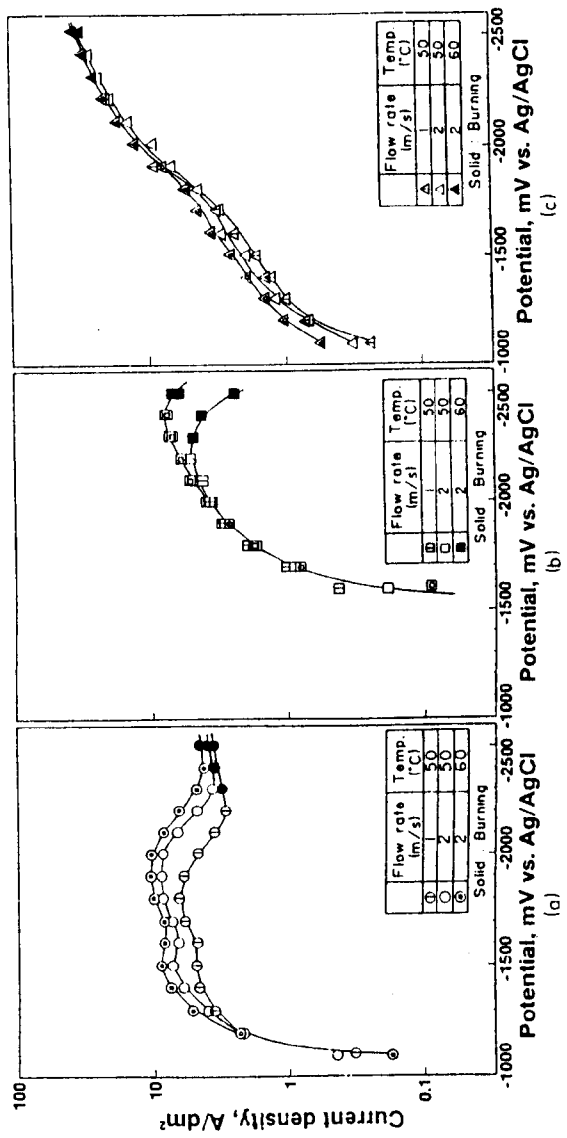


FIGURE 2.17: Effect of Flow Rate and Temperature on the Partial Polarisation Curves for the Deposition of Zinc-Manganese from a Sulphate-Citrate Bath (33)(34)

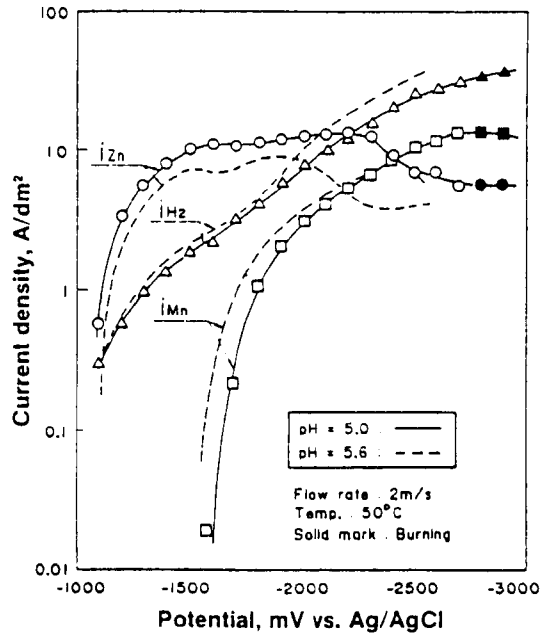


FIGURE 2.18: Effect of pH on the Partial Polarisation Curves for the Deposition of Zinc-Manganese from a Sulphate-Citrate Bath ⁽³³⁾⁽³⁴⁾

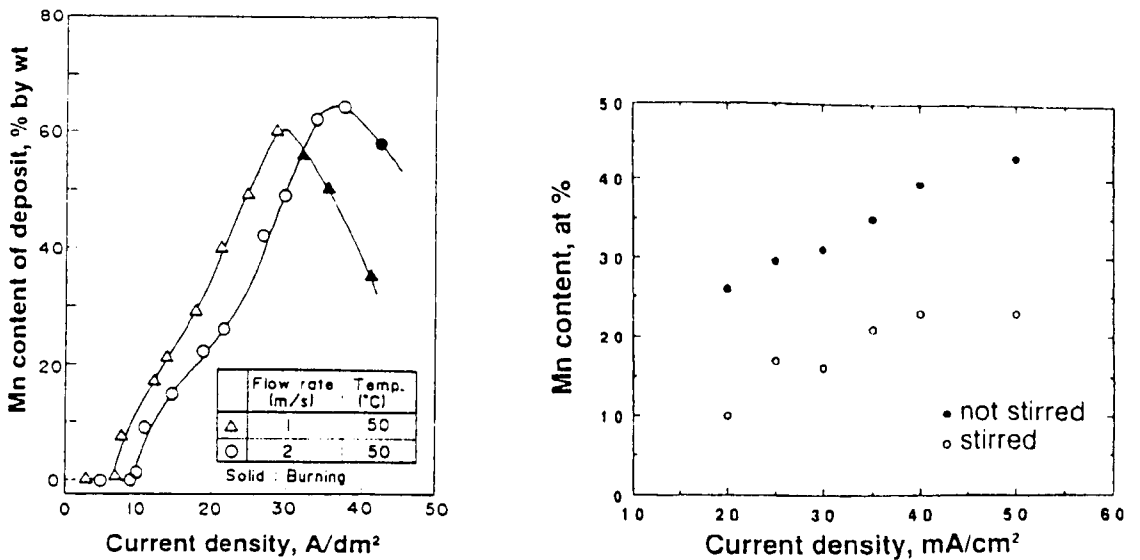


FIGURE 2.19: Effect of Flow Rate on the Manganese Content of the Deposit Produced from a Sulphate-Citrate Bath ⁽³³⁾⁽³⁴⁾⁽³⁷⁾

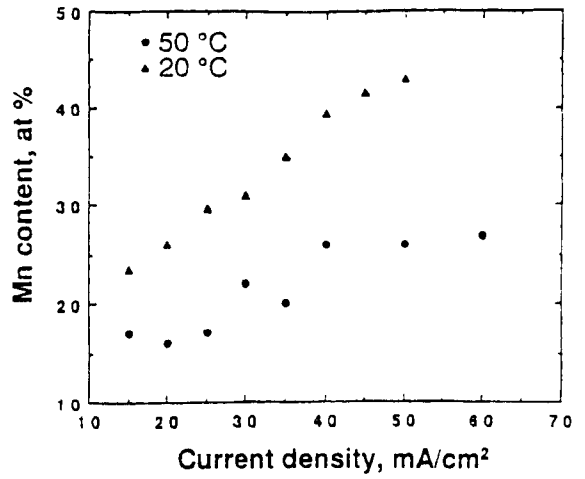
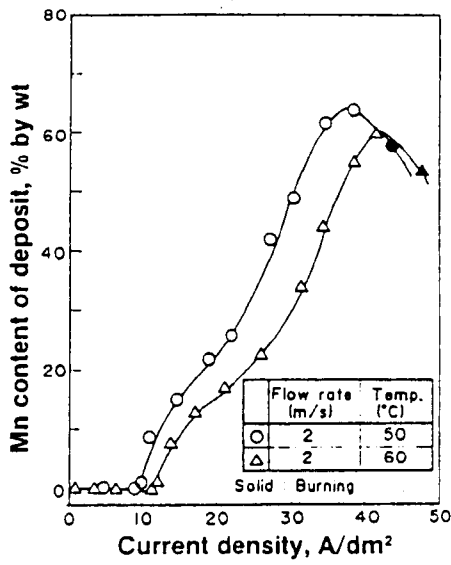


FIGURE 2.20: Effect of Temperature on the Manganese Content of the Deposit Produced from a Sulphate-Citrate Bath ⁽³³⁾⁽³⁴⁾⁽³⁷⁾

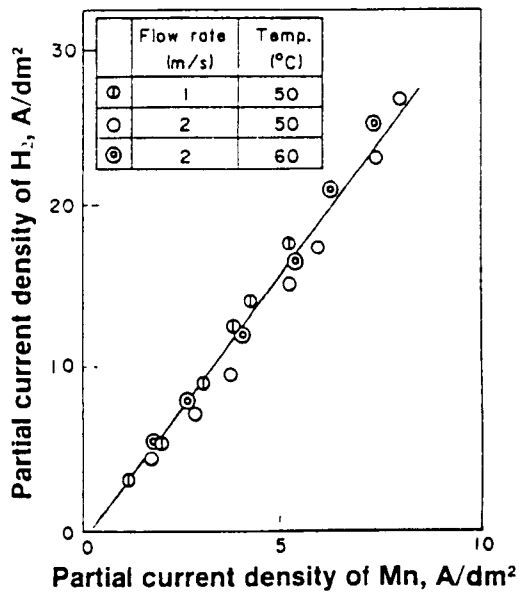


FIGURE 2.21: Relationship Between Partial Current Densities of Hydrogen and Zinc During Zinc-Manganese Deposition from a Sulphate-Citrate Bath ⁽³³⁾⁽³⁴⁾

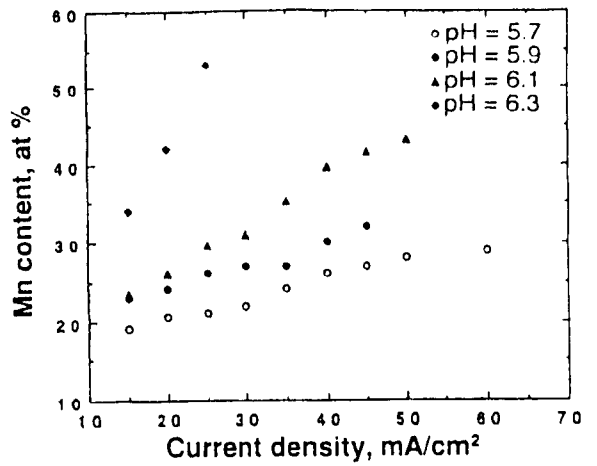
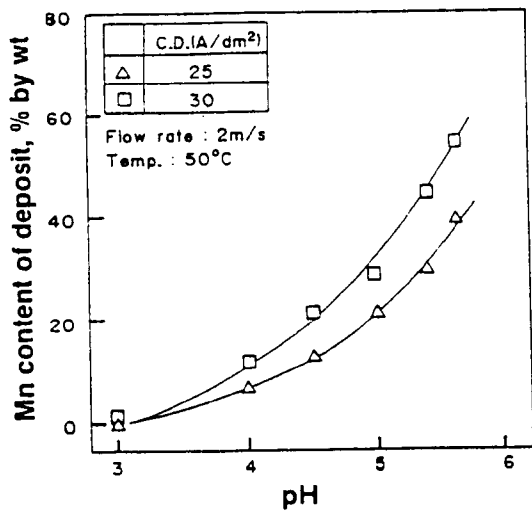


FIGURE 2.22: Effect of Bath pH on the Manganese Content of the Deposit Produced from a Sulphate-Citrate Bath ⁽³³⁾⁽³⁴⁾⁽³⁷⁾

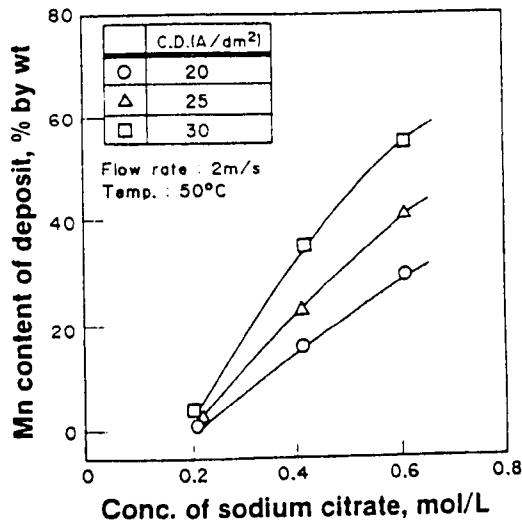


FIGURE 2.23: Effect of Sodium Citrate Content of the Bath on the Manganese Content of the Deposit Produced from a Sulphate-Citrate Bath ⁽³³⁾⁽³⁴⁾

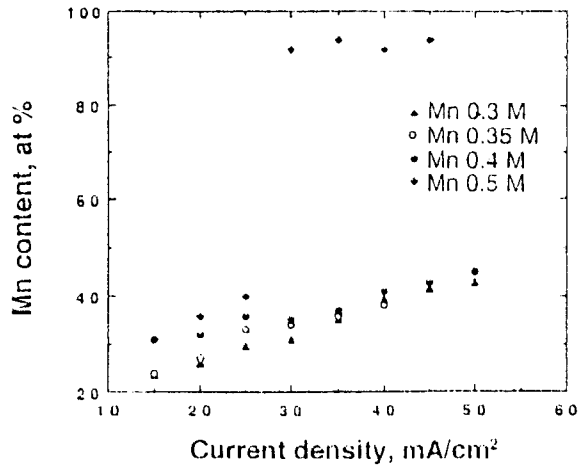


FIGURE 2.24: Effect of Manganese Content of the Bath on the Manganese Content of the Deposit Produced from a Sulphate-Citrate Bath ⁽³⁷⁾

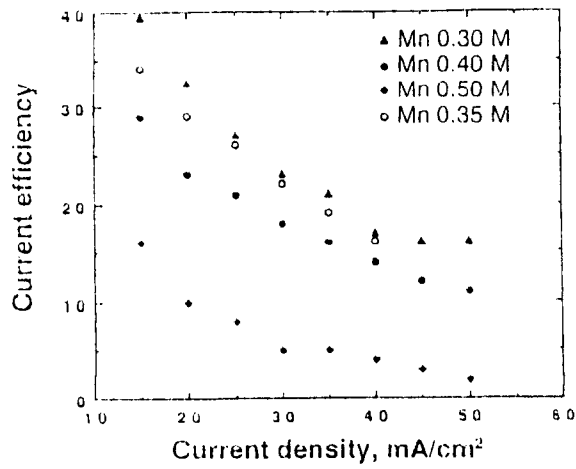


FIGURE 2.25: Effect of Manganese Content of the Bath on the Cathode Current Efficiency for Deposition from a Sulphate-Citrate Bath ⁽³⁷⁾

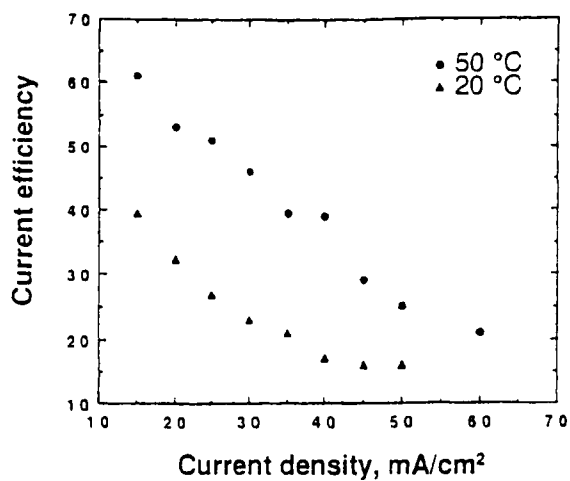


FIGURE 2.26: Effect of Temperature on the Cathode Current Efficiency for Deposition from a Sulphate-Citrate Bath ⁽³⁷⁾

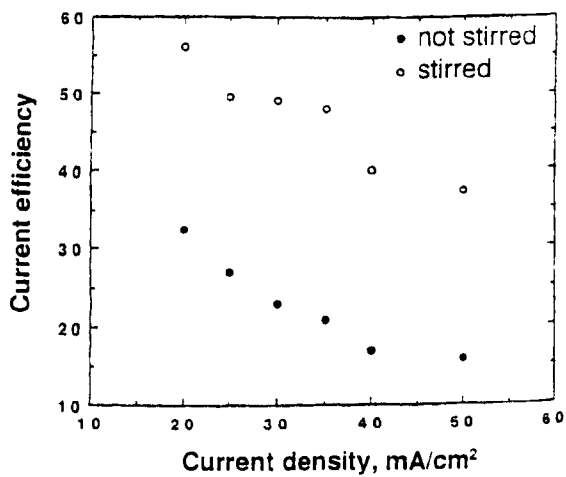


FIGURE 2.27: Effect of Flow Rate on the Cathode Current Efficiency for Deposition from a Sulphate-Citrate Bath ⁽³⁷⁾

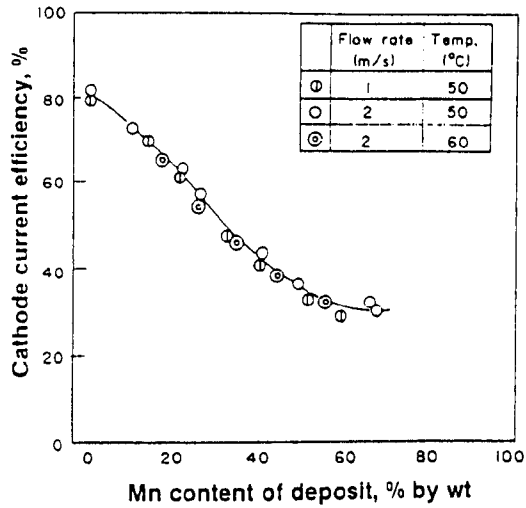


FIGURE 2.28: Relationship Between Manganese Content of the Deposit and Cathode Current Efficiency for Deposition from a Sulphate-Citrate Bath ⁽³³⁾⁽³⁴⁾

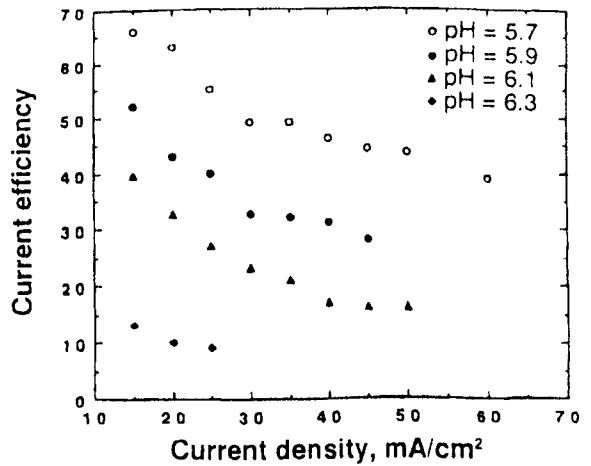
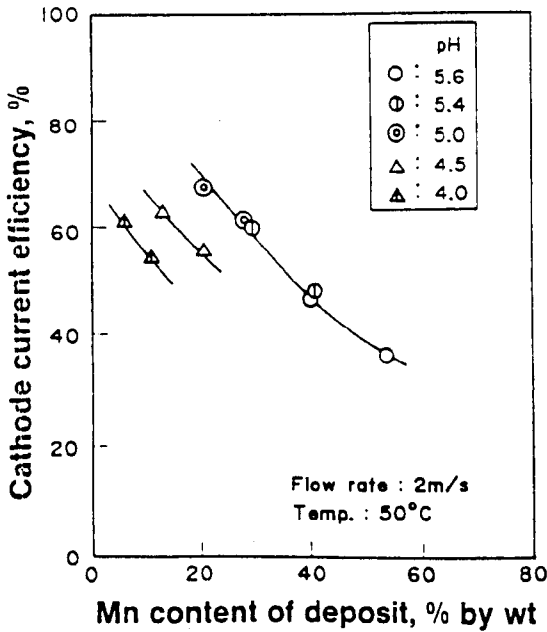


FIGURE 2.29: Effect of pH on the Manganese Content of the Deposit and Cathode Current Efficiency for Deposition from a Sulphate-Citrate Bath ⁽³³⁾⁽³⁴⁾⁽³⁷⁾

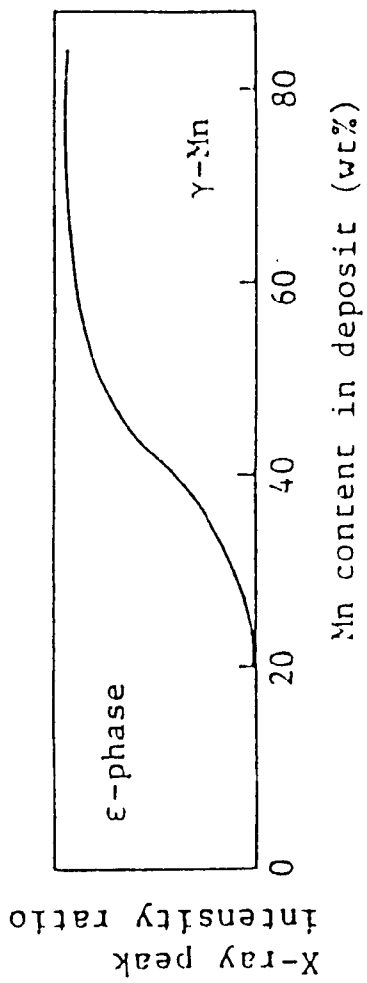


FIGURE 2.30: Phase Composition of Electrodeposited Zinc-Manganese Alloys ⁽²⁶⁻²⁸⁾⁽³⁹⁾⁽⁴⁴⁾⁽⁴⁵⁾

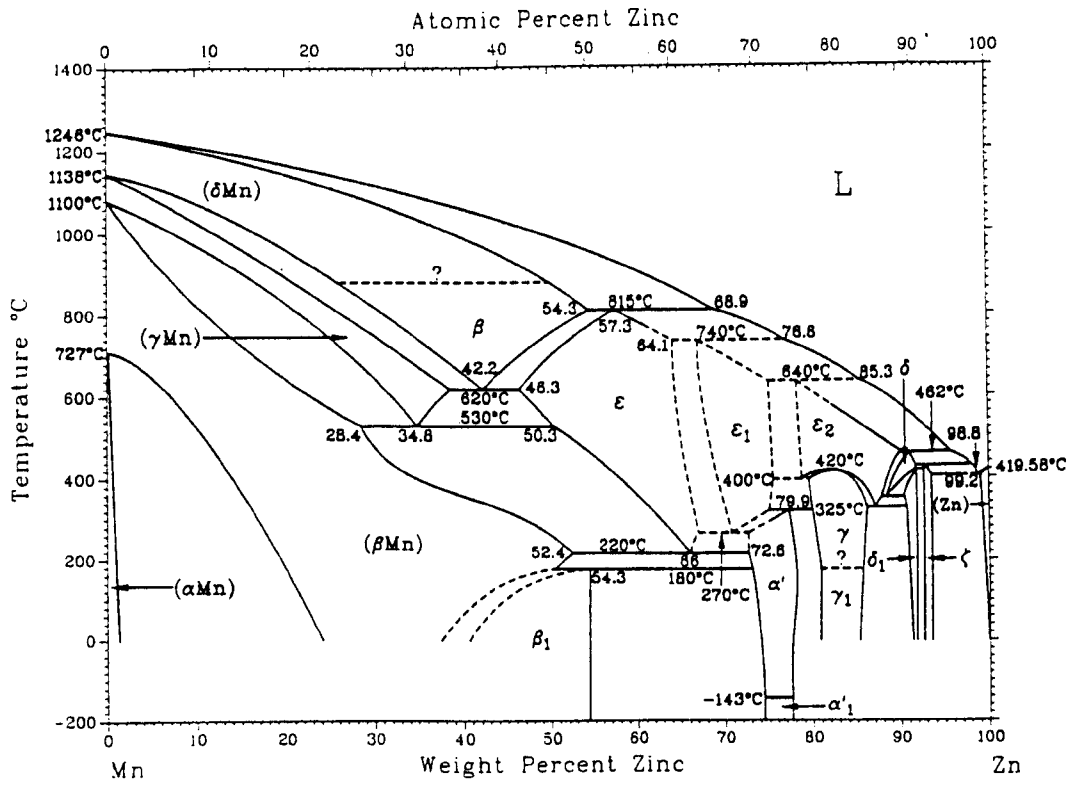


FIGURE 2.31: The Manganese-Zinc Equilibrium Diagram ⁽⁴⁷⁾
 (H. Okamoto and L. E. Tanner, 1990)

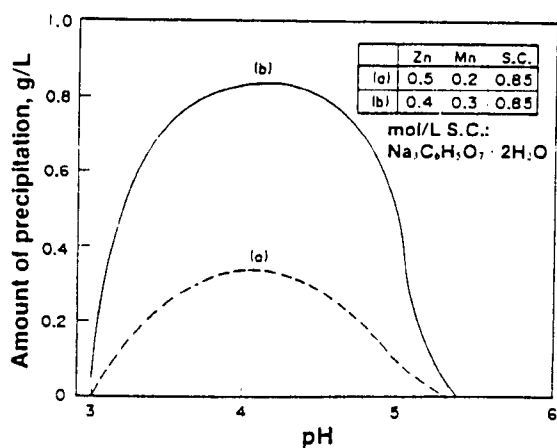


FIGURE 2.32: Relationship Between pH and Precipitation from the Sulphate-Citrate Bath after 20 Days at 50°C ⁽³³⁾⁽³⁴⁾

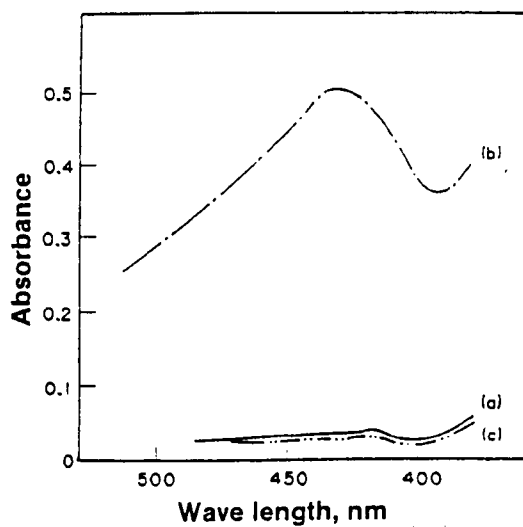


FIGURE 2.33: Effect of Treatment with Metallic Zinc on the Absorbance Spectrum of the Sulphate-Citrate Bath ⁽³³⁾⁽³⁴⁾

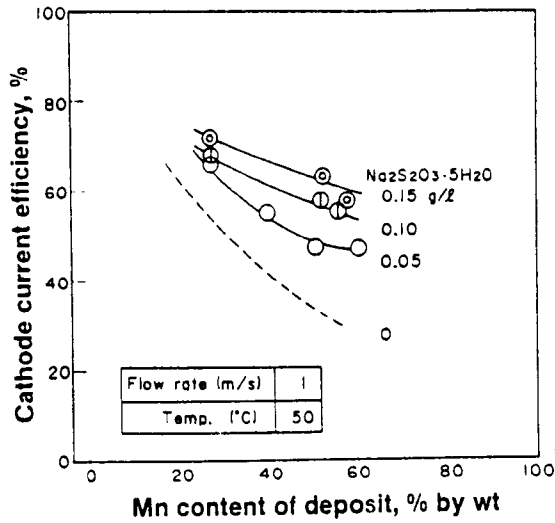


FIGURE 2.34: Effect of Sodium Thiosulphate Additions on the Cathode Current Efficiency for Deposition from the Sulphate-Citrate Bath ⁽³³⁾⁽³⁴⁾

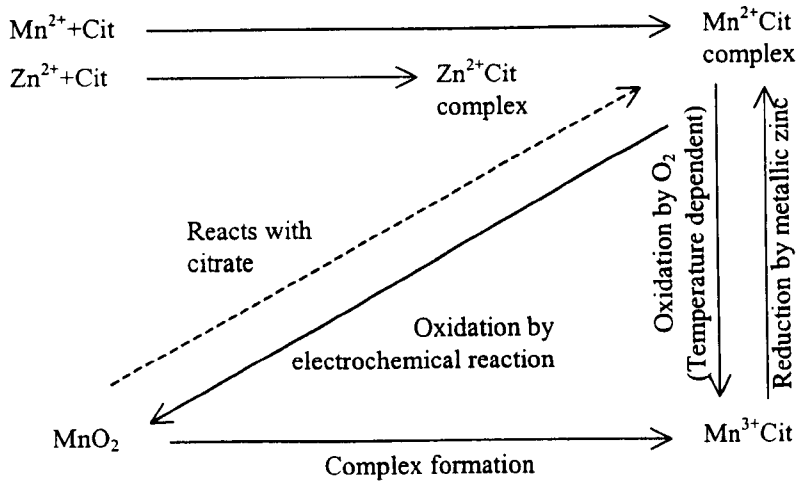


FIGURE 2.35: Chemical Reactions of Manganese and Zinc During Zinc-Manganese Deposition from the Sulphate-Citrate Bath ⁽⁶⁰⁾

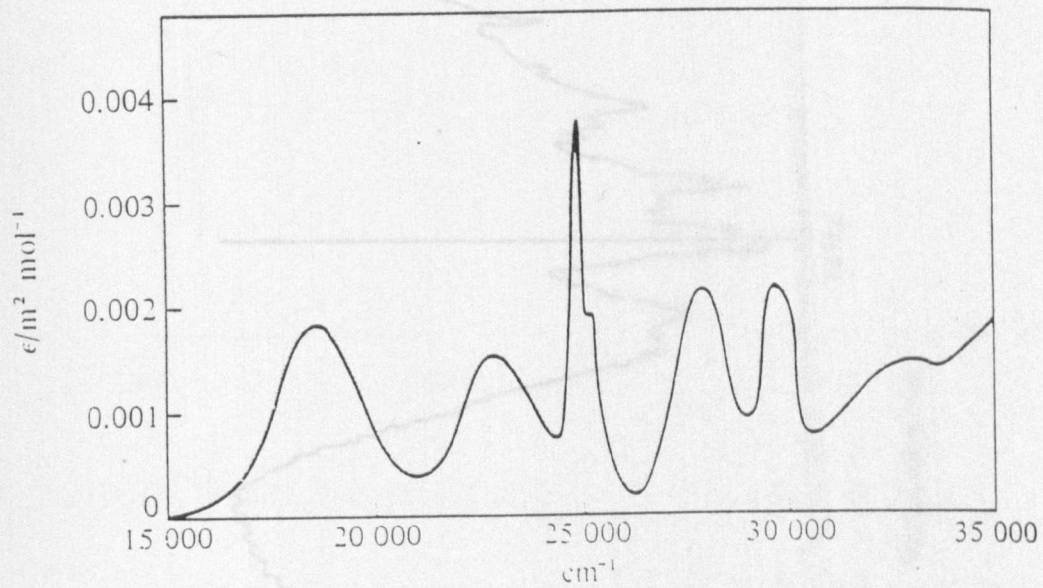


FIGURE 2.36: The Electronic Absorption Spectrum for $[\text{Mn}(\text{H}_2\text{O})_6]^{2+}$ (61)

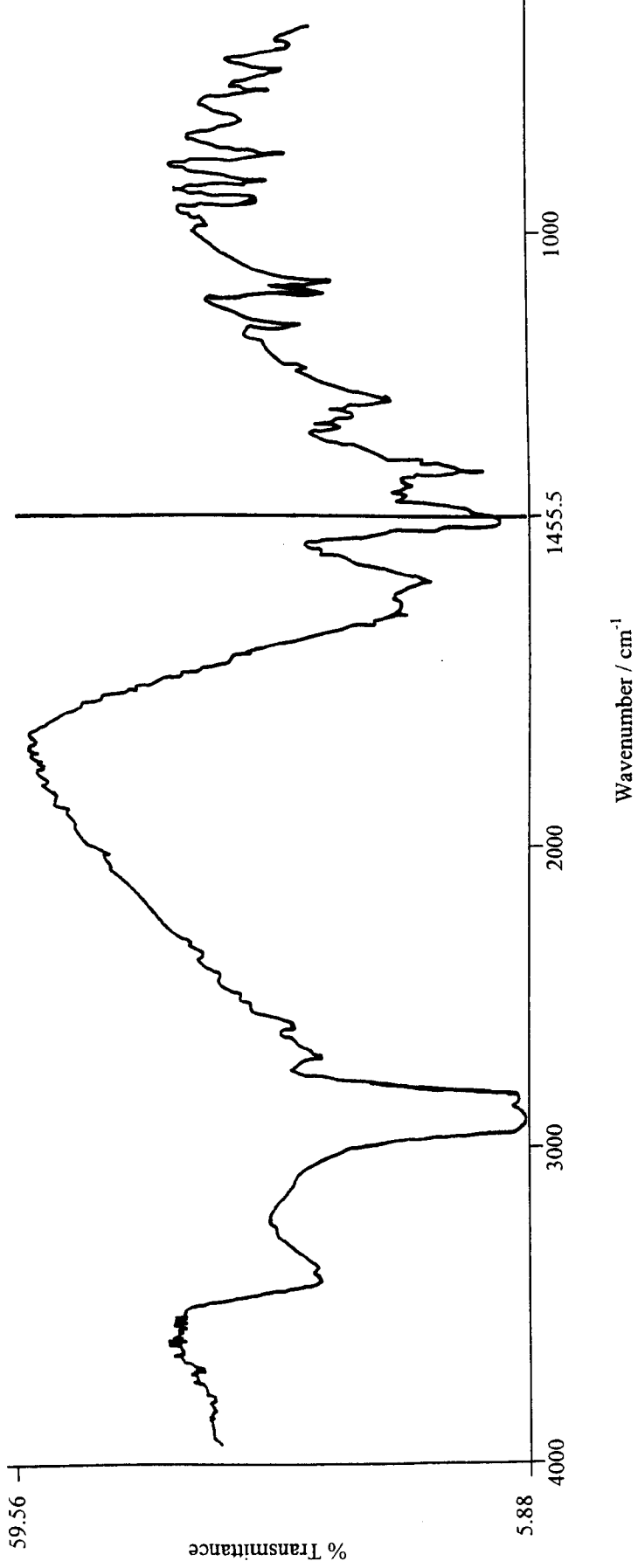
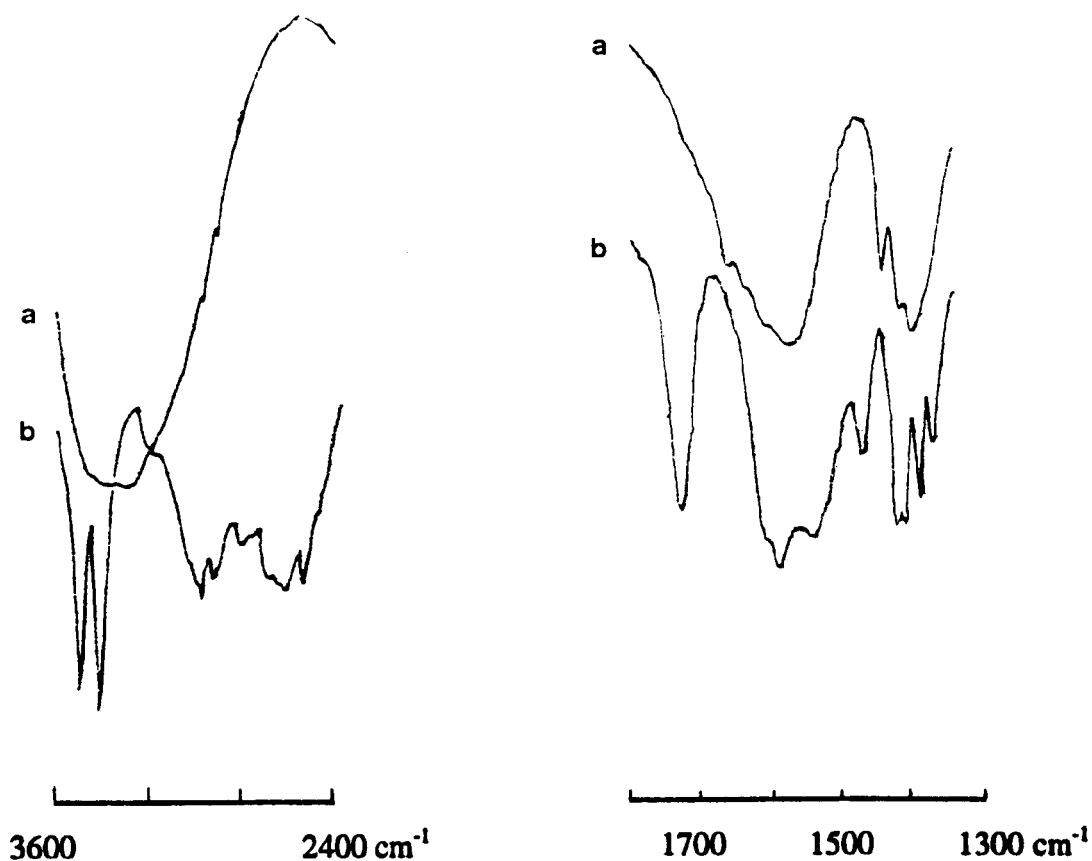


FIGURE 2.37: Infrared Spectrum for Zinc Citrate ⁽⁶⁵⁾



a) $[\text{Mn}(\text{H}_2\text{O})_6][\text{Mn}(\text{C}_6\text{H}_5\text{O}_7)\cdot\text{H}_2\text{O}]_2\cdot 2\text{H}_2\text{O}$

b) $\text{Mn}(\text{C}_6\text{H}_5\text{O}_7)\cdot\text{H}_2\text{O}$

Region	Assignment	$[\text{Mn}(\text{H}_2\text{O})_6][\text{Mn}(\text{C}_6\text{H}_5\text{O}_7)\cdot\text{H}_2\text{O}]_2\cdot 2\text{H}_2\text{O}$	$\text{Mn}(\text{C}_6\text{H}_5\text{O}_7)\cdot\text{H}_2\text{O}$
I	O-H stretch in water	3350 b,m	3490 s
A	O-H stretch		3400 s
D	C=O stretch		1728 s
D'/I	COO⁻ antisymmetric stretch + H-O-H bending in water	1655 sh	
D'	COO⁻ antisymmetric stretch	1611 sh 1575 s	1586 s 1550 sh
D''	COO⁻ symmetric stretch and O-H bending	1448 m 1421 m 1402 m	1470 w 1441 m 1418 m 1403 m 1394 m

Key to adsorption: s strong, m medium, w weak, sh shoulder, b broad

FIGURE 2.38: Infrared Spectra for Manganese Citrate Complexes (KBr Disc) ⁽⁶⁶⁾

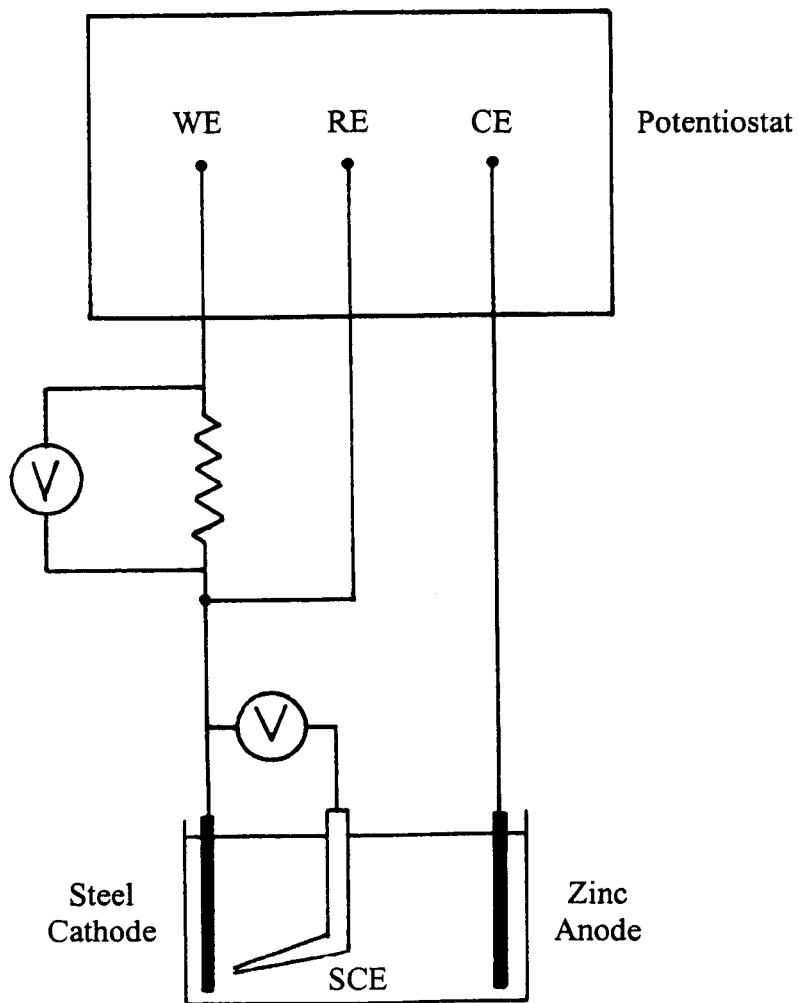
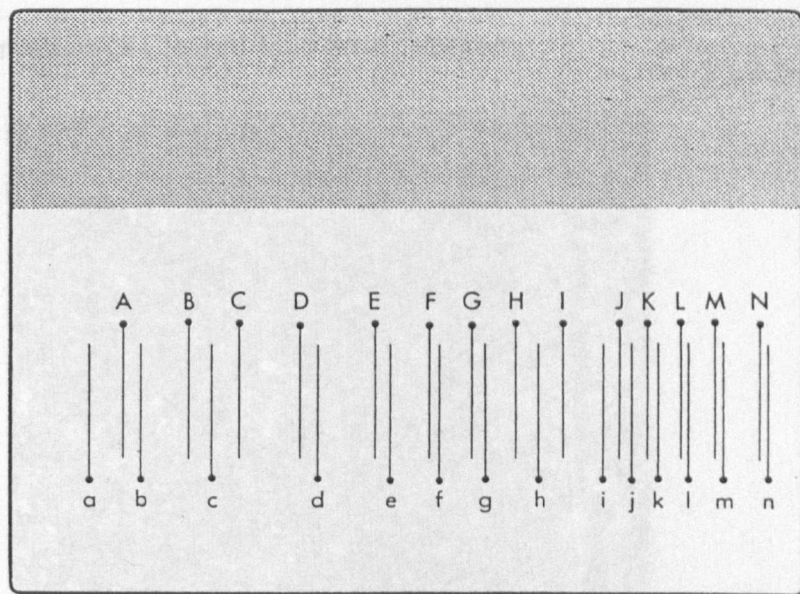


FIGURE 3.1: Three-Electrode Galvanostatic Circuit

Current applied amperes	Current Density—amp/ft ²													
	Position on Hull Cell panel													
	A	B	C	D	E	F	G	H	I	J	K	L	M	N
1	40	30	25	20	15	12	10	8	6	4	3	2	1	0.5
2	80	60	50	40	30	24	20	16	12	8	6	4	2	1
3	120	90	75	60	45	36	30	24	18	12	9	6	3	1.5
5	200	150	125	100	75	60	50	40	30	20	15	10	5	2.5



Current applied amperes	Current density—amp/dm ²													
	Position on Hull Cell panel													
	a	b	c	d	e	f	g	h	i	j	k	l	m	n
1	5	4	3	2	1.5	1.25	1.0	0.75	0.5	0.4	0.3	0.2	0.1	0.05
2	10	8	6	4	3	2.5	2	1.5	1	0.8	0.6	0.4	0.2	0.1
3	15	12	9	6	4.5	3.75	3	2.25	1.5	1.2	0.9	0.6	0.3	0.15
5	25	20	15	10	7.5	6.25	5	3.75	2.5	2.0	1.5	1.0	0.5	0.25

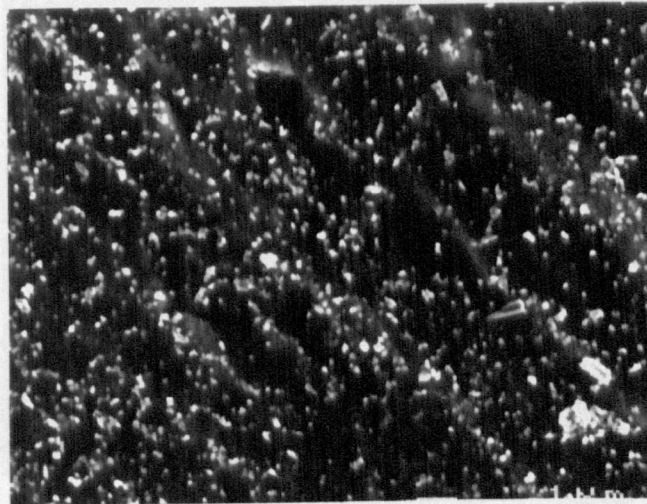
FIGURE 3.2: The Current Densities Represented on a Hull Cell Panel ⁽⁶⁸⁾



1 μ m

$\times 5000$

FIGURE 4.1: SEM Micrograph of Cleaned Mild Steel Substrate



a) -850mV
(Gold coated)

1 μ m

$\times 5000$

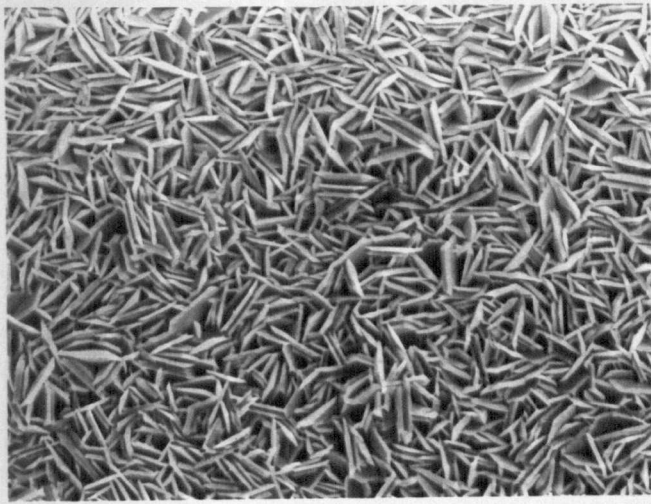


b) -1050mV
(Gold coated)

1 μ m

$\times 5000$

FIGURE 4.2: SEM Micrographs of Zinc-Manganese Deposited from a Standard Bath (pH5.6, room temperature)



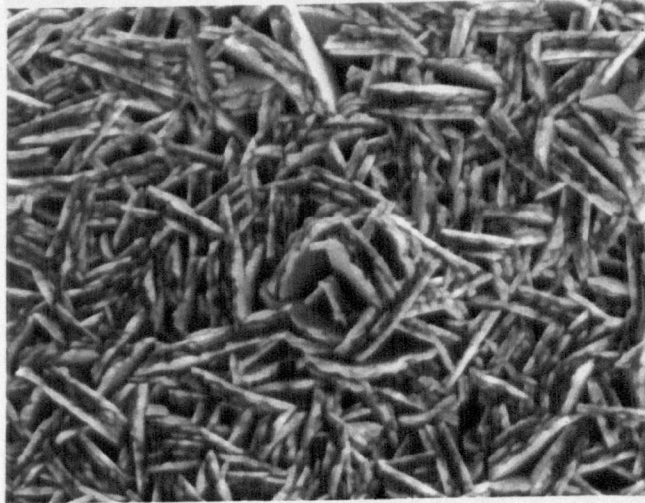
a) 0.15Adm⁻²

1μm

× 5000

1μm

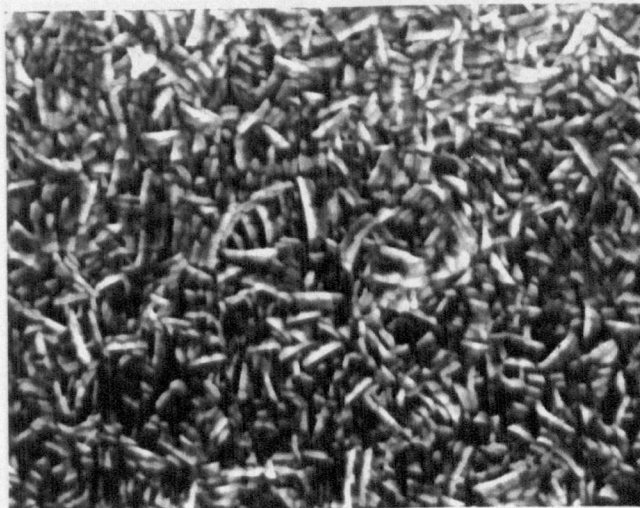
× 10000



b) 0.3Adm⁻²

1μm

× 10000



c) 0.6Adm⁻²

1μm

× 10000

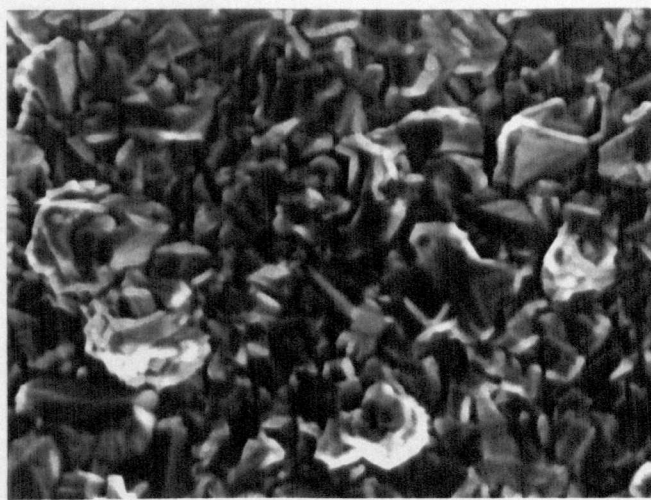
FIGURE 4.3: SEM Micrographs of Zinc-Manganese Deposited from a Standard Bath (pH5.6, room temperature)



a) 0.9Adm^{-2}

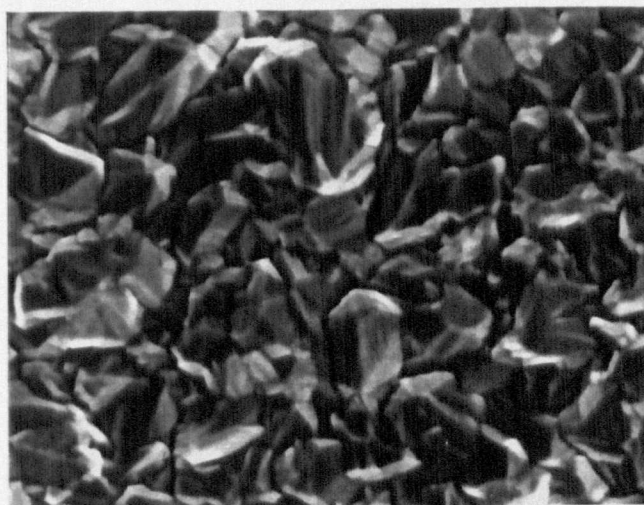
$1 \mu\text{m}$

$\times 5000$



$1 \mu\text{m}$

$\times 10000$



b) 1.2Adm^{-2}

$1 \mu\text{m}$

$\times 10000$



c) 1.5Adm^{-2}

$1 \mu\text{m}$

$\times 10000$

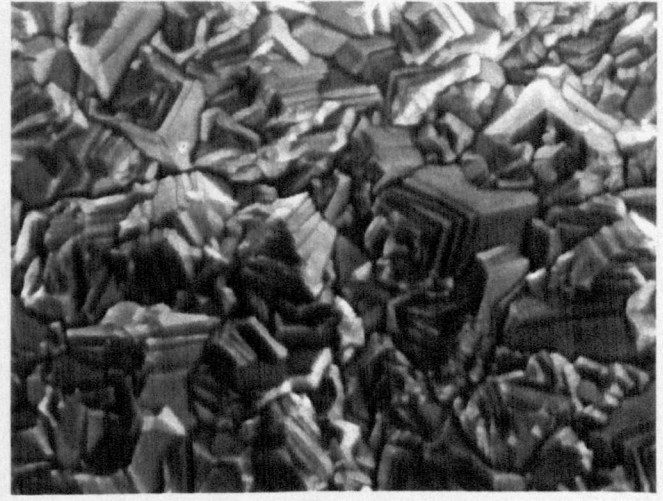
FIGURE 4.4: SEM Micrographs of Zinc-Manganese Deposited from a Standard Bath (pH5.6, room temperature)



a) 2.25Adm^{-2}

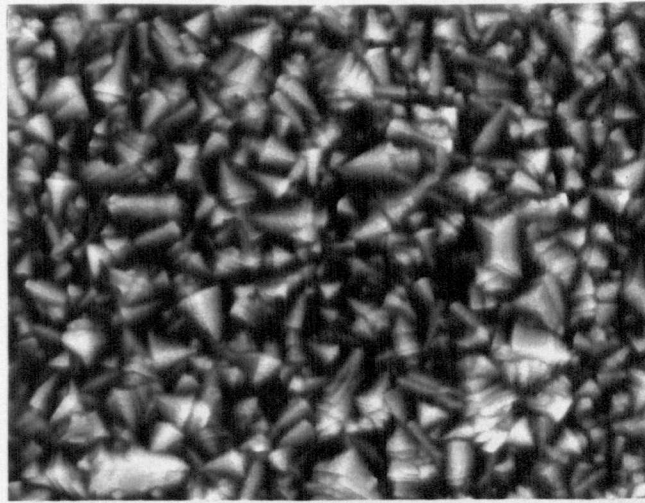
$1 \mu\text{m}$

$\times 5000$



$1 \mu\text{m}$

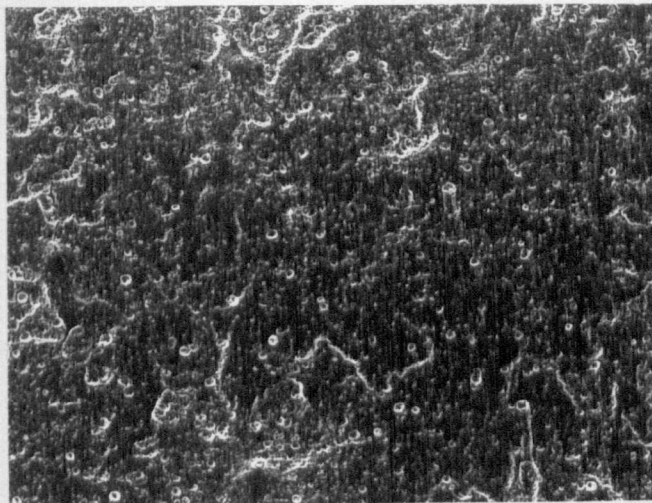
$\times 10000$



b) 3Adm^{-2}

$1 \mu\text{m}$

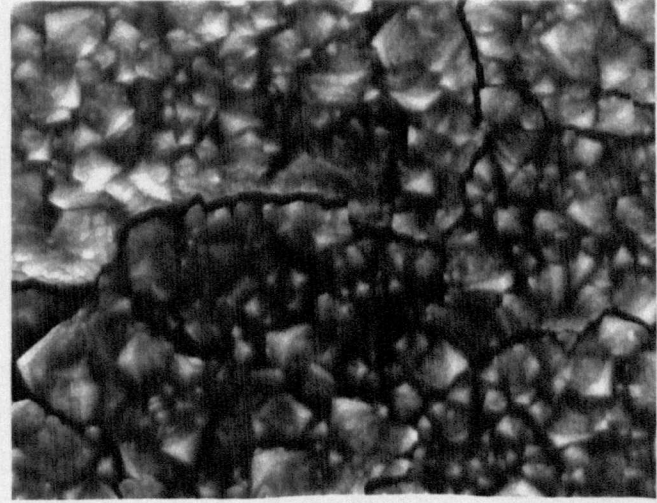
$\times 5000$



c) 3.75Adm^{-2}

$100 \mu\text{m}$

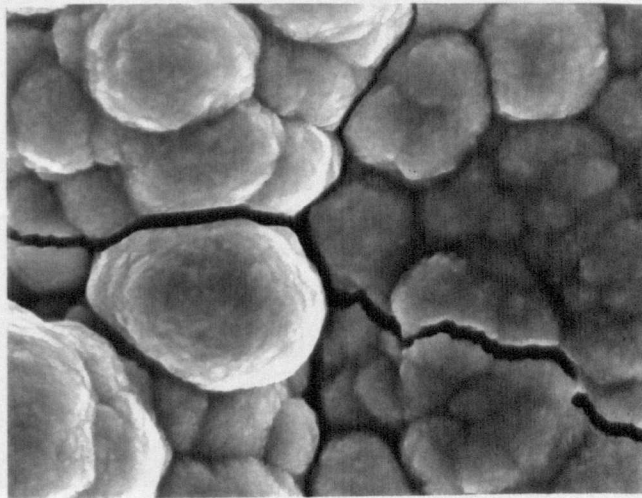
$\times 200$



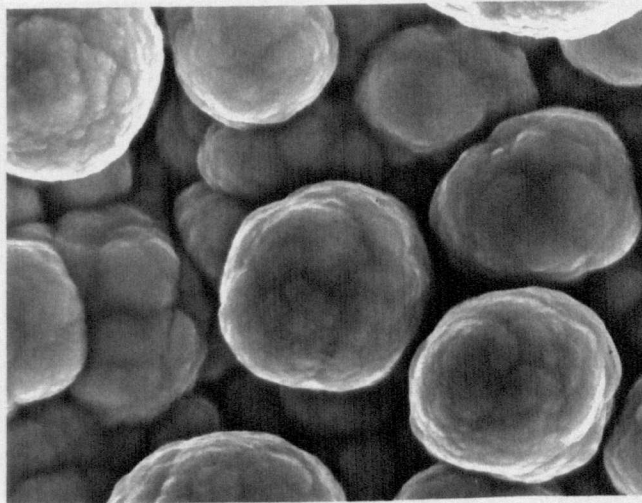
$1 \mu\text{m}$

$\times 5000$

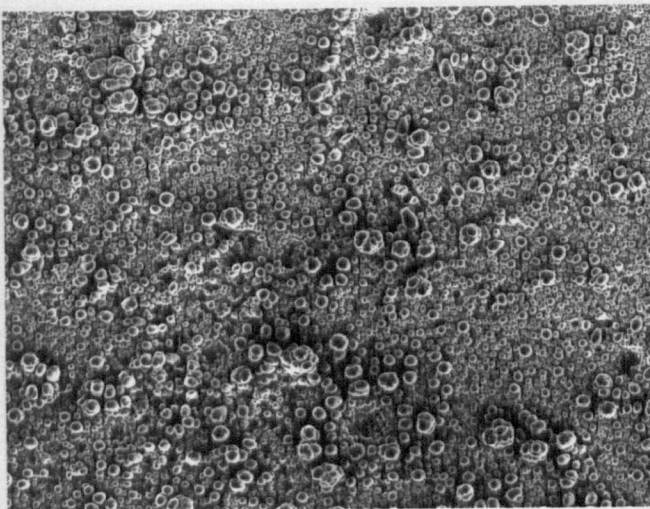
FIGURE 4.5: SEM Micrographs of Zinc-Manganese Deposited from a Standard Bath (pH5.6, room temperature)



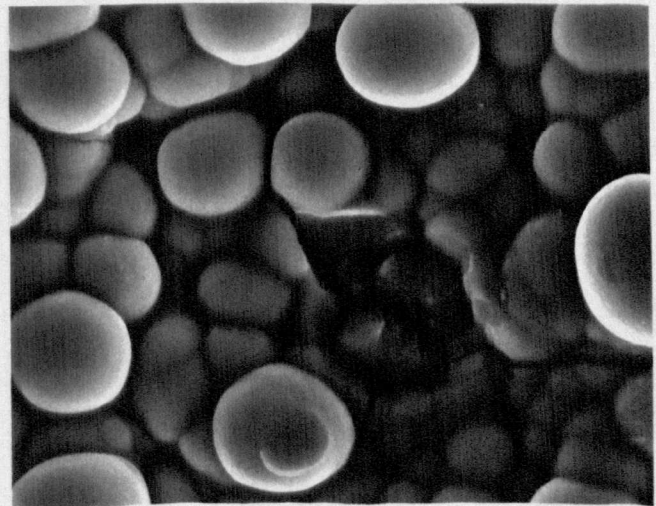
a) 4.5Adm^{-2} $\overline{1\mu\text{m}}$ $\times 5000$



b) 6Adm^{-2} $\overline{1\mu\text{m}}$ $\times 5000$

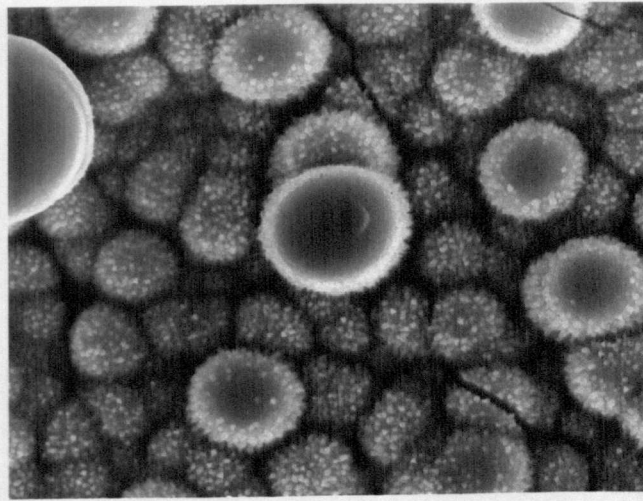


c) 9Adm^{-2} $\overline{100\mu\text{m}}$ $\times 200$



$\overline{1\mu\text{m}}$ $\times 5000$

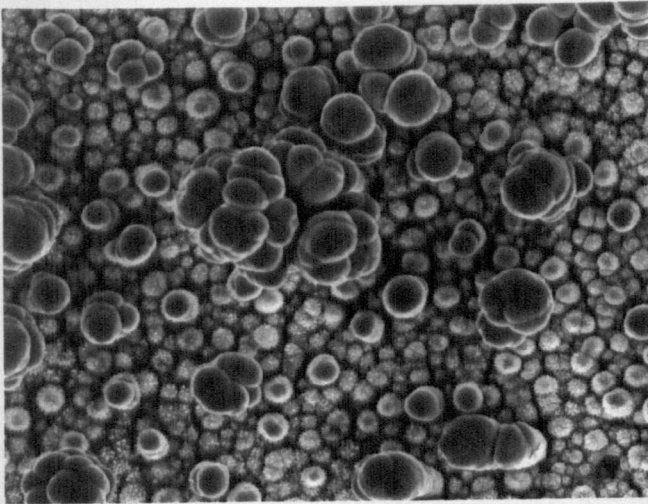
FIGURE 4.6: SEM Micrographs of Zinc-Manganese Deposited from a Standard Bath (pH5.6, room temperature)



a) 12Adm^{-2}

$1\mu\text{m}$

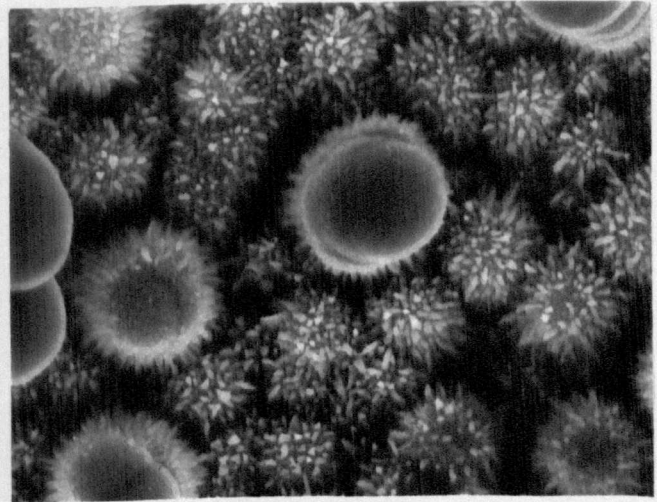
$\times 5000$



b) 15Adm^{-2}

$10\mu\text{m}$

$\times 1000$



$1\mu\text{m}$

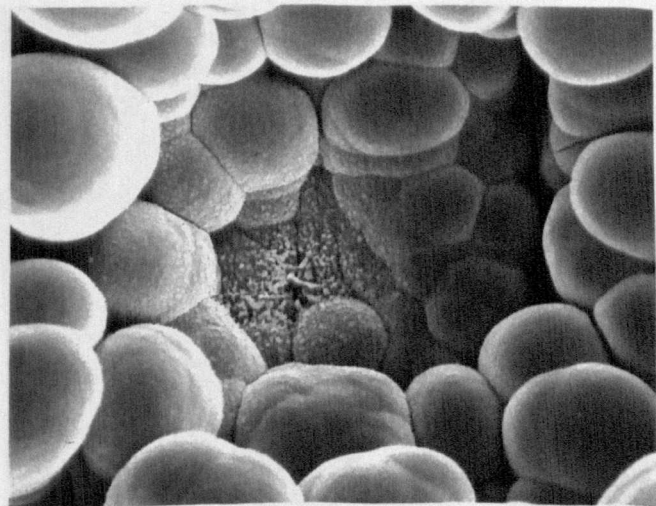
$\times 5000$



c) 20Adm^{-2}

$100\mu\text{m}$

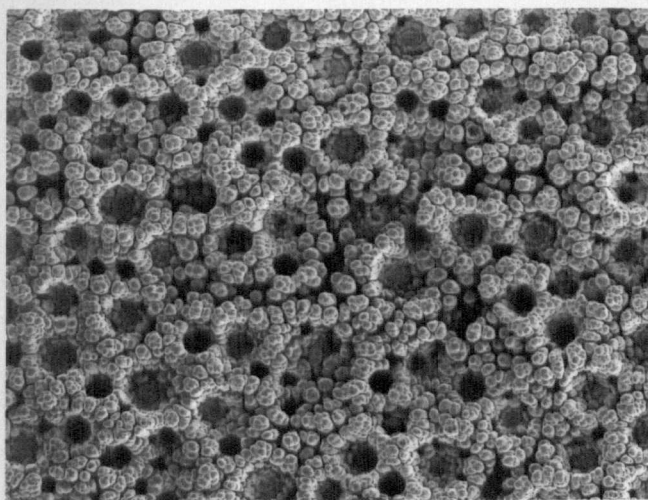
$\times 200$



$1\mu\text{m}$

$\times 5000$

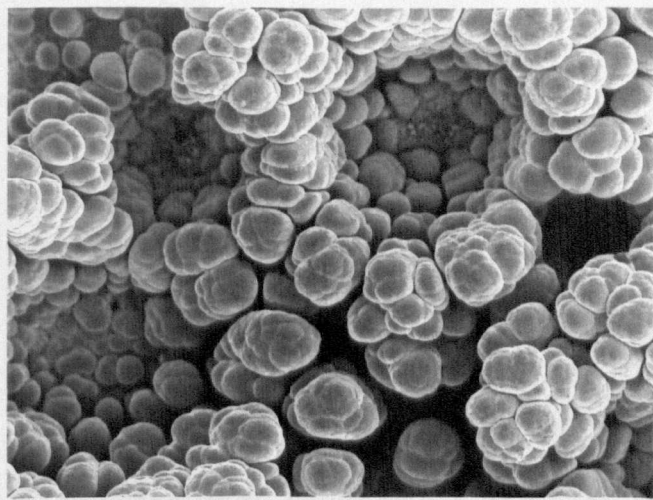
FIGURE 4.7: SEM Micrographs of Zinc-Manganese Deposited from a Standard Bath (pH5.6, room temperature)



a) 30Adm^{-2}

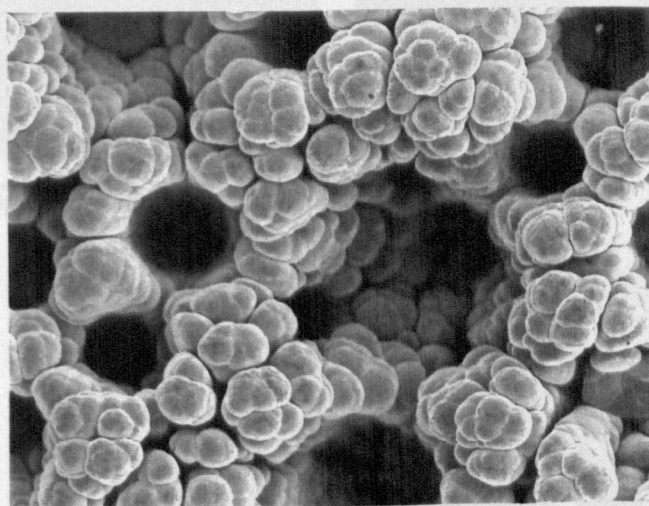
$100\mu\text{m}$

$\times 200$



$10\mu\text{m}$

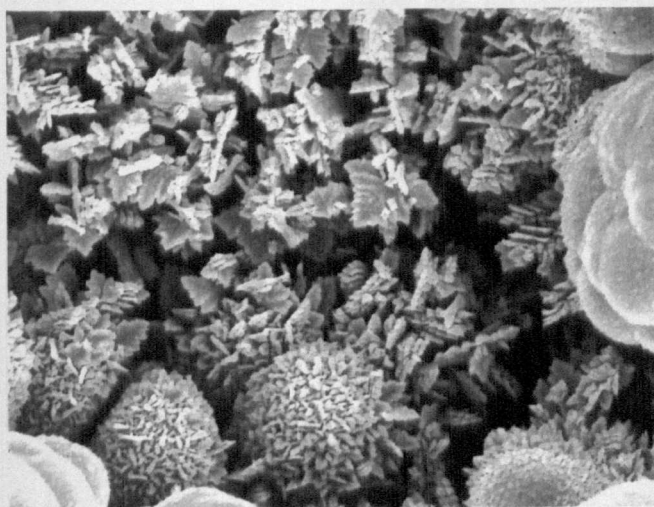
$\times 1000$



b) 40Adm^{-2}

$10\mu\text{m}$

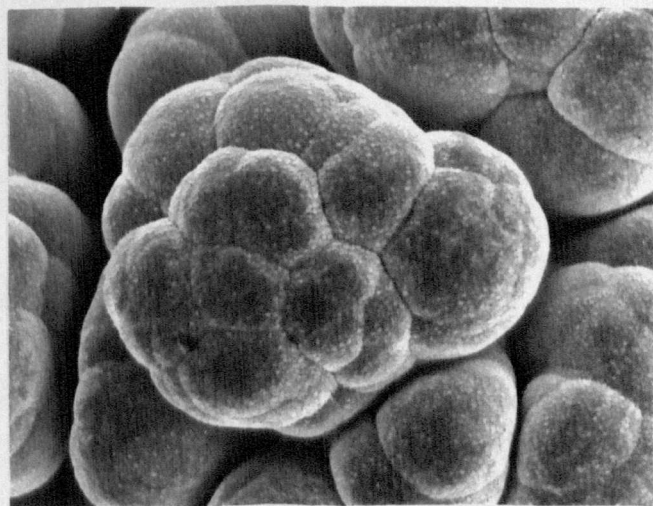
$\times 1000$



c) 40Adm^{-2} (Hole)

$1\mu\text{m}$

$\times 5000$

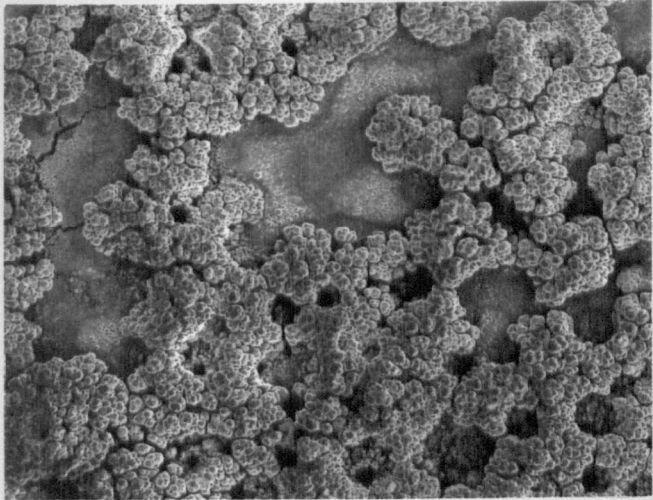


d) 40Adm^{-2} (Peak)

$1\mu\text{m}$

$\times 5000$

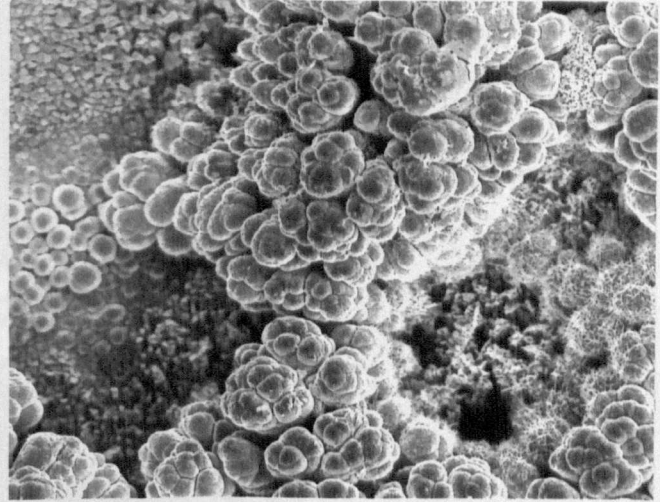
FIGURE 4.8: SEM Micrographs of Zinc-Manganese Deposited from a Standard Bath (pH5.6, room temperature)



a) 50Adm^{-2}

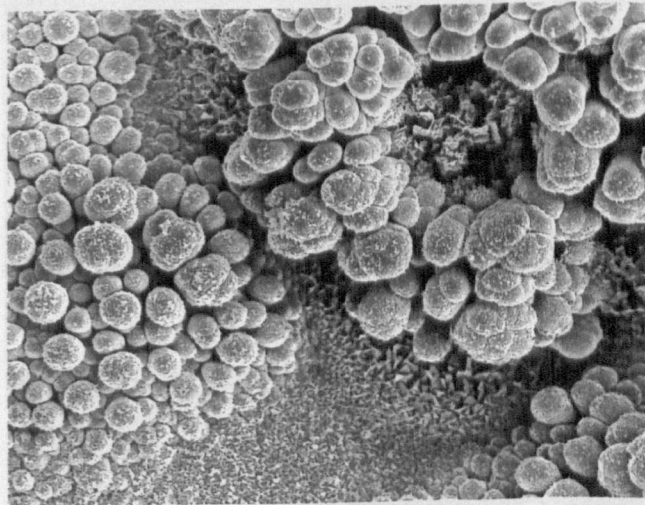
$100 \mu\text{m}$

$\times 200$



$10 \mu\text{m}$

$\times 1000$

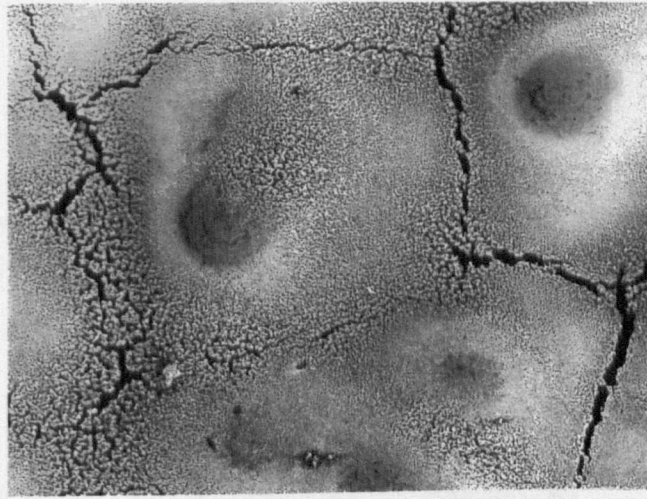


b) 60Adm^{-2}

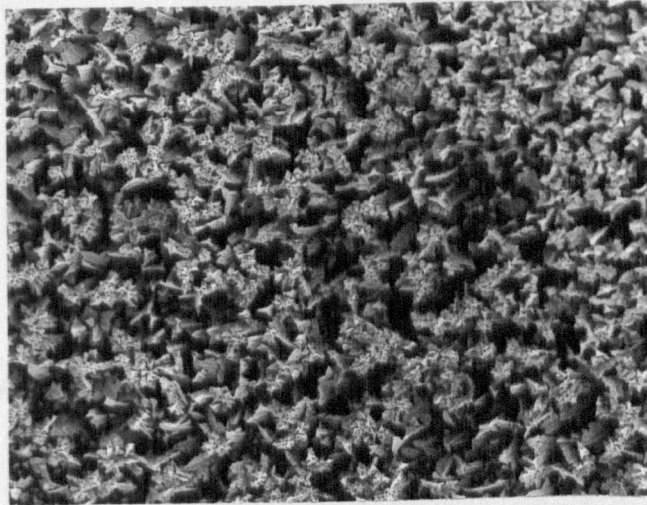
$10 \mu\text{m}$

$\times 1000$

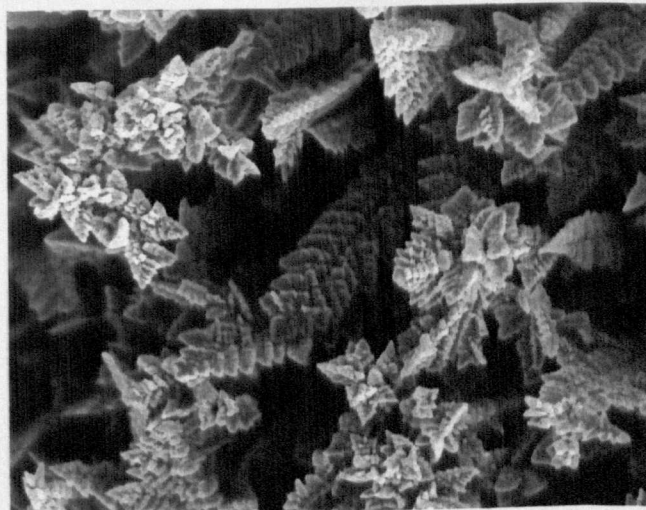
FIGURE 4.9: SEM Micrographs of Zinc-Manganese Deposited from a Standard Bath (pH5.6, room temperature)



a) 70Adm^{-2} $100\mu\text{m}$ $\times 200$



b) 70Adm^{-2} $10\mu\text{m}$ $\times 1000$



c) 70Adm^{-2} $1\mu\text{m}$ $\times 5000$

FIGURE 4.10: SEM Micrographs of Zinc-Manganese Deposited from a Standard Bath (pH5.6, room temperature)

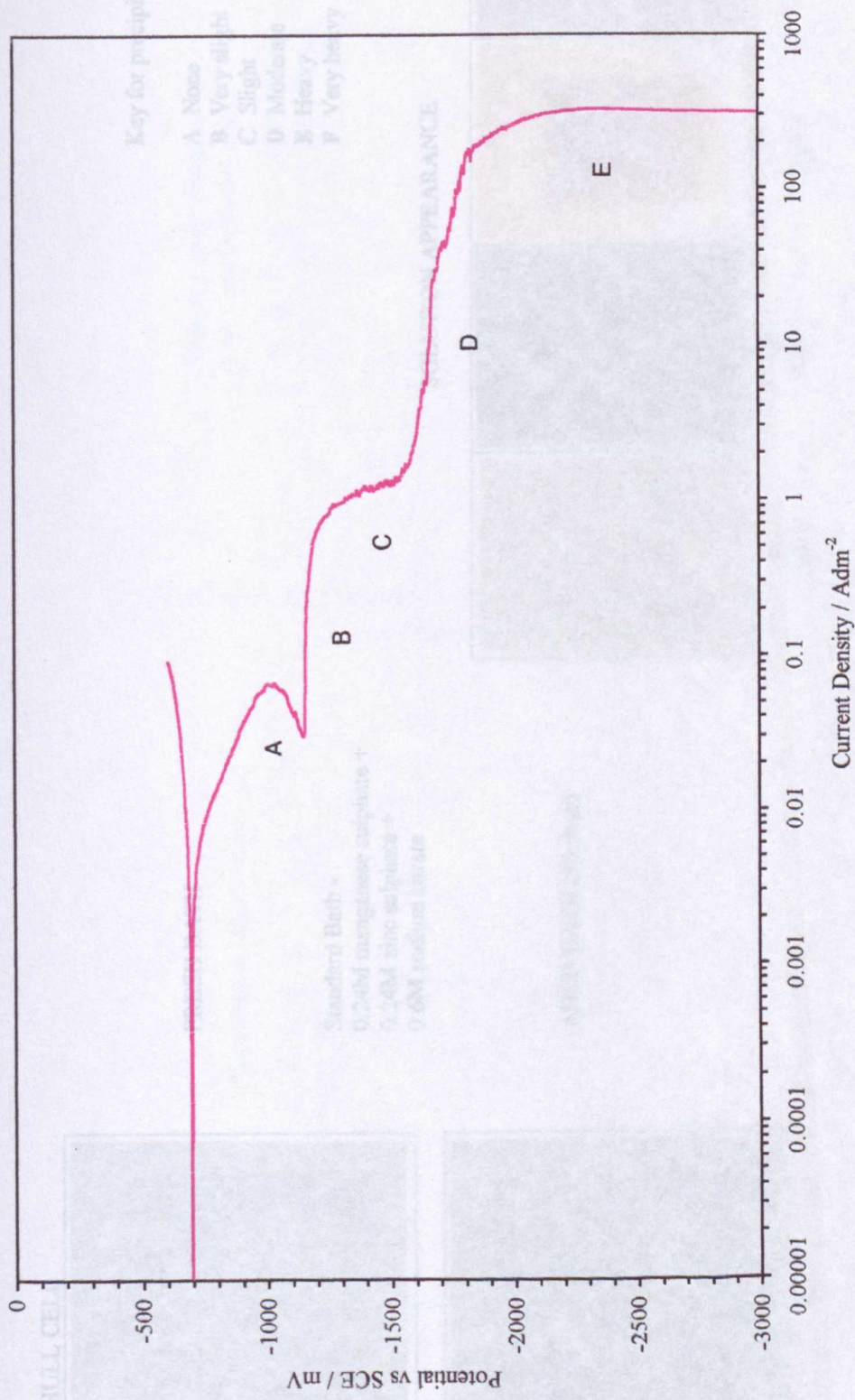
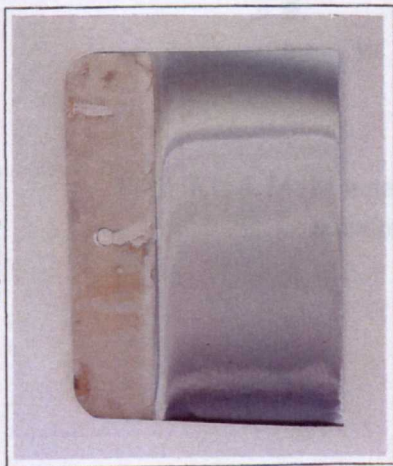


FIGURE 4.11: Zinc-Manganese Electrodeposition from a Standard Bath (25°C, pH5.6)

HULL CELL



FRESH BATH

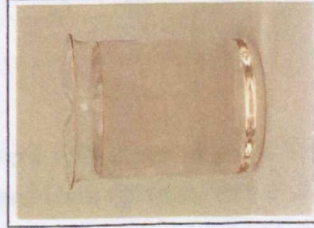
Standard Bath -
 0.24M manganese sulphate +
 0.24M zinc sulphate +
 0.6M sodium citrate

AGED BATH (30 days)

Key for precipitation:

- A** None
- B** Very slight
- C** Slight
- D** Moderate
- E** Heavy
- F** Very heavy

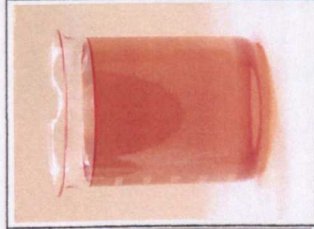
SOLUTION APPEARANCE



A
Day 1



B
Day 3



C
Day 9



D
Day 30

FIGURE 4.12: The Zinc-Manganese Standard Bath (pH5.6, Room Temperature)



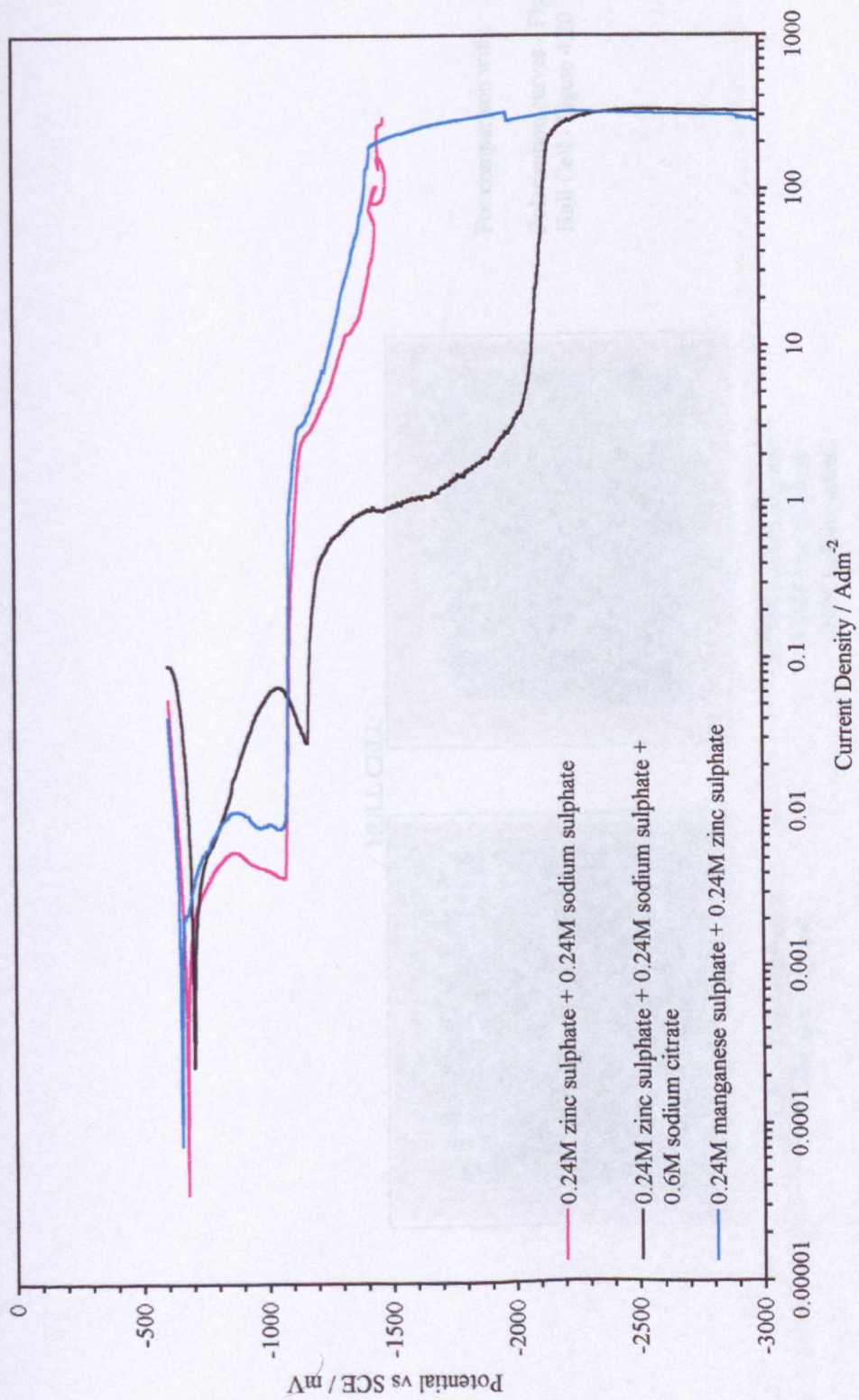
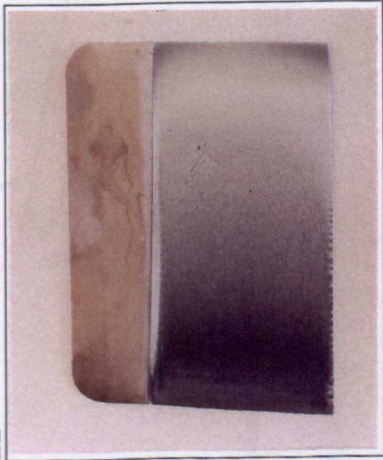


FIGURE 4.15: Effect of Sodium Citrate on Zinc Electrodeposition (25°C, pH5.6)

HULL CELL



0.24M sodium sulphate +
0.24M zinc sulphate



0.24M sodium sulphate +
0.24M zinc sulphate +
0.6M sodium citrate

For comparison with:

Polarisation curves - Figures 4.15, 4.21
Hull Cell - Figure 4.20

FIGURE 4.16: Effect of Sodium Citrate on Zinc Electrodeposition (pH5.6, Room Temperature)

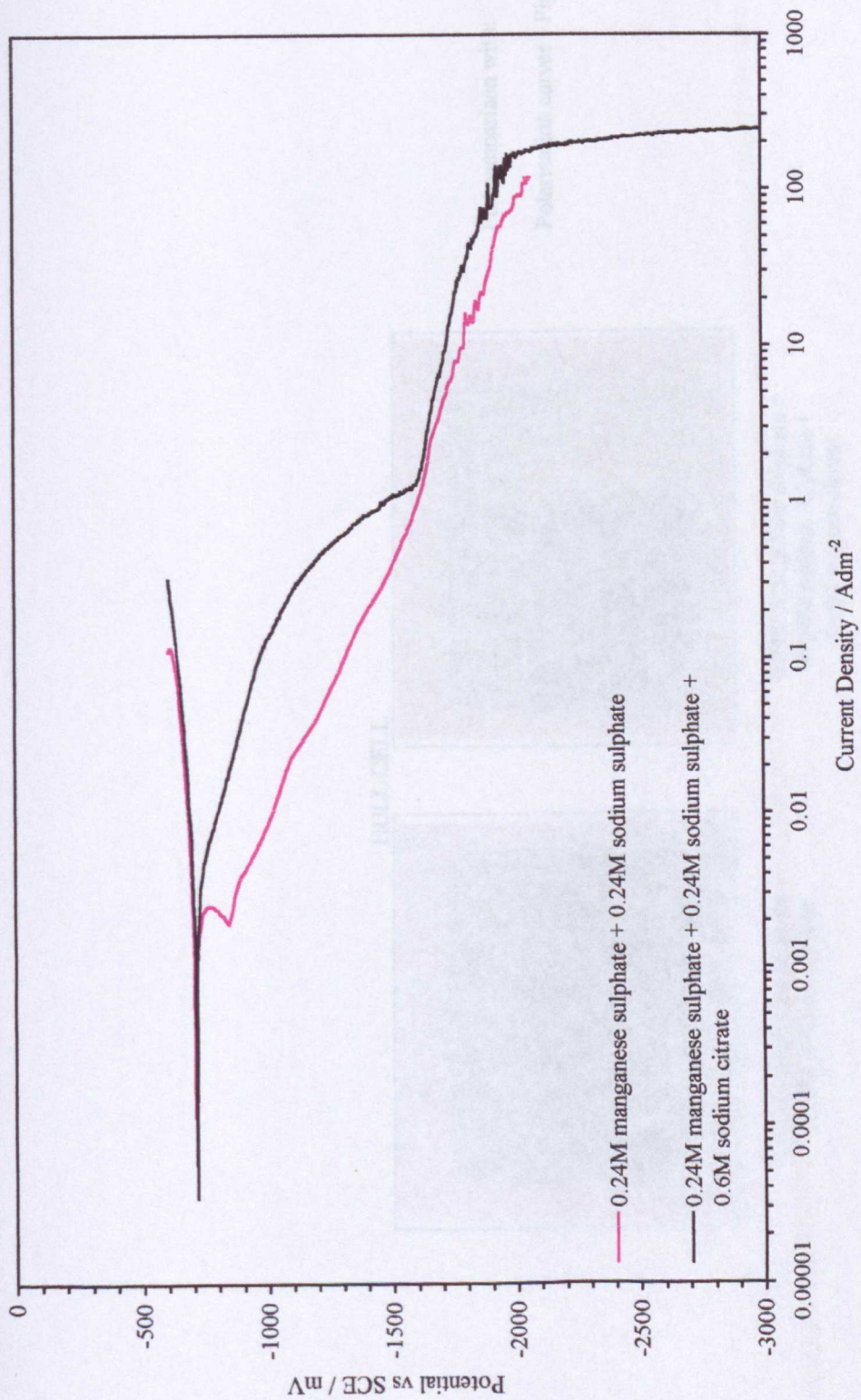
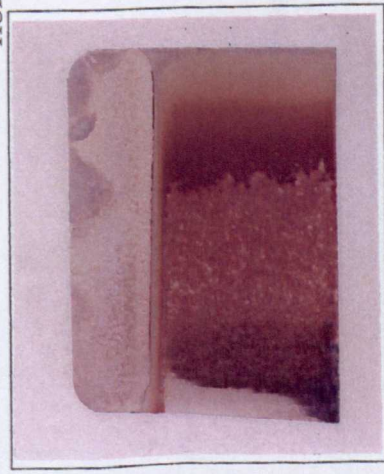


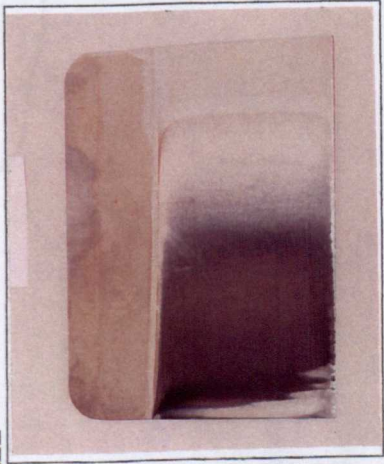
FIGURE 4.17: Effect of Sodium Citrate on Manganese Electrodeposition (25°C, pH5.6)



HULL CELL



0.24M manganese sulphate +
0.24M sodium sulphate



0.24M manganese sulphate +
0.24M sodium sulphate +
0.6M sodium citrate

For comparison with:

Polarisation curves - Figures 4.17, 4.21

FIGURE 4.18: Effect of Sodium Citrate on Manganese Electrodeposition (pH5.6, Room Temperature)

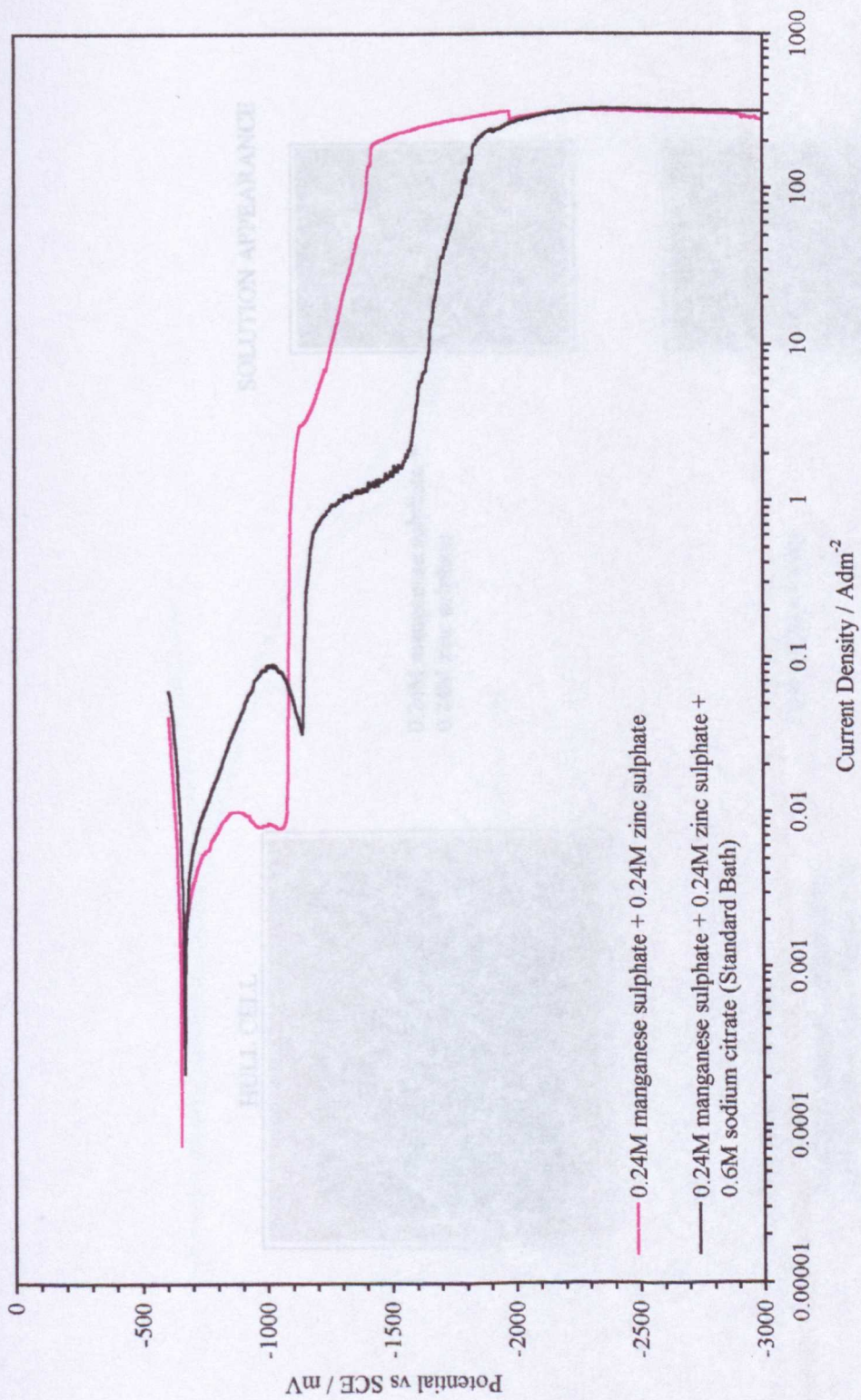
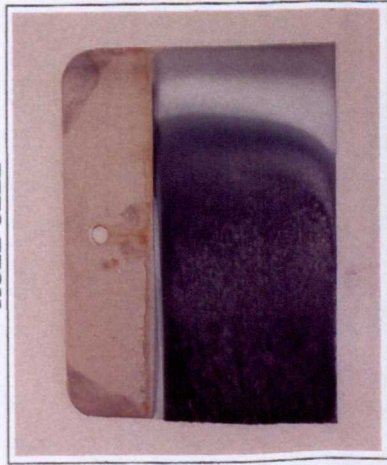
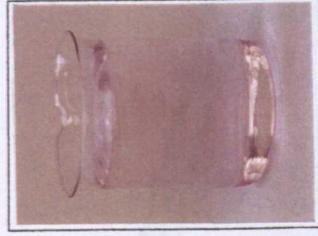


FIGURE 4.19: Effect of Sodium Citrate on Zinc-Manganese Electrodeposition from a Standard Bath (25°C, pH5.0)

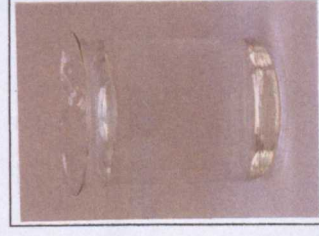
HULL CELL



SOLUTION APPEARANCE



0.24M manganese sulphate +
0.24M zinc sulphate



0.6M sodium citrate

For comparison with:

Polarisation curves - Figure 4.19
Hull Cells/Solutions - Figure 4.12

FIGURE 4.20: Constituent Solutions for the Zinc-Manganese Standard Bath (pH5.0, Room Temperature)

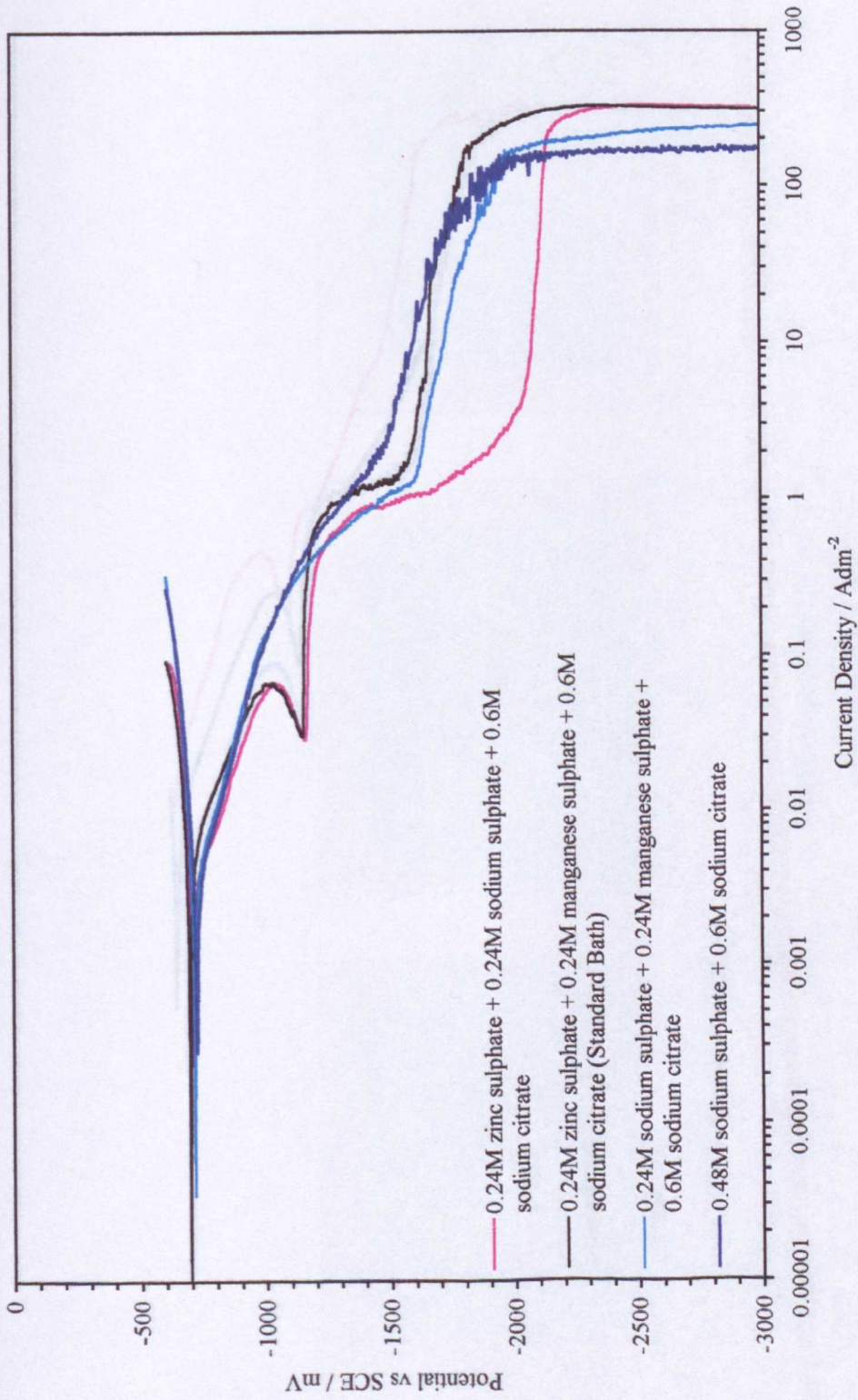


FIGURE 4.21: Constituent Curves for Zinc-Manganese Electrodeposition from a Standard Bath (25°C, pH5.6)

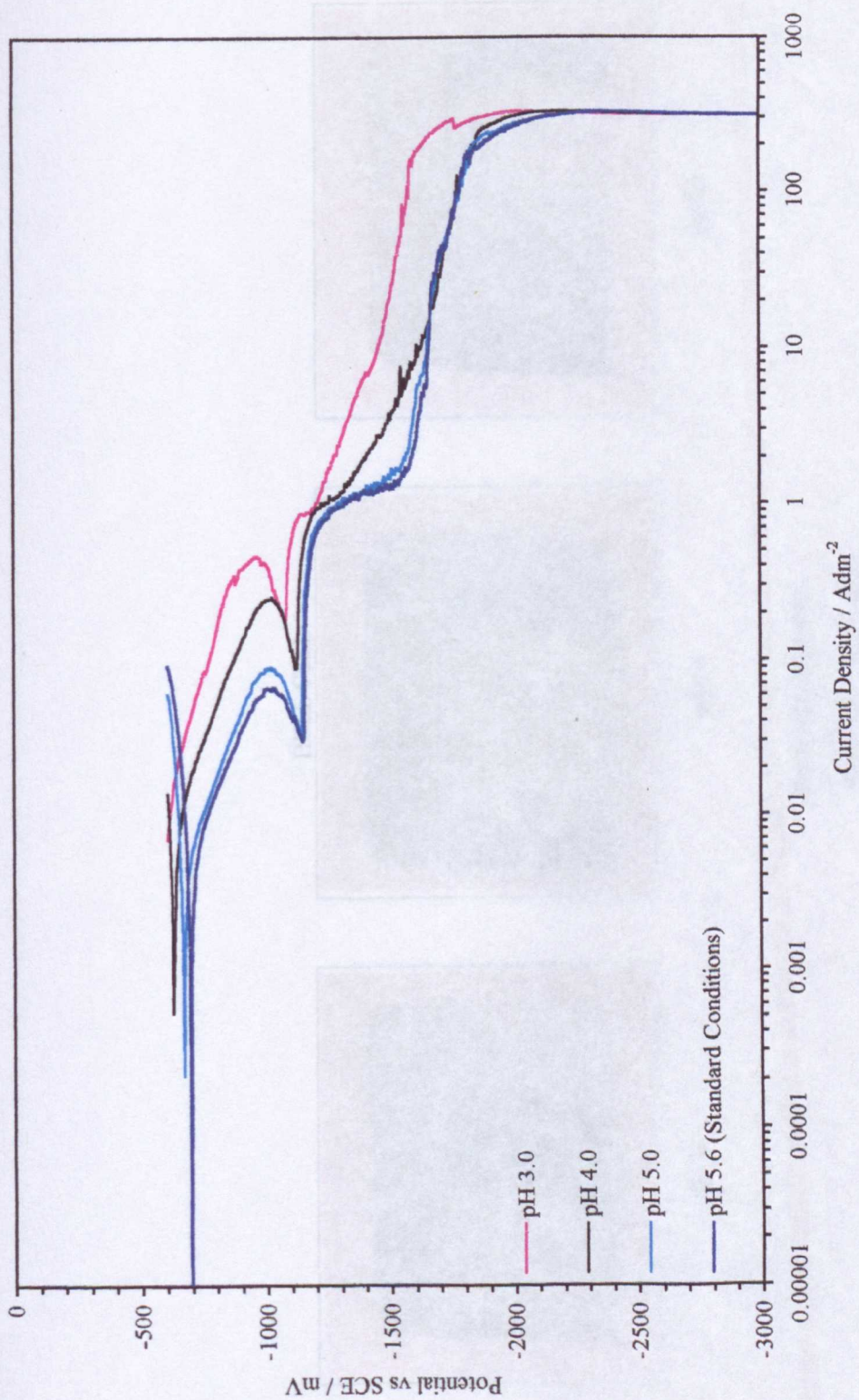
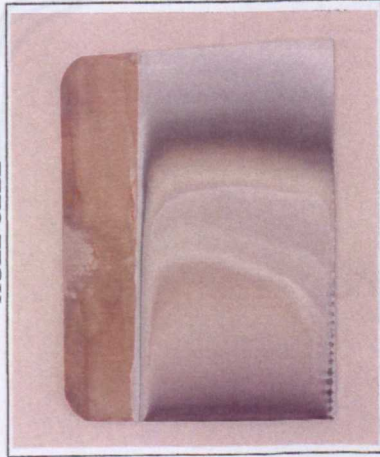


FIGURE 4.22: Effect of pH on Zinc-Manganese Electrodeposition from a Standard Bath (25°C)

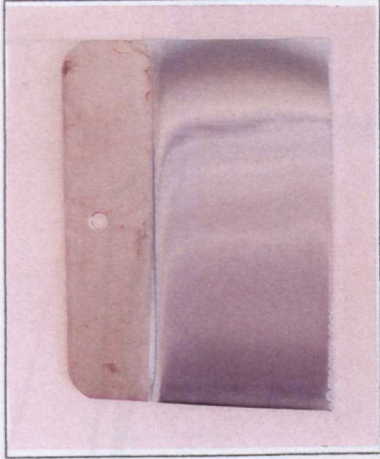
HULL CELL



pH3.0



pH4.0



pH5.0

For comparison with:

Hull Cells - Figure 4.12

FIGURE 4.23: Effect of pH on a Zinc-Manganese Standard Bath (Room Temperature)

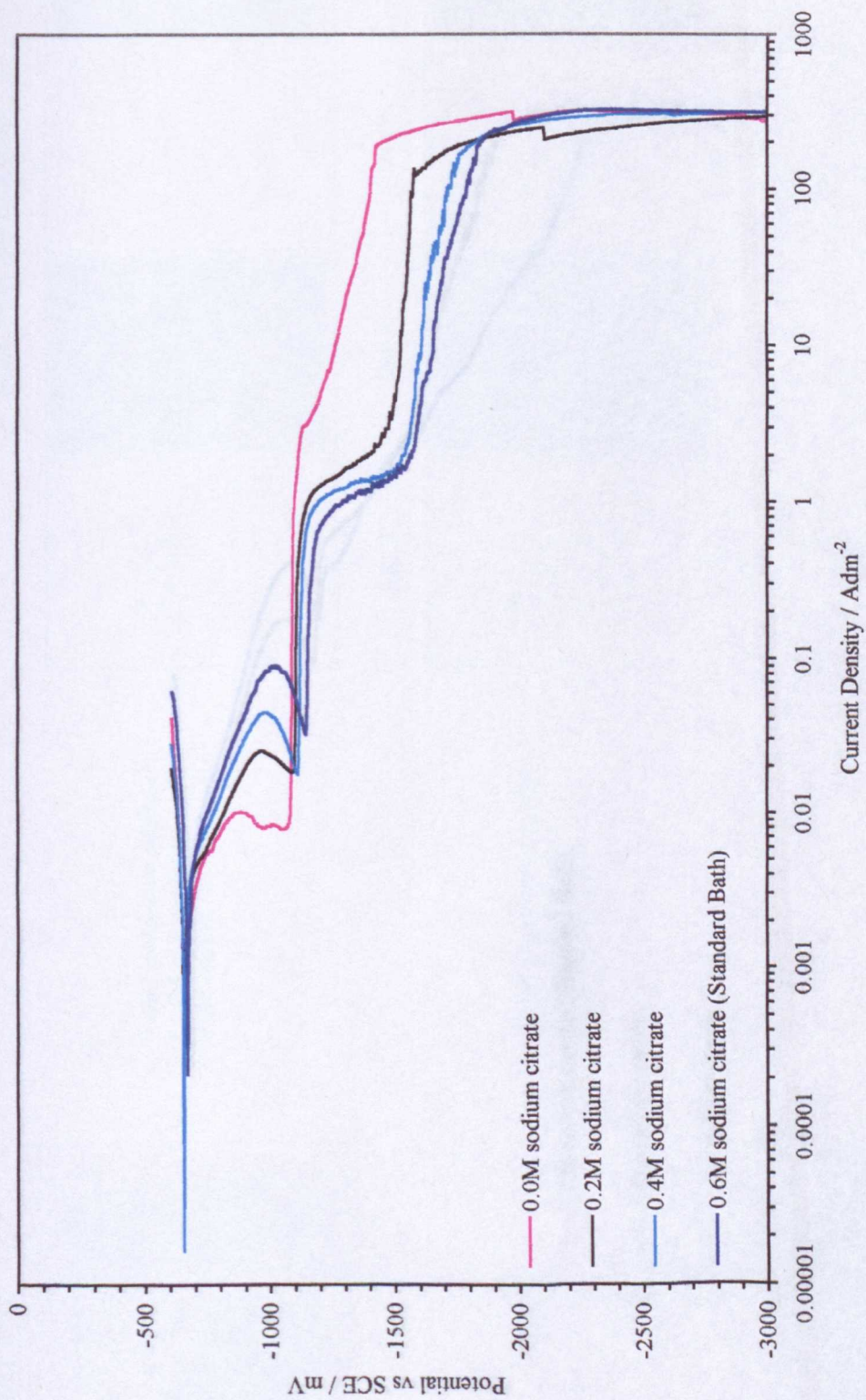


FIGURE 4.24: Effect of Sodium Citrate Content on Zinc-Manganese Electrodeposition from a Standard Bath (25°C, pH5.0)

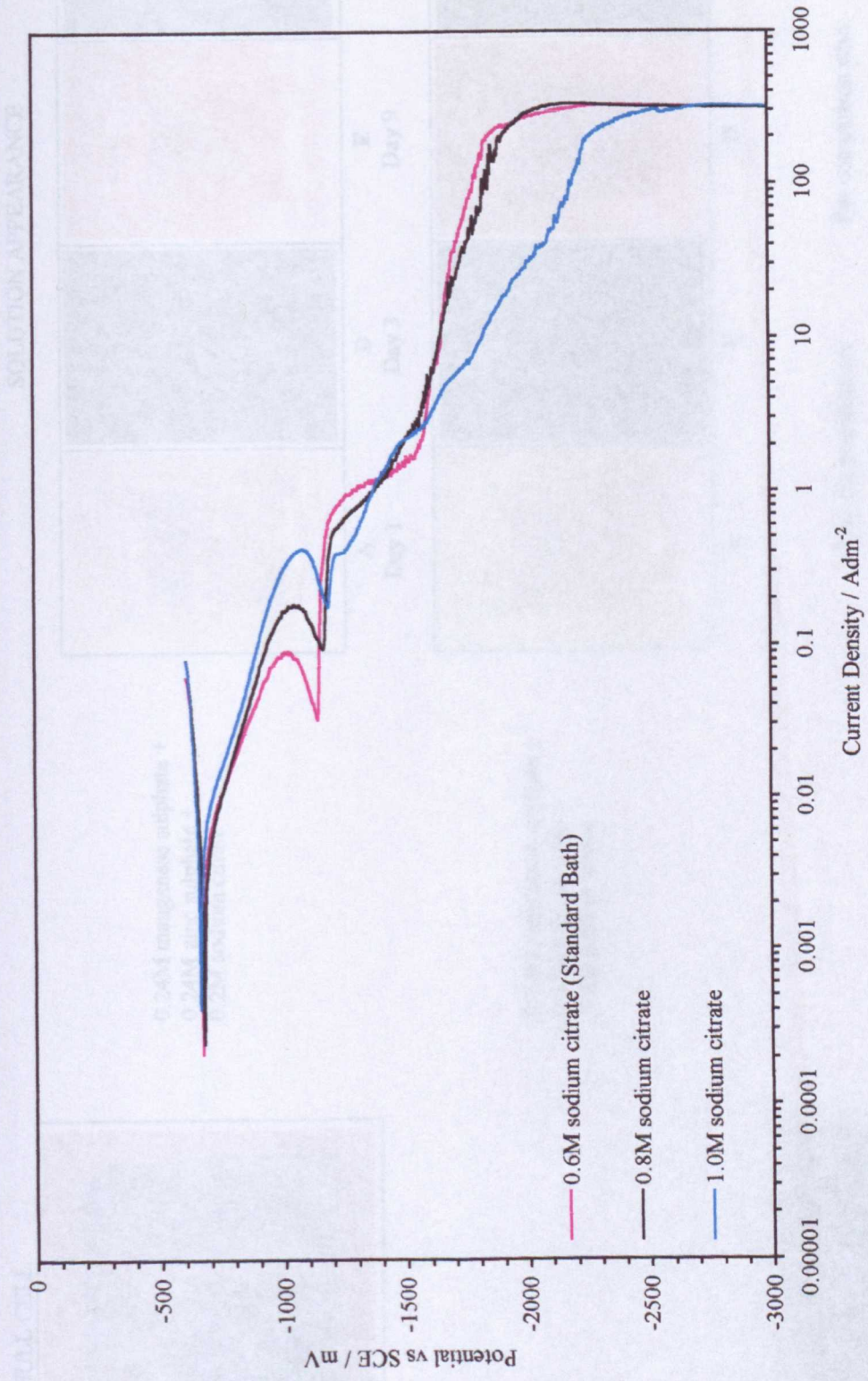


FIGURE 4.25: Effect of Sodium Citrate Content on Zinc-Manganese Electrodeposition from a Standard Bath (25°C, pH5.0)

HULL CELL



0.24M manganese sulphate +
0.24M zinc sulphate +
0.2M sodium citrate

0.24M manganese sulphate +
0.24M zinc sulphate +
0.4M sodium citrate

0.24M manganese sulphate +
0.24M zinc sulphate +
1.0M sodium citrate

SOLUTION APPEARANCE

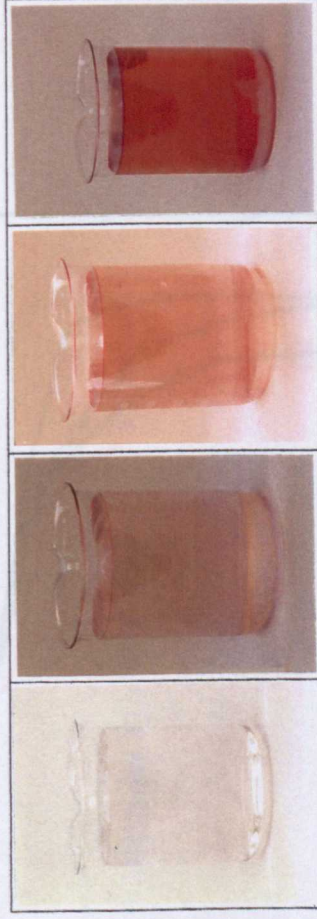


A
Day 1

D
Day 3

E
Day 9

E
Day 30



A

C

D

E

Key for precipitation:

- A None
- B Very slight
- C Slight
- D Moderate
- E Heavy
- F Very heavy

For comparison with:

Polarisation curves - Figures 4.24, 4.25
Hull Cells/Solutions - Figure 4.12



FIGURE 4.26: Effect of Sodium Citrate Content on a Zinc-Manganese Standard Bath (pH5.0, Room Temperature)

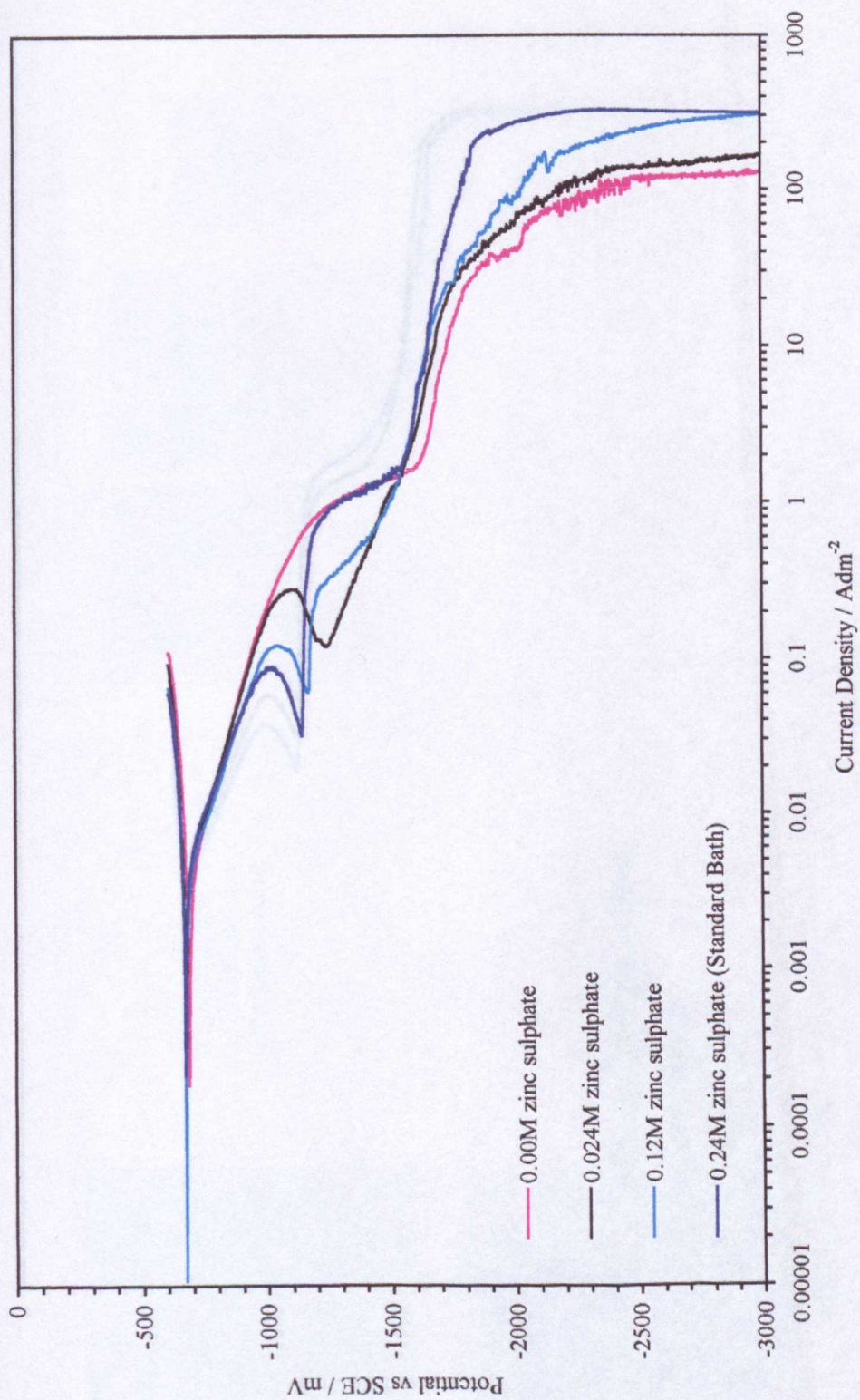


FIGURE 4.27: Effect of Zinc Sulphate Content on Zinc-Manganese Electrodeposition from a Standard Bath (25°C, pH5.0)

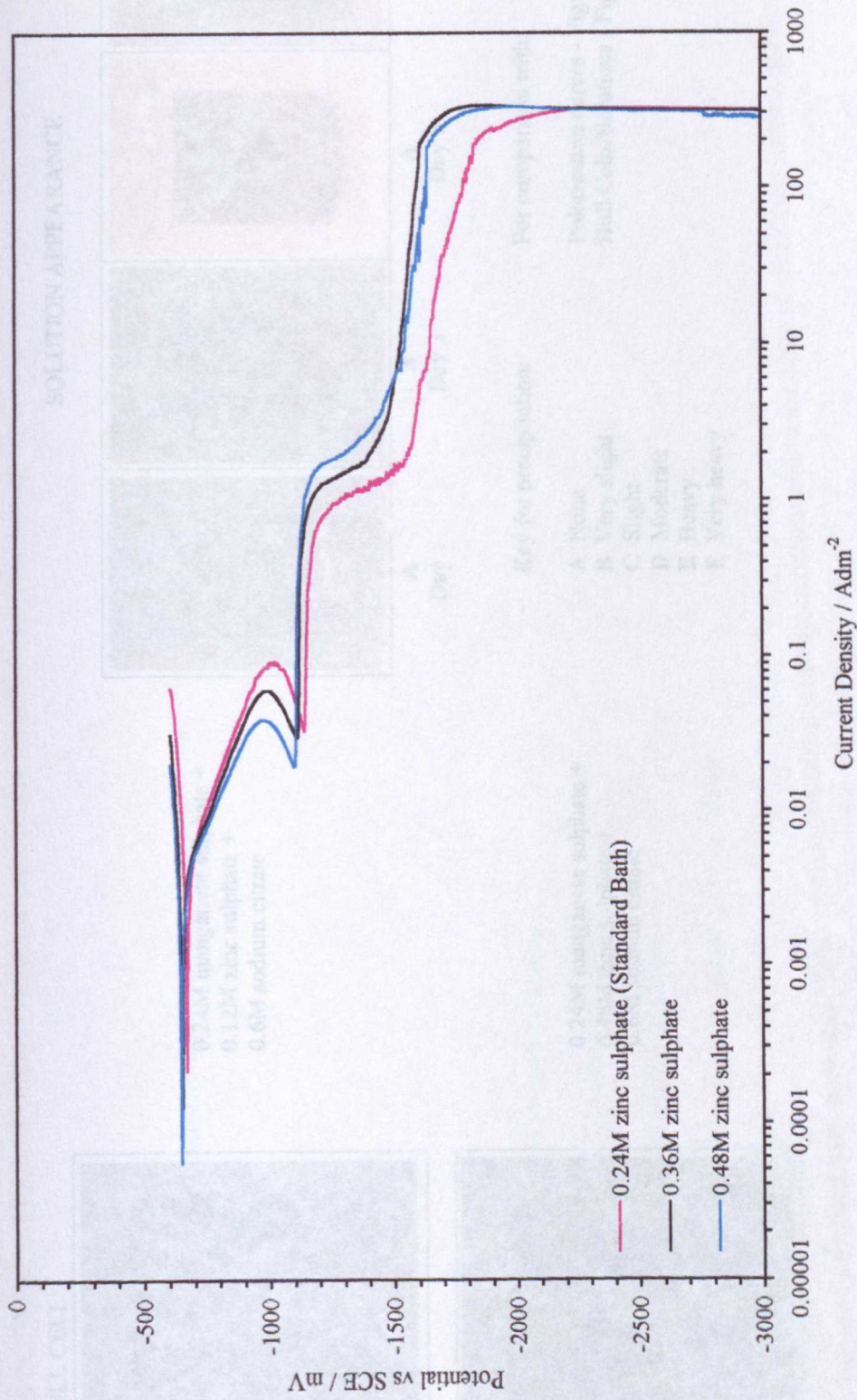
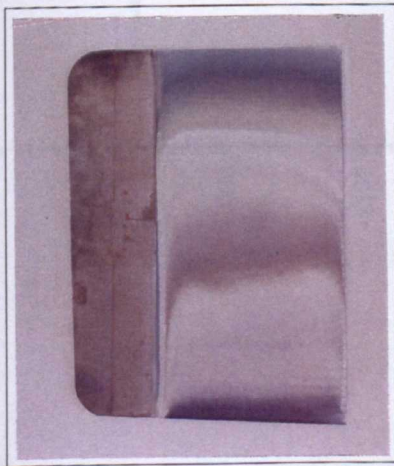


FIGURE 4.28: Effect of Zinc Sulphate Content on Zinc-Manganese Electrodeposition from a Standard Bath (25°C, pH5.0)

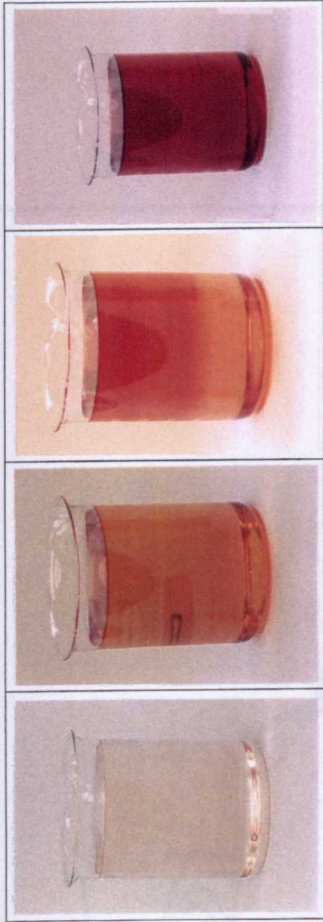
HULL CELL



0.24M manganese sulphate +
0.12M zinc sulphate +
0.6M sodium citrate

0.24M manganese sulphate +
0.48M zinc sulphate +
0.6M sodium citrate

SOLUTION APPEARANCE



A
Day 1

A
Day 3

A
Day 9

B
Day 30

Key for precipitation:

- A None
- B Very slight
- C Slight
- D Moderate
- E Heavy
- F Very heavy

For comparison with:

Polarisation curves - Figures 4.27, 4.28
Hull Cells/Solutions - Figure 4.12

FIGURE 4.29: Effect of Zinc Sulphate Content on a Zinc-Manganese Standard Bath (pH5.0, Room Temperature)

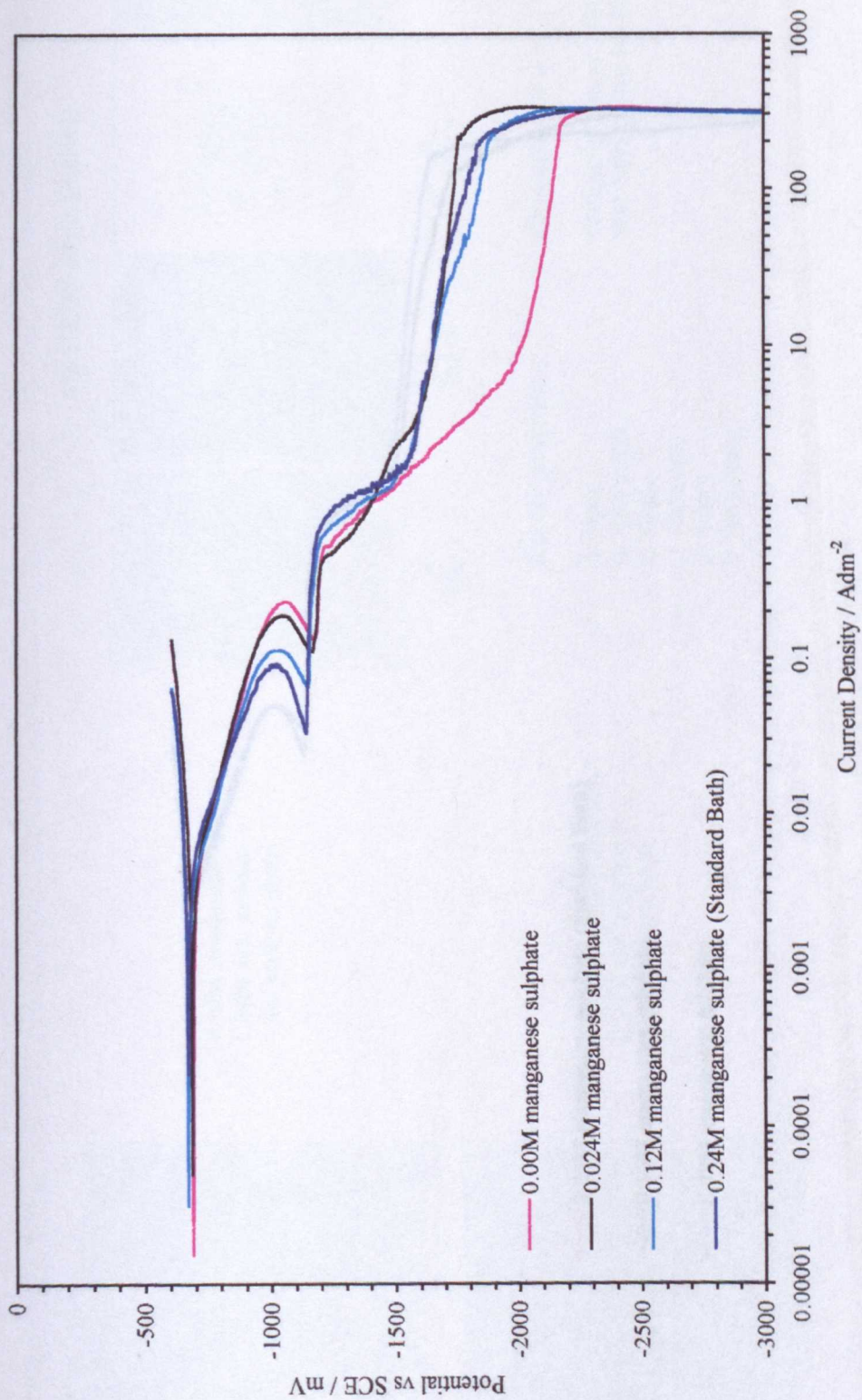


FIGURE 4.30: Effect of Manganese Sulphate Content on Zinc-Manganese Electrodeposition from a Standard Bath (25°C, pH5.0)

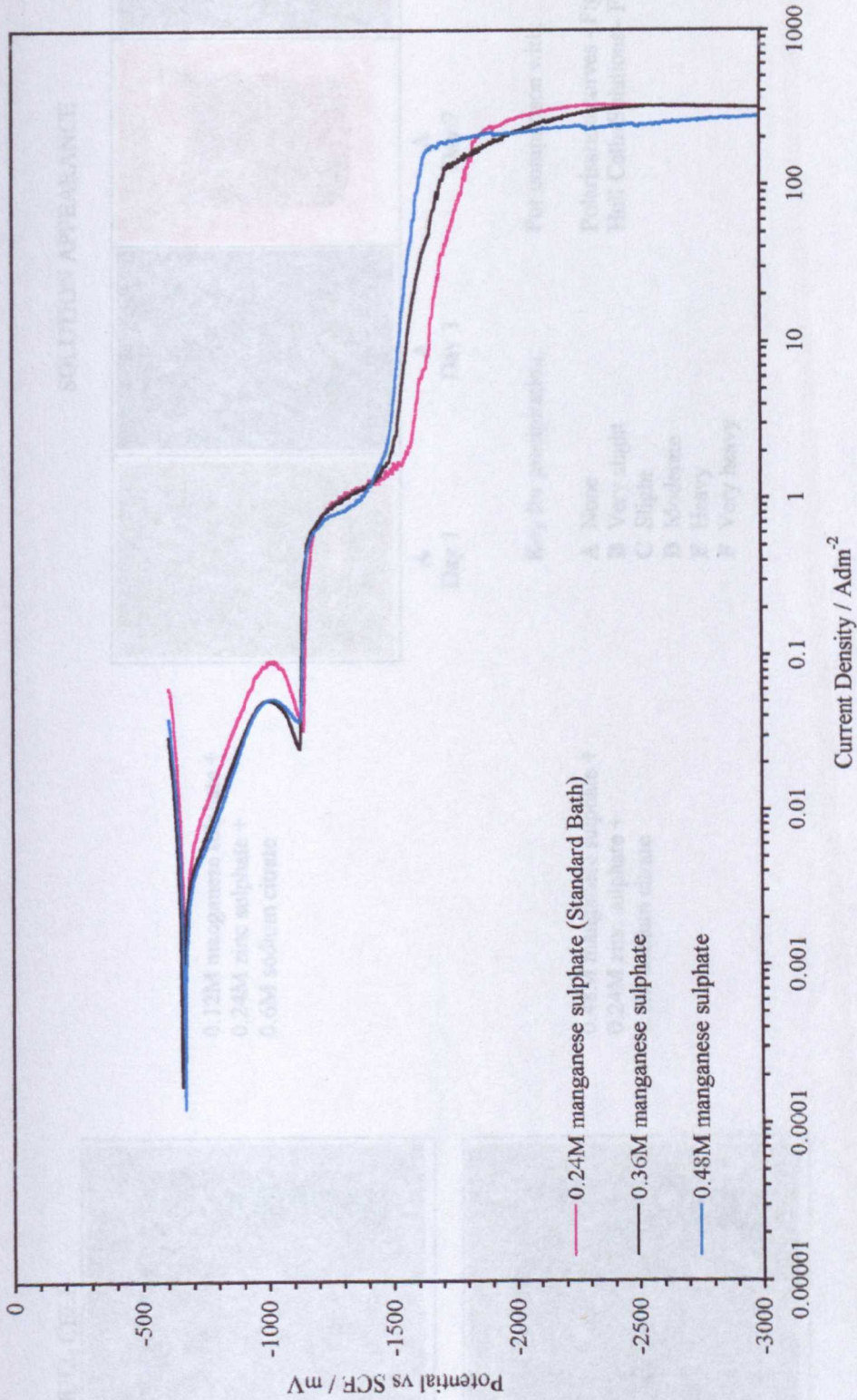
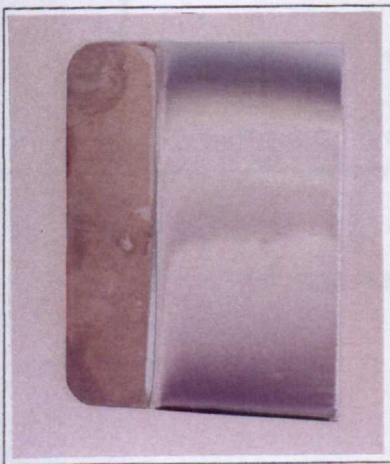
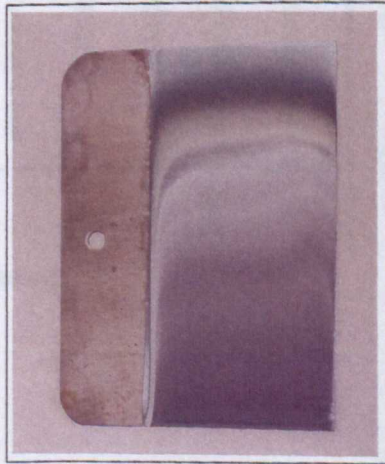


FIGURE 4.31: Effect of Manganese Sulphate Content on Zinc-Manganese Electrodeposition from a Standard Bath (25°C, pH5.0)

HULL CELL

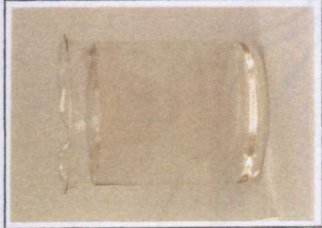


0.12M manganese sulphate +
0.24M zinc sulphate +
0.6M sodium citrate

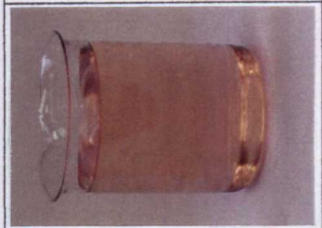


0.48M manganese sulphate +
0.24M zinc sulphate +
0.6M sodium citrate

SOLUTION APPEARANCE



A
Day 1



A
Day 3



A
Day 9



A
Day 30

Key for precipitation:

- A** None
- B** Very slight
- C** Slight
- D** Moderate
- E** Heavy
- F** Very heavy

For comparison with:

- Polarisation curves - Figures 4.30, 4.31
- Hull Cells/Solutions - Figure 4.12

FIGURE 4.32: Effect of Manganese Sulphate Content on a Zinc-Manganese Standard Bath (pH5.0, Room Temperature)

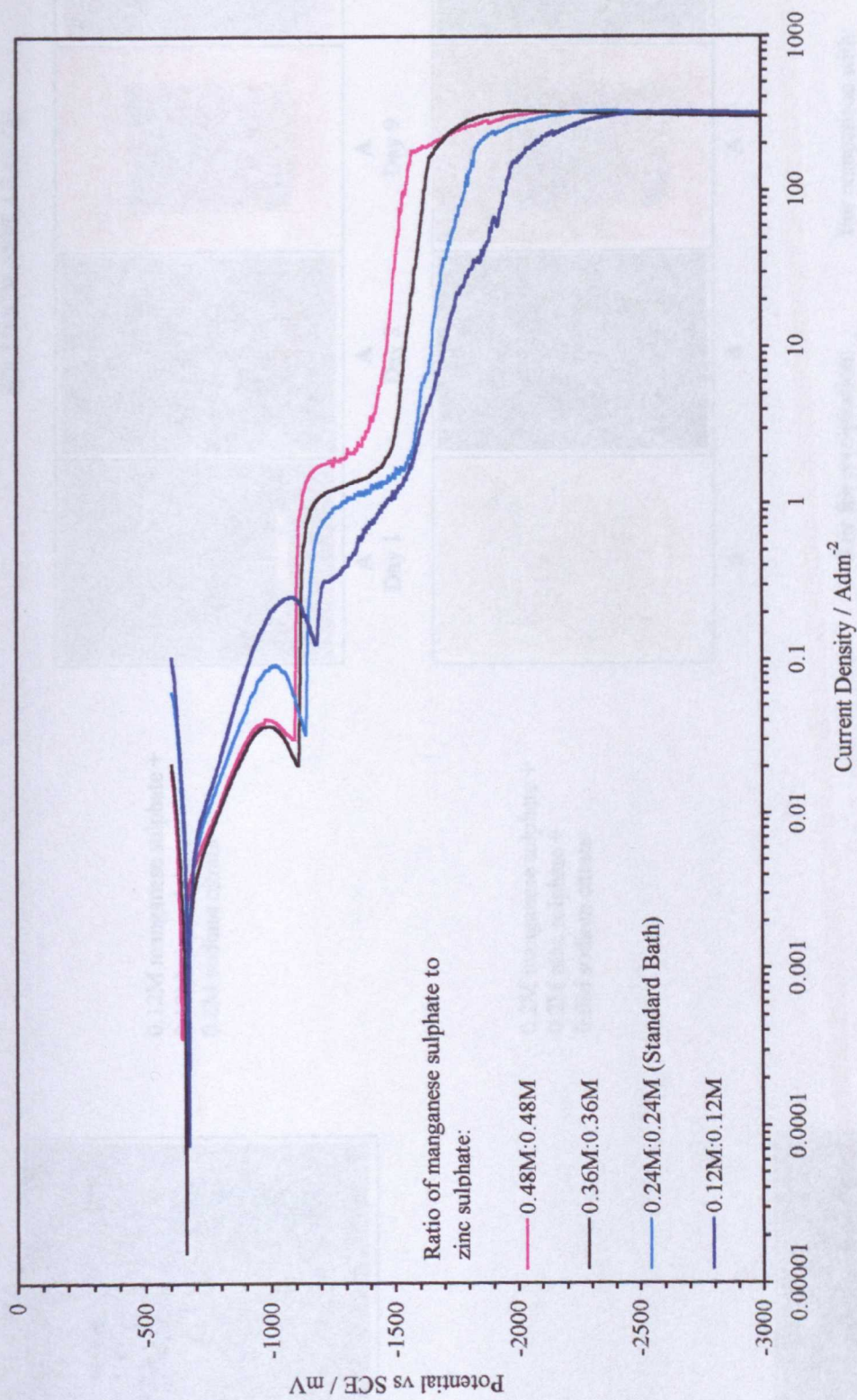
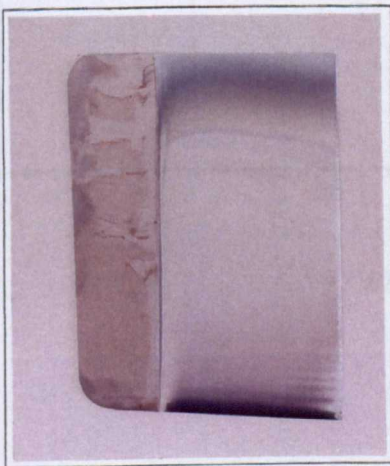


FIGURE 4.33: Effect of Metal Salt Content on Zinc-Manganese Electrodeposition from a Standard Bath (25°C, pH5.0)

HULL CELL

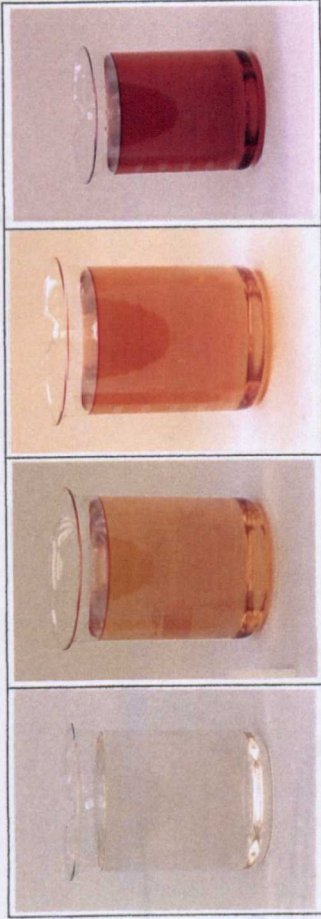


0.12M manganese sulphate +
0.12M zinc sulphate +
0.6M sodium citrate

0.2M manganese sulphate +
0.2M zinc sulphate +
0.6M sodium citrate

0.48M manganese sulphate +
0.48M zinc sulphate +
0.6M sodium citrate

SOLUTION APPEARANCE

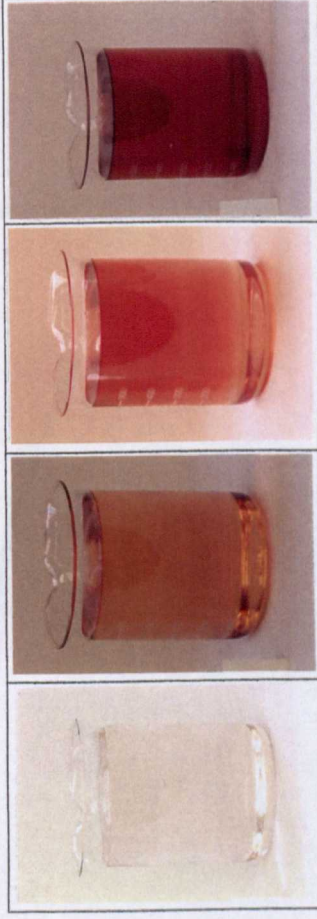


A
Day 1

A
Day 3

A
Day 9

A
Day 30



A

A

A

C

Key for precipitation:

- A None
- B Very slight
- C Slight
- D Moderate
- E Heavy
- F Very heavy

For comparison with:

- Polarisation curves - Figure 4.33
- Hull Cells/Solutions - Figure 4.12

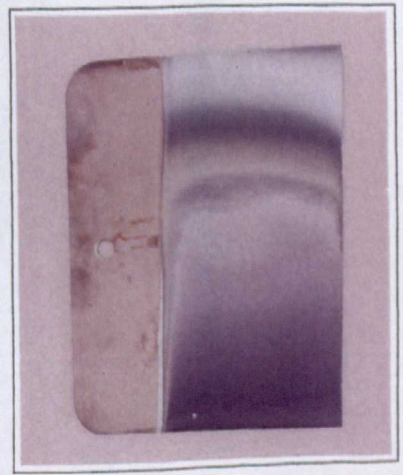


FIGURE 4.34: Effect of Metal Salt Content on a Zinc-Manganese Standard Bath (pH5.0, Room Temperature)

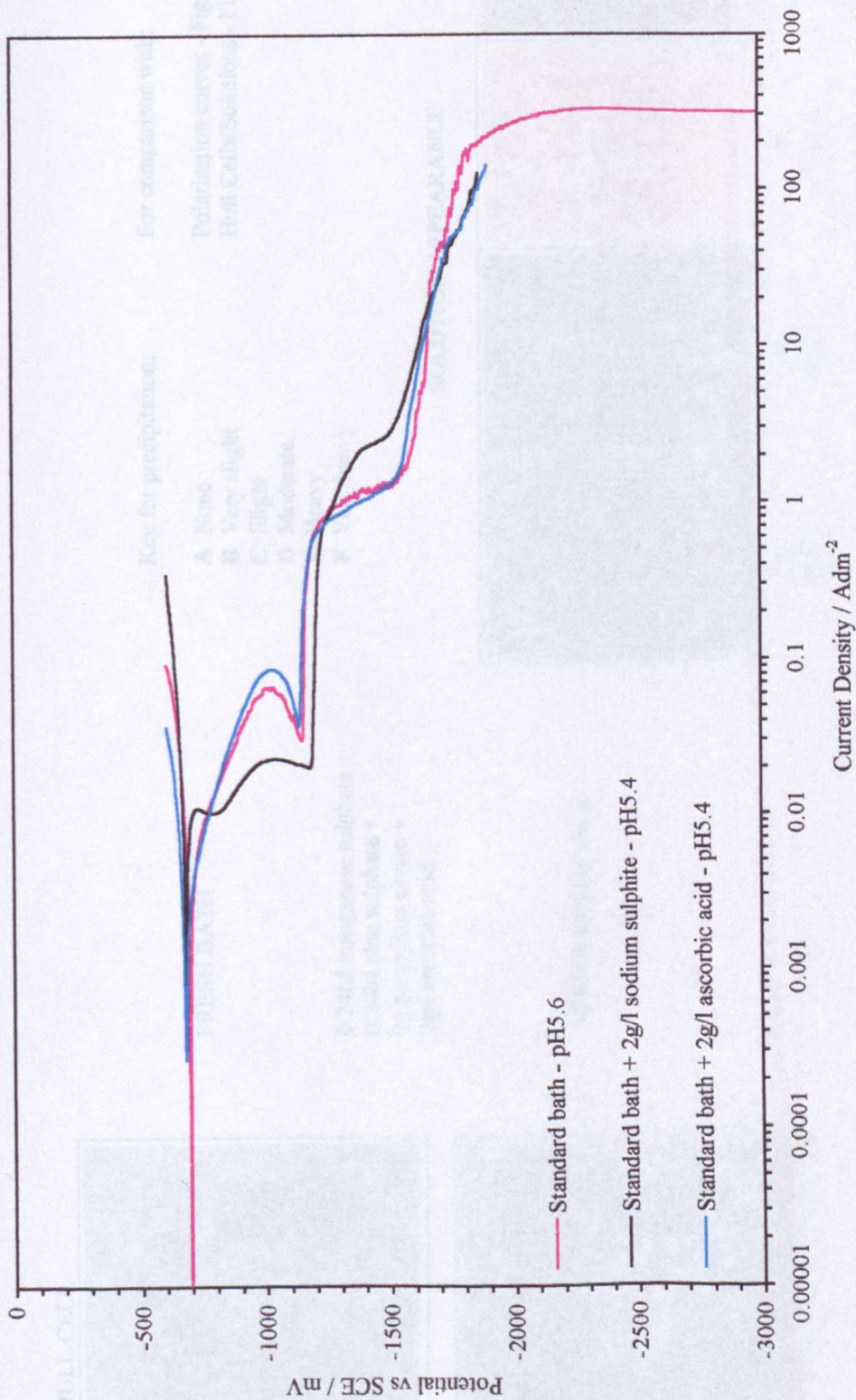
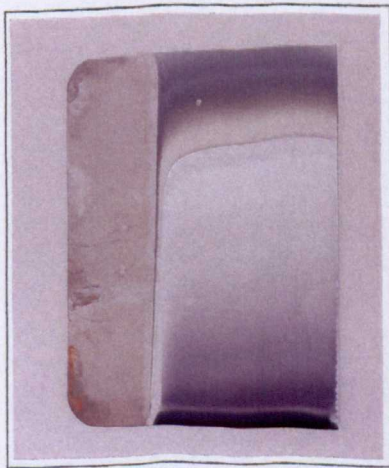


FIGURE 4.35: Effect of Additions on Zinc-Manganese Electrodeposition from a Standard Bath (25°C)

HULL CELL



FRESH BATH

0.24M manganese sulphate +
 0.24M zinc sulphate +
 0.6M sodium citrate +
 2g/l ascorbic acid

AGED BATH (30 days)

Key for precipitation:

- A None
- B Very slight
- C Slight
- D Moderate
- E Heavy
- F Very heavy

For comparison with:

Polarisation curves - Figures 4.35, 4.39
 Hull Cells/Solutions - Figure 4.12, 4.37

SOLUTION APPEARANCE

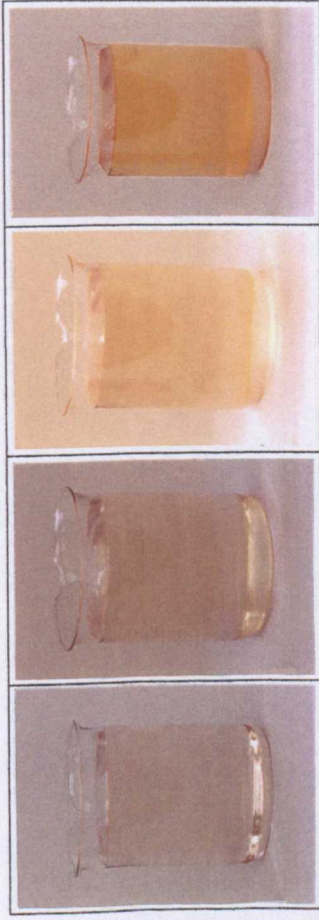
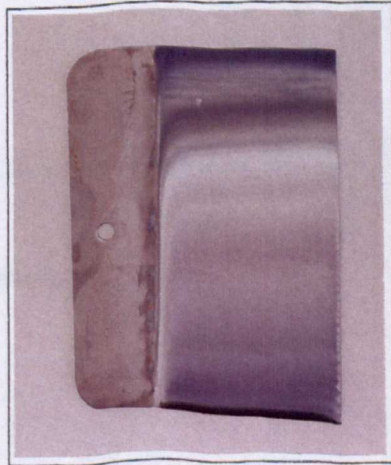
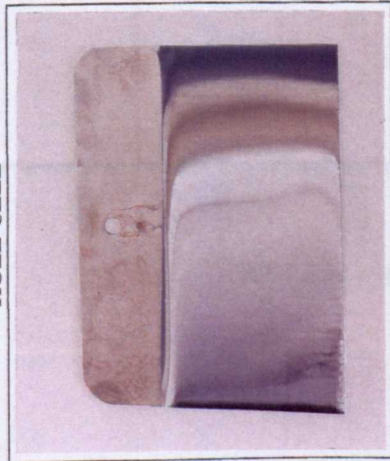


FIGURE 4.36: Effect of 2g/l Ascorbic Acid Addition to a Zinc-Manganese Standard Bath (pH5.5, Room Temperature)

HULL CELL



FRESH BATH

0.24M manganese sulphate +
 0.24M zinc sulphate +
 0.6M sodium citrate +
 2g/l sodium sulphite

AGED BATH (30 days)

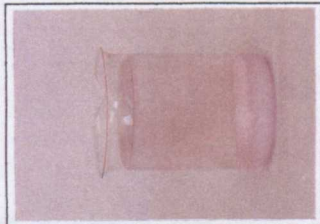
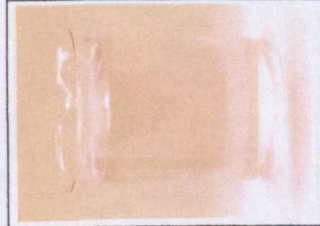
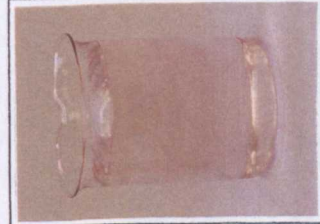
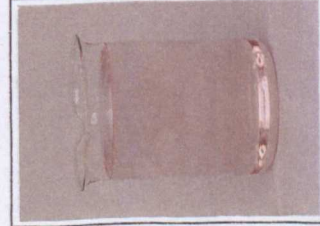
Key for precipitation:

- A** None
- B** Very slight
- C** Slight
- D** Moderate
- E** Heavy
- F** Very heavy

For comparison with:

Polarisation curves - Figures 4.35, 4.40
 Hull Cells/Solutions - Figure 4.12, 4.36

SOLUTION APPEARANCE



A
Day 1

B
Day 3

C
Day 9

D
Day 30

FIGURE 4.37: Effect of 2g/l Sodium Sulphite Addition to a Zinc-Manganese Standard Bath (pH5.5, Room Temperature)

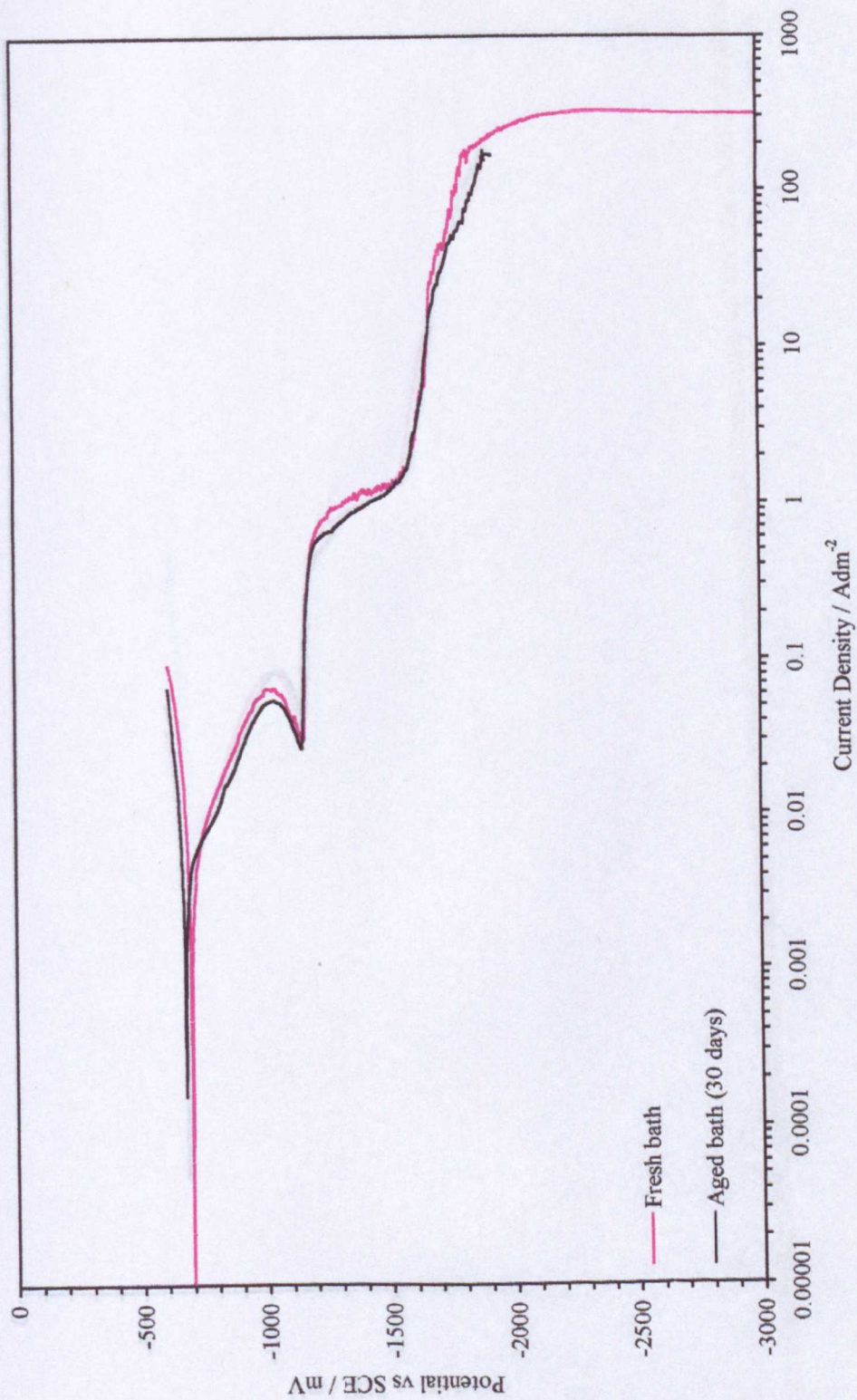


FIGURE 4.38: Effect of Bath Aging on Zinc-Manganese Electrodeposition from a Standard Bath (25°C, pH5.6)

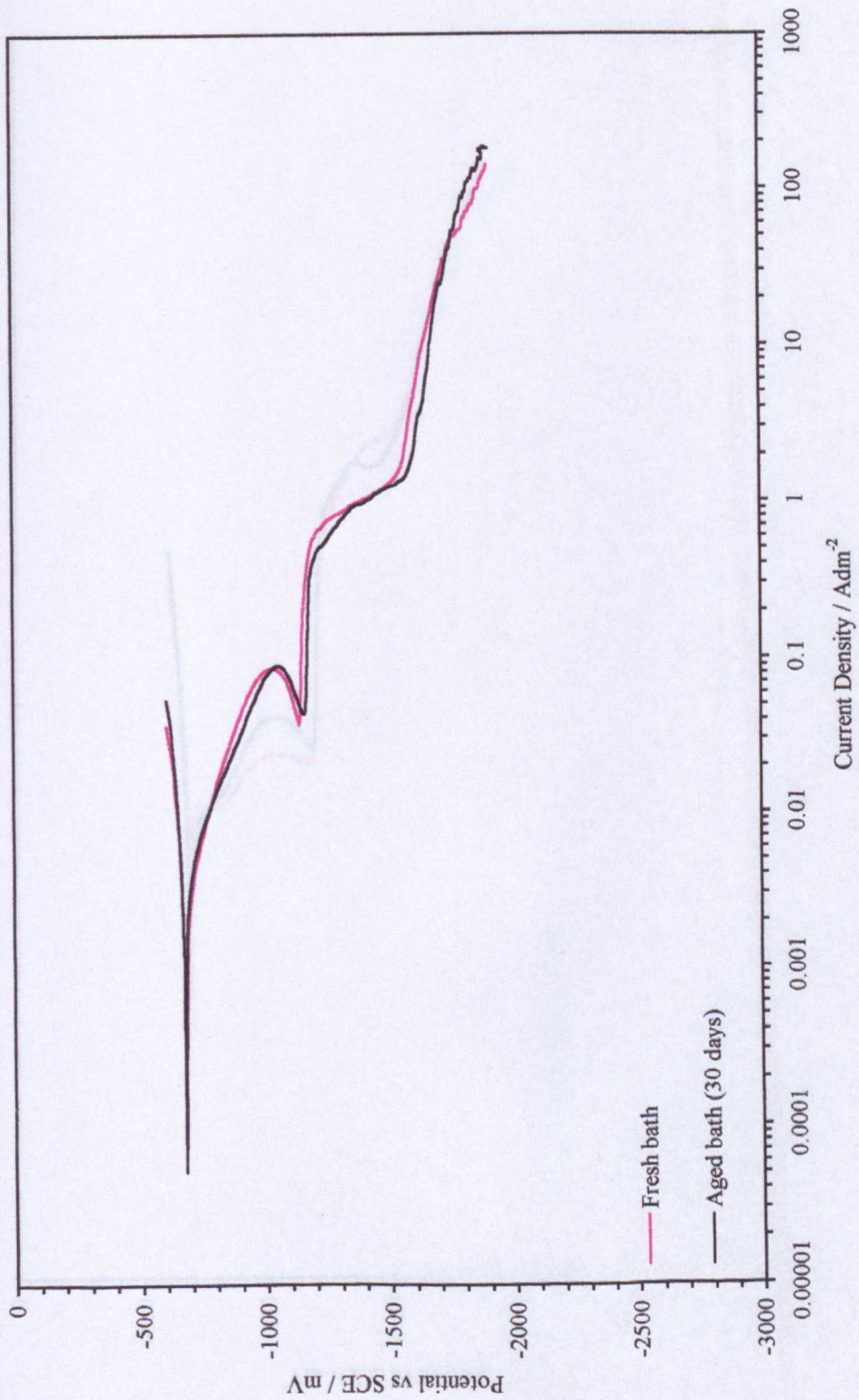


FIGURE 4.39: Effect of Bath Aging on Zinc-Manganese Electrodeposition from a Standard Bath with 2g/l Ascorbic Acid Addition (25°C, pH5.4)

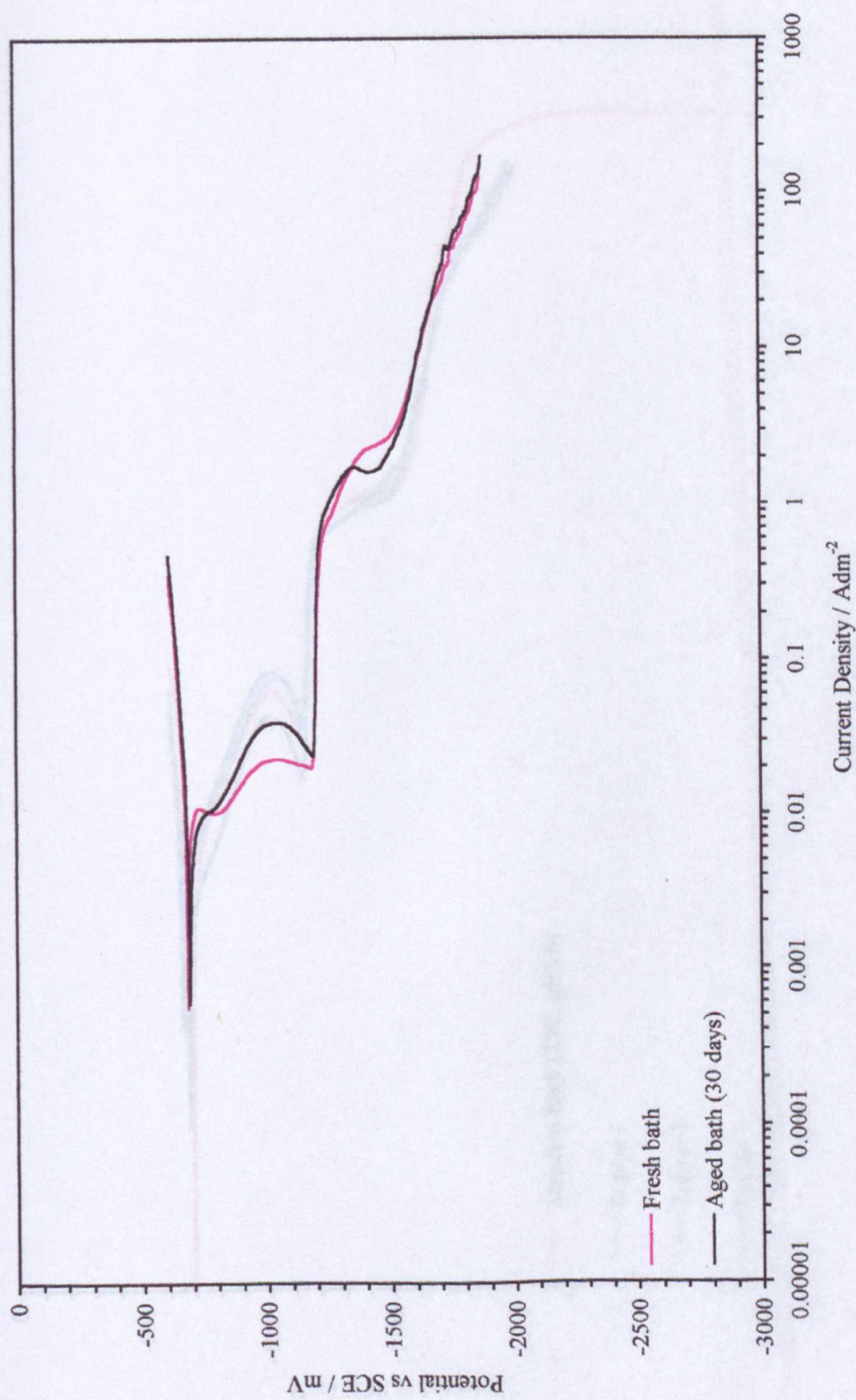


FIGURE 4.40: Effect of Bath Aging on Zinc-Manganese Electrodeposition from a Standard Bath with 2g/l Sodium Sulphite Addition (25°C, pH5.4)

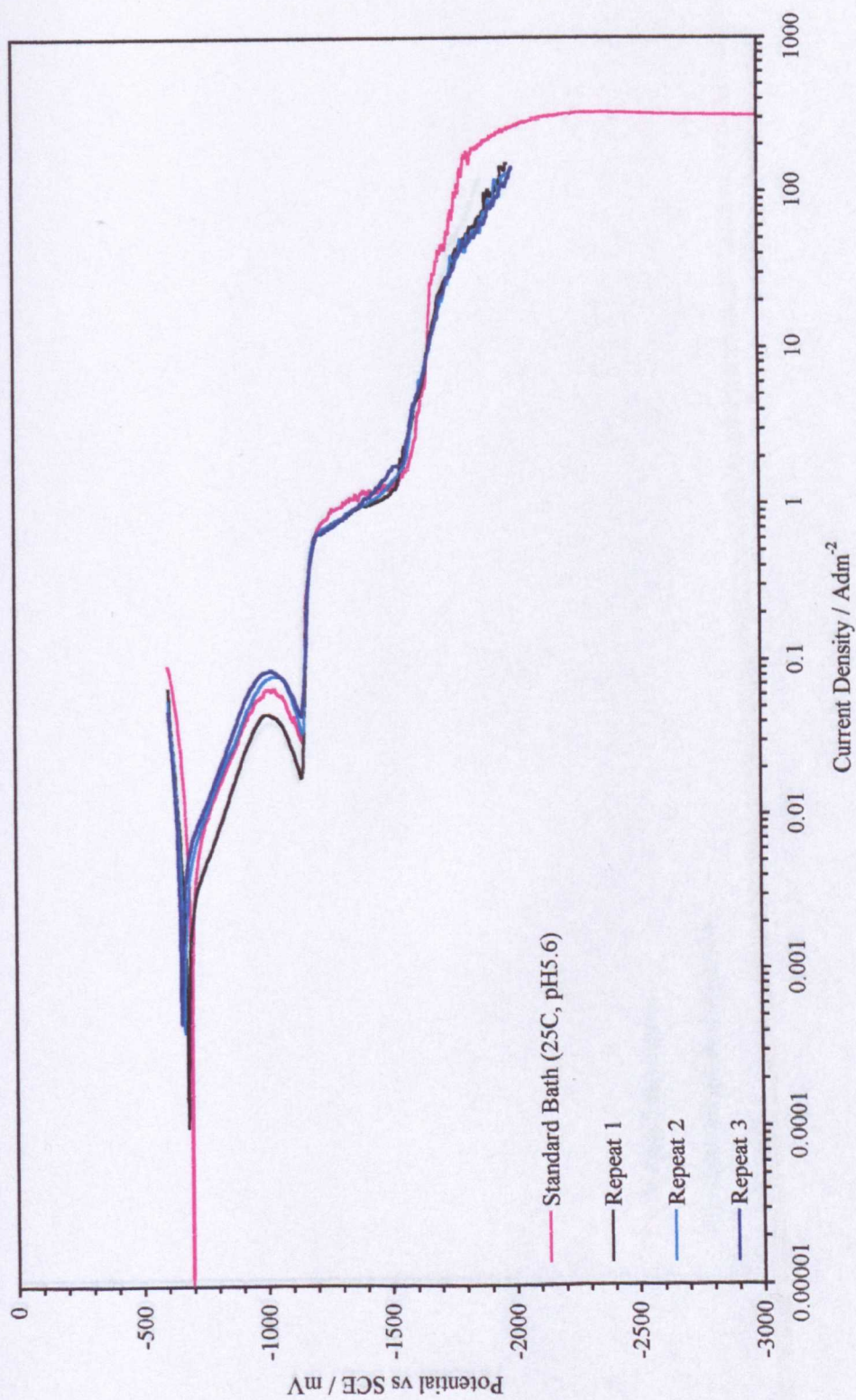


FIGURE 4.41: Effect of Repeated Use of the Zinc-Manganese Standard Bath (25°C, pH5.6)

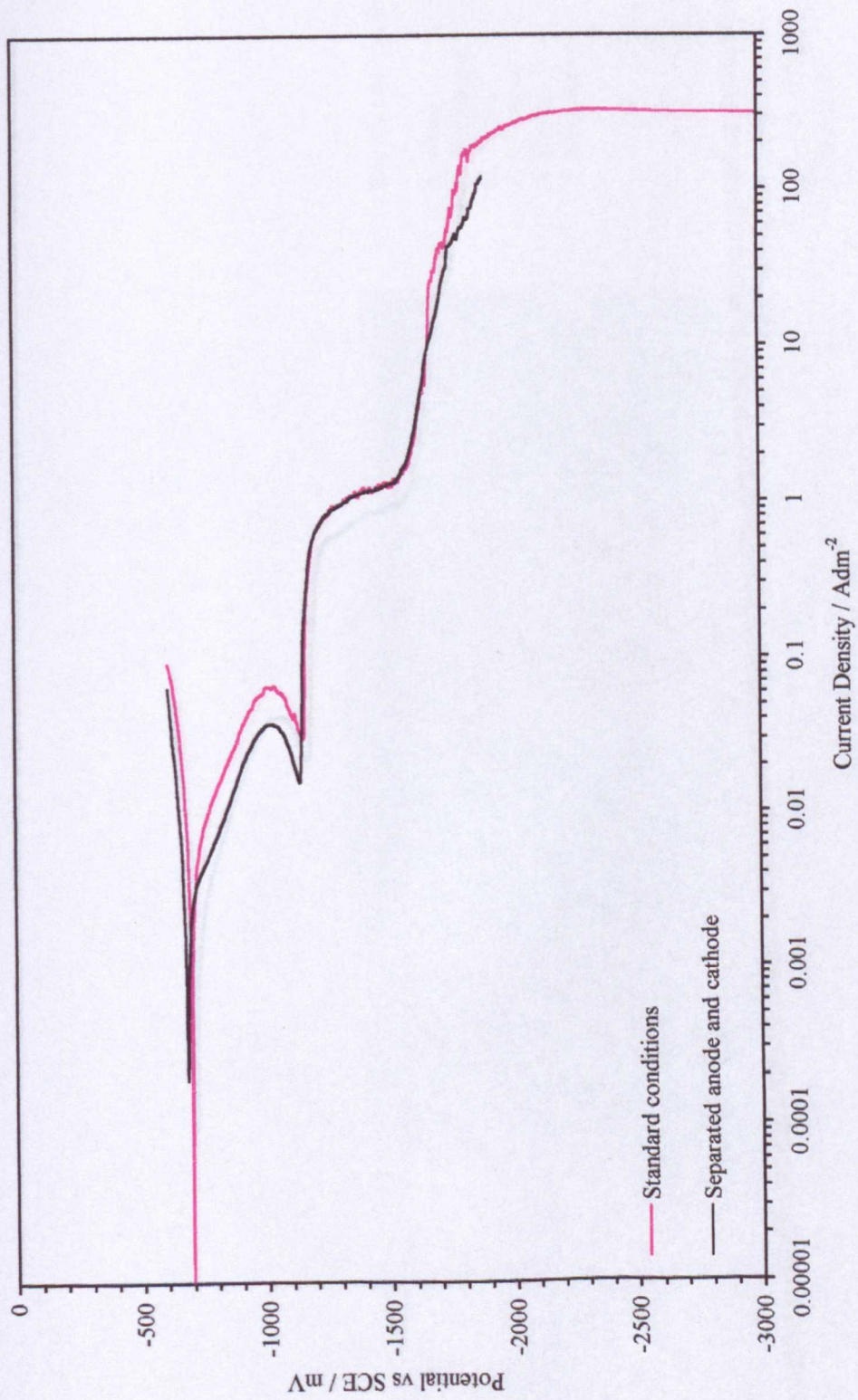


FIGURE 4.42: Effect of Anode and Cathode Separation on Zinc-Manganese Electrodeposition from a Standard Bath (25°C, pH5.6)

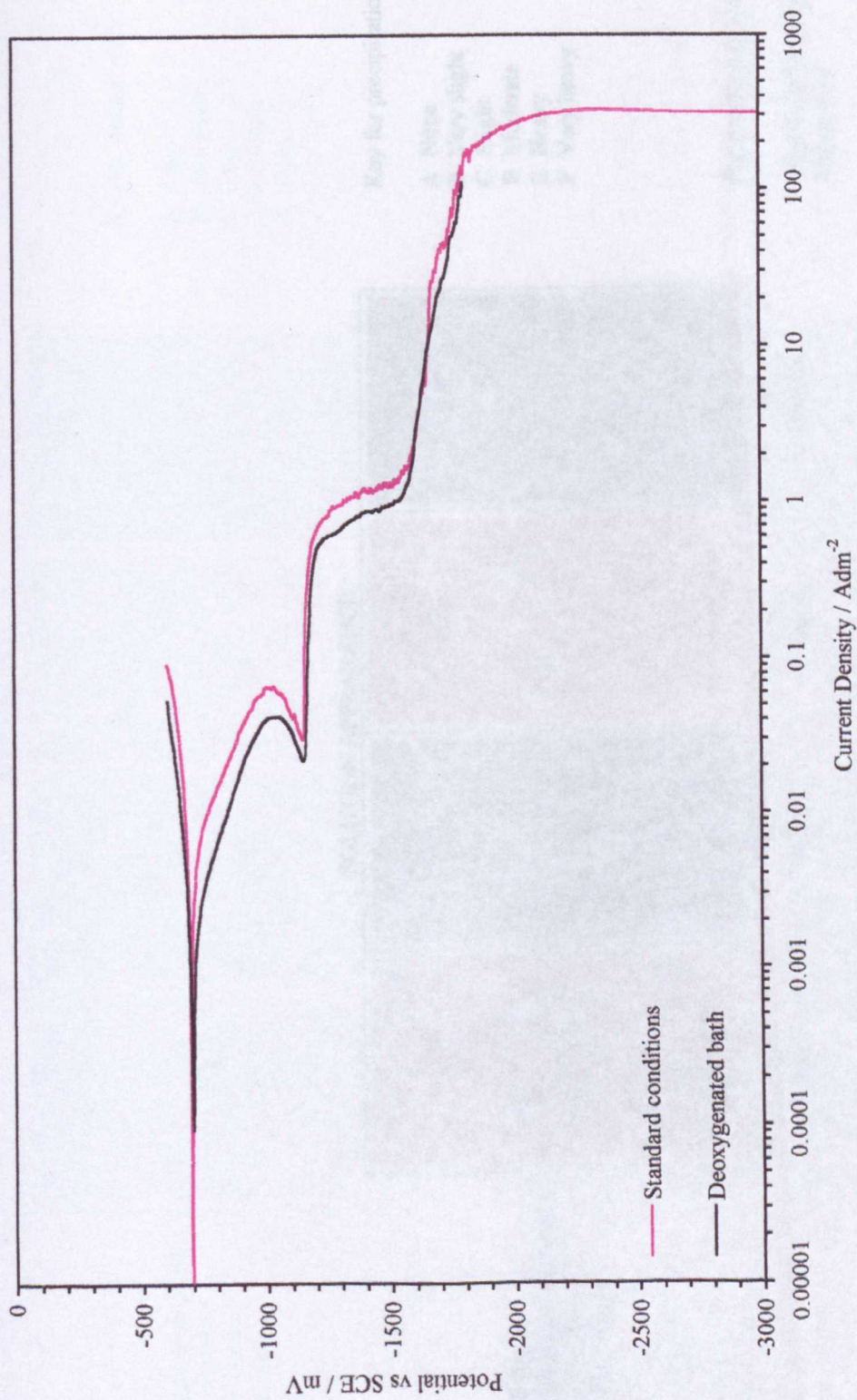


FIGURE 4.43: Effect of Oxygen Content on Zinc-Manganese Electrodeposition from a Standard Bath (25°C, pH5.6)

SOLUTION APPEARANCE



Standard Bath -
 0.24M manganese sulphate +
 0.24M zinc sulphate +
 0.6M sodium citrate

Key for precipitation:

- A None
- B Very slight
- C Slight
- D Moderate
- E Heavy
- F Very heavy

For comparison with:

Hull Cells/Solutions -
 Figure 4.12

FIGURE 4.44: Effect of Exclusion of the Atmosphere from a Zinc-Manganese Standard Bath (pH5.6, Room Temperature)

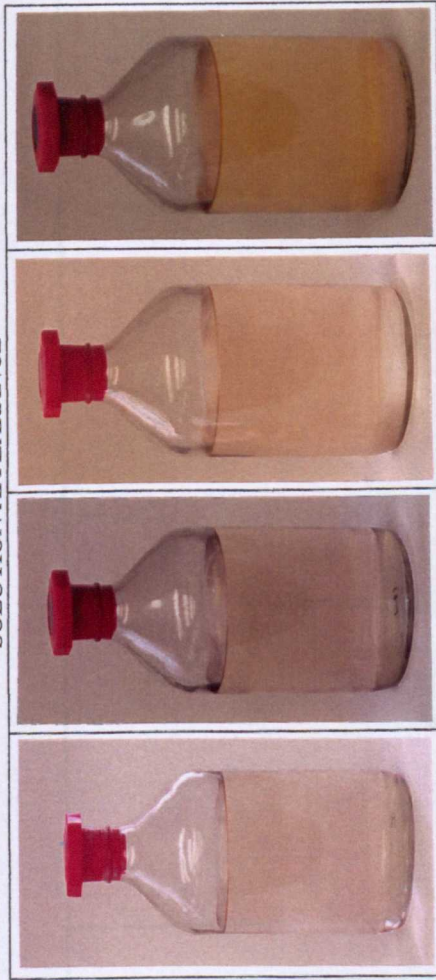
SOLUTION APPEARANCE

Key for precipitation:

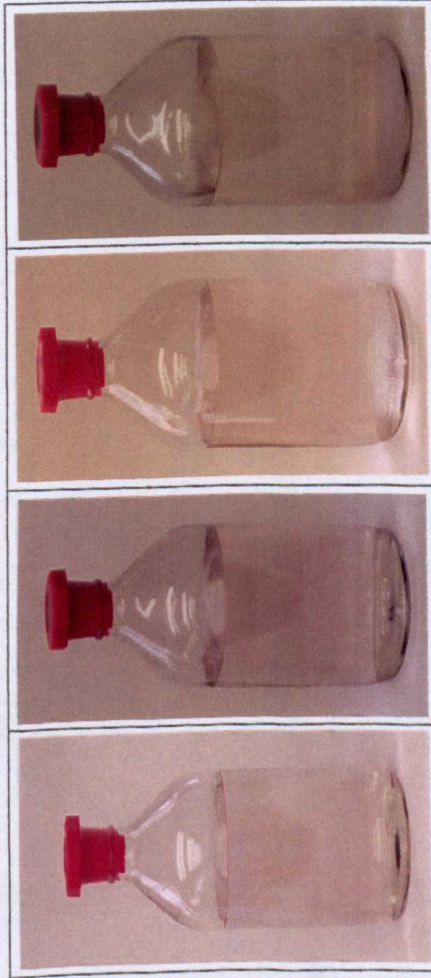
- A None
- B Very slight
- C Slight
- D Moderate
- E Heavy
- F Very heavy

For comparison with:

Hull Cells/Solutions -
 Figures 4.12, 4.36, 4.37, 4.44



0.24M manganese sulphate +
 0.24M zinc sulphate +
 0.6M sodium citrate +
 2g/l ascorbic acid



0.24M manganese sulphate +
 0.24M zinc sulphate +
 0.6M sodium citrate +
 2g/l sodium sulphite

FIGURE 4.45: Effect of Exclusion of the Atmosphere from a Zinc-Manganese Standard Bath with Additions (pH5.6, Room Temperature)

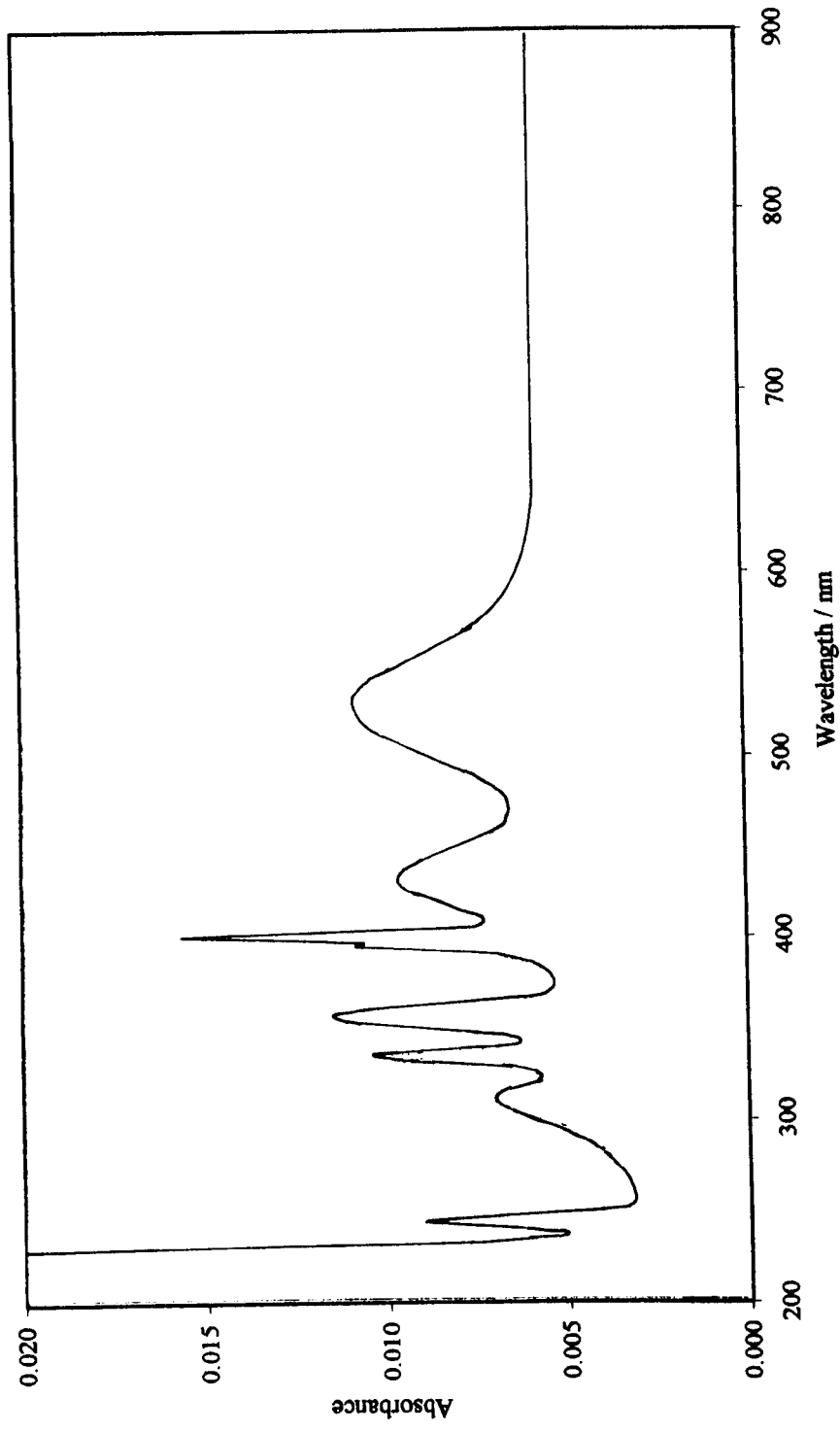


FIGURE 4.46: Ultraviolet and Visible Spectrum for a Freshly Prepared 0.48M Manganese Sulphate Solution (pH4.4, Room Temperature).
(Background: Double Distilled Water)

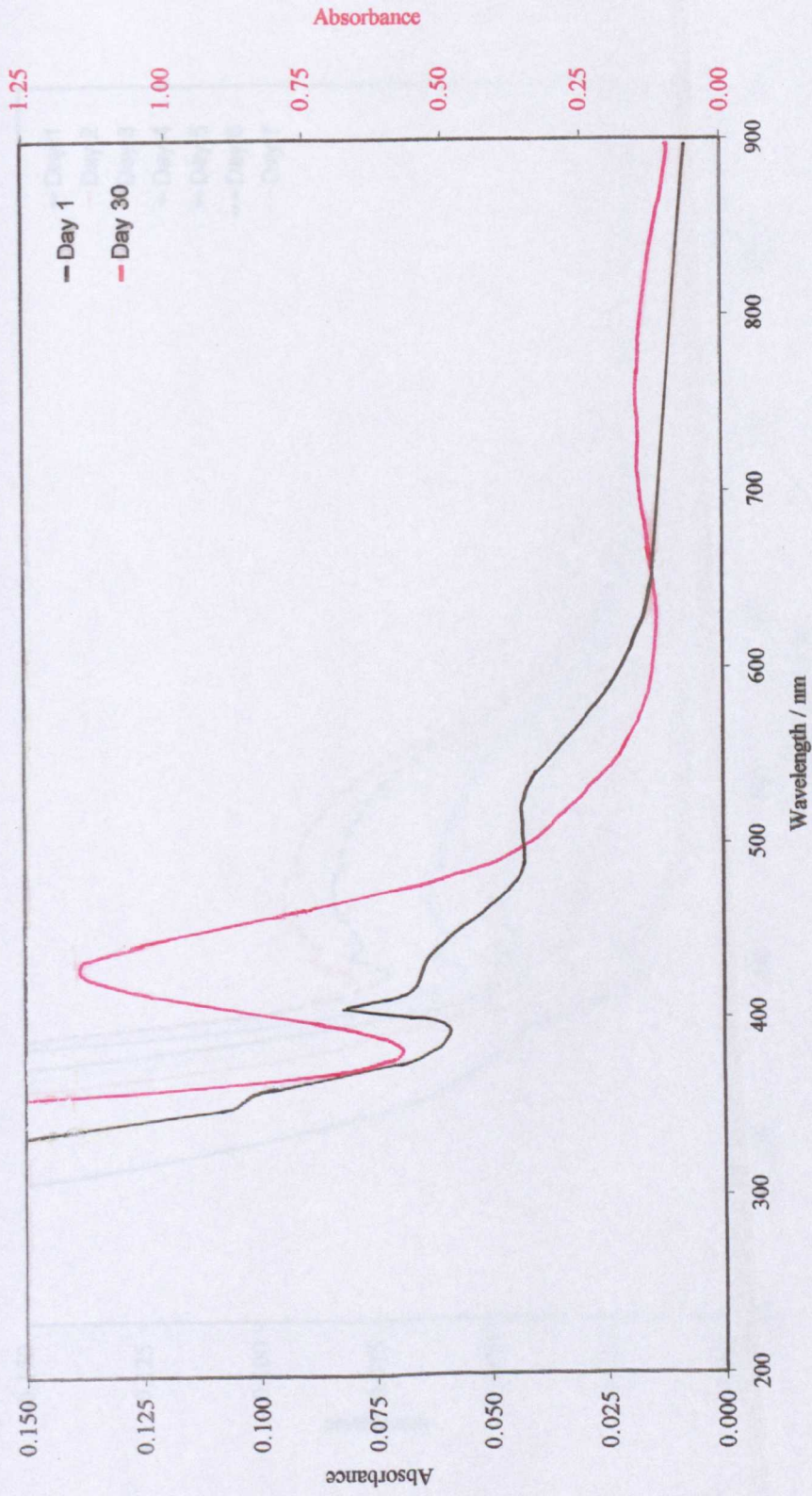


FIGURE 4.47: Effect of Aging on the Ultraviolet and Visible Spectrum for a Solution of 0.48M Manganese Sulphate and 0.6M Sodium Citrate (pH5.6, Room Temperature)
 (Background: Double Distilled Water)

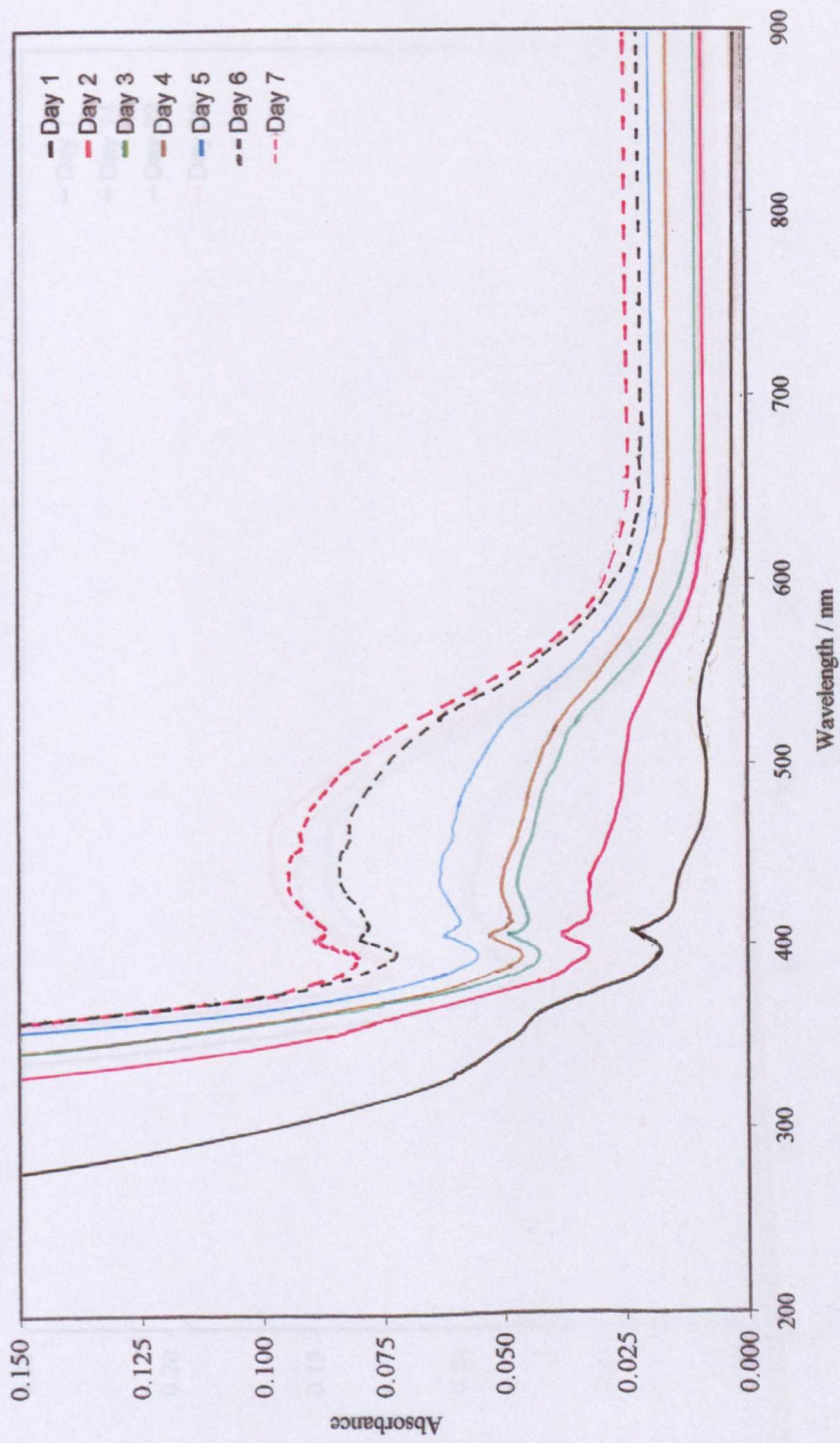


FIGURE 4.48: Effect of Aging on the Ultraviolet and Visible Spectrum for a Standard Bath (pH5.6, Room Temperature) - Day 1 to Day 7 (Background: Double Distilled Water)

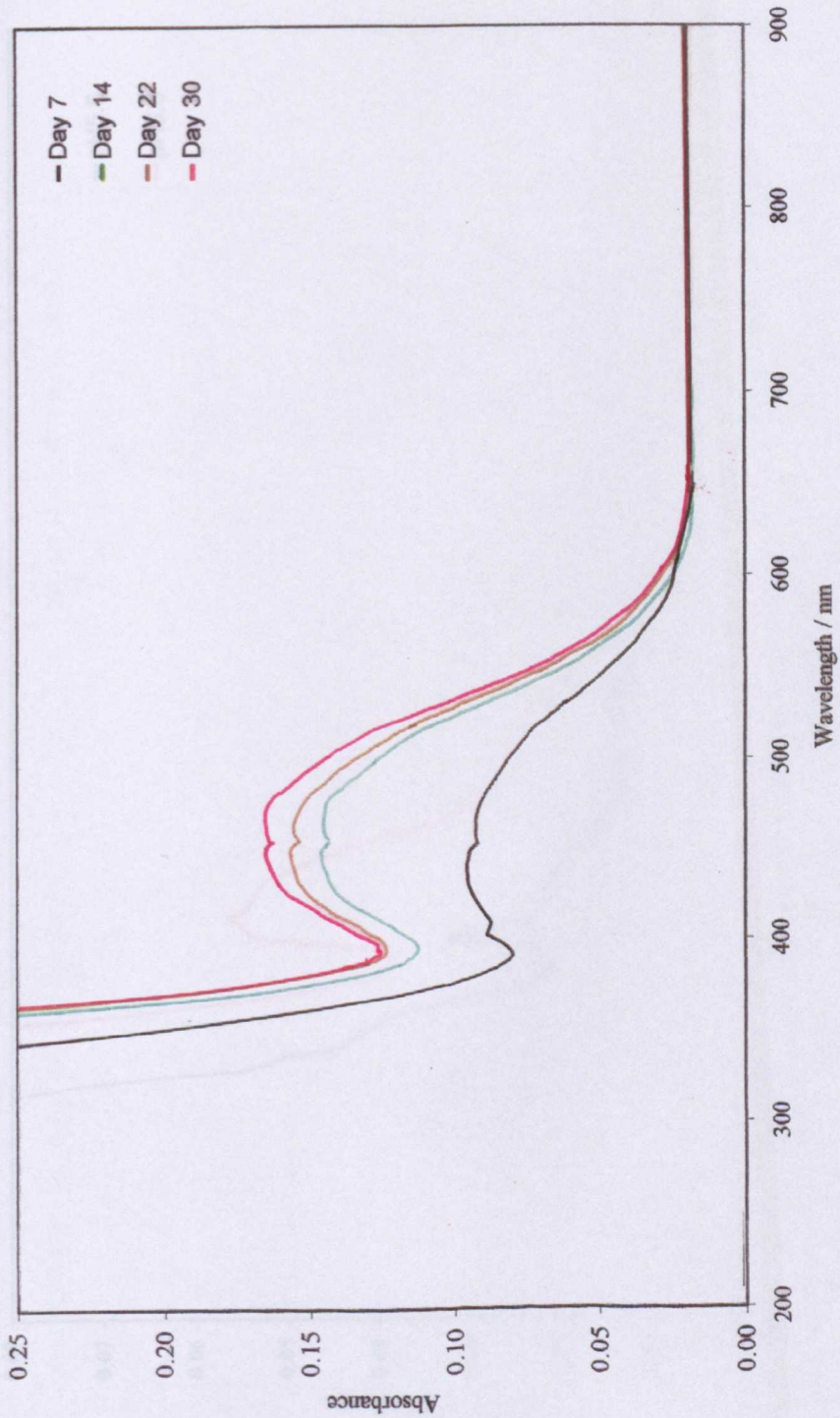


FIGURE 4.49: Effect of Aging on the Ultraviolet and Visible Spectrum for a Standard Bath (pH 5.6, Room Temperature) - Day 7 to Day 30 (Background: Double Distilled Water)

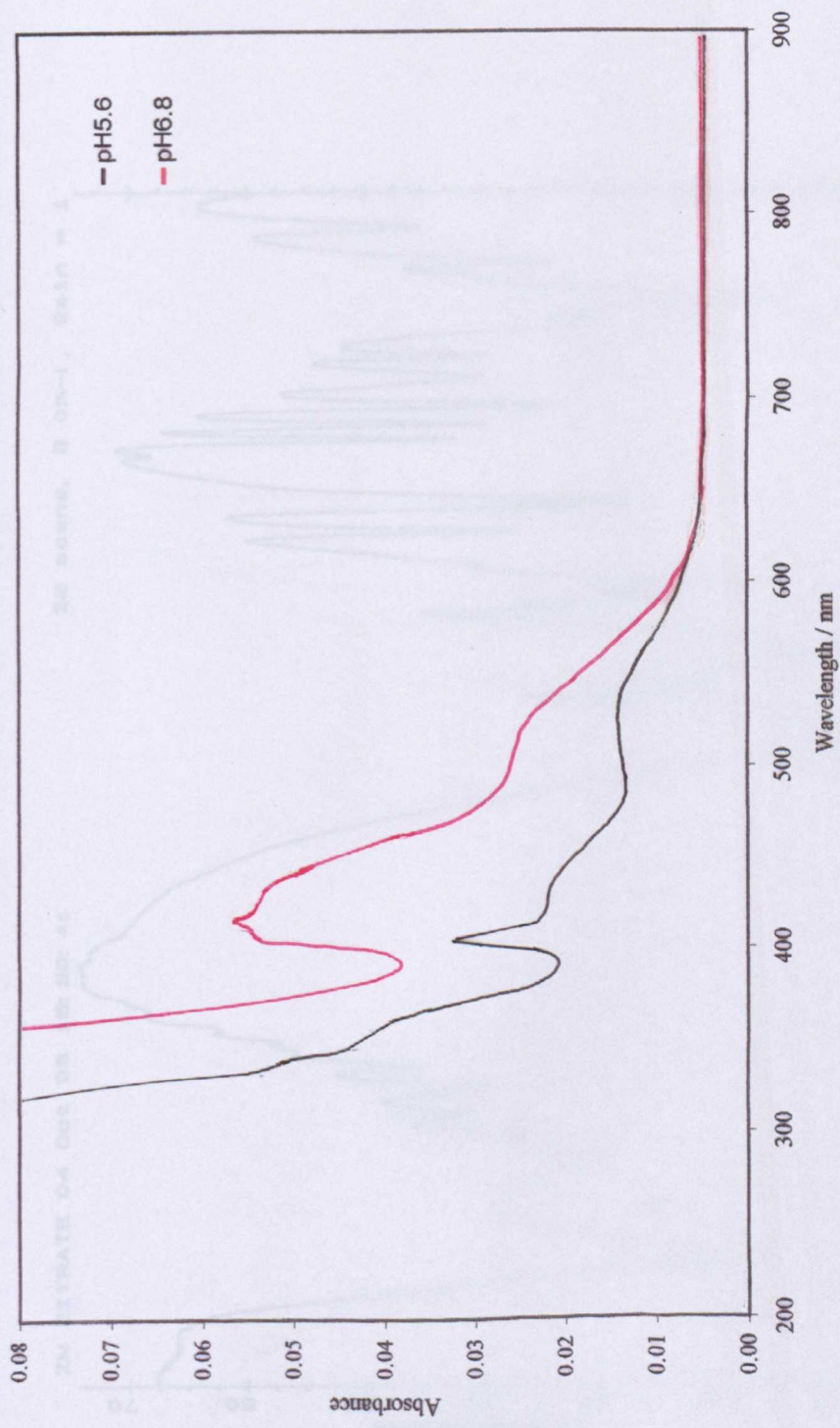


FIGURE 4.50: Effect of pH on the Ultraviolet and Visible Spectrum for a Freshly Prepared Solution of 0.24M Manganese Sulphate and 0.6M Sodium Citrate (Background: Double Distilled Water)

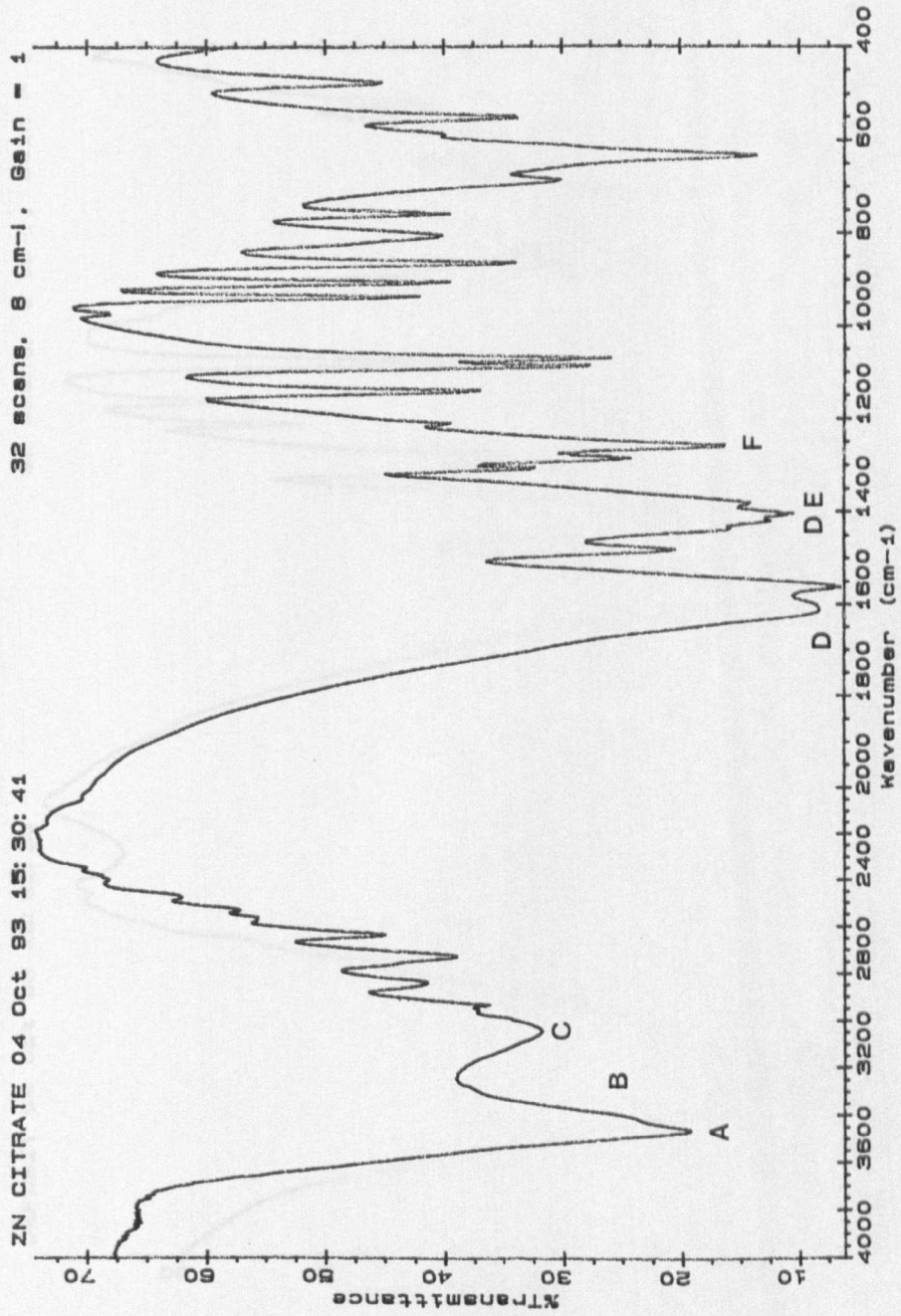


FIGURE 4.51: Infrared Spectrum for Zinc Citrate (KBr disc)

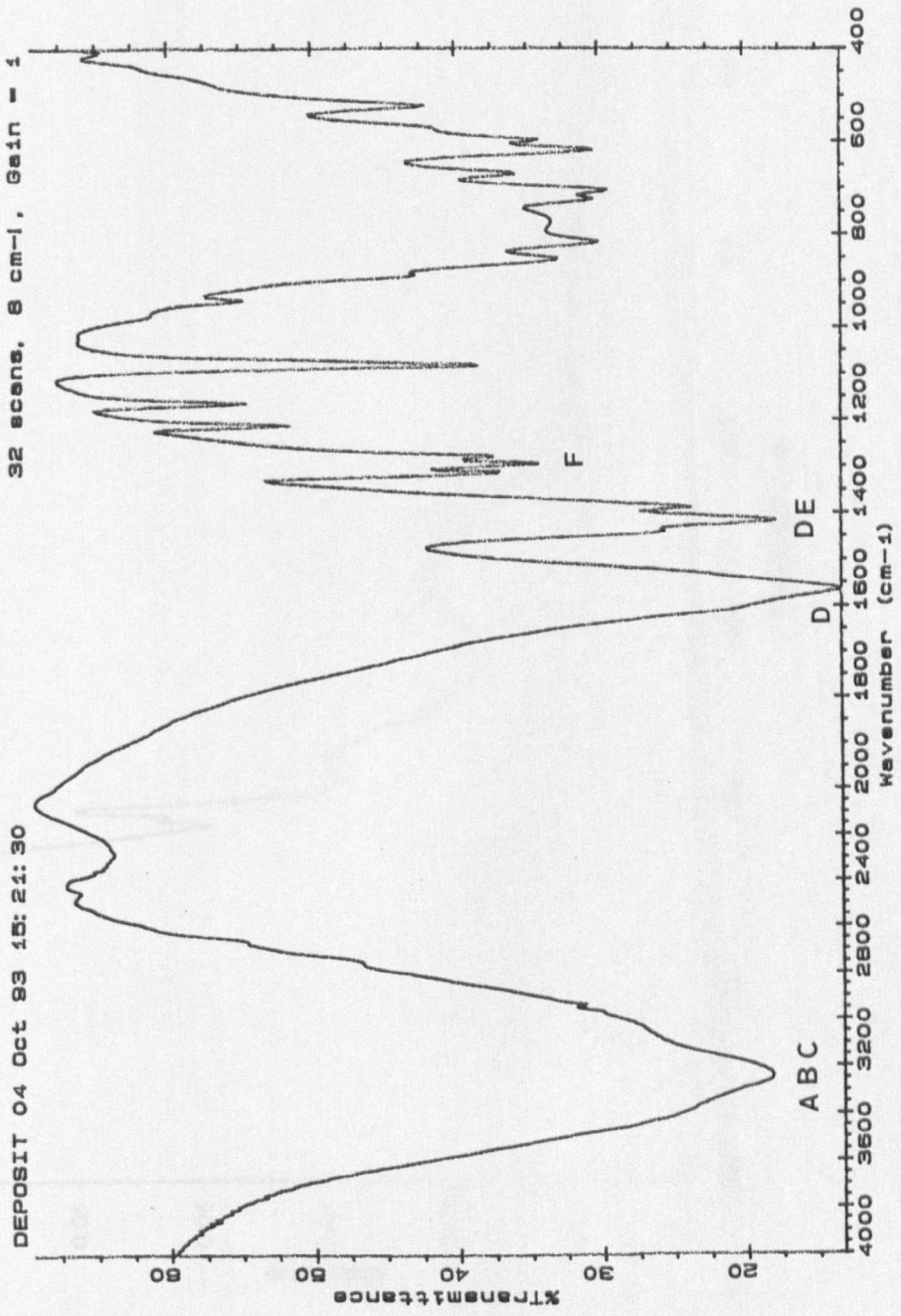


FIGURE 4.52: Infrared Spectrum for the Precipitate from a Standard Bath (KBr disc)

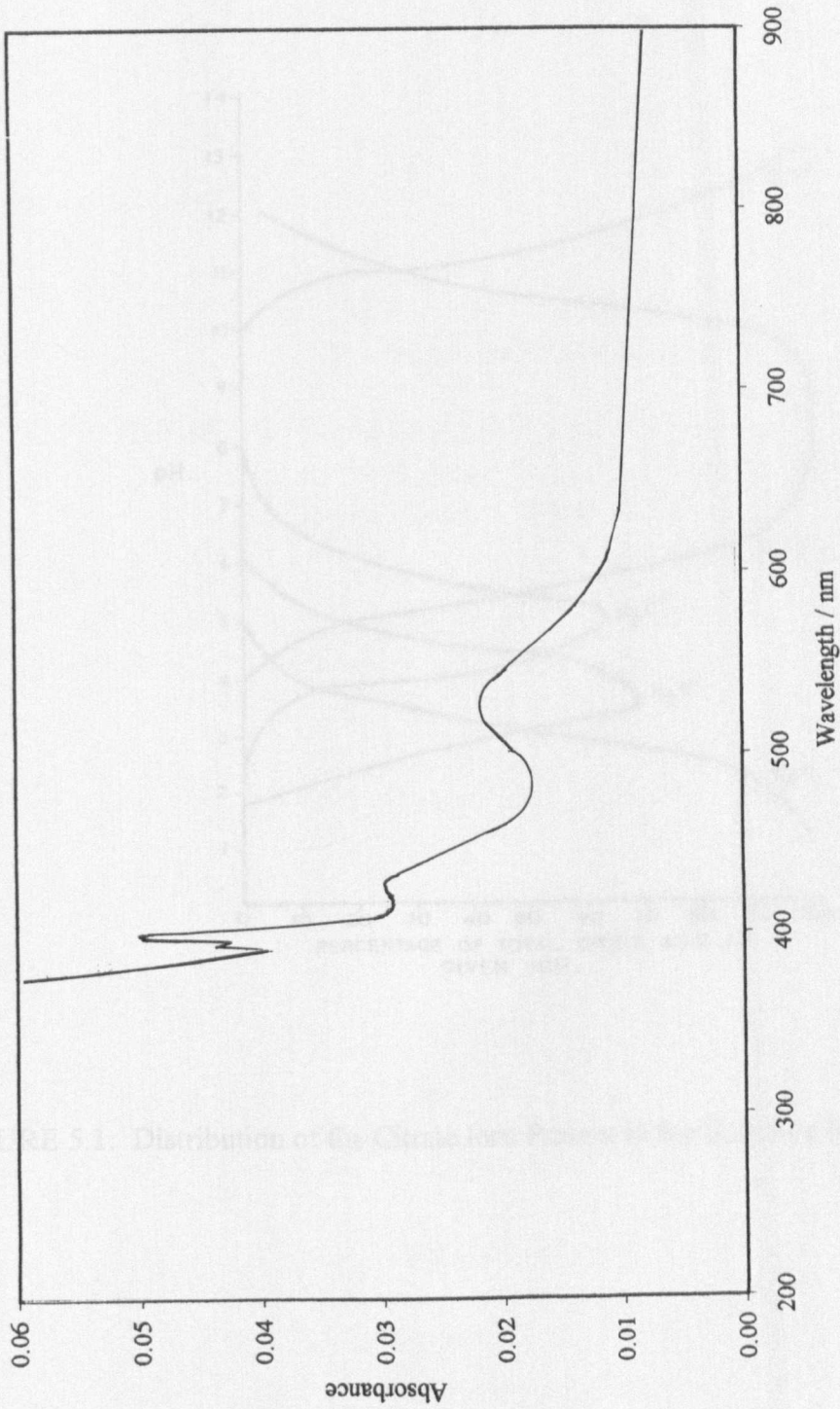


FIGURE 4.53: Ultraviolet and Visible Spectrum for the Precipitate Produced in a Standard Bath (Background: 20% (by vol) nitric acid)

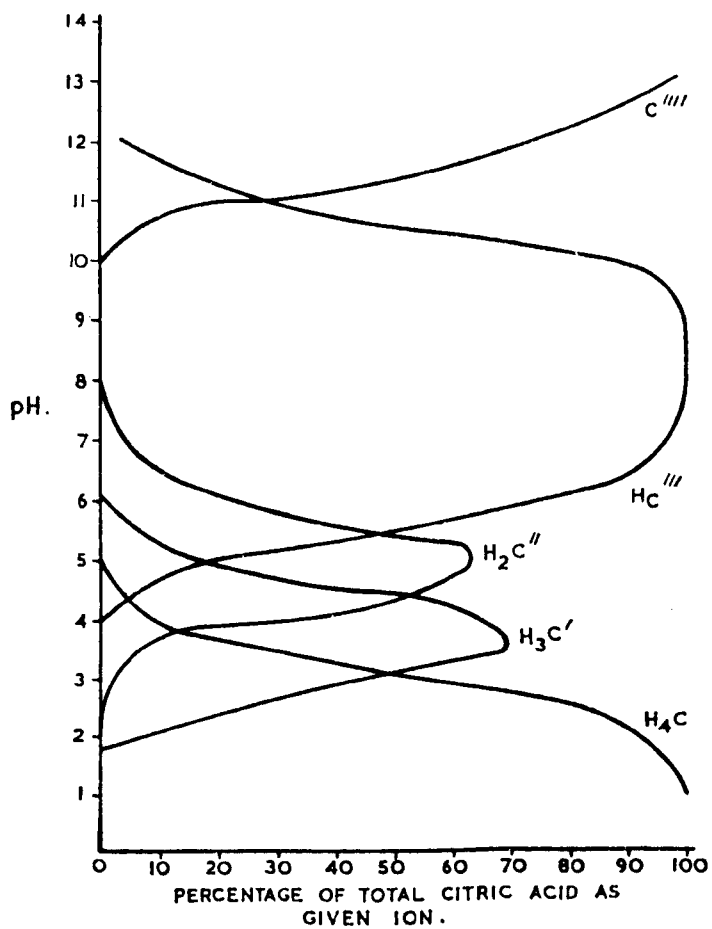


FIGURE 5.1: Distribution of the Citrate Ions Present in the Bath as a Function of pH ⁽⁷⁹⁾

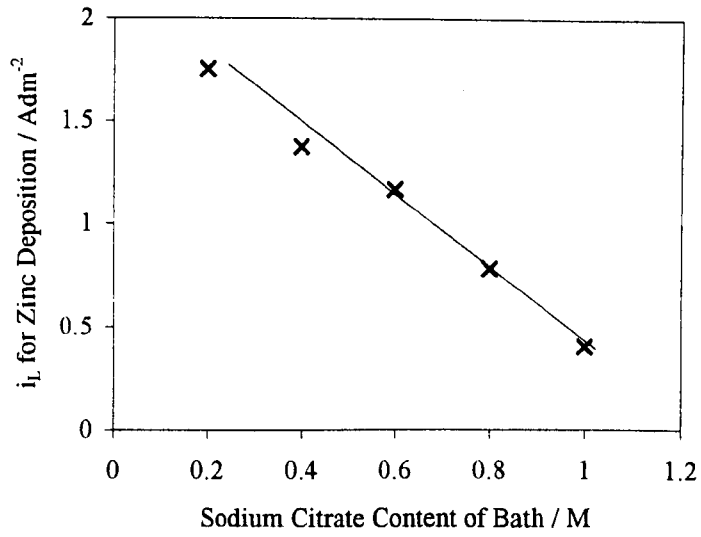


FIGURE 5.2: The Dependence of Zinc deposition i_L on the Sodium Citrate Content of the Bath (From Figures 4.24 and 4.25)

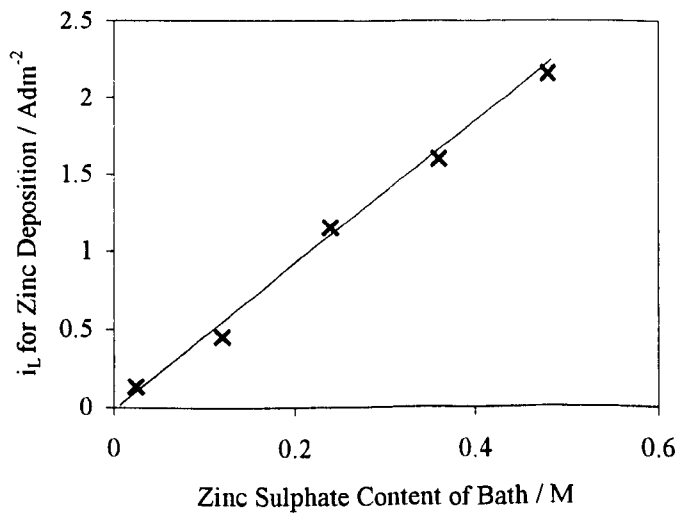


FIGURE 5.3: The Dependence of Zinc Deposition i_L on the Zinc Sulphate Content of the Bath (From Figures 4.27 and 4.28)

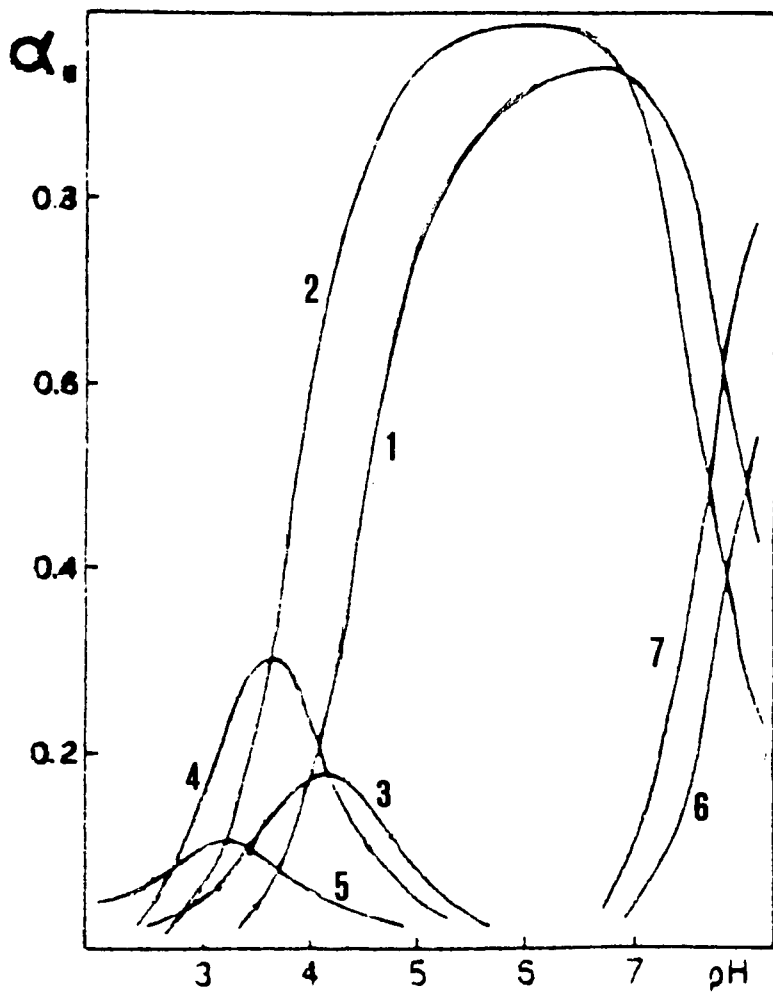
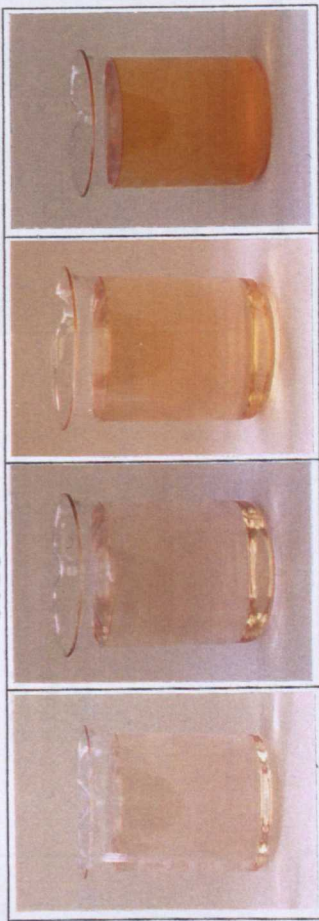


FIGURE 5.4: Distribution of Zinc and Manganese Citrate Species Present in the Bath as a Function of pH ⁽⁷⁶⁾

Key: 1 MnCit^- 2 ZnCit^- 3 MnCitH^0 4 ZnCitH^0
 5 MnCitH_2^+ 6 $\text{Mn}_2\text{Cit}_2\text{H}_2^{4-}$ 7 $\text{Zn}_2\text{Cit}_2\text{H}_2^{4-}$

SOLUTION APPEARANCE

0.2M manganese sulphate +
 0.2M zinc sulphate +
 0.6M sodium citrate +
 2g/l ascorbic acid



A
Day 1

A
Day 3

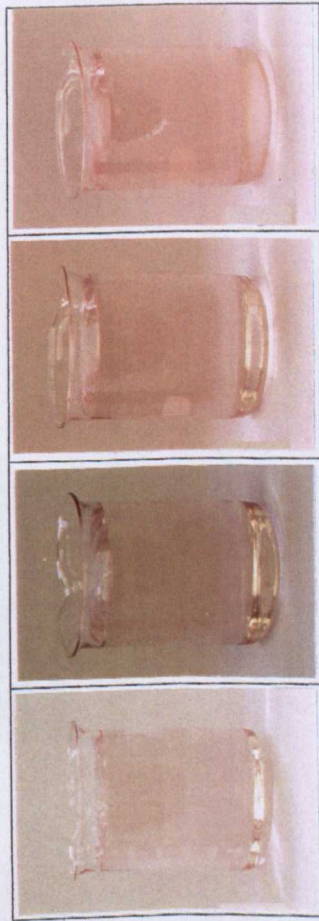
A
Day 9

C
Day 30

Key for precipitation:

- A None
- B Very slight
- C Slight
- D Moderate
- E Heavy
- F Very heavy

0.2M manganese sulphate +
 0.2M zinc sulphate +
 0.6M sodium citrate +
 2g/l sodium sulphite



A

A

A

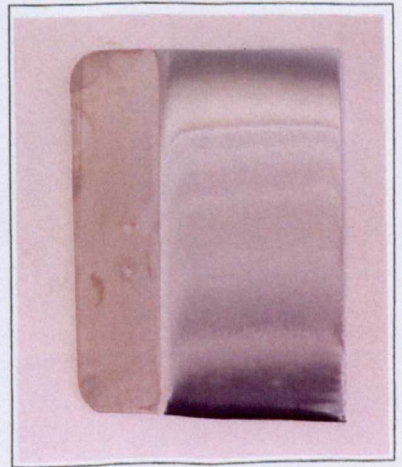
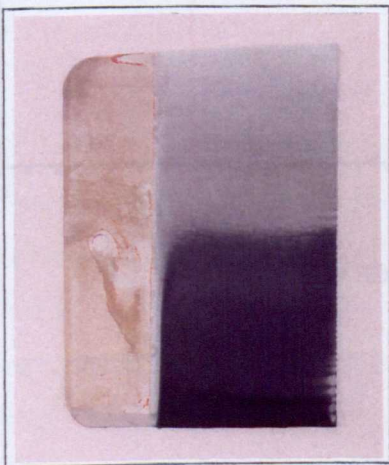
C

For comparison with:

Hull Cells/Solutions -
 Figures 4.12, 4.36, 4.37

FIGURE 5.6: Effect of Decrease in Metal Salt Content on a Zinc-Manganese Standard Bath with Additions (pH5.6, Room Temperature)

HULL CELL



0.24M manganese sulphate +
0.24M zinc sulphate +
0.6M ammonium citrate

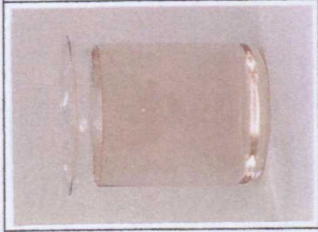
0.24M manganese sulphate +
0.24M zinc sulphate +
0.6M citric acid

(pH altered with ammonia solution)

0.24M manganese sulphate +
0.24M zinc sulphate +
0.6M citric acid

(pH altered with 20% (by volume)
sodium hydroxide)

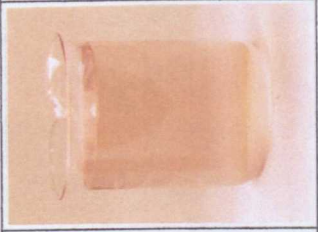
SOLUTION APPEARANCE



A
Day 1



B
Day 3



D
Day 9



D
Day 30

Key for precipitation:

- A** None
- B** Very slight
- C** Slight
- D** Moderate
- E** Heavy
- F** Very heavy

For comparison with:

- Polarisation curves - Figure 6.2
- Hull Cells/Solutions - Figure 4.12

FIGURE 6.1: Effect of Citrate Type on a Zinc-Manganese Standard Bath (pH 5.6, Room Temperature)

ACKNOWLEDGEMENTS

Finally, I would like to express my gratitude to the following individuals for their generous financial and administrative support. I am indebted to Professor J S Li Leach and Professor J V W for their facilities. I am indebted to the SRC for their support of this project, and particularly appreciate the supervision of Dr B R Pearson. My heartfelt thanks go to all the staff who have kept me smiling and working hard in my early days. I much appreciated the support and expertise of "Team R" and the staff of the departmental technical who have made my work would like to thank the staff of the department for producing a number of excellent reports. I would like to thank the staff of the department for their patient advice and assistance. To all my friends and relatives who have supported me in this project - you may never know just how much I appreciate it because I'll probably never tell you what I really think. Kynastons, Leacy, Anne and Peter, and especially Mark. I will never be able to adequately express my appreciation to my father and Robert, and Ben Boden, for his invaluable advice and guidance throughout this project. He has patiently shown me the way many times. This project was finished for you. Yours,

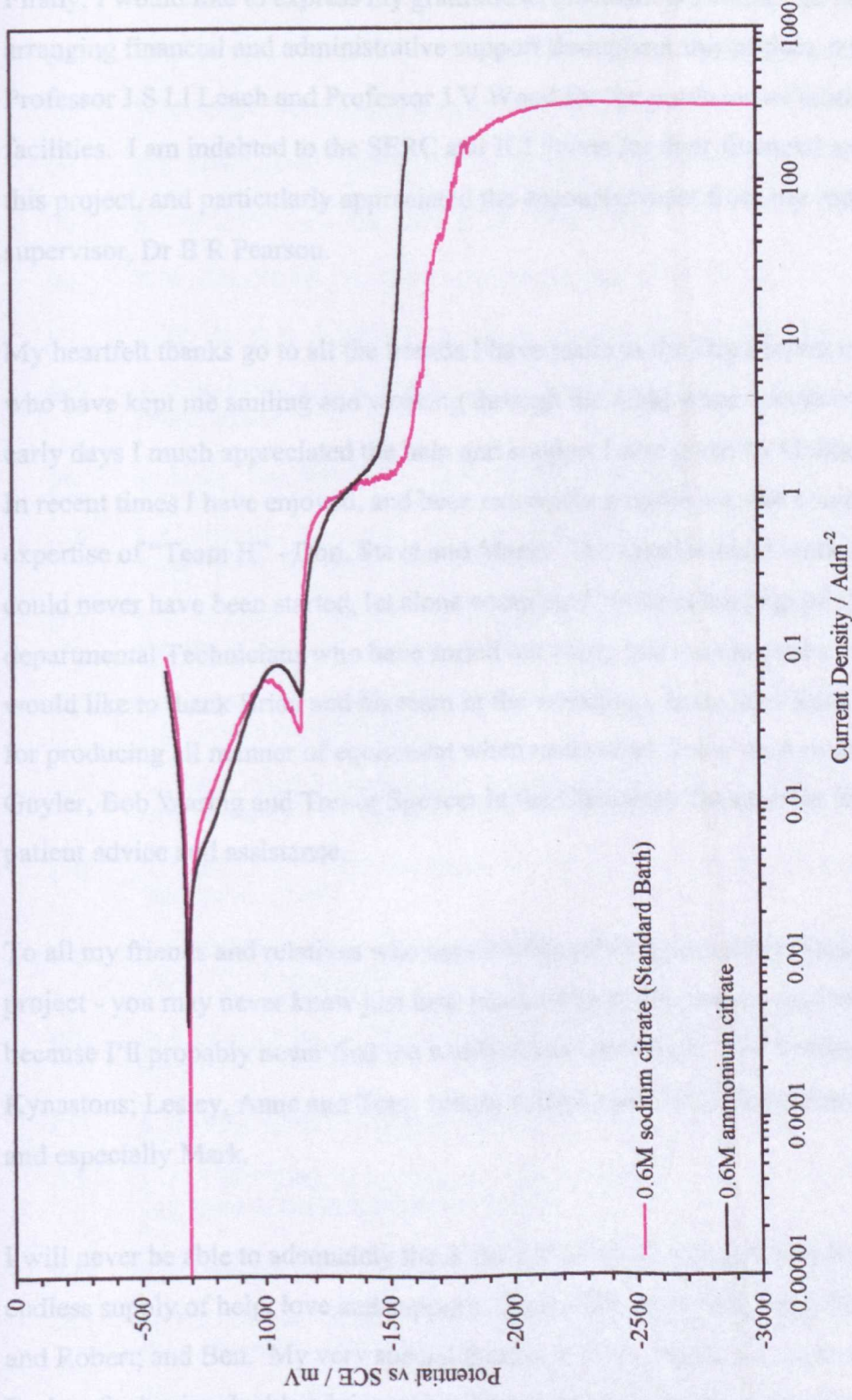


FIGURE 6.2: Effect of Citrate Type on Zinc-Manganese Electrodeposition from a Standard Bath (25°C, pH5.6)

ACKNOWLEDGEMENTS

Firstly, I would like to express my gratitude to Professor S J Harris for his patience in arranging financial and administrative support throughout this project, and to Professor J S Ll Leach and Professor J V Wood for the provision of laboratory facilities. I am indebted to the SERC and ICI Paints for their financial sponsorship of this project, and particularly appreciated the encouragement from my industrial supervisor, Dr B R Pearson.

My heartfelt thanks go to all the friends I have made in the Department over the years who have kept me smiling and working through the night when necessary! In the early days I much appreciated the help and support I was given by Graham and Peter. In recent times I have enjoyed, and been extremely grateful for, the company and expertise of "Team H" - Don, Steve and Maria. The experimental work in this project could never have been started, let alone completed, without the help of all the departmental Technicians who have sorted out many last minute crises. In particular I would like to thank Brian and his team in the workshop, Jenny and Julie, and Frank for producing all manner of equipment when necessary! I also wish to thank Mark Guyler, Bob Waring and Trevor Spencer in the Chemistry Department for their patient advice and assistance.

To all my friends and relatives who have continually supported me throughout this project - you may never know just how much I appreciate you unless I tell you here, because I'll probably never find the words at any other time: The Preisers; The Kynastons; Lesley, Anne and Tom; Julian, Adrian and Carrie; Julie; Jamie; the Reles; and especially Mark.

I will never be able to adequately thank the following amazing people for their endless supply of help, love and support: Mum, Dad and Peter; Mair, Tim, William and Robert; and Ben. My very special thanks go to my friend and supervisor, Dr P J Boden, for his invaluable advice and guidance, moral support and inexhaustible enthusiasm. He has patiently shown me the light at the end of the tunnel so many times. This project was finished for you. Thank you - with love.

REFERENCES

- (1) J. O'CONNOR, J. BOWEN. *Plant Engineering*, File No. 6530; (25 Oct 1984); P62-64
- (2) M. F. LICHTENSTADTER. *J. Protective Coatings and Linings*, 3 (8), (Aug 1986); P36-43
- (3) W. R. EAST. *Mats. Eng. (Cleveland)*, 104 (3), (Mar 1987); P26-29
- (4) H.E. TOWNSEND. *Materials Performance*, (Oct 1991); P60-65
- (5) R. WINAND. *Surf. Coat. Technol*, 37, (1989); P65-87
- (6) E. W. BROOMAN. *Plat. Surf. Finish*, 80 (2), (Feb 1993); P29-35
- (7) G. W. LOAR, K. R. ROMER, T. J. AOE. *Plat. Surf. Finish*, 78 (3), (Mar 1991); P74-79
- (8) F. C. PORTER, A. M. STONEMAN, R. G. THILTHORPE. *Trans. Inst. Metal Finish.*, 66, (1988); P28-33
- (9) R. SARD. *Plat. Surf. Finish.*, 74 (2), (Feb 1987); P30-34
- (10) L. L. SHREIR. "Corrosion. Vol. 1: Metal/Environment Reactions." Publ. Newnes-Butterworths; Second Edition (1976)
- (11) L. L. SHREIR. "Corrosion. Vol. 2: Corrosion Control." Publ. Newnes-Butterworths; Second Edition (1976)
- (12) J. M WEST. "Electrodeposition and Corrosion Processes." Publ. Van Nostrand Reinhold Co. Ltd.; Second Edition (1970)
- (13) P.J. GELLINGS. "Introduction to Corrosion Prevention and Control." Publ. Delft University Press, Delft, The Netherlands; Revised Edition (1985)
- (14) J. C. SCULLY. "The Fundamentals of Corrosion." Publ. Pergamon Press, Oxford, England; Third Edition (1990)
- (15) E. H. LYONS. "Modern Electroplating." Ed. F. A. Lowenheim. Publ. J. Wiley and Sons Inc., USA; Third Edition (1974)
- (16) F. A. LOWENHEIM. "Electroplating." Publ. McGraw-Hill Book Co, New York, USA; (1978)
- (17) A. DAMJANOVIC. *Plating*, 52 (10), (1965); P1017
- (18) J. O'M. BOCKRIS, D. M. DRAZIC. "Electrochemical Science." Publ. Taylor and Francis Ltd., London, England; First Edition (1972)
- (19) M. STERN, A. L GEARY. *J. Electrochem. Soc.*, 104 (1), (Jan 1957); P56-63
- (20) M. POURBAIX. "Atlas of Electrochemical Equilibria in Aqueous Solutions." Publ. Pergamon Press, Oxford, England; (1966)
- (21) A. BRENNER. "Electrodeposition of Alloys. Principles and Practice. Vol I.;" Publ. Academic Press Inc, New York/London; (1963)
- (22) G. D. WILCOX, D. R. GABE. *Corrosion Science*, 35 (5-8), (1993); P1251-1258

- (23) G. D. WILCOX, B. PETERSEN. *Trans. Inst. Metal Finish.*, 74 (4), (1996); P115-118
- (24) A. BRENNER. "Electrodeposition of Alloys. Principles and Practice. Vol II.;" Publ. Academic Press Inc, New York/London; (1963)
- (25) a) A. B. TRIPLER JR, J. E. BRIDE, J. A. GURKLIS, C. L. FAUST. "An Investigation of Electrodeposited Alloys for Protection of Steel Aircraft Parts." Air Force Tech. Report No. 5692, Suppl. 2; Materials Lab, Wright Air Development Centre, Cincinnati, Ohio, USA; (1952)
- b) C. L. FAUST, A. B. TRIPLER JR, C. R. KONECNY, W. C. SCHICKER. "An Investigation of Electrodeposited Alloys for Protection of Steel Aircraft Parts." Air Force Tech. Report No. 5692, Suppl. 3; Materials Lab, Wright Air Development Centre, Cincinnati, Ohio, USA; (1952)
- c) A. B. TRIPLER JR, G. FULLER, C. L. FAUST. "An Investigation of Electrodeposited Alloys for Protection of Steel Aircraft Parts." Air Force Tech. Report No. 5692, Suppl. 4; Materials Lab, Wright Air Development Centre, Cincinnati, Ohio, USA; (1953)
- (26) M. SAGIYAMA, T. URAKAWA, T. ADANIYA, T. HARA. *Conf. Proc: SAE Corrosion (Coatings And Steel)*; 24-28 Feb 1986; Detroit, Mi, USA; P107-117
- (27) T. HARA, M. SAGIYAMA, T. URAKAWA, T. ADANIYA, Y. FUKUDA, Y. TSUCHIYA. *Nippon Kokan Technical Report – Overseas*, 48, (Feb 1987); P29-37
- (28) T. HARA, M. SAGIYAMA, T. URAKAWA, T. ADANIYA, Y. FUKUDA, Y. TSUCHIYA. *Nippon Kokan Technical Report – Overseas*, 114, (1986); P8-15
- (29) D. R. GABE, G. D. WILCOX, A. JAMANI, B. R. PEARSON. *Metal Finish.*, 91 (8), (Aug 1993); P34-36
- (30) D. R. GABE, G. D. WILCOX, A. JAMANI, B. R. PEARSON. *Conf. Proc.: Interfinish '92 Intl. Congr. for Surface Finishing*; Oct 1992; Sao Paulo, Brazil
- (31) M. SELVAM, S. GURUVIAH. *B. Electrochem*, 5 (5), (May 1989); P352-358
- (32) T. AKIYAMA, H. FUKUSHIMA, T. URAKAWA. *Conf. Proc.: 1st Intl. Conf. on Processing Materials for Properties*; Honolulu, Hawaii, USA; 7-10 Nov 1993; P601-604
- (33) M. SAGIYAMA, T. URAKAWA, T. ADANIYA, T. HARA, Y. FUKUDA. *Conf. Proc: AESF 5th Cont. Strip Plat. Symp*; 5-7 May 1987; Dearborn, Mi, USA; Paper VI; P1-16
- (34) M. SAGIYAMA, T. URAKAWA, T. ADANIYA, T. HARA, Y. FUKUDA. *Plat. Surf. Finish.*, 74 (11), (Nov 1987); P77-82
- (35) J.M. WEST. "Basic Corrosion and Oxidation." Publ. Ellis Horwood Ltd, Chichester, England; (1980)
- (36) A. URAKAWA, M. SAGIYAMA, T. ADANIYA, T. HARA. *Trans. ISIJ*, 23 (8), (1983); B-292
- (37) M. EYRAUD, A. GARNIER, F. MAZERON, J. CROUSIER. *Plat. Surf. Finish.*, (Jan 1995); P63-70
- (38) F. I. DANILOV, D. A. SUKHOMLIN, V. V. GERASIMOV, V. A. POPOVICH. *Soviet Electrochem.*, 28 (2), (1992); P171-174
- (39) ANON. *Automotive Engineering*, 94 (5), (May 1986); P56-60

- (40) G. GOVINDARAJAN, V. RAMAKRISHNAN, S. RAMAMURTHI, V. SUBRAMANIAN, N. V. PARTHASARADHY. *Bull. Electrochem.*, 5 (6), (June 1989); P422-426
- (41) B. BOZZINI, F. PAVAN, G. BOLLINI, P.L. CAVALLOTTI. Private Communication of Paper; Politecnico di Milano and Soc. Pneumatici Pirelli, Italy
- (42) M. Y. FOO, G. D. WILCOX, D. R. GABE. "New Materials and Technologies in Surface Finishing for Better Corrosion and Tribology Properties." East Report (1993); Swabisch Gmund
- (43) B. WIELAGE, S. STEINHAUSER, D. NICKELMANN. *Galvanotechnik*, 89 (3), (1998); P724-730
- (44) T. URAKAWA, M. SAGIYAMA, T. ADANIYA, T. HARA. *J. Iron and Steel Inst. of Jpn*, 72 (8), (1986); P968-975; (In Japanese)
- (45) T. URAKAWA, M. SAGIYAMA, T. ADANIYA, T. HARA. *Trans. Iron and Steel Inst. of Jpn*, 26 (2), (1986); B-67
- (46) T. WATANABE, T. KUBOTA, M. YAMASHITA, T. URAKAWA, M. SAGIYAMA. *Conf. Proc.: Corrosion-Resistant Automotive Sheet Steels – in conjunction with 1988 World Materials Congr.*; Chicago, Illinois, USA; 24-30 Sept 1988; P15-20
- (47) H. BAKER. "ASM Handbook. Vol. 3: Alloy Phase Diagrams." Publ. ASM Intl., Ohio, USA; (1992)
- (48) JOINT COMMITTEE ON POWDERED DIFFRACTION STANDARDS (JCPDS). *Powder Diffraction File: PDF-2 Database Sets 1-41*. Publ. Intl. Centre for Diffraction Data, Swarthmore, PA, USA.
- (49) ASTM B117-97. "Standard Practice for Operating Salt Spray (Fog) Apparatus." Publ. ASTM, West Conshohocken, PA, USA (1999)
- (50) M. SELVAM, S. GURUVIAH. *Bull. Electrochem.*, 6 (5), (May 1990); P485-486
- (51) C. J. SLUNDER, W. K. BOYD. "Zinc: Its Corrosion Resistance." Publ. International Lead Zinc Research Organisation Inc., Triangle Park, New York, USA; Second Edition (1983)
- (52) B. W. ROACH. *Welding And Metal Fabrication*, 56 (4), (May/June 1988); P167-168, 170
- (53) E. A. BRANDES, G. B. BROOK. "Smithells Metals Reference Book." Publ. Butterworth-Heinemann Ltd., Oxford, England; Seventh Edition (1992)
- (54) A. SULCIUS, G. BUINEVICIENE, B. STULPINAS. *Bull. Electrochem.*, 7 (2), (Feb 1991); P81-81
- (55) A. SULCIUS, G. BUINEVICIENE, B. STULPINAS. *Soviet Electrochem.*, 24 (9), (Mar 1989); P1172-1174
- (56) R. MURTI, N. RAZDAN, G. E. ERMOLINA. *Indian J. Technol.*, 26, (Oct 1988); P495-500
- (57) R. KASHYAP, S. K. SRIVASTAVA, S. C. SRIVASTAVA. *Surf. Coat. Technol.*, 28 (2), (1986); P129-137
- (58) Y. SUGIMOTO ET AL; *Conf. Proc: 179th Meeting Of Electrochem. Soc;* 5-10 May 1991; Washington DC, USA
- (59) T. AGLADZE, S. BAGAEV, D. GABE, V. KUDRYAVTSEV, C. RAUB, S. SCHACHAMEYER, N. SPYRELIS, T. TSUPAK. *Trans. Inst. Metal Finish.*, 75 (1), (1997); P30-34

- (60) H. H. IWATA, T. URAKAWA, T. HARA. *Trans. ISIJ*, **28** (2), (1988); Paper B-64
- (61) N. N. GREENWOOD, A. EARNSHAW. "Chemistry of the Elements." Publ. Pergamon Press; First Edition Reprint (1990)
- (62) R. A. NYQUIST, R. O. KAGEL. "Infrared Spectra of Inorganic Compounds (3800-45cm⁻¹)." Publ. Academic Press Inc, USA; (1971)
- (63) L. J. BELLAMY. "The Infra-Red Spectra of Complex Molecules." Publ. Methuen and Co. Ltd., London, England; Second Edition (1958)
- (64) D. H. WILLIAMS, I. FLEMING. "Spectroscopic Methods in Organic Chemistry." Publ. McGraw-Hill Publishing Co., London, England; Fifth Edition, (1995)
- (65) ICN FLOW. Private Communication. Chemical manufacturers, Thame, Oxon, England.
- (66) T. FUJITA. *Chem. and Pharm. Bull.*, **30** (10), (Oct 1982); P3461-3465
- (67) C. J. POUCHERT. "The Aldrich Library of Infrared Spectra."; Publ. Aldrich Chemical Co. Inc.; Edition III (1981)
- (68) W. CANNING AND CO. LTD. "Canning Handbook on Electroplating." Publ. W. Canning and Co. Ltd, Birmingham, England (1970); Twenty First Edition
- (69) M. F. MATHIAS, C. M. VILLA, T. W. CHAPMAN. *J. Appl. Electrochem.*, **20**, (1990); P1-10
- (70) R. H. DAHM, R. J. LATHAM. *Trans. Inst. Metal Finish.*, **71** (2), (1993); P77-79
- (71) BRITISH STANDARDS INSTITUTE. "Code of Practice for Cleaning and Preparation of Metal Surfaces." CP 3012: 1972
- (72) D. R. GABE, G. D. WILCOX. *Trans. Inst. Metal Finish.*, **71** (2), (1993); P71-73
- (73) G. A. OTTEWILL, B. A. PLUNKETT, F. C. WALSH. *Trans. Inst. Metal Finish.*, **71** (4), (Nov 1993); P166-170
- (74) A. H. SULLY. "Manganese." Publ. Butterworths Scientific Publications, London; (1995)
- (75) C. S. BARRETT, T. B. MASSALSKI. "Structure of Metals. Crystallographic Methods, Principles and Data." Publ. Pergamon Press. Third Revised Edition (1980)
- (76) P. AMICO, P. G. DANIELE, V. CUCINOTTA, E. RIZZARELLI, S. SAMMARTANO. *Inorganica Chimica Acta*, **36**, (1979); P1-7
- (77) W. L. MASTERTON, E. J. SLOWINSKI, C. L. STANITSKI. "Chemical Principles with Qualitative Analysis." Publ. Saunders College Publishing; Sixth Edition (1985)
- (78) R. L. DROSTE. "Theory and Practice of Water and Wastewater Treatment." Publ. J. Wiley and Sons Inc, USA; (1997)
- (79) J. BROWN, D. G. KINGERLEY, V. ASHWORTH, M. J. WILLETT. *Chemistry and Industry*, (27 Sept 1969); P1369-1378
- (80) J. S. LI. LEACH, B. R. PEARSON, A. RAHMAT. *Conf. Proc.*; 10th Intl. Cong. on Metallic Corrosion; 7-11 Nov 1987; Madras, India (1987); P563-569
- (81) R. PARSONS. "Handbook of Electrochemical Constants." Publ. Butterworths Scientific Publications, London, England; (1959)

- (82) R. C. WEAST. "Handbook of Chemistry and Physics." Publ. CRC Press, Cleveland, Ohio; Fifty Fifth Edition (1974)
- (83) H. YAN, J. DOWNES, P. J. BODEN, S. J. HARRIS. *Philosophical Magazine A*, **70** (2), (1994); P391-404
- (84) H. REMY. "Treatise on Inorganic Chemistry. Vol II." Publ. Elsevier Publishing Co., Amsterdam; (1956)
- (85) W. H. SAFRANEK. "The Properties of Electrodeposited Metals and Alloys. A Handbook." Publ. AESF, Florida, USA; (1986)
- (86) S. J. ROSE, R.E. GUSTAR, D. R. MIHARA, R. I. BIDKLEY, H. G. M. EDWARDS, A KNOWLES. *Trans. Inst. Metal Finish.*, **73** (1), (1993); P11-14
- (87) R. I. BICKLEY, H. G. M. EDWARDS, R.GUSTAR, S. J. ROSE. *J. Mol. Struct.*, **246** (3-4), (1991); P217-228
- (88) D. G. KINGERLEY. Private Communication. Department of Materials Engineering and Materials Design, University of Nottingham, England
- (89) A. V. PAVLINOVA, A. I. SHNAREVICH. *Russ. J. Inorganic Chem.*, **5** (12), (Dec 1960); P1331-1333
- (90) G. WILKINSON (Ed). "Comprehensive Co-ordination Chemistry. Vol 2: Ligands." Publ. Pergamon Press; First Edition (1987)
- (91) A. I. SHNAREVICH. *Russ. J. Inorganic Chem.*, **8** (9), (Sept 1963); P1083-1086
- (92) J. K. KLEWICKI, J. J. MORGAN. *Environ. Sci. Technol.*, **32**, (1998); P2916-2922
- (93) J. J. MORGAN. Private Communication at jjjbm@cco.caltech.edu
- (94) B. COTTON, G. WILKINSON, P. L GAUS. "Basic Inorganic Chemistry." Publ. J. Wiley and Sons Inc.; Second Edition (1987)
- (95) L. GMELIN. "Gmelin Handbuch Der Anorganischen Chemie. Vol. D2: Mn Koordinationsverbindungen." Publ. Springer-Verlag, Heidelberg, Germany; Eighth Edition (1980); (In German)
- (96) J. A. DUFFY. "General Inorganic Chemistry." Publ. Longman Group Ltd., London; Second Edition (1974)
- (97) R. J. KELLER. "The Sigma Library of FT-IR Spectra. Vol. 2." Publ. Sigma Chemical Co. Inc., St. Louis, Missouri, USA; First Edition (1986)
- (98) J. P. GLUSKER, H. L. CARRELL. *J. Mol. Struct.*, **15**, (1973); P151-159
- (99) H. L. CARRELL, J. P. GLUSKER. *Acta Cryst.*, **B29**, (1973); P638-640
- (100) BEILSTEIN Database 1988-1989. Beilstein Institut fur Literatur der Organischen Chemie; Distributed by Beilstein Informationssysteme GmbH, Frankfurt, Germany
- (101) A. J. VAGRAMYAN, Z. A. SOLOV'EVA. "Technology of Electrodeposition." (Translated from Russian by A. Behr.) Publ. Robert Draper Ltd, Teddington; (1961)
- (102) M. GONSALVES. "The Electrodeposition and Chemistry of Manganese." MPhil Thesis (1990); Department of Chemistry, University of Southampton, England

- (103) L. G. SILLEN, A. E. MARTELL. "Stability Constants of Metal-Ion Complexes." Publ. The Chemical Society, London; (1971)
- (104) K. D. MAGERS, C. G. SMITH, D.T. SAWYER. *Inorg. Chem.*, 17 (3), (March 1978); P515-523
- (105) D. SCHLAIN, J. D. PRATER. *Trans. Electrochem. Soc.*, 94 (2), (Aug 1948); P58-73, 374-375
- (106) J. H. JACOBS, P. E. CHURCHWARD. *Trans. Electrochem. Soc.*, 94 (3), (Sep 1948); P108-121, 379-381
- (107) A. E. EDWARDS, W.E BRADT. *Trans. Electrochem. Soc.*, 73, (Apr 1938); P337-352
- (108) W. E. BRADT, L. R. TAYLOR. *Trans. Electrochem. Soc.*, 73, (Apr 1938); P327-335
- (109) M. GONSALVES, D. PLETCHER. *J. Electroanal. Chem.*, 285, (1990); P185-193
- (110) R. MURTI, N. RAZDAN, G. E. ERMOLINA. *J. Indian Technol.*, 24, (May 1986); P270-274
- (111) W. A. BELL. *Trans. Inst. Metal Finish.*, 31, (1954); P466-475
- (112) C. L. MANTELL. *Trans. Electrochem. Soc.*, 94 (5), (Nov 1948); P232-243, 388-389

APPENDICES

APPENDIX 1

COATING MASS RELATED TO THICKNESS

In the diagrams and results of Sagiya et al ⁽²⁶⁻²⁸⁾⁽³³⁾⁽³⁴⁾, the amount of coating deposited is given as mass per unit area. For comparative purposes, this can be converted to a coating thickness using the following method.

Assuming the mass of the coating to comprise solely of zinc and manganese (with no inclusions such as oxides or hydroxides):

$$\text{Density, } \rho = \frac{\text{Mass}}{\text{Volume}} = \frac{\text{Mass}}{\text{Area} \times \text{Thickness}}$$

Therefore:

$$\text{Thickness} = \frac{\text{Mass}}{\text{Area}} \times \frac{1}{\rho}$$

Since the alloy comprises both zinc and manganese:

$$\text{Thickness} = \frac{\text{Mass}}{\text{Area}} \times \frac{1}{\rho_{\text{Zn}} \cdot \text{wt}\%_{\text{Zn}} + \rho_{\text{Mn}} \cdot \text{wt}\%_{\text{Mn}}}$$

Since:

$$\rho_{\text{Zn}} = 7.14 \times 10^6 \text{ gm}^{-3}$$

$$\rho_{\text{Mn}} = 7.20 \times 10^6 \text{ gm}^{-3}$$

Then, at the extremes of pure zinc and pure manganese:

$$\text{Thickness of } 20 \text{ gm}^{-3} \text{ zinc} = 1.40 \mu\text{m}$$

$$\text{Thickness of } 20 \text{ gm}^{-3} \text{ manganese} = 1.39 \mu\text{m}$$

So, 20 gm^{-3} of alloy is approximately equal to $1.40 \mu\text{m}$.

APPENDIX 2

CLEANING PROCEDURE FOR MILD STEEL

The method followed throughout this work for the preparation of the mild steel specimens is described below:

- Wipe panels to remove macroscopic dirt and grease.
- Pre-clean in “Inhibisol” (1,1,1 trichloroethane), removing surface debris with a cotton wool swab.
- Distilled water rinse.
- Hot alkaline soak in 80g/l “Enbond HD 162” at 80°C for 30 minutes.
- Distilled water rinse.
- Electroclean at 6 to 7Adm⁻² in “Endox 114” at 60°C:
 - Anodic for 60 seconds
 - Cathodic for 30 seconds
 - Anodic for 30 seconds
- Distilled water rinse.
- Acid pickle in 10% (by volume) sulphuric acid at room temperature for 30 seconds.
- Distilled water rinse.
- Anodic electroclean at 6 to 7Adm⁻² in “Endox 114” at 60°C for 15 seconds.

- Distilled water rinse.
- Electroplate immediately.

The above steps should be performed sequentially without delay. It was necessary to apply any "Fortolac" lacquer after degreasing in "Inhibisol". This solvent cracked the lacquer which caused unstable potential and current readings during experiments. The lacquer was designed to withstand the remainder of the cleaning process.

"Enbond HD162" and "Endox 114" were obtained from IMASA Ltd, Slough, and "Fortolac" and "Inhibisol" from W. Canning and Co Ltd, Birmingham.

APPENDIX 3

OPERATING CONDITIONS FOR THE COPPER COULOMETER

A coulometer is a small electrochemical cell in which the deposition process is chosen such that all the current flowing is used for only one electrode process. That is, metal deposition occurs with 100% cathode efficiency.

The copper coulometer used in this research is that described by Cannings⁽⁶⁸⁾ and was self-produced. The composition of the solution was:

Copper sulphate, pentahydrate	150g/l
Sulphuric acid	50g/l
Ethanol	50g/l

The anode and cathode were copper and of similar size.

APPENDIX 4

CALCULATION OF CATHODE CURRENT EFFICIENCY

The cathode current efficiency (also known as cathode efficiency) is the proportion of the total cathode current which is used in depositing the metal concerned.

Faraday's Laws of electrolysis can be applied to electroplating such that:

- 1) The mass of metal deposited is proportional to the quantity of charge passed.

That is

$$Q = It \quad \text{(Equation A4.1)}$$

Where Q is the charge passed in Asec, or Coulombs, for a current I flowing over a time t.

- 2) For the same charge passed, the mass of metal deposited is proportional to its chemical equivalent.

The Faraday is defined as the quantity of electricity required to deposit one gram equivalent of metal, or 1F (= 96480Cmol⁻¹) deposits

$$w = \frac{A}{z}$$

where w is the equivalent weight, A is the atomic weight of the metal and z is the valency of the metal ions in solution.

Therefore, 1C (= 1Asec) deposits

$$w = \frac{A}{96480z} = \frac{A}{zF}$$

And a charge of Q Asec will deposit, according to Equation A4.1

$$w = \frac{QA}{zF} = \frac{ItA}{zF} \quad (\text{Equation A4.2})$$

An assumption is made in this equation that the electrodeposition of metal occurs at 100% cathode current efficiency. This is also assumed to be the case in the copper coulometer. So, from Equation A4.2

$$w_{\text{Cu}} = \frac{ItA_{\text{Cu}}}{z_{\text{Cu}}F}$$

where w_{Cu} is the mass of copper deposited, A is the atomic weight of copper and z_{Cu} is the valency of copper which is 2 in sulphate solution. The quantity of charge passed (It) in coulombs can be calculated.

Similarly, for zinc-manganese electrodeposition:

$$w_{\text{Zn/Mn}} = \frac{It}{F} \left(\frac{A_{\text{Mn}} \cdot \text{wt}\%_{\text{Mn}}}{z_{\text{Mn}}} + \frac{A_{\text{Zn}} \cdot \text{wt}\%_{\text{Zn}}}{z_{\text{Zn}}} \right) \quad (\text{Equation A4.3})$$

where $\text{wt}\%_{\text{Mn}}$ and $\text{wt}\%_{\text{Zn}}$ are the alloy percentages of manganese and zinc respectively.

Since the same quantity of current is passed during zinc-manganese electrodeposition as during copper deposition and the composition of the alloy is known, this equation allows the calculation of the theoretical mass of zinc-manganese which would be deposited at 100% efficiency. This equation assumes that zinc and manganese deposition are the only processes occurring which contribute to the mass of the deposit.

The actual mass of zinc-manganese deposited is found by experimentation, so the cathode current efficiency for metal deposition at this current can be found using:

$$\text{Cathode Current Efficiency} = \frac{\text{Actual mass of Zn - Mn}}{\text{Theoretical mass of Zn - Mn}} \times 100\%$$

The proportion of this current which is not used for metal deposition and is consumed by secondary electrode processes is given by taking this percentage from 100%.

APPENDIX 5

CALCULATION OF TIME REQUIRED TO ELECTROPLATE A GIVEN THICKNESS

From Equation A4.3, the mass of zinc-manganese deposited as an electroplate will be given by

$$w_{Zn/Mn} = \frac{It}{F} \left(\frac{A_{Mn} \cdot wt\%_{Mn}}{z_{Mn}} + \frac{A_{Zn} \cdot wt\%_{Zn}}{z_{Zn}} \right) \quad (\text{Equation A5.1})$$

where $wt\%_{Mn}$ and $wt\%_{Zn}$ are the alloy percentages of manganese and zinc respectively.

Since

$$\rho = \frac{w}{v}$$

where ρ is the density of the metal deposited and v is the volume, then the mass of metal deposited can also be written as

$$w_{Zn/Mn} = v \left(\rho_{Mn} \cdot wt\%_{Mn} + \rho_{Zn} \cdot wt\%_{Zn} \right)$$

Substituting this into Equation A5.1

$$v \left(\rho_{Mn} \cdot wt\%_{Mn} + \rho_{Zn} \cdot wt\%_{Zn} \right) = \frac{It}{F} \left(\frac{A_{Mn} \cdot wt\%_{Mn}}{z_{Mn}} + \frac{A_{Zn} \cdot wt\%_{Zn}}{z_{Zn}} \right)$$
$$\underline{T} = \frac{Fv \left(\rho_{Mn} \cdot wt\%_{Mn} + \rho_{Zn} \cdot wt\%_{Zn} \right)}{I \left(\frac{A_{Mn} \cdot wt\%_{Mn}}{z_{Mn}} + \frac{A_{Zn} \cdot wt\%_{Zn}}{z_{Zn}} \right)}$$

The densities of manganese and zinc are 7.20gcm^{-3} and 7.14gcm^{-3} respectively, and the atomic weights are 54.94 and 65.37 respectively. So, the time taken in seconds to electroplate zinc-manganese of average thickness $1\mu\text{m}$ onto an area of 1dm^2 will be given by

$$\underline{T} = \frac{964.8}{i} \frac{(7.20 \cdot \text{wt \%}_{\text{Mn}} + 7.14 \cdot \text{wt \%}_{\text{Zn}})}{(27.47 \cdot \text{wt \%}_{\text{Mn}} + 32.69 \cdot \text{wt \%}_{\text{Zn}})} \quad (\text{Equation A5.2})$$

where i is the current density in Adm^{-2} .

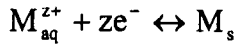
If the system operates at less than 100% cathode current efficiency, then the charge passed needs to be divided by the cathode current efficiency.

So, for example, at a current density of 10Adm^{-2} the deposit was found to contain 41% manganese and 59% zinc which was deposited at a cathode current efficiency of 48.18%. Therefore, the substrate should be electroplated for 47 seconds to give a deposit of average thickness $1\mu\text{m}$.

APPENDIX 6

DERIVATION OF THE NERNST EQUATION

Consider the equilibrium in Equation 1.1:



An activation energy barrier exists for both processes as shown in Figure A6.1.

Reduction of one mole of metal ions to the metallic state requires the passage of z Faradays, or a quantity of electricity zF coulombs. Passage of charge zF through the potential difference of E volts across the double layer constitutes electrical work of zFE joules. This work done by the system, at constant temperature and pressure, is equal to the decrease in free energy of the system, $-\Delta G$. Hence, the free energy change of a reversible electrode reaction is related to the potential by:

$$\Delta G = -zFE \quad (\text{Equation A6.1})$$

The rate of the anodic dissolution process is described by i_+ , while i_- represents the rate of the cathodic discharge process. These rates proceed according to the Arrhenius equation, such that:

$$i_+ = k_A [M_{\text{s}}] \exp\left(-\frac{\Delta G_A^*}{RT}\right)$$

and:

$$i_- = k_C [M_{\text{aq}}^{z+}] [e^{-}] \exp\left(-\frac{\Delta G_C^*}{RT}\right)$$

where k_A and k_C are the corresponding rate constants which contain terms relating the vibration frequency of atoms in the solid, the charge on the species and the Faraday constant. The activities of the products and reactants are denoted by square brackets and are considered to be unity for the metal ions and electrons in the metal.

ΔG_A^* and ΔG_C^* are the standard free energy changes in joules mol⁻¹ for the formation of the transition state from lattice and solution respectively for the system in equilibrium.

According to Equation 1.4, at equilibrium $i_+ = |i_-| = i_0$, so:

$$i_0 = k_A \exp\left(-\frac{\Delta G_A^*}{RT}\right) = k_C [M_{\text{aq}}^{z+}] \exp\left(-\frac{\Delta G_C^*}{RT}\right) \quad (\text{Equation A6.2})$$

Therefore:

$$\frac{\exp(-\Delta G_A^* / RT)}{\exp(-\Delta G_C^* / RT)} = \frac{k_C}{k_A} [M_{\text{aq}}^{z+}]$$

In terms of $\Delta G = \Delta G_C^* - \Delta G_A^*$ and from Equation A6.1:

$$\exp\left(-\frac{\Delta G}{RT}\right) = \frac{k_C}{k_A} [M_{\text{aq}}^{z+}] = \exp\left(\frac{zFE_{\text{eq}}}{RT}\right)$$

Taking natural logarithms:

$$\frac{zFE_{\text{eq}}}{RT} = \ln\left(\frac{k_C}{k_A}\right) + \ln[M_{\text{aq}}^{z+}]$$

or:

$$E_{\text{eq}} = \frac{RT}{zF} \ln\left(\frac{k_C}{k_A}\right) + \frac{RT}{zF} \ln[M_{\text{aq}}^{z+}]$$

When M_{aq}^{z+} is unity, $E_{\text{eq}} = E^0$. So, the first term on the right hand side of this equation must be equal to the standard equilibrium potential, E^0 .

Therefore:

$$E_{\text{eq}} = E^0 + \frac{RT}{zF} \ln[M_{\text{aq}}^{z+}] \quad (\text{Equation A6.3})$$

and, since $\log x = 2.303 \ln x$, then at 25°C:

$$E_{\text{eq}} = E^0 + \frac{0.059}{z} \log[M_{\text{aq}}^{z+}] \quad (\text{Equation A6.4})$$

In addition, since:

$$\text{pH} = -\log[H^+]$$

this can be written as:

$$E_{\text{eq}} = E^0 - 0.059 \text{pH} \quad (\text{Equation A6.5})$$

Equations A6.3, A6.4 and A6.5 are forms of the Nernst equation. It is applicable only when the system is reversible. In a more generalised form

$$E_{\text{eq}} = E^0 + \frac{RT}{zF} \ln \frac{[\text{oxidised state}]}{[\text{reduced state}]} \quad (\text{Equation A6.6})$$

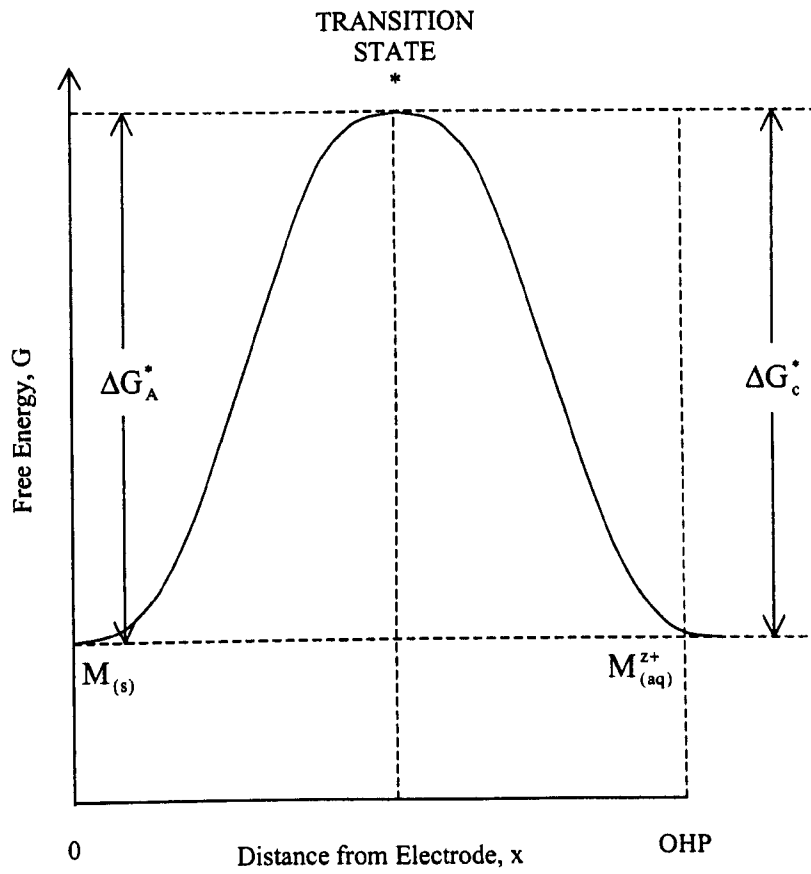


FIGURE A6.1: Electrode Reaction Free Energy Profile for a Reversible Process $M_{(aq)}^{z+} + ze^{-} \leftrightarrow M_{(s)}$ in Equilibrium

APPENDIX 7

DERIVATION OF THE TAFEL EQUATION

If an electrode is cathodically polarised, the equilibrium of Figure A6.1 will be altered as shown in Figure A7.1. The transition state can now only be formed by applying extra potential. This change in potential from the equilibrium state is known as the cathodic overpotential, η_c . For a process solely under activation control, this comprises entirely activation overpotential, $\eta_{act,C}$, and to reduce M^{z+} ions will require change in the magnitudes of free energy from ΔG_C^* and ΔG_A^* to:

$$(\Delta G_C^*)' = \Delta G_C^* + (1 - \beta)zF\eta_{act,C}$$

and

$$(\Delta G_A^*)' = \Delta G_A^* + \beta zF\eta_{act,C}$$

The activation overpotential, $\eta_{act,C}$, serves two functions. Firstly, part of it (a fraction $(1 - \beta)$) assists the cathodic process. Secondly, a fraction β retards the anodic process. β is known as the symmetry factor. A metal ion crossing the double layer would experience increasing influence from the overpotential, and the full value if it reached the electrode surface. However, only a fraction of it, $(1 - \beta)$, is required to produce the transition state which occurs at an intermediate distance.

The rates of the processes proceed according to the Arrhenius equation, such that

$$\begin{aligned} i_- &= k_c [M_{aq}^{z+}] \exp\left(-\frac{\{\Delta G_C^* + (1 - \beta)zF\eta_{act,C}\}}{RT}\right) \\ &= k_c [M_{aq}^{z+}] \exp\left(-\frac{\Delta G_C^*}{RT}\right) \exp\left(-\frac{(1 - \beta)zF\eta_{act,C}}{RT}\right) \end{aligned}$$

and

$$\begin{aligned}
 i_+ &= k_A \exp\left(-\frac{\{\Delta G_A^* - \beta z F \eta_{\text{act,C}}\}}{RT}\right) \\
 &= k_A \exp\left(-\frac{\Delta G_A^*}{RT}\right) \exp\left(\frac{\beta z F \eta_{\text{act,C}}}{RT}\right)
 \end{aligned}$$

Using Equation A6.4, these can be simplified to:

$$i_- = i_0 \exp\left(\frac{-(1-\beta)zF\eta_{\text{act,C}}}{RT}\right) \quad \text{(Equation A7.1)}$$

and

$$i_+ = i_0 \exp\left(\frac{\beta z F \eta_{\text{act,C}}}{RT}\right) \quad \text{(Equation A7.2)}$$

When the system is cathodically polarised, equilibrium does not occur and a net cathodic reaction results. The net cathodic current density, $i_{\text{net,C}}$, is given by:

$$\begin{aligned}
 |i_{\text{net,C}}| &= |i_-| - i_+ \\
 &= i_0 \exp\left(\frac{-(1-\beta)zF\eta_{\text{act,C}}}{RT}\right) - i_0 \exp\left(\frac{\beta z F \eta_{\text{act,C}}}{RT}\right) \quad \text{(Equation A7.3)}
 \end{aligned}$$

As the cathodic overpotential increases above 0.052V⁽¹⁰⁾, the second term representing anodic dissolution becomes negligible. In this case:

$$|i_{\text{net,C}}| \cong i_0 \exp\left(\frac{-(1-\beta)zF\eta_{\text{act,C}}}{RT}\right)$$

Taking natural logarithms and rearranging gives:

$$\eta_{\text{act,C}} = -\frac{RT}{(1-\beta)zF} \ln\left(\frac{|i_{\text{net,C}}|}{i_0}\right)$$

$$= \frac{RT}{(1-\beta)zF} \ln i_0 - \frac{RT}{(1-\beta)zF} \ln |i_{\text{net,C}}|$$

or, in base ten logarithms:

$$\eta_{\text{act,C}} = \frac{2.303RT}{(1-\beta)zF} \lg i_0 - \frac{2.303RT}{(1-\beta)zF} \lg |i_{\text{net,C}}| \quad (\text{Equation A7.4})$$

If the electrode was polarised anodically, similar calculations would produce an expression for the anodic overpotential, η_A , such that:

$$\eta_{\text{act,A}} = -\frac{2.303RT}{\beta zF} \lg i_0 + \frac{2.303RT}{\beta zF} \lg i_{\text{net,A}} \quad (\text{Equation A7.5})$$

Equations A7.4 and A7.5 are Tafel equations, which are usually expressed in the generalised form:

$$\eta_{\text{act}} = a + b \lg i_{\text{net}} \quad (\text{Equation A7.6})$$

A plot of η versus $\lg i$ should be a straight line for a process under activation control with a slope of b_C or b_A , where:

$$b_C = -\frac{2.303RT}{(1-\beta)zF} \quad \text{and} \quad b_A = \frac{2.303RT}{\beta zF}$$

Equation A7.6 shows that $\eta_{\text{act}} = 0$ for $\lg i = \lg i_0$. Thus, extrapolation of the linear Tafel plot to $\eta_{\text{act}} = 0$ gives the value of i_0 .

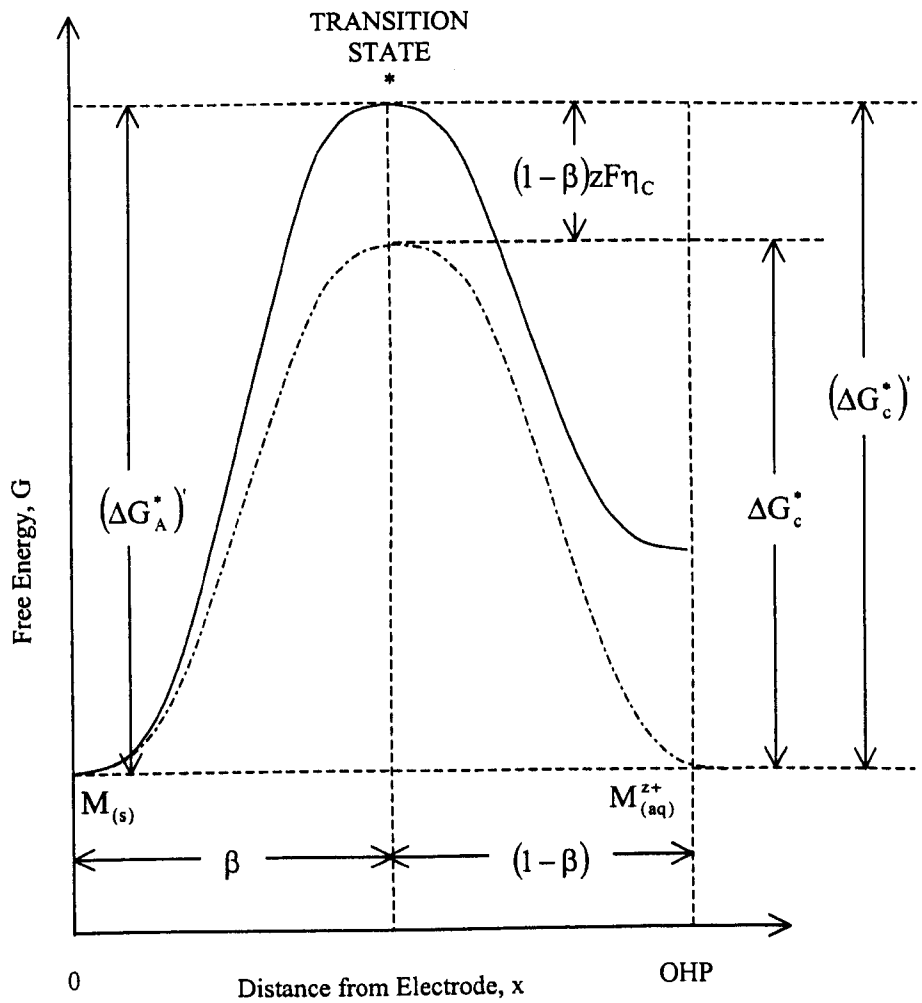


FIGURE A7.1: Effect of Cathodic Polarisation on the Electrode Reaction Free Energy Profile for a Process in Equilibrium

- Electrode in equilibrium
- Electrode cathodically polarised

APPENDIX 8

DERIVATION OF EQUATIONS FOR THE LIMITING CURRENT DENSITY AND CONCENTRATION OVERPOTENTIAL

At a net cathodic current density, $i_{\text{net,C}}$, the total amount of M^{z+} ions deposited at the cathode surface will be $i_{\text{net,C}}/zF \text{ mol sec}^{-1}$. These are replaced by diffusion and migration until an equilibrium concentration, c_e , is established in the Outer Helmholtz Plane. Across the diffusion layer, of thickness δ_N , the metal ion concentration decreases from the bulk value, c_0 , to c_e at the double layer as shown in Figure 2.1.

The diffusion rate of M^{z+} ions across this layer is given by Fick's First Law such that:

$$J = -D \frac{\delta c}{\delta x} = -D \frac{(c_e - c_0)}{\delta_N} = D \frac{(c_0 - c_e)}{\delta_N} \quad \text{mol sec}^{-1} \text{ m}^{-2}$$

This assumes that there is a linear concentration gradient through the diffusion layer. D is the diffusion coefficient of the species M^{z+} .

Assuming that transport is entirely by diffusion then, under steady-state conditions, the total amount deposited is equal to that arriving at the cathode. So:

$$\frac{i_{\text{net,C}}}{zF} = D \frac{(c_0 - c_e)}{\delta_N} \quad \text{(Equation A8.1)}$$

At the limiting current density, i_L , the concentration of M^{z+} at the cathode surface is zero. That is:

$$\frac{i_L}{zF} = \frac{Dc_0}{\delta_N} \quad (\text{Equation A8.2})$$

or

$$i_L = \frac{zFDc_0}{\delta_N} \quad (\text{Equation A8.3})$$

Dividing Equation A8.1 by A8.2 gives:

$$\frac{c_e}{c_0} = 1 - \frac{i_{\text{net,C}}}{i_L}$$

Using a Nernst-type relationship as derived in equation A6.3, the equilibrium potentials corresponding to the bulk and surface concentrations respectively are given by:

$$E_0 = E^0 + \frac{RT}{zF} \ln c_0 \quad \text{and} \quad E_e = E^0 + \frac{RT}{zF} \ln c_e$$

Hence, the application of cathodic current density $i_{\text{net,C}}$ has produced a concentration polarisation, $\eta_{\text{conc,C}}$, of:

$$\begin{aligned} \eta_{\text{conc,C}} = E_e - E_0 &= \frac{RT}{zF} \ln \frac{c_0}{c_e} = \frac{RT}{zF} \ln \left(1 - \frac{|i_{\text{net,C}}|}{i_L} \right) \\ &= \frac{2.303RT}{zF} \log \left(1 - \frac{|i_{\text{net,C}}|}{i_L} \right) \quad (\text{Equation A8.4}) \end{aligned}$$

The limiting current density in Equation A8.3 has been derived by assuming that transport is solely by diffusion. If migration also occurs then the migration rate of M^{z+} ions down the potential gradient is given by:

$$\frac{i_{\text{net,C}} t}{zF} \text{ mol sec}^{-1} \text{ m}^{-2}$$

where \underline{t} is the transport number of the ions, that is, the fraction of the metal ions arriving at the electrode by migration. Adding this to the right hand side of equation A8.1 gives, for a cathodic process:

$$i_L = \frac{zFDc_0}{(1-\underline{t})\delta_N} \quad \text{(Equation A8.5)}$$